

Universiteit
Leiden
The Netherlands

Multimodality imaging in metabolic heart disease

Ng, A.

Citation
Ng, A. (2021, March 23). *Multimodality imaging in metabolic heart disease*. Retrieved from https://hdl.handle.net/1887/3157141

Version:	Publisher's Version
License:	Licence agreement concerning inclusion of doctoral thesis in the Institutional Repository of the University of Leiden
Downloaded from:	https://hdl.handle.net/1887/3157141

Note: To cite this publication please use the final published version (if applicable).

Cover Page



Universiteit Leiden



The handle https://hdl.handle.net/1887/3157141 holds various files of this Leiden University dissertation.

Author: Ng, A.
Title: Multimodality imaging in metabolic heart disease
Issue Date: 2021-03-23

Multimodality Imaging in

Metabolic Heart Disease

Multimodality Imaging In Metabolic Heart Disease

The studies described in this thesis were performed at the Department of Cardiology of Leiden University Medical Center, Leiden, The Netherlands, and Department of Cardiology, Princess Alexandra Hospital, Brisbane, Queensland, Australia

Cover: Arnold CT Ng
Lay-out and print:
ISBN: 978-94-6361-534-1

Copyright© Arnold CT Ng, Leiden, The Netherlands. All rights reserved. No part of this book may be reproduced or transmitted, in any form or by any means, without permission of the author.

Multimodality Imaging in Metabolic Heart Disease

Proefschrift

ter verkrijging van
de graad van Doctor aan de Universiteit Leiden,
op gezag van rector magnificus prof.dr.ir. H. Bijl,
volgens besluit van het college voor promoties
te verdedigen op dinsdag 23 maart 2021
klokke 10.00 uur
door
Arnold CT Ng
Geboren te Malaysia in 1976

Promotor

Prof. Dr. .J. Bax

Co-promotor

Dr. V. Delgado

Leden promotiecommissie

Prof.dr.ir. J.H.C. Reiber
Prof.dr. N.R. Biermasz
Prof. Dr. J.W de Fijter
Prof. Dr. F. Cosentino (Karolinska University Hospital, Sweden)
Prof. Dr. D. Leung (South Western Sydney Clinical School, University of New South Wales, Sydney, Australia)
Dr. N.A. Marsan

Dedicated to my family:

Carolina, Allison, Adelyne, Diyen

TABLE OF CONTENTS

	General introduction and outline of thesis	9
Chapter 1	Multimodality Imaging in Diabetic Heart Disease *Curr Probl Cardiol. 2011;36(1):9-47*	25
Chapter 2	Findings from Left Ventricular Strain and Strain Rate Imaging in Asymptomatic Patients with Type 2 Diabetes Mellitus *Am J Cardiol. 2009;104(10):1398-401*	65
Chapter 3	Impact of Diabetes and Increasing Body Mass Index Category on Left Ventricular Systolic and Diastolic Function *J Am Soc Echocardiogr. 2018;31(8):916-925*	77
Chapter 4	Myocardial Steatosis and Biventricular Strain and Strain Rate Imaging in Patients with Type 2 Diabetes Mellitus *Circulation. 2010;122(24):2538-44*	99
Chapter 5	Association Between Diffuse Myocardial Fibrosis by Cardiac Magnetic Resonance Contrast-Enhanced T1 Mapping and Subclinical Myocardial Dysfunction in Diabetic Patients: A Pilot Study *Circ Cardiovasc Imaging. 2012 Jan;5(1):51-9*	115
Chapter 6	Impact of Epicardial Adipose Tissue, Left Ventricular Myocardial Fat Content and Interstitial Fibrosis on Myocardial Contractile Function *Circ Cardiovasc Imaging. 2018;11(8):e007372*	137
Chapter 7	Defining Subclinical Myocardial Dysfunction and Implications for Patients with Diabetes Mellitus and Preserved Ejection Fraction *Am J Cardiol. 2019;124(6):892-898*	159
	Summary and conclusions	177
	Samenvatting en conclusies	183
	List of publications	187
	Curriculum Vitae	203
	Acknowledgements	205

General introduction and outline of thesis

Epidemiology of obesity and diabetes

There is currently a growing worldwide epidemic of obesity and type 2 diabetes mellitus (DM). In the last 40 years, the number of obese adults has increased 6-fold to an estimated 640 million worldwide.[1] Obesity is a risk factor for cardiovascular diseases and some cancers, but is the strongest risk factor for developing DM. The latest estimates by the International Diabetes Federation suggested that there are 425 million diabetics in 2017, and is projected to increase by 48% to 629 million by 2045.[2] Furthermore, an estimated 212 million adults aged 20-79 years are unaware of their DM diagnosis, and DM accounted for 10.7% of global all-cause mortality (higher than the combined deaths from infectious diseases).[2] Global healthcare expenditure for DM patients aged 20-79 years grew from US$ 232 billion in 2007 to US$ 727 billion in 2017, a three-fold increase within 10 years.[2]

Although coronary atherosclerosis (i.e. coronary heart disease [CHD]) is the most common and well recognized complication arising from obesity and DM, patients often can develop cardiac structural and functional changes independent of CHD that are detrimental and associated with long term adverse outcomes.[3-5] Known as metabolic heart disease, it is characterized by altered myocardial energetics with mitochondrial dysfunction, abnormal substrate usage with steatosis, cardiac autonomic neuropathy and increased interstitial collagen deposition.[6, 7] These pathological processes initially result in subclinical myocardial contractile dysfunction with preservation of left ventricular (LV) ejection fraction (EF), but eventually progresses to overtly reduced LVEF.[8-11]

Myocardial metabolism

In a normal heart, there is a balance between myocardial oxygen delivery (supply) and metabolism (demand). Adenosine triphosphate (ATP) is the primary molecule that provides energy to drive myocardial contraction and is primarily produced within the mitochondria via oxidative phosphorylation. The heart normally uses both glucose and free fatty acids as energy substrates for ATP production via the citric acid cycle (Krebs cycle) (Figure 1).[12] Acetyl coenzyme A (acetyl-CoA) is the key molecule that delivers the acetyl group to the Krebs cycle to produce reduced nicotinamide adenine dinucleotide (NADH) and CO_2. NADH is subsequently used by the oxidative phosphorylation pathway to generate ATP (Figure 1).

Within the mitochondria, 10-40% of acetyl-CoA is produced from the oxidation of glucose/pyruvate via the glycolysis pathway, and 60-90% is produced via β-oxidation of free fatty acids.[12] Under normal physiological conditions, 70–90% of the free fatty acids entering the myocytes are immediately oxidized and 10–30% enter the intracellular triglyceride pool.[13] This intracellular triglyceride pool is an important source of fatty

acids, with the rate of lipolysis and its contribution to overall myocardial ATP production being inversely related to the concentration of exogenous free fatty acids. Increased ATP production from increased cardiac work is due to increased ATP hydrolysis and oxidative phosphorylation, but the total ATP pool remains relatively constant.[14]

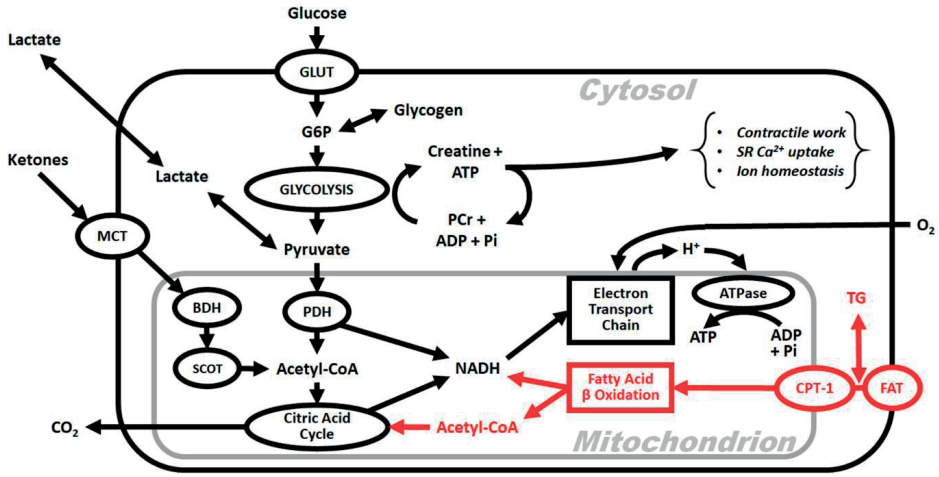


Figure 1. *Graphical representation of myocardial substrate metabolism. Cardiac myocytes utilizes glucose, free fatty acid, and ketones as energy substrates to produce ATP. Majority of the ATP is produced via oxidative phosphorylation in the mitochondria. BDH: β-hydroxybutyrate dehydrogenase; CPT-1: carnitine palmitoyltransferase-1; FAT: fatty acid transporter/CD36; G6P: glucose 6-phosphate; GLUT: glucose transporters; MCT: monocarboxylic acid transporters; PCr: phosphocreatine; PDH: pyruvate dehydrogenase; SCOT: succinyl-CoA-3-oxaloacid CoA transferase; SR: sarcoplasmic reticulum. Adapted from Stanley et al. and Karwi et al.*[12, 15]

Although the heart can utilize both glucose and free fatty acid for metabolism, obese and diabetic patients preferentially uses free fatty acid as its main energy source despite the prevailing hyperglycemia. Consequently, there is a shift in myocardial energy production towards mitochondrial free fatty acid β-oxidation, and the excess free fatty acid is converted and stored as triglycerides within the cellular cytoplasm (i.e. steatosis).[16, 17] Although the intracellular triglyceride is inert, it reflects the increased concentration of free fatty acid in the myocardium. The high concentration of free fatty acid inhibits pyruvate dehydrogenase which impairs the mitochondrial citric acid cycle and ATP production.[6] The excessive free fatty acid exceeds the mitochondrial β-oxidative capacity and leads to accumulation of toxic lipid intermediates such as ceramide and diacylglycerol, causing cellular apoptosis, replacement fibrosis and myocardial contractile dysfunction.[18, 19]

There is a direct relationship between myocardial steatosis and contractile dysfunction. Previous animal study demonstrated that LV contractile function is less when free fatty

acids rather than glucose are the sole exogenous energy substrate.[20] In humans, myocardial steatosis is associated with LV diastolic dysfunction.[21] Currently, myocardial steatosis can be quantified by magnetic resonance spectroscopy (MRS) as well as multi-echo cardiac magnetic resonance (CMR) methods to reconstruct water- and fat-separated images.

Myocardial steatosis

Magnetic resonance spectroscopy

Magnetic resonance spectroscopy (MRS) is a non-invasive tool that can quantify myocardial metabolism. It can be performed on any atom that has an odd number of nucleons (i.e. protons and neutrons) within its nucleus, such as hydrogen/proton (^{1}H), carbon (^{13}C) and phosphorus (^{31}P). When these nuclei are subjected to a magnetic field, they will align and precess about the axis of the magnetic field at a specific frequency (Figure 2). However, the nuclei of atoms in a molecule (e.g. water [H_2O] or lipid methylene [–CH_2–] or CH_3 moieties) are shielded from the applied magnetic field by the circulating electron, resulting in slight differences in the resonant frequencies of the nucleus depending on the chemical bonds within the molecule. These chemical shifts are measured in parts per million (ppm) of the main resonant frequency.

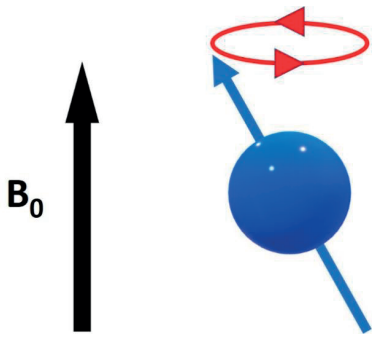


Figure 2. *Representation of a proton precession (red arrows) about the axis of the applied magnetic field (B0).*

In biological tissue, ^{1}H is the most abundant nucleus to perform MRS. For in-vivo ^{1}H-MRS, water resonates at 4.7 ppm whilst the lipid methylene [–CH_2–] and CH_3 moieties resonate at 1.2 and 0.9 ppm respectively (Figure 3). Due to the intense concentration of water compared to lipids within the myocardium, water suppression techniques are applied to attenuate the water peak in order to quantify the lipid signals. As the heart moves within the mediastinum due to systolic/diastolic motions and within the chest cavity due to respiration, MRS of the myocardium is usually performed with both cardiac and respiratory gating. This usually result in long scan durations in order to achieve

adequate spectrograms to quantify intramyocardial triglyceride content.[22] Furthermore, the placement of the volume-of-interest is usually limited to the proximal and mid interventricular septum to avoid potential contamination from epicardial adipose tissue (EAT). Presently, ^{1}H-MRS is considered the clinical gold-standard for quantifying intramyocardial triglyceride content.

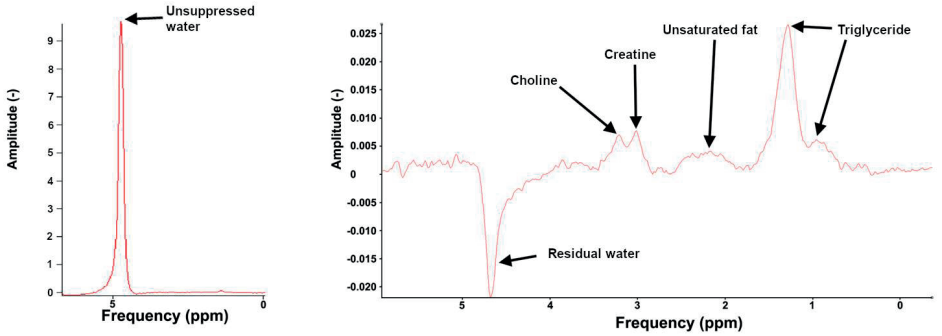


Figure 3. *Quantification of myocardial triglyceride content by ^{1}H-MRS. Examples of unsuppressed (left panel) and water-suppressed (right panel) spectra. The water-suppressed spectrum shows the peaks from triglyceride, unsaturated fat, creatine and choline. Myocardial triglyceride content is calculated and expressed as a percentage that is based on the signal amplitude of myocardial triglyceride divided by the signal amplitude of water. In patients with obesity or diabetes, the triglyceride peaks will be increased relative to the water peak, resulting in a higher ratio.*

Water-fat separated imaging

Intramyocardial fat can also be quantified using multi-echo Dixon water and fat separated imaging with variable projection (VARPRO).[23-25] It similarly exploits differences in resonance frequencies between water and fat to quantify intramyocardial fat content. The VARPRO method utilizes ≥ 3 echo times to derive water-only, fat-only, in-phase and out-of-phase images using a single breathhold.[23-25] This method provides excellent discrimination between water and fat, and the images generally have low signal-to-noise ratio (Figure 4).

Unlike ^{1}H-MRS, this technique permits quantification of regional and global intramyocardial fat content. Images are also obtained in a single breath-hold. Most importantly, it can be coupled with other multiparametric CMR techniques such as T1 mapping and late gadolinium enhancement. However, VARPRO will tend to overestimate myocardial triglyceride content compared to ^{1}H-MRS due to its inherent T1 bias.

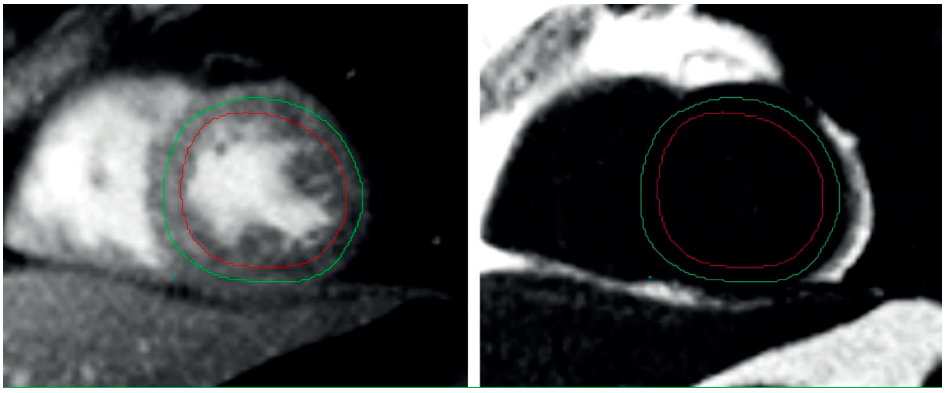


Figure 4. *Quantification of myocardial fat. Example of a Dixon multiecho gradient variable projection (VARPRO) sequence with fat–water separation imaging in a healthy individual. Left panel is the water-only image and right panel is the fat-only image. Myocardial fat content is calculated and expressed as a percentage that is based on the mean pixel signal intensity of the left ventricular fat-only image divided by the mean pixel signal intensity of the left ventricular water-only image, multiplied by 100.*

Epicardial adipose tissue

Epicardial adipose tissue (EAT) may also play an important role in cardiac substrate utilization. It is embryologically similar to mesenteric and omental visceral fat, having developed from the splanchnopleuric mesoderm.[26] EAT is bounded between the epicardium and pericardium, and is not separated from the underlying myocardium by any fibrous tissue. It lies directly over the myocardium, preferentially within the atrioventricular and interventricular grooves following the coronary arteries, right ventricular free wall and around both atria.[27] Previous study has suggested that EAT may act as a lipid store for the myocardium, and directly releases free fatty acids for myocardial lipid and energy homeostasis.[28] Both increasing obesity and diabetes are directly associated with increased EAT volume, and there is a direct correlation between EAT thickness and myocardial steatosis.[29] Increased EAT volume is also independently associated with various cardiac pathologies including increased LV mass, myocardial dysfunction, left atrial dysfunction, atrial fibrillation and CHD.[30-38] Total EAT volume can be accurately quantified using 3-dimensional imaging techniques modalities such as computed tomography (CT) and CMR (Figure 5), and are superior to 2-dimensional techniques such as echocardiography that offers only linear measurements.[26]

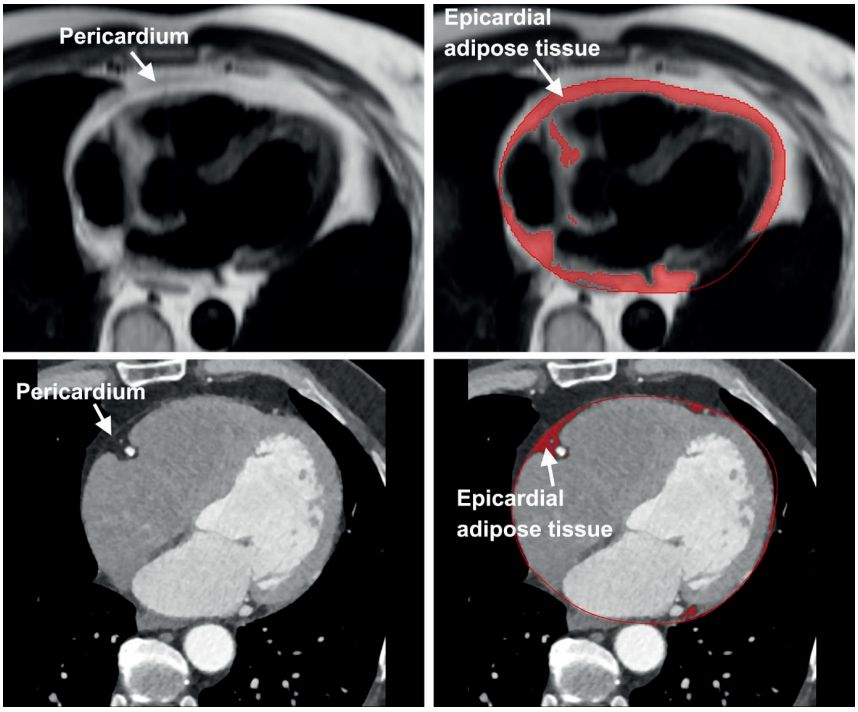


Figure 5. *Quantification of epicardial fat volume. Examples of epicardial fat volume quantification with the use of cardiac magnetic resonance black blood imaging (top 2 panels) in a patient with diabetes, and CT (bottom 2 panels) in a healthy individual. In the top left panel, the pericardium is the thin rim of black line surrounding the heart in black blood imaging. Therefore, epicardial adipose tissue is bounded between the pericardium and the epicardium, and appears bright in black blood imaging. In top right panel, the computer software automatically highlights and calculate the total epicardial adipose tissue volume based on pixel signal intensity. In bottom left panel, the pericardium is the thin rim of bright line on CT coronary angiogram. In bottom right panel, the computer software automatically highlights and calculate the total epicardial adipose tissue volume based on Hounsfield units. Patients with obesity or diabetes usually have larger epicardial adipose tissue volume compared to normal healthy individuals.*

Myocardial interstitial fibrosis

Patients with metabolic heart disease can develop increased interstitial fibrosis leading to increased LV stiffness, impaired systolic and diastolic function, and eventual clinical heart failure. Unlike “traditional” late gadolinium enhancement that is dependent on relative regional differences in contrast distribution, recent advent of CMR with T1 mapping allows quantification of diffuse LV interstitial fibrosis by means of calculating post-contrast T1 time or extracellular volume (ECV) fraction.[39] Post-contrast T1 time and ECV fraction calculations rely on T1 shortening of extracellular gadolinium contrast that accumulates within the extracellular space (Figure 6). Large histological validation studies have demonstrated an excellent correlation between post-contrast T1 time and fibrosis burden on endomyocardial biopsies.[40, 41]

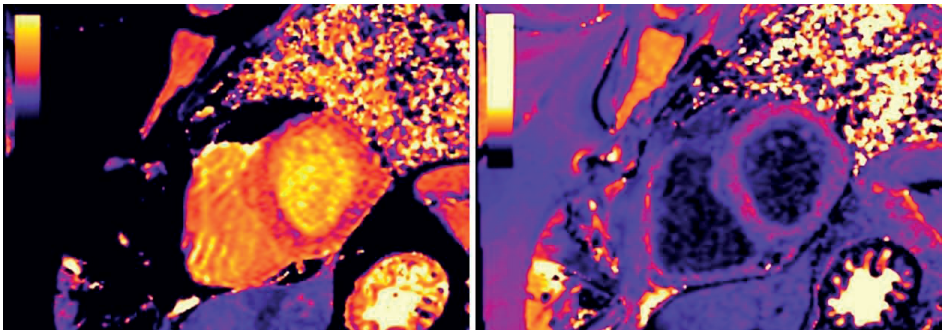


Figure 6. *Quantification of interstitial fibrosis. CMR with T1 mapping allows the quantification of diffuse interstitial fibrosis in the left ventricle by calculation of extracellular volume (ECV) fraction with the use of left ventricular native (left panel) and post-contrast (right panel) T1 maps.*

In a small head-to-head comparison study, native T1 time had no correlation with histological collagen volume fraction, and ECV fraction may be superior to post-contrast T1 time.[42] From the CMR technical perspective, the advantages of ECV fraction over post-contrast T1 time includes independence of magnetic field strength, the type of T1 mapping sequence, and timing of post-contrast image acquisition.

Myocardial contractile function

There is extensive literature on the prognostic value of LVEF in predicting patient morbidity and mortality.[43-45] However, LVEF is an insensitive measure of LV systolic function and is usually preserved during the early stages of the disease process where there are only subtle reductions in myocardial contractility. This early subtle reduction in myocardial contractile function before appearance of clinical symptoms is known as subclinical myocardial dysfunction and can be detected using advanced echocardiographic techniques such as 2-dimensional (2D) strain imaging.

Strain is a dimensionless index and is defined as the amount of deformation (i.e. change in length) normalised to its original length. It is represented by the symbol ε and expressed mathematically as:

$$Strain\ (\varepsilon)\ = \frac{L - L_0}{L_0} \times 100\%$$

where L is the length of myocardium after deformation (i.e. end-systole) and L_0 is the original length (i.e. end-diastole). By convention, strain is defined as positive when the myocardium is lengthening, and defined as negative when the myocardium is shortening. As shown in Figure 7, LV myocardial contraction is comprised of longitudinal shortening (negative strain), circumferential shortening (negative strain), and radial thickening (positive strain).

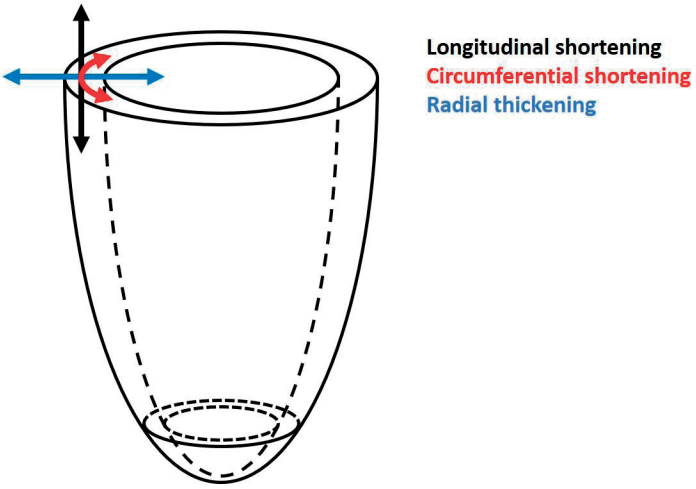


Figure 7. *Graphical representation of the left ventricular myocardial contraction according to the cardiac axis. During systole, there is longitudinal shortening (black arrow) from the basal to apical motion of the left ventricle, circumferential shortening (red arrow) in the short axis, and radial thickening (blue arrow) in the short axis.*

Of these 3 strain directions, longitudinal strain is primarily determined by subendocardial fibers and is the most sensitive indicator of subclinical myocardial dysfunction. This is due to the endocardium having the lowest oxygen tension compared to the epicardium and is therefore most vulnerable to relative ischemia even with subtle reductions in myocardial blood flow.[46] Compared to LVEF, longitudinal strain is a superior prognosticator for all-cause mortality and cardiovascular morbidity.[47] Figure 8 shows the derivation of peak global longitudinal strain from the 3 apical views.

Objectives and outline of thesis

The objectives of this thesis were to elucidate the pathogenesis of metabolic heart disease, evaluate the associated changes in myocardial structure and contractile function, and determine the long-term prognostic implications of subclinical myocardial dysfunction on all-cause mortality.

Chapter 1 summarizes the utility of various advanced cardiac imaging modalities in elucidating the pathogenesis of metabolic heart disease. Next, echocardiographic 2D speckle tracking strain analysis was used to detect subclinical myocardial contractile dysfunction in diabetic (Chapter 2) and obese (Chapter 3) patients with preserved LVEF. In Chapters 4-6, CMR and cardiac CT were used to evaluate the associations between myocardial steatosis, interstitial fibrosis and EAT with subclinical myocardial contractile dysfunction. Finally, the thesis will conclude with the prognostic implications of sub-

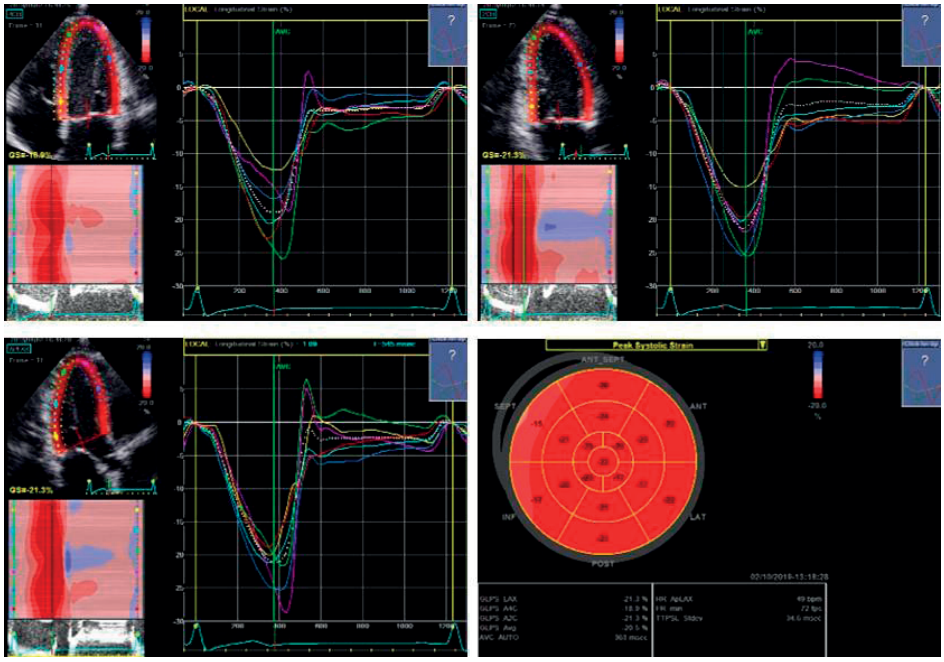


Figure 8. *Example of 2D speckle tracking analyses. Individual longitudinal strain measurements are initially performed from the 4-chamber (top left panel), 2-chamber (top right panel) and 3-chamber (bottom left panel) views. Individual longitudinal strain curves are generated from each view and combined to automatically display a bull's eye map with the average peak global longitudinal strain (bottom right panel).*

clinical myocardial contractile dysfunction and its incremental clinical usefulness using decision curve analysis (Chapter 7).

In this thesis, all patients had normal LVEF and peak global longitudinal strain (GLS) was used to detect subclinical myocardial contractile dysfunction. In Chapters 2 and 3, GLS was used to evaluate the impact of DM and obesity on myocardial contractility. In Chapters 3 to 6, the thesis explored the association between GLS and pathogenesis of metabolic heart disease (i.e. steatosis, interstitial fibrosis and epicardial adipose tissue [EAT] volume). In Chapter 7, the prognostic significance and clinical usefulness of GLS was evaluated.

REFERENCE LIST

(1) Trends in adult body-mass index in 200 countries from 1975 to 2014: a pooled analysis of 1698 population-based measurement studies with 19.2 million participants. *Lancet* 2016;387:1377-1396.

(2) Cho NH, Shaw JE, Karuranga S, Huang Y, da Rocha Fernandes JD, Ohlrogge AW, Malanda B. IDF Diabetes Atlas: Global estimates of diabetes prevalence for 2017 and projections for 2045. *Diabetes Res Clin Pract* 2018;138:271-281.

(3) Dandamudi S, Slusser J, Mahoney DW, Redfield MM, Rodeheffer RJ, Chen HH. The prevalence of diabetic cardiomyopathy: a population-based study in Olmsted County, Minnesota. *J Card Fail* 2014;20:304-309.

(4) Liu JH, Chen Y, Yuen M, Zhen Z, Chan CW, Lam KS, Tse HF, Yiu KH. Incremental prognostic value of global longitudinal strain in patients with type 2 diabetes mellitus. *Cardiovasc Diabetol* 2016;15:22.

(5) Ng ACT, Prevedello F, Dolci G, Roos CJ, Djaberi R, Bertini M, Ewe SH, Allman C, Leung DY, Marsan NA, Delgado V, Bax JJ. Impact of Diabetes and Increasing Body Mass Index Category on Left Ventricular Systolic and Diastolic Function. *J Am Soc Echocardiogr* 2018;31:916-925.

(6) Falcao-Pires I, Leite-Moreira AF. Diabetic cardiomyopathy: understanding the molecular and cellular basis to progress in diagnosis and treatment. *Heart Fail Rev* 2012;17:325-344.

(7) Cavalera M, Wang J, Frangogiannis NG. Obesity, metabolic dysfunction, and cardiac fibrosis: pathophysiological pathways, molecular mechanisms, and therapeutic opportunities. *Transl Res* 2014;164:323-335.

(8) Pazin-Filho A, Kottgen A, Bertoni AG, Russell SD, Selvin E, Rosamond WD, Coresh J. HbA 1c as a risk factor for heart failure in persons with diabetes: the Atherosclerosis Risk in Communities (ARIC) study. *Diabetologia* 2008;51:2197-2204.

(9) Kenchaiah S, Evans JC, Levy D, Wilson PW, Benjamin EJ, Larson MG, Kannel WB, Vasan RS. Obesity and the risk of heart failure. *N Engl J Med* 2002;347:305-313.

(10) Di SB, Galandauer I, Aronow WS, McClung JA, Alas L, Salabay C, Belkin RN. Prevalence of left ventricular diastolic dysfunction in obese persons with and without diabetes mellitus. *Am J Cardiol* 2005;95:1527-1528.

(11) Horwich TB, Fonarow GC. Glucose, Obesity, Metabolic Syndrome, and Diabetes: Relevance to Incidence of Heart Failure. *J Am Coll Cardiol* 2010;55:283-293.

(12) Stanley WC, Recchia FA, Lopaschuk GD. Myocardial substrate metabolism in the normal and failing heart. *Physiol Rev* 2005;85:1093-1129.

(13) Lopaschuk GD, Ussher JR, Folmes CD, Jaswal JS, Stanley WC. Myocardial fatty acid metabolism in health and disease. *Physiol Rev* 2010;90:207-258.

(14) Balaban RS, Heineman FW. Control of mitochondrial respiration in the heart in vivo. *Mol Cell Biochem* 1989;89:191-197.

(15) Karwi QG, Uddin GM, Ho KL, Lopaschuk GD. Loss of Metabolic Flexibility in the Failing Heart. *Front Cardiovasc Med* 2018;5:68.

(16) McGavock JM, Lingvay I, Zib I, Tillery T, Salas N, Unger R, Levine BD, Raskin P, Victor RG, Szczepaniak LS. Cardiac Steatosis in Diabetes Mellitus: A 1H-Magnetic Resonance Spectroscopy Study. *Circulation* 2007;116:1170-1175.

(17) Ng ACT, Strudwick M, van der Geest RJ, Ng ACC, Gillinder L, Goo SY, Cowin G, Delgado V, Wang WYS, Bax JJ. Impact of Epicardial Adipose Tissue, Left Ventricular Myocardial Fat Content, and Interstitial Fibrosis on Myocardial Contractile Function. *Circ Cardiovasc Imaging* 2018;11:e007372.

(18) Schaffer JE. Lipotoxicity: when tissues overeat. *Curr Opin Lipidol* 2003;14:281-287.

(19) Chokshi A, Drosatos K, Cheema FH, Ji R, Khawaja T, Yu S, Kato T, Khan R, Takayama H, Knoll R, Milting H, Chung CS, Jorde U, Naka Y, Mancini DM, Goldberg IJ, Schulze PC. Ventricular assist device implantation corrects myocardial lipotoxicity, reverses insulin resistance, and normalizes cardiac metabolism in patients with advanced heart failure. *Circulation* 2012;125:2844-2853.

(20) Burkhoff D, Weiss RG, Schulman SP, Kalil-Filho R, Wannenburg T, Gerstenblith G. Influence of metabolic substrate on rat heart function and metabolism at different coronary flows. *Am J Physiol* 1991;261:H741-H750.

(21) Rijzewijk LJ, van der Meer RW, Smit JWA, Diamant M, Bax JJ, Hammer S, Romijn JA, De Roos A, Lamb HJ. Myocardial Steatosis Is an Independent Predictor of Diastolic Dysfunction in Type 2 Diabetes Mellitus. *J Am Coll Cardiol* 2008;52:1793-1799.

(22) Gillinder L, Goo SY, Cowin G, Strudwick M, van der Geest RJ, Wang WY, Ng AC. Quantification of Intramyocardial Metabolites by Proton Magnetic Resonance Spectroscopy. *Front Cardiovasc Med* 2015;2:24.

(23) Hernando D, Haldar JP, Sutton BP, Ma J, Kellman P, Liang ZP. Joint estimation of water/fat images and field inhomogeneity map. *Magn Reson Med* 2008;59:571-580.

(24) Kellman P, Hernando D, Shah S, Zuehlsdorff S, Jerecic R, Mancini C, Liang ZP, Arai AE. Multiecho dixon fat and water separation method for detecting fibrofatty infiltration in the myocardium. *Magn Reson Med* 2009;61:215-221.

(25) Kellman P, Hernando D, Arai AE. Myocardial Fat Imaging. *Curr Cardiovasc Imaging Rep* 2010;3:83-91.

(26) Sacks HS, Fain JN. Human epicardial adipose tissue: a review. *Am Heart J* 2007;153:907-917.

(27) Iacobellis G, Corradi D, Sharma AM. Epicardial adipose tissue: anatomic, biomolecular and clinical relationships with the heart. *Nat Clin Pract Cardiovasc Med* 2005;2:536-543.

(28) Nelson RH, Prasad A, Lerman A, Miles JM. Myocardial uptake of circulating triglycerides in nondiabetic patients with heart disease. *Diabetes* 2007;56:527-530.

(29) Malavazos AE, Di LG, Secchi F, Lupo EN, Dogliotti G, Coman C, Morricone L, Corsi MM, Sardanelli F, Iacobellis G. Relation of echocardiographic epicardial fat thickness and myocardial fat. *Am J Cardiol* 2010;105:1831-1835.

(30) Marwan M, Achenbach S. Quantification of epicardial fat by computed tomography: why, when and how? *J Cardiovasc Comput Tomogr* 2013;7:3-10.

(31) Patel VB, Shah S, Verma S, Oudit GY. Epicardial adipose tissue as a metabolic transducer: role in heart failure and coronary artery disease. *Heart Fail Rev* 2017;22:889-902.

(32) Oikonomou EK, Antoniades C. The role of adipose tissue in cardiovascular health and disease. *Nat Rev Cardiol* 2018.

(33) Iacobellis G, Leonetti F, Singh N, Sharma M. Relationship of epicardial adipose tissue with atrial dimensions and diastolic function in morbidly obese subjects. *Int J Cardiol* 2007;115:272-273.

(34) Iacobellis G, Ribaudo MC, Zappaterreno A, Iannucci CV, Leonetti F. Relation between epicardial adipose tissue and left ventricular mass. *Am J Cardiol* 2004;94:1084-1087.

(35) Nyman K, Graner M, Pentikainen MO, Lundbom J, Hakkarainen A, Siren R, Nieminen MS, Taskinen MR, Lundbom N, Lauerma K. Cardiac steatosis and left ventricular function in men with metabolic syndrome. *J Cardiovasc Magn Reson* 2013;15:103.

(36) Ng AC, Delgado V, Bertini M, van der Meer RW, Rijzewijk LJ, Hooi ES, Siebelink HM, Smit JW, Diamant M, Romijn JA, de RA, Leung DY, Lamb HJ, Bax JJ. Myocardial steatosis and biventricular strain and strain rate imaging in patients with type 2 diabetes mellitus. *Circulation* 2010;122:2538-2544.

(37) Zhao L, Harrop DL, Ng ACT, Wang WYS. Epicardial Adipose Tissue Is Associated With Left Atrial Dysfunction in People Without Obstructive Coronary Artery Disease or Atrial Fibrillation. *Can J Cardiol* 2018;34:1019-1025.

(38) Ng AC, Goo SY, Roche N, van der Geest RJ, Wang WY. Epicardial Adipose Tissue Volume and Left Ventricular Myocardial Function Using 3-Dimensional Speckle Tracking Echocardiography. *Can J Cardiol* 2016;32:1485-1492.

(39) Schelbert EB, Messroghli DR. State of the Art: Clinical Applications of Cardiac T1 Mapping. *Radiology* 2016;278:658-676.

(40) Iles L, Pfluger H, Phrommintikul A, Cherayath J, Aksit P, Gupta SN, Kaye DM, Taylor AJ. Evaluation of Diffuse Myocardial Fibrosis in Heart Failure With Cardiac Magnetic Resonance Contrast-Enhanced T1 Mapping. *J Am Coll Cardiol* 2008;52:1574-1580.

(41) Sibley CT, Noureldin RA, Gai N, Nacif MS, Liu S, Turkbey EB, Mudd JO, van der Geest RJ, Lima JA, Halushka MK, Bluemke DA. T1 Mapping in cardiomyopathy at cardiac MR: comparison with endomyocardial biopsy. *Radiology* 2012;265:724-732.

(42) Miller CA, Naish JH, Bishop P, Coutts G, Clark D, Zhao S, Ray SG, Yonan N, Williams SG, Flett AS, Moon JC, Greiser A, Parker GJ, Schmitt M. Comprehensive validation of cardiovascular magnetic resonance techniques for the assessment of myocardial extracellular volume. *Circ Cardiovasc Imaging* 2013;6:373-383.

(43) Pocock SJ, Wang D, Pfeffer MA, Yusuf S, McMurray JJ, Swedberg KB, Ostergren J, Michelson EL, Pieper KS, Granger CB. Predictors of mortality and morbidity in patients with chronic heart failure. *Eur Heart J* 2006;27:65-75.

(44) Hillege HL, Nitsch D, Pfeffer MA, Swedberg K, McMurray JJ, Yusuf S, Granger CB, Michelson EL, Ostergren J, Cornel JH, de ZD, Pocock S, Van Veldhuisen DJ. Renal function as a predictor of outcome in a broad spectrum of patients with heart failure. *Circulation* 2006;113:671-678.

(45) Schou M, Torp-Pedersen C, Gustafsson F, Abdulla J, Kober L. Wall motion index, estimated glomerular filtration rate and mortality risk in patients with heart failure or myocardial infarction: a pooled analysis of 18,010 patients. *Eur J Heart Fail* 2008;10:682-688.

(46) Goodwill AG, Dick GM, Kiel AM, Tune JD. Regulation of Coronary Blood Flow. *Compr Physiol* 2017;7:321-382.

(47) Kalam K, Otahal P, Marwick TH. Prognostic implications of global LV dysfunction: a systematic review and meta-analysis of global longitudinal strain and ejection fraction. *Heart* 2014;100:1673-1680.

(48) Trends in adult body-mass index in 200 countries from 1975 to 2014: a pooled analysis of 1698 population-based measurement studies with 19.2 million participants. *Lancet* 2016;387:1377-1396.

(49) Ng AC, Delgado V, Djaberi R, Schuijf JD, Boogers MJ, Auger D, Bertini M, De Roos A, van der Meer RW, Lamb HJ, Bax JJ. Multimodality imaging in diabetic heart disease. *Curr Probl Cardiol* 2011;36:9-47.

1

Multimodality Imaging in Diabetic Heart Disease

Arnold C.T. Ng, Victoria Delgado, Roxanna Djaberi, Joanne D. Schuijf, Mark J. Boogers, Dominique Auger, Matteo Bertini, Albert de Roos, Rutger W. van der Meer, Hildo J. Lamb, Jeroen J. Bax

Curr Probl Cardiol. 2011;36(1):9-47

ABSTRACT

Diabetic heart disease is currently defined as left ventricular dysfunction that occurs independently of coronary artery disease and hypertension. Its underlying etiology is likely to be multifactorial, acting synergistically together to cause myocardial dysfunction. Multimodality cardiac imaging such as echocardiography, nuclear, computed tomography and magnetic resonance imaging can provide invaluable insight into different aspects of the disease process, from imaging at the cellular level for altered myocardial metabolism to microvascular and endothelial dysfunction, autonomic neuropathy, coronary atherosclerosis, and finally interstitial fibrosis with scar formation. Furthermore, cardiac imaging is pivotal in diagnosing diabetic heart disease. Thus, the aim of the present review is to illustrate the role of multimodality cardiac imaging in elucidating the underlying pathophysiological mechanisms of diabetic heart disease.

INTRODUCTION

Diabetes mellitus is the most common endocrine disease in the world. Recent estimates from the World Health Organization indicate that more than 170 million people worldwide have diabetes, and that number is projected to increase to more than 360 million by the year 2030.[1, 2] Diabetic patients are at an increased risk of developing cardiovascular disease,[3] and can develop heart failure independent of myocardial ischemia.[4] Similarly, the incidence of diabetes is also increased in patients with heart failure.[5, 6] Epidemiological studies have established diabetes as an independent risk factor for developing heart failure, even after correcting for the presence of coronary artery disease.[3, 4, 7] Since it was first described by Rubler et al. more than 3 decades ago,[8] diabetic cardiomyopathy is currently defined as left ventricular (LV) dysfunction that occurs independently of significant coronary artery disease and hypertension.[9] However, the clinical spectrum of diabetes and heart failure is wide, ranging from subclinical disease to overt clinical heart failure. Thus, the term diabetic cardiomyopathy is usually reserved for diabetic patients with overt myocardial dysfunction with signs and symptoms of congestive heart failure.[8] In contrast, diabetic heart disease is a better description for diabetic patients with evidence of subclinical myocardial dysfunction without overt heart failure symptoms.

Various mechanisms underlie the etiology of diabetic heart disease, including processes such as altered myocardial metabolism with subsequent steatosis and lipotoxicity, endothelial dysfunction with microvascular disease, autonomic neuropathy, altered myocardial structure with fibrosis and atherosclerosis.[10] Often, these processes are not mutually exclusive, but act synergistically together and result in myocardial dysfunction. Multimodality imaging such as echocardiography, nuclear imaging, computed tomography (CT) and magnetic resonance imaging (MRI) can all reveal different etiological aspects of diabetic heart disease (Table 1). The present manuscript will illustrate the role of multimodality cardiac imaging in elucidating the pathogenesis of diabetic heart disease, starting from imaging at the cellular level for altered myocardial metabolism to microvascular and endothelial dysfunction, autonomic neuropathy, coronary atherosclerosis, and finally interstitial fibrosis with scar formation. Furthermore, features of myocardial diastolic and systolic dysfunction that are consequent to these pathophysiological processes will also be examined.

Table 1. *Pathogenesis of diabetic heart disease and the applications of multimodality imaging in elucidating the underlying mechanisms*

Altered metabolism
Magnetic resonance spectroscopy
Endothelial dysfunction and microvascular disease
Flow mediated dilatation
Stress echocardiography
Myocardial contrast echocardiography
Nuclear myocardial perfusion imaging
Positron emission tomography
Contrast-enhanced magnetic resonance imaging
Cardiac autonomic dysfunction
123-iodine metaiodobenzylguanidine (^{123}I MIBG) SPECT
Positron emission tomography
Coronary atherosclerosis
Coronary artery calcium scoring
Coronary CT angiography
Myocardial structural changes with fibrosis
Echocardiographic intergrated backscatter
Magnetic resonance imaging

SPECT: single photon emission computed tomography; CT: computed tomography

A) IMAGING THE PATHOGENESIS OF DIABETIC HEART DISEASE

1. Altered metabolism

Increasingly, evidence is emerging that diabetic patients have myocardial functional and structural changes that are independent of coronary artery disease or hypertension.[9-11] Although the mechanisms leading to diabetic heart disease are complex and not fully understood, one of the pathophysiological causes is the excessive fatty acid accumulation within organs such as the heart (known as steatosis), eventually leading to irreversible cellular death through complex mechanisms (also known as lipotoxicity).[12-14]

Under physiological conditions, fatty acids are normally absorbed through the intestines and are mostly stored as triglycerides within adipocytes with minimal accumulation within other tissues such as the heart. However, increased nutritional fatty acid intake and increased lipolysis in diabetes or obesity will lead to increased free fatty acid delivery to non-adipose tissues.[13-15] When the amount of free fatty acids uptake by the heart exceeds its oxidative capacity, excessive fatty acids will be stored as triglycerides within the myocyte cytoplasm. However, part of the fatty acid is redirected into non-oxidative

pathways giving rise to toxic fatty acid intermediates such as ceramide. These toxic fatty acid intermediates disrupt normal cellular signalling and alter myocyte function and structure by complex mechanisms, eventually leading to cellular apoptosis and replacement fibrosis. Thus, it is currently accepted that intracellular triglycerides are probably inert, but are reflective of the increased intracellular concentrations of toxic fatty acid intermediates. At present, myocardial triglycerides can be quantified by using hydrogen 1 magnetic resonance spectroscopy (^{1}H MRS).[16]

Magnetic resonance spectroscopy. Currently, ^{1}H MRS can be performed using MR systems with a high field strength (1.5 Tesla or above). Often, cardiac and respiratory motion triggering are employed to improve the reliability and spectral quality of myocardial ^{1}H MRS by reducing cardiac and respiratory motion artefacts, and reduce the chance of contamination by signals arising from the epicardial fat.[17] A typical myocardial ^{1}H MR spectrum will display signals arising from water, creatine, choline and fat (Figure 1). As the water signal is approximately 100-1000 times that of the fat signal, acquisition of ^{1}H MR spectra both with and without water suppression is essential for reliable quantification of intramyocardial triglyceride content. Using dedicated software, signal amplitudes from the intracellular triglycerides and water are quantified and expressed as triglyceride/water ratio.

Several studies have utilized ^{1}H MRS to relate myocardial triglyceride content and LV function in healthy volunteers, and in obese and diabetic patients.[16, 18-22] It is known that myocardial triglyceride content increases with normal physiological aging, and is inversely correlated with the age-related decline in myocardial function.[21] Similarly, myocardial triglyceride content is increased in obese and diabetic patients.[19, 20, 23] Furthermore, the accumulation of myocardial triglyceride was associated with myocardial dysfunction in these patients. These findings are in agreement with experimental animal studies showing direct toxic effects of fatty acid intermediates on the myocardium.[24, 25]

Several human studies have examined the reversibility of myocardial dysfunction associated with steatosis. Both Hammer et al. and Schrauwen-Hinderling et al. have demonstrated that weight loss was able to partially reverse myocardial triglyceride accumulation in diabetic and obese patients respectively, and this was associated with improvements in LV function.[18, 26] In contrast, there is currently conflicting evidence on the role of medications in reducing intramyocardial triglyceride accumulation.[22, 27] For example, Zib and co-workers demonstrated that pioglitazone (a thiazolidinedione which increases whole-body insulin sensitivity) significantly reduced myocardial and hepatic triglyceride contents, but there were no significant changes in LV mass and ejection fraction (EF).[27] On the other hand, van der Meer and co-workers demonstrated

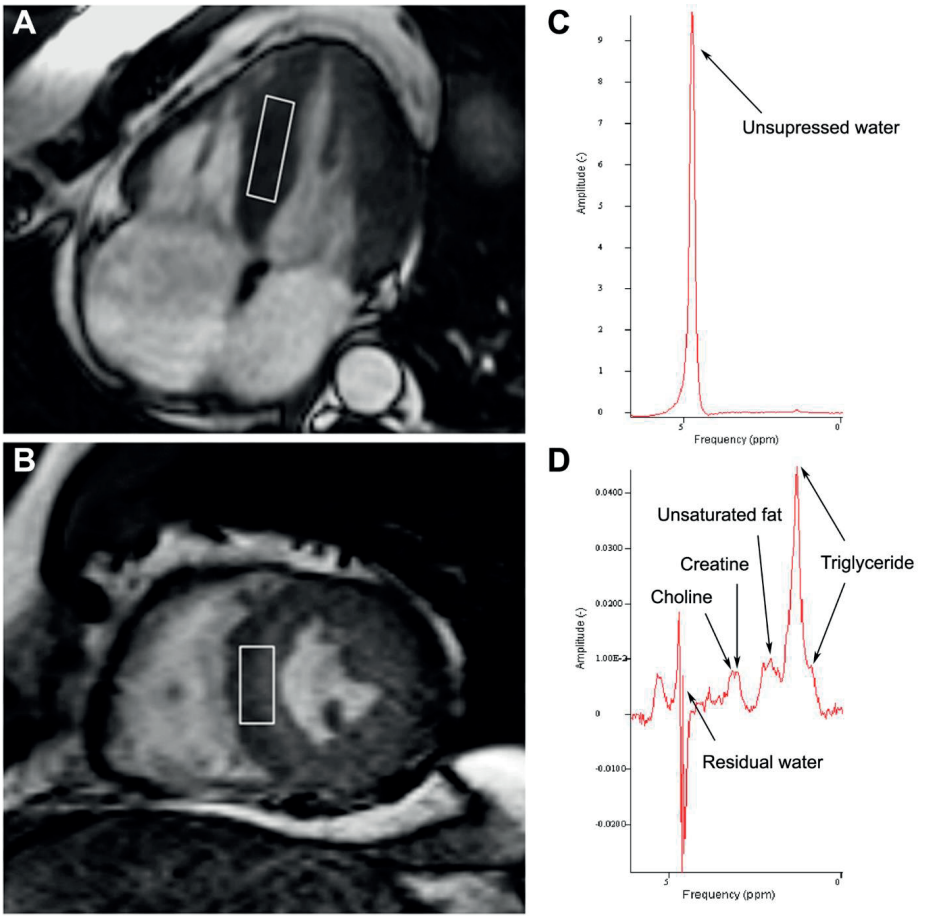


Figure 1. *Examples of image acquisition and spectra from a patient. Panel A and B: 4-chamber and short axis views with the volume of interest placed in the interventricular septum; Panel C: Typical unsuppressed spectrum showing the water peak; Panel D: Typical water-suppressed spectrum showing the various peaks from triglyceride, unsaturated fat, creatine and choline. The amplitudes of the spectra are in arbitrary units, and concentrations of triglyceride are usually expressed as a ratio relative to the peak water amplitude.*

significant improvement in LV diastolic function in diabetic patients treated with pioglitazone, but myocardial triglyceride content remained unchanged.[22] Future studies are clearly needed to further investigate the role of medications in reversing myocardial steatosis. However, as previously noted, intracellular triglycerides are probably inert, and the relationship between myocardial triglyceride accumulation and LV dysfunction likely represents an association rather than a causal relationship. Furthermore, there is currently no evidence to suggest that myocardial triglyceride accumulation will eventually result in clinical heart failure.

2. Endothelial dysfunction and microvascular disease

One of the mechanisms underlying diabetic cardiomyopathy is the presence of endothelial dysfunction and microvascular disease. The normal function of endothelial cells is to maintain vascular homeostasis in order to ensure adequate blood flow and nutrient delivery to tissues while preventing thrombosis and leukocyte diapedesis.[28] This is performed through the competing and opposing synthesis and release of nitric oxide (which causes smooth muscle relaxation and vasodilatation) and vasoconstrictor prostanoids and endothelin (which results in vasoconstriction). Endothelial-derived nitric oxide protects against atherosclerosis by preventing platelet and leukocyte adhesion to the vascular wall, and inhibition of smooth muscle cell proliferation.[29-31] Reduction or loss of endothelial nitric oxide availability results in monocyte and vascular smooth muscle cell migration into the vascular intima layer and the formation of macrophage foam cells, the initial stages of atherosclerosis.[32] In diabetic patients, the associated hyperglycemia, increased circulating free fatty acids levels and insulin resistance lead to increased mitochondrial superoxide generation, reduced endothelial nitric oxide production with reciprocal increase in vasoconstrictor prostanoids and endothelin syntheses. This will eventually result in endothelial dysfunction and atherosclerosis.[32, 33] Furthermore, dysregulation of vascular smooth muscle function is exacerbated by impairments in sympathetic nervous system function, as is often seen in diabetic autonomic neuropathy (see below).[34] Various imaging techniques such as flow mediated dilatation (FMD), stress echocardiography, myocardial contrast echocardiography, nuclear perfusion imaging, positron emission tomography (PET) and contrast-enhanced MRI may be employed to evaluate endothelial function and microvascular disease.

Flow mediated dilation. FMD of the brachial artery provides a non-invasive estimation of systemic endothelial function.[35] In this method, the brachial artery diameter is measured using B-Mode ultrasound or a wall-tracking system, before and after an increase in shear stress that is induced by reactive hyperemia. FMD is thus defined as the percentage change in diameter of the brachial artery and measures the function of endothelium dependent vasodilatation (Figure 2). The observed brachial artery dilatation has been shown to be closely related to coronary endothelial function and vasoreactivity.[36]

FMD has been widely used in research to study the natural course of endothelial function with age and its role in the initiation and progression of vascular disease.[37] For example, FMD ranges from approximately 20% in young adults to 0% in patients with established CAD, while mean FMD values were also reduced (range 0-12%) in diabetic patients.[38] Often, diabetic patients may show evidence of myocardial perfusion defects without a corresponding obstructive epicardial coronary artery disease, suggestive of endothelial dysfunction with microvascular disease.[39] Accordingly, a recent study demonstrated a

significant lower FMD in diabetic patients with perfusion defects compared to those without perfusion defects on single photon emission computed tomography (SPECT) (FMD 3.6 ± 2.4% vs. 6.4 ± 2.6%, p < 0.001), despite the absence of obstructive coronary disease.[40] This observation emphasizes the potential role of endothelial dysfunction and corresponding microvascular disease on myocardial perfusion in diabetic patients.

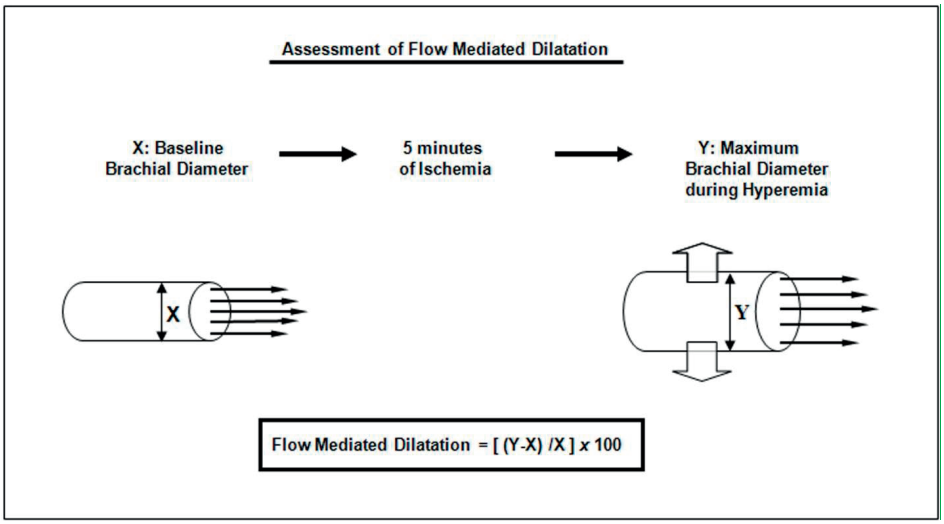


Figure 2. *Assessment of flow mediated dilatation. The brachial artery is visualized distal to the elbow using ultrasonography. Next, ischemia is induced in the forearm distal to the location of the transducer by inflating a blood pressure cuff for 5 minutes at a pressure of at least 200 mmHg. After cuff deflation, ultrasonography is continued for 5 minutes with measurements at approximately 30-second intervals. Widest lumen diameter is used as maximal vasodilation achieved during reactive hyperemia. Flow mediated dilatation is expressed as the percentage change relative to the baseline diameter.*

Detection of microangiopathy by stress echocardiography. Previous echocardiographic studies have also evaluated the relationship between myocardial blood flow and LV systolic and diastolic dysfunction in diabetic patients.[41, 42] Fang et al. evaluated 41 diabetic patients with normal resting LVEF and without coronary artery disease as demonstrated by a normal dobutamine stress echocardiography.[41] Systolic myocardial velocity (Sm) was measured at rest and at peak dobutamine dose with color-coded tissue Doppler imaging. Compared to healthy controls, diabetic patients showed significantly reduced resting Sm (4.2 ± 0.9 cm/s vs. 4.7 ± 0.9 cm/s, p = 0.012). At peak dobutamine dose, Sm increased in diabetic patients and controls reaching comparable values (8.9 ± 1.8 cm/s vs. 9.6 ± 2.1 cm/s, p = not significant).[41] Therefore, this normal response to stress suggested that ischemic etiology might not be a cause for the resting left ventricular systolic dysfunction. These results were later confirmed by another study from the same group using myocardial contrast echocardiography to assess myocardial blood flow.[42]

***Detection of microangiopathy by myocardial contrast echocardiography*.** Echocardiographic microbubble contrast agents are normally used for LV opacification to enhance endocardial border detection, thus improving the accuracies of LV volume quantification and wall motion analyses. In addition, the microbubble contrast agents also permit evaluation of myocardial perfusion and myocardial blood flow.[43] As these microbubble contrast agents have similar microvascular rheology as red blood cells, they stay within the intravascular compartment. Using a low mechanical index during imaging, these microbubbles resonate and appear bright on echocardiography. When a high mechanical index ultrasound pulse is transmitted, the microbubbles are destroyed within the myocardium, thereby reducing the myocardial contrast intensity to nearly zero. The rate of replenishment within the myocardium is thus dependent on the presence of intact microvasculature and myocardial blood flow rate, and the intensity at which the contrast effect plateaus is dependent on myocardial blood volume. Thus, normally perfused myocardium appears as enhanced myocardium, whereas those areas with impaired perfusion appear as dark or patchy areas (Figures 3A and 3B).

In a study by Moir and co-workers who recruited 26 healthy controls and 22 type 2 diabetic patients with normal LVEF and absent coronary artery disease, the relationship between myocardial flow reserve post-stress and myocardial function was explored.[42] Myocardial blood flow and function were quantified by myocardial contrast echocardiography and tissue Doppler strain/strain rate imaging respectively. Compared to controls, resting longitudinal peak systolic strain (-14.4 ± 4.6% vs. -18.7 ± 3.1%, p = 0.006) was significantly lower in diabetic patients, but resting myocardial blood flow was comparable (5.1 ± 3.5 vs. 4.6 ± 3.2, p = 0.62). Post-stress, myocardial blood flow reserve was significantly lower in diabetic patients (2.4 ± 1.0 vs. 3.8 ± 2.1, p = 0.01). However, there was no correlation between myocardial blood flow reserve and resting myocardial function (Figure 3C). Thus, the authors concluded that although subclinical myocardial dysfunction and microvascular disease may coexist, it may not be the sole causative factor in diabetic heart disease.

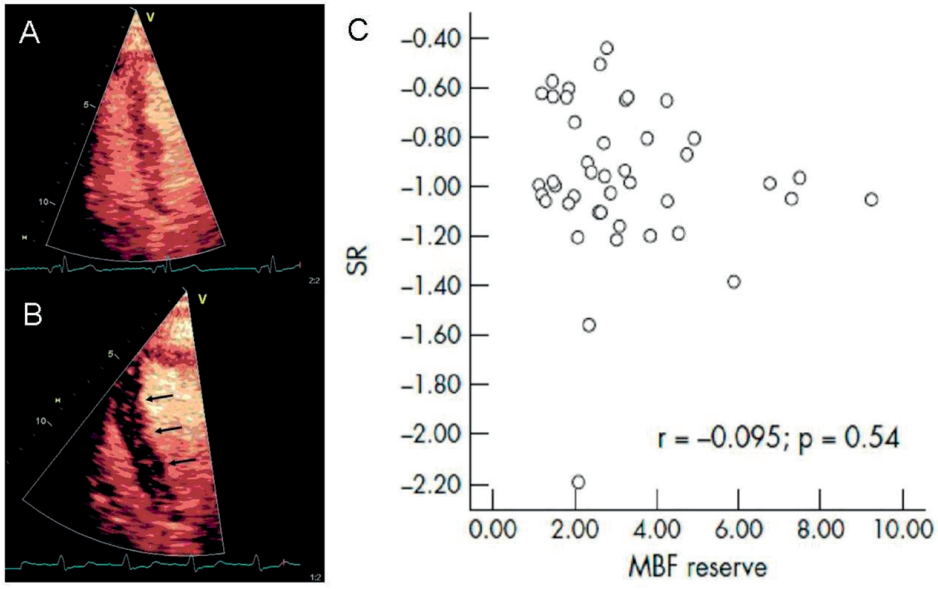


Figure 3. *Examples of myocardial contrast echocardiography assessing myocardial blood flow. After a high mechanical index ultrasound pulse, the microbubbles are initially destroyed before returning to reperfuse the myocardium. Areas with normal myocardial blood flow show a homogeneous replenishment of the myocardium (panel A). In contrast, areas with impaired perfusion appear as dark patchy, non-replenished areas (arrows, panel B). In diabetic cardiomyopathy, myocardial blood flow reserve post-stress did not correlated with resting myocardial function as assessed by tissue Doppler strain rate imaging (panel C).*
SR: strain rate; MBF: myocardial blood flow. Adapted with permission from Moir et al. Heart 2006;92:1414–1419.

Nuclear myocardial perfusion imaging. Myocardial perfusion imaging by thallium-201 or technetium-99m sestamibi SPECT is a widely used and validated non-invasive tool for the diagnosis of myocardial ischemia. ECG-gated SPECT allows both quantitative evaluation of cardiac function and myocardial perfusion to detect ischemia during exercise testing or pharmacological stress with adenosine, dipyridamole or dobutamine (Figure 4).[44] The presence of myocardial perfusion defects during stress is due to heterogeneous flow distribution as a result of two potential mechanisms: obstructive epicardial coronary artery disease due to atherosclerosis and subsequently reduced flow during stress;[45] or insufficient vasomotor response in the coronary microvasculature due to endothelial dysfunction resulting in relative hypoperfusion during stress.[46]

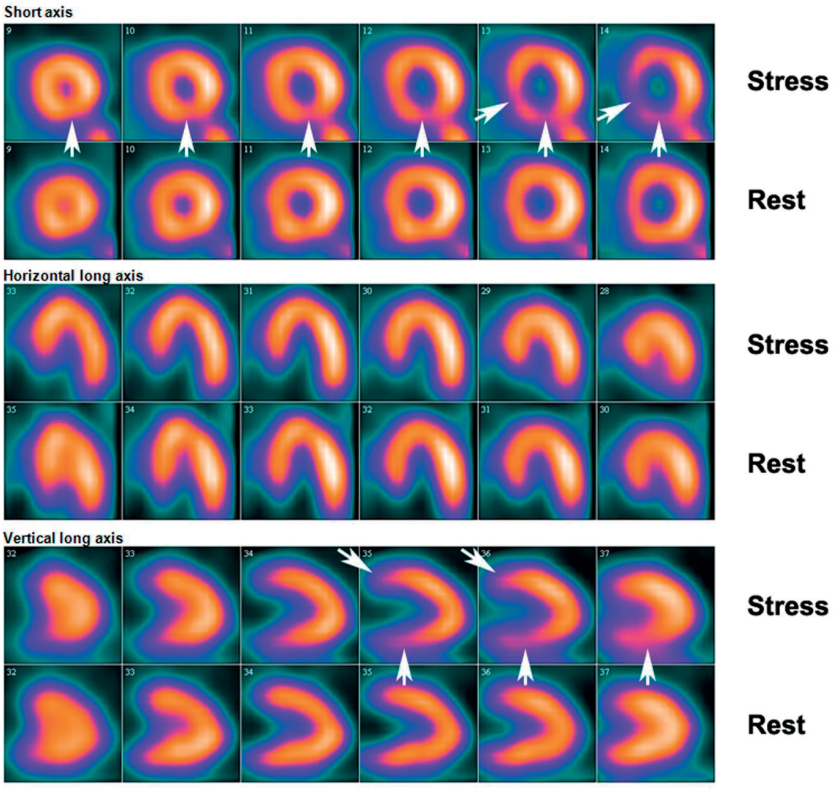


Figure 4. *Myocardial perfusion using gated SPECT at rest and after adenosine stress. Resting images and stress images in the short axis, horizontal and vertical long axes are depicted. In the current example, no persistent perfusion defects were observed. Reversible perfusion defects were observed in the inferior, inferoseptal, anterior and anteroseptal regions (arrows).*

The prevalence of myocardial perfusion defects as assessed by SPECT myocardial perfusion imaging in asymptomatic diabetic patients ranges from 20 – 40% in several prospective studies,[47-49] and the prognostic value of SPECT myocardial perfusion imaging in diabetic patients has been confirmed in several previous studies.[48-50] For example, in a large cohort of 1271 diabetic patients, Kang et al. described a favorable cardiovascular prognosis in patients with a normal myocardial perfusion SPECT study (coronary event rates 1-2% per year), which increases to 3 – 4% per year in patients with mild perfusion defects, to > 7% per year for patients with moderate to severe perfusion defects. The incremental cardiovascular predictive value of SPECT in diabetic patients has been attributed to both the direct detection of underlying obstructive epicardial coronary disease, and its ability to reflect on endothelial dysfunction within the coronary microvasculature.[51]

It has been previously shown that coronary endothelial dysfunction is a precursor to overt atherosclerosis and is reversible to a certain extent, such as with statin therapies.[52, 53] Accordingly, in the Detection of Ischemia in Asymptomatic Diabetics (DIAD) study, inducible myocardial ischemia at baseline was shown to resolve in up to 79% of asymptomatic patients with diabetes at 3 years follow-up.[54] This resolution was suggested by the authors to be secondary to improvements in endothelial dysfunction and stabilization of atherosclerotic plaques as a result of treatment with statins, aspirin and angiotensin-converting enzyme inhibitors.

Positron emission tomography. Although SPECT imaging is routinely used in the clinical setting, image quality may be suboptimal in obese and female diabetic patients due to attenuation artifacts. As such, assessment of myocardial perfusion by PET may be a good alternative in situations where SPECT imaging quality is suboptimal.[55] Myocardial perfusion imaging by PET uses high energy gamma photons produced by positron-emitting radionuclides, and has superior spatial resolution compared to conventional SPECT.[56] By combining readily available attenuation correction algorithms for photon attenuation, scatter and random events, PET imaging can provide a truly quantitative measure of myocardial blood flow (in ml/min/g) and coronary flow reserve in absolute terms.[57-59] Thus far, this technique has been applied in research to examine coronary microvascular reactivity in various study populations.[60-64] Several studies have demonstrated dysregulation of myocardial microvascular reactivity in diabetic patients.[62-64] For example, Kjaer and co-workers demonstrated endothelial dysfunction using ^{13}N-ammonia PET imaging in type 2 diabetic patients without evidence of epicardial coronary disease compared to normal controls.[62] Similarly, Prior and co-workers demonstrated a significantly lower total vasodilator capacity in normotensive diabetic (-17%) and hypertensive diabetic (-34%) patients compared to insulin sensitive individuals.[64]

Magnetic resonance perfusion imaging. In MRI, myocardial perfusion imaging relies on the injection of a gadolinium-based paramagnetic contrast agent which alters the relaxation properties of the proton nuclei in its vicinity. The subsequent transit of the contrast agent through the cardiovascular system and into the myocardium can be detected using pulse sequences which focus on T_1 weighted images (Figure 5). Thus, using dipyridamole as a pharmacological stressor, magnetic resonance perfusion imaging allows non-invasive quantification of myocardial perfusion during baseline conditions and during maximal hyperemia.

There are currently a limited number of studies that have assessed MRI myocardial perfusion imaging in diabetic patients. In a small study by Taskiran et al., 19 type 1 diabetic patients were compared against 10 healthy controls.[65] All the diabetic patients had no

major microvascular disease, and were divided into the presence or absence of autonomic neuropathy. After induction of maximal hyperemia by dipyridamole, myocardial perfusion index was significantly lower in diabetic patients with autonomic neuropathy compared to those without neuropathy or normal controls ($p < 0.001$). Thus, altered myocardial perfusion associated with autonomic neuropathy may be a potential pathophysiological mechanism underlying the increased mortality observed in diabetic patients.

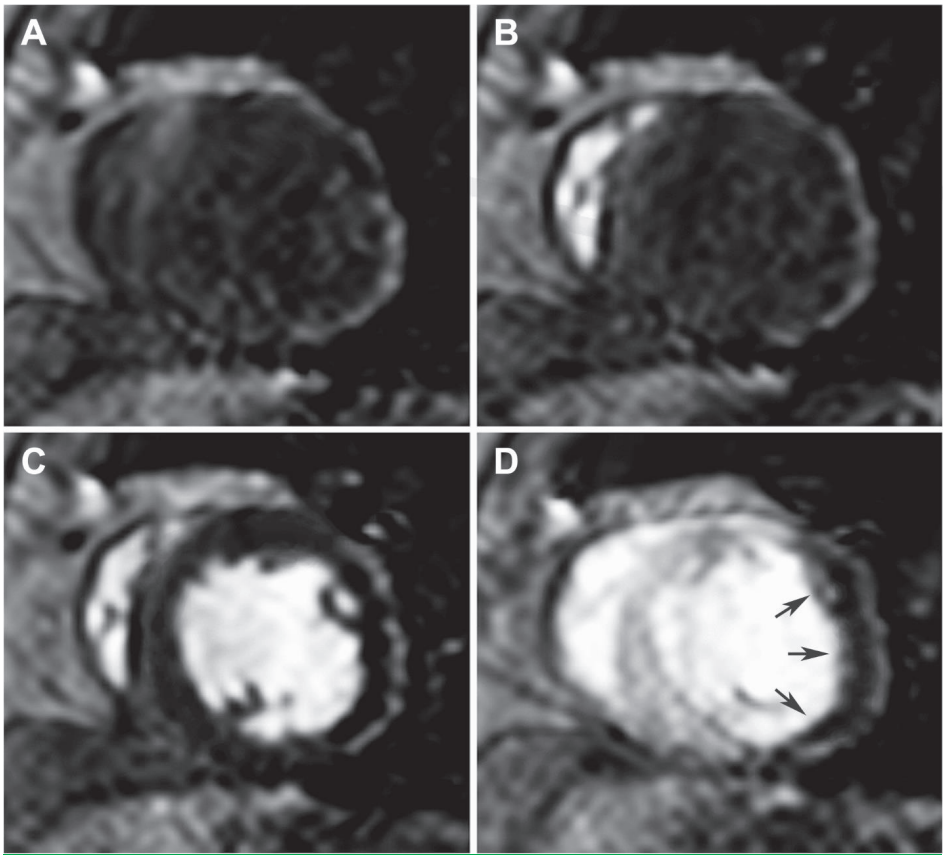


Figure 5. *Example of myocardial perfusion imaging by magnetic resonance imaging during the first pass of an intravenously injected contrast bolus. Prior to contrast injection, the blood pool, right and left ventricular myocardium are dark (Panel A). Following contrast injection, contrast enhancement is then first observed in the right ventricular cavity (Panel B), followed by the left ventricular cavity (Panel C), and finally followed by enhancement of the myocardium (Panel D). The present patient had a large perfusion defect in the postero-lateral wall (arrows).*

3. Cardiac autonomic dysfunction

Diabetic neuropathies are a heterogeneous group of diabetic complications that affects different parts of peripheral nervous system. Its pathophysiology is likely to be multifactorial, involving alterations in metabolism, micro- and macrovascular dysfunction, deficiency of neurohormonal growth factor and autoimmune nerve damage.[66] Although diabetic autonomic neuropathy can affect every system in the body, cardiac autonomic neuropathy (CAN) is particularly associated with an increased risk of silent myocardial infarction and sudden cardiac death, thus contributing to significant cardiovascular morbidity and mortality.[67] The prevalence of CAN in type 2 diabetic patients is estimated to be around 20 – 30% of patients.[68] Clinical manifestations of CAN include the presence of resting tachycardia (heart rate > 100 beats/min), postural hypotension (fall in systolic blood pressure > 20mmHg or diastolic blood pressure > 10mmHg upon standing) without an appropriate reflex increase in heart rate, exercise intolerance due to blunting of cardiac output in response to exercise, or silent myocardial infarction.[69, 70]

The presence of CAN conveys a poor clinical outcome. Previous meta-analysis by Vinik and co-workers assessed the prognostic value of CAN in diabetic patients.[70] Using the pooled analyses from 12 studies involving a total of 1486 study subjects, they estimated that the pooled prevalence rate risk for silent myocardial infarction in diabetic patients was 1.96 (95% confidence interval 1.53 – 2.51, $p < 0.001$).[70] In the same review, the pooled estimate of the relative risk for mortality, based on 15 studies with 2900 patients, was 2.14 (95% confidence interval 1.83 – 2.51, $p < 0.0001$) for diabetic patients with CAN. Thus, it was estimated that the 5 year mortality rate is 5 times higher in diabetic patients with CAN compared to patients without evidence of CAN.[69, 70] Therefore, early diagnosis and recognition of CAN is crucial as it may impact on the clinical decision making of these patients.

Diagnosis of CAN involves assessment of both parasympathetic and sympathetic nervous system using a range of different tests. Assessment of parasympathetic nervous system includes the resting heart rate, beat-to-beat variation with deep breathing (E:I ratio), 30:15 heart rate ratio with standing, Valsalva ratio, and spectral analysis of heart rate variation.[69] Assessment of sympathetic nervous system includes the resting heart rate, spectral analysis of heart rate variation, postural blood pressure, hand grip blood pressure, cold pressor response, sympathetic skin galvanic response, sudorometry, and cutaneous blood flow.[69] However, all these tests are indirect assessments of the autonomic nervous system and are less sensitive than direct assessments by cardiac radionuclide imaging with SPECT or PET.[71, 72]

Currently, SPECT and PET imaging are available for the assessment of cardiac sympathetic adrenergic innervation and activation.[72-74] Essentially, adrenergic nerve imaging is based on two principles; synthesis of false neurotransmitters (catecholamine analogs) or the labeling of true adrenergic neurotransmitters. Both techniques allow evaluation of abnormalities in cardiac sympathetic innervation by visualizing the uptake and storage of radiolabeled neurotransmitters transported into the presynaptic nerve terminals.

123-iodine metaiodobenzylguanidine (^{123}I MIBG) SPECT. Abnormalities in sympathetic innervation can be assessed using 123-iodine metaiodobenzylguanidine (^{123}I MIBG), a norepinephrine analog that is taken up and accumulated in the presynaptic nerve terminals.[68, 75, 76] Currently, ^{123}I MIBG represents the most commonly used tracer in clinical cardiology to evaluate cardiac sympathetic innervation patterns.[76] Planar and tomographic SPECT images are acquired 10-20 minutes (early) or 3-4 hours (late) after MIBG administration. From the planar images, semi-quantitative measurements such as heart-to-mediastinum (H/M) ratio and cardiac washout rate are used to evaluate global sympathetic innervation. SPECT images are used to assess regional abnormalities in sympathetic innervation as depicted in Figure 6. At present, several studies using ^{123}I MIBG imaging have demonstrated the presence of global and regional abnormalities in sympathetic innervation in diabetic patients.[68, 75, 77] Turpeinen and co-workers performed ^{123}I MIBG scintigraphy to evaluate regional abnormalities in sympathetic innervation pattern in 7 type 1 and 13 type 2 diabetic patients.[77] Type 2 diabetic patients showed reduced ^{123}I MIBG uptake in the inferoposterior segments compared to type 1 diabetic patients. However, conventional indirect measures of autonomic function by power spectral analysis of heart rate variability failed to detect any differences between the 2 groups.

Nagamachi and co-workers subsequently evaluated the prognostic value of cardiac MIBG imaging by retrospectively evaluating 144 type 2 diabetic patients for the occurrence of cardiac events (arrhythmia, heart failure or acute myocardial infarction), and all-cause mortality.[68] After a mean follow-up period of 7.2 ± 3.2 years, 17 (11.8%) patients experienced a cardiac event, of which 7 died. An additional 9 patients died due to non-cardiac causes. On multivariate analysis, the presence of CAN (relative risk 6.75, 95% confidence interval 1.16 – 39.3, p = 0.03) was an independent predictor of cardiac events on follow-up. Similarly, the presence of CAN (relative risk 17.1, 95% confidence interval 1.07 – 27.9, p = 0.04) and a reduced H/M ratio on delayed ^{123}I MIBG imaging (relative risk 6.0, 95% confidence interval 1.18 – 30.6, p = 0.04) were independent predictors of all-cause mortality.

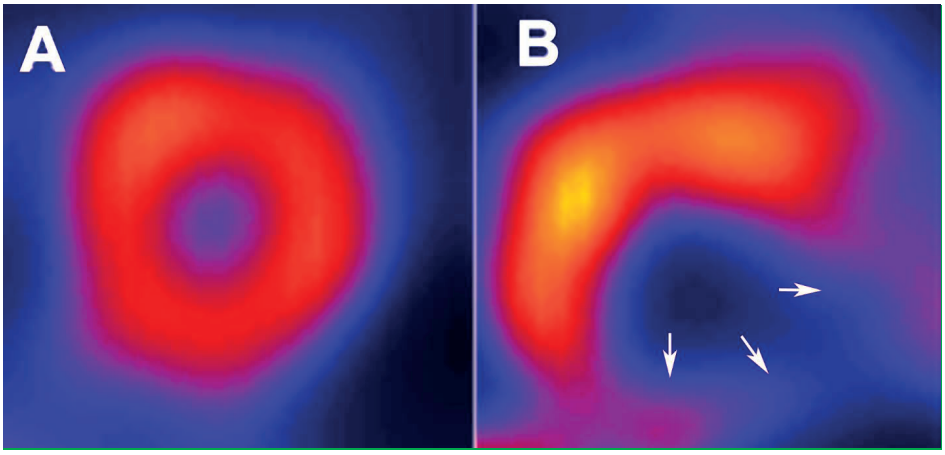


Figure 6. *Sympathetic innervation as assessed with ^{123}I MIBG SPECT imaging. Panel A: Example of a patient with normal sympathetic innervation on ^{123}I MIBG SPECT imaging. Panel B: Example of a patient with regional abnormalities as assessed with ^{123}I MIBG SPECT imaging (arrows).*

Positron emission tomography. PET imaging is the only technique that permits absolute quantification of myocardial sympathetic innervation pattern. Using carbon-11 metahydroxyephedrine (^{11}C HED) in PET imaging has the advantage of accurately detecting regional abnormalities in sympathetic innervation. Stevens and co-workers evaluated regional abnormalities in cardiac sympathetic innervation with ^{11}C HED PET imaging in 29 diabetic patients and compared to 10 healthy subjects.[72] The diabetic patients were categorized into the presence of mild or severe diabetic autonomic neuropathy. Using the absolute difference in tracer uptake of the myocardium, the extent of regional sympathetic denervation was expressed as the percentage of the LV in all subjects with diabetes. The study showed that the extent of regional sympathetic denervation was significantly larger in patients with severe autonomic neuropathy as compared to patients with mild autonomic neuropathy (48 ± 19% vs. 6 ± 5%, $p < 0.01$). Furthermore, there was evidence of sympathetic dysinnervation with increased innervation in the basal myocardial segments but decreased innervation in the apical myocardial segments (Figure 7). Thus, this observed regional myocardial variation in sympathetic innervation and could contribute to myocardial electrical instability and potentially life-threatening arrhythmias.

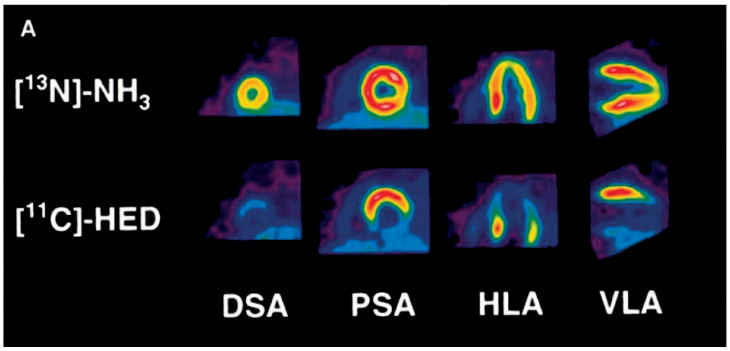


Figure 7. *PET imaging of a patient with severe diabetic autonomic neuropathy. Top row: short and long axis images of the left ventricle showing normal blood flow as indicated by homogenous ^{13}N NH_3 tracer uptake. Bottom row: extensive abnormalities in ^{11}C HED PET imaging. The basal myocardial segments showed excessively high ^{11}C HED retention suggestive of increased innervation, whereas there was decreased innervation in the apical myocardial segments as demonstrated by absent tracer uptake. Adapted with permission from Stevens et al., J Am Coll Cardiol 1998;31:1575-1584.*

4. Coronary atherosclerosis

As previously alluded to, the presence of microvascular disease and endothelial dysfunction in diabetic patients are often the precursors of vascular atherosclerosis. Although the presence of significant coronary stenosis will result in myocardial dysfunction and is thus strictly not considered as "diabetic heart disease", its prevalence in diabetic patients is higher than non-diabetics, and is associated with significant cardiovascular morbidity and mortality.[78] Furthermore, the presence of coronary atherosclerosis without significant luminal narrowing may not be entirely benign.[79] Indeed, previous studies have demonstrated that myocardial infarction and unstable angina are frequently caused by coronary lesions deemed to be non-significant prior to the event.[80, 81] Thus, it may be useful to identify and risk-stratify patients into normal coronary arteries without atherosclerosis, non-significant coronary artery disease, and significant coronary artery disease. At present, computed tomography (CT) techniques such as coronary artery calcium (CAC) scoring and coronary CT angiography (CTA) are considered the most robust imaging techniques for non-invasive visualization of coronary atherosclerosis.

Coronary artery calcium scoring. CAC score can characterize the location and burden of coronary atherosclerosis by detecting calcium present within atherosclerotic plaques. Image acquisition for CAC scoring typically involves acquiring multiple, non-contrast, thick slice images of the entire heart. Using a cut-off value of greater than 130 Hounsfield units to define calcium, coronary calcifications can be identified as bright white structures on the CT images (Figure 8).

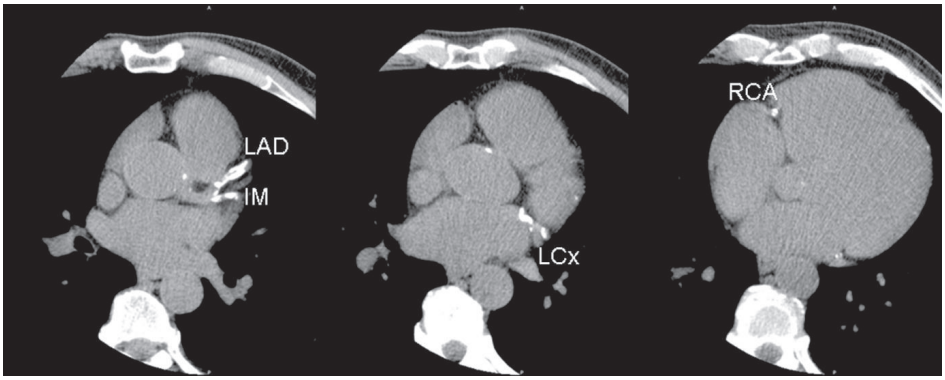


Figure 8. *Example of a diabetic patient with extensive coronary calcification in all 3 coronary arteries. Total coronary calcium score was 1599. IM: intermediate branch; LAD: left anterior descending coronary artery; LCx: left circumflex artery; RCA: right coronary artery.*

Semi-quantification of coronary calcium is commonly expressed by the Agatston score, which uses the plaque size, density and a weighting factor to calculate a value ranging from 0 (absence of detectable calcium) to over 1000 (indicating the presence of extensive coronary calcifications). Importantly, there is a clear relationship between the CAC score and the extent of coronary atherosclerosis, as well as the presence of significant coronary stenosis.[82] However, the association between CAC score and extent of coronary atherosclerosis is not linear as severe coronary stenosis can occur at sites with limited calcium deposition. Likewise, extensive CAC scores can be observed in the absence of significant luminal narrowing. Thus, rather than being a diagnostic test for obstructive CAD, CAC scoring may be more valuable as a risk stratification tool to identify at-risk patients with underlying atherosclerosis who might benefit from further investigations.

In the general population, CAC scoring has indeed been shown to provide strong prognostic information. An elevated CAC score has consistently been associated with increased mortality and adverse cardiovascular events, independently of coronary risk factors.[83] Similar findings have been observed in diabetic patients.[84] In one of the largest series to date, Raggi et al. compared baseline CAC scores and outcomes among 9474 non-diabetic and 903 diabetic patients.[84] During a mean follow-up period of 5 years, CAC score was identified as the best predictor of all-cause mortality in both diabetic and non-diabetic individuals (Figure 9).

Moreover, further analysis revealed that for each level of CAC score, mortality was higher in diabetic patients compared to non-diabetics. Thus, CAC scoring may be a promising tool in identifying diabetic patients with increased likelihood of coronary events who might benefit from further functional evaluation and more aggressive, individually targeted preventive treatment strategies. Indeed, Anand and co-workers recently

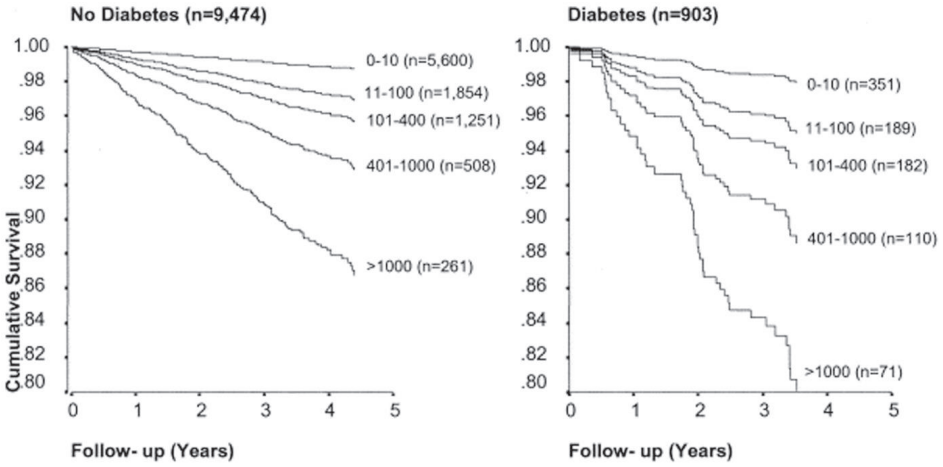


Figure 9. *Cox proportional hazards survival demonstrating significantly lower survival with increasing coronary artery calcium scores by electron beam computed tomography. Comparison of survival curves show that diabetic patients have significantly lower survival with each coronary artery calcium score category compared to non-diabetic patients. Adapted with permission from Raggi et al. J Am Coll Cardiol 2004;43:1663-1669.*

demonstrated in 510 asymptomatic type 2 diabetic patients that while the incidence of ischemia was low in patients with no or limited CAC, the likelihood of ischemia increases with higher CAC scores (Figure 10).[85]

Coronary CT angiography. More detailed information on the coronary anatomy can be derived from non-invasive contrast-enhanced coronary CTA which permits direct visualization of the coronary arteries (Figure 11). Particularly with the newer generations of multi-detector row CT scanners (64-slice and higher), high sensitivities and specificities can be obtained for the detection of significant coronary stenoses. Importantly, this high diagnostic accuracy has been shown to be maintained in the presence of diabetes.[86, 87] The advantage of this technique is the high negative predictive value which approaches 100%. Notably, coronary CTA is also unlikely to miss severe coronary artery diseases such as left main or three-vessel diseases. Moreover, this technique allows identification of coronary atherosclerotic plaques in the absence of calcium or stenosis, thus permitting visualization of early, subclinical atherosclerotic disease. To a limited extent, information on plaque composition can also be derived, although it is less precise and detailed as compared to invasive techniques such as intravascular ultrasound (IVUS) or optical coherence tomography.

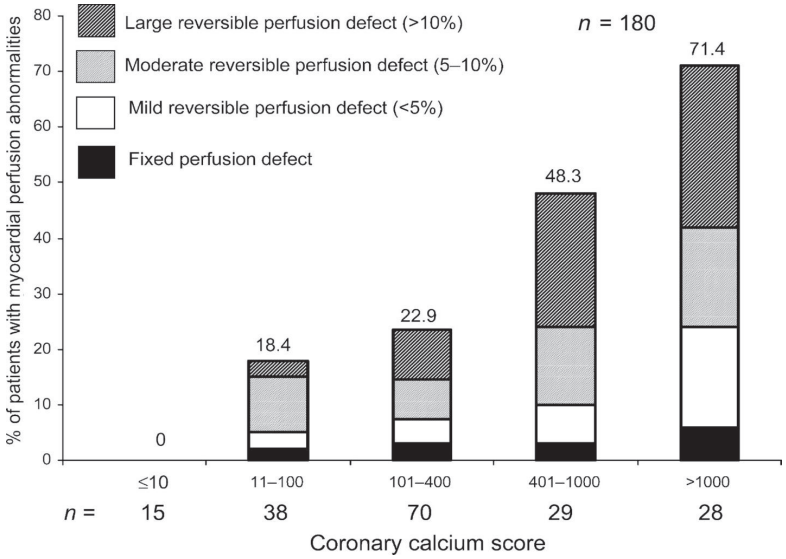


Figure 10. *Relationship between the extent of coronary calcification and the prevalence/severity of myocardial perfusion abnormality. Increasing coronary artery calcium score was associated with both an increased incidence of perfusion abnormalities, and larger perfusion defects. Adapted with permission from Anand et al. Eur Heart J 2006;27:713-721.*

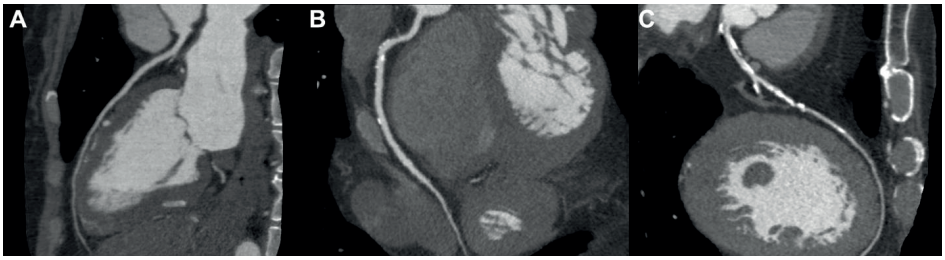


Figure 11. *Evaluation of coronary artery disease with coronary CT angiography in patients with type 2 diabetes. Panel A: curved multiplanar reformation (cMPR) of the left anterior descending coronary artery without any evidence of atherosclerosis. Panel B: cMPR of the right coronary artery revealing diffuse atherosclerosis in the absence of significant stenosis. Panel C: cMPR of the left anterior descending coronary artery revealing extensive atherosclerosis with multiple significant (> 50% luminal narrowing) lesions.*

Using coronary CTA, Pundziute et al. recently demonstrated that diabetic patients have more extensive, diffuse coronary atherosclerosis compared to matched non-diabetic patients.[88] Interestingly, this increased plaque burden was mainly attributable to an increased number of non-obstructive lesions, while the incidence of significant stenosis was similar amongst both populations. In a smaller population, these observations were later confirmed by the same group using MSCT and invasive plaque imaging with grey-scale and virtual histology IVUS (VH IVUS) (Figure 12).[89]

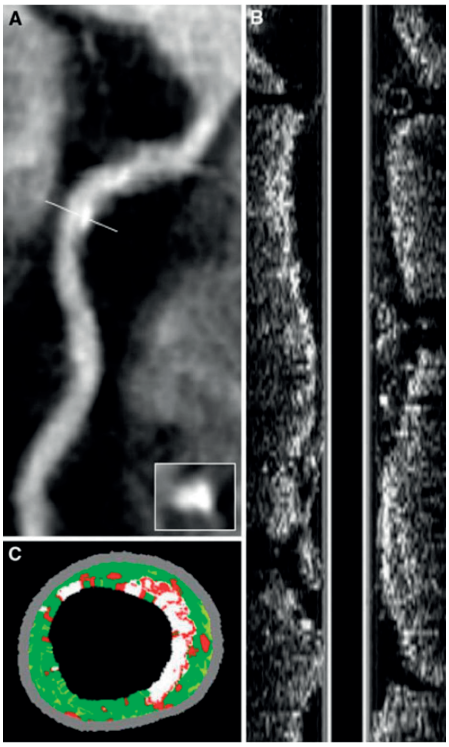


Figure 12. *Example of coronary atherosclerosis in a type 2 diabetic patient as demonstrated by coronary CTA (Panel A), gray-scale intravascular ultrasound (IVUS, Panel B), and virtual histology IVUS (VH IVUS, Panel C). Panel A: Curved multiplanar reformation of the right coronary artery by CTA demonstrated diffuse atherosclerosis along the course of the artery, and a mixed plaque was observed in the proximal part of the artery in both longitudinal and transverse images. Panel B: The presence of diffuse atherosclerosis was confirmed in longitudinally reconstructed IVUS image. Panel C: Corresponding VH IVUS image at the minimal luminal area site of the atherosclerotic plaque, demonstrating the features of a fibrocalcific plaque. Fibrous areas were marked in green, fibro-fatty in yellow, calcium in white and necrotic core in red. Adapted with permission from Pundziute et al., J Nucl Cardiol 2009;16:376-383.*

Diabetic patients had significantly higher plaque burden and more calcified lesions than non-diabetics.[89] In another study composed of 80 asymptomatic type 2 diabetic patients, Ambrose and co-workers compared CAC scoring and CTA and demonstrated that CTA may reveal substantial plaque burden even in patients with zero or low CAC scores (Figure 13).[90] Thus, coronary CTA may be more accurate in evaluating the presence and extent of coronary atherosclerosis in diabetic patients compared to CAC scoring. Preliminary results suggest that CTA has an incremental prognostic information over baseline clinical variables in both diabetic and non-diabetic patients.[91]

5. Myocardial structural changes with fibrosis

Although the etiology of diabetic heart disease is multifactorial, the final common pathway is accelerated myocyte apoptosis, formation of advanced glycation end-products, and development of interstitial fibrosis.[92-94] Several animal and human studies have demonstrated increased interstitial fibrosis in diabetic patients.[92-94] These structural changes lead to increased LV stiffness, impaired systolic and diastolic function, and ultimately the development of clinical heart failure. As such, both echocardiography and MRI can be used to detect and quantify myocardial fibrosis.

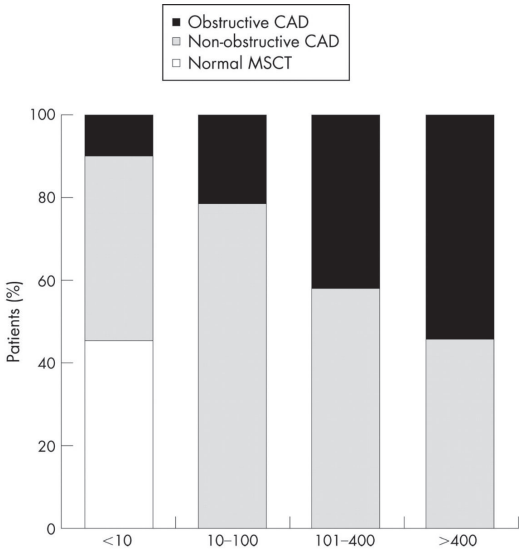


Figure 13. *Bar graph demonstrating the distribution of both obstructive and non-obstructive coronary artery disease per coronary artery calcium score category in asymptomatic type 2 diabetic patients. Diabetic patients can have significant plaque burden despite zero or low (< 10) calcium score. Adapted with permission from Scholte et al. Heart 2008;94:290-295.*

Echocardiographic integrated backscatter. Integrated backscatter analysis using 2-dimensional echocardiography has been used to non-invasively evaluate myocardial fibrosis.[95] The increased deposition of collagen alters the ultrasound reflectivity (backscattering) of the myocardial tissue and previous study has demonstrated a linear correlation between the myocardial backscatter magnitude and the amount of fibrosis content on histology.[95] The measurement of myocardial integrated backscatter is usually performed in the parasternal long-axis view by placing a region of interest in the interventricular septum and the posterior wall (Figure 14). The value of myocardial integrated backscatter obtained at end-diastole is corrected by the integrated backscatter value of the pericardium, thereby providing the calibrated integrated backscatter value.

In diabetic patients without hypertension or coronary artery disease, the myocardial ultrasound reflectivity is significantly increased compared to healthy age matched controls, suggesting the presence of increased myocardial fibrosis.[96] This observation was later confirmed by Fang and co-workers, who included 48 diabetic patients without coronary artery disease and normal LVEF, 45 diabetic patients with left ventricular hypertrophy, 45 patients with only left ventricular hypertrophy and 48 normal controls.[97] Calibrated integrated backscatter at the interventricular septum and posterior wall were significantly higher in the three groups of patients as compared to controls. Furthermore, diabetic patients with concomitant LV hypertrophy had the highest calibrated integrated

backscatter value (Figure 14). Similar trends were observed in the LV myocardial function as determined by tissue Doppler-derived strain analyses. Therefore, the presence of subclinical myocardial dysfunction in diabetic heart disease is associated with the presence of increased myocardial fibrosis. This observation of increased myocardial fibrosis was in concordance with histological studies of diabetic hearts without significant coronary disease that showed increased collagen deposition in the perivascular and interstitial regions.[94, 98, 99]

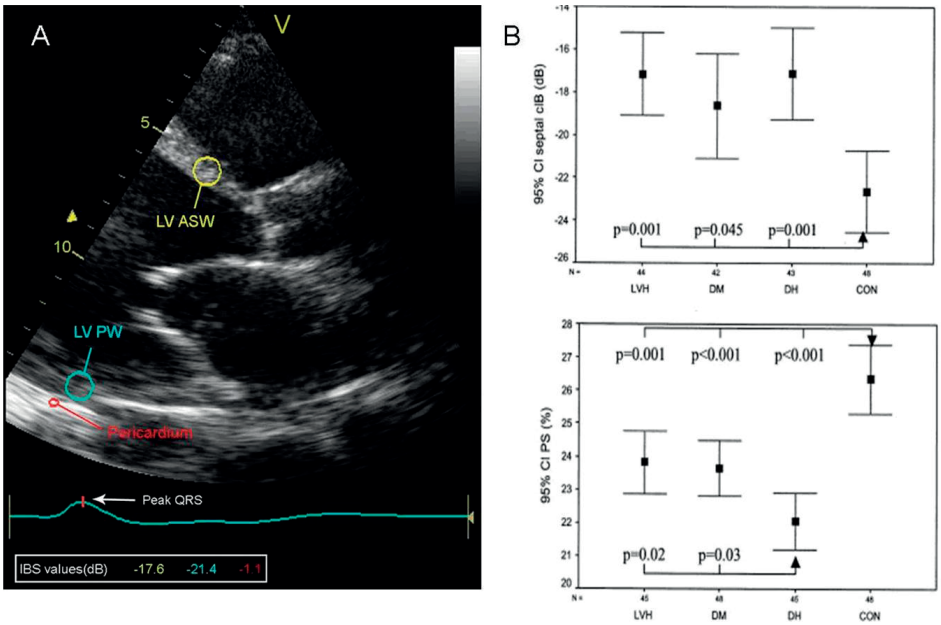


Figure 14. *Evaluation of myocardial fibrosis with integrated backscatter. From LV parasternal long-axis view (panel A), the ultrasound reflectivity or integrated backscatter of the myocardium is measured at the interventricular septum and posterior wall, and corrected for the pericardial integrated backscatter value. Compared to normal controls, diabetic patients and non-diabetic patients with LV hypertrophy had significantly lower longitudinal peak strain and higher myocardial integrated backscatter value. However, diabetic patients with LV hypertrophy had the highest myocardial integrated backscatter with the lowest longitudinal peak strain. PS: cIB: calibrated integrated backscatter; CON: control; DH: diabetic patients with left ventricular hypertrophy; DM: diabetic patients; LVH: patients with left ventricular hypertrophy; PS: peak strain. Adapted with permission from Fang et al. J Am Coll Cardiol 2003;41:611–7.*

Magnetic resonance imaging. Currently, MRI with delayed contrast enhancement (DCE) is the gold standard for non-invasive visualization of myocardial scar tissue. This technique is based on an inversion recovery pulse sequence and delayed imaging of the heart at approximately 10 – 20 minutes after administration of gadolinium-based contrast agents. Due to the chemical charge and molecular size of these gadolinium-based contrast agents, they rapidly diffuse from the intravascular to extracellular space, but do

not enter the intracellular space. Consequently, contrast accumulates within infarcted or scarred myocardial tissues. By selecting an appropriate inversion time to "null" normal myocardium, scar tissue will appear as bright hyperenhanced regions (Figure 15). The ability of MRI DCE to accurately depict scar tissue has been previously validated.[100] In the seminal paper by Kim et al., ex-vivo DCE images were displayed next to histopathological specimens of infarcted myocardial tissues, providing compelling evidence that the extent of delayed enhancement on MRI corresponded to histopathological infarct size.[100]

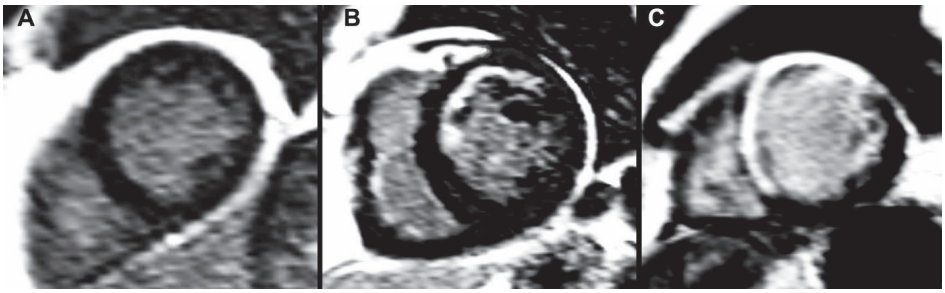


Figure 15. *Examples of MRI delayed contrast-enhanced images. Panel A: normal study without evidence of delayed enhancement. Note that the normal myocardium appears black due to nulling by the inversion recovery pulse sequence. Panel B: non-transmural scarring in the anteroseptal and anterior segments appearing as white hyperenhanced regions indicative of previous subendocardial infarction in the left anterior descending artery territory. Panel C: transmural scarring in the septal, anteroseptal and anterior walls.*

Kwong and co-workers demonstrated the prognostic value of identifying DCE in a cohort of 107 diabetic patients without previous clinical history of myocardial infarction.[101] The presence of DCE, indicative of silent myocardial infarction, was associated with significantly higher all-cause mortality compared to diabetic patients without DCE (log rank $p = 0.02$). On multivariate analysis, the presence of DCE was the strongest independent predictor of major adverse cardiac outcomes (combination all-cause mortality, new acute myocardial infarction, hospitalization for unstable angina or heart failure, ventricular arrhythmias requiring implantable cardiac defibrillators, and acute cerebrovascular accidents) and all-cause mortality.

B) IMAGING LEFT VENTRICULAR MYOCARDIAL DYSFUNCTION IN DIABETIC HEART DISEASE

Although the etiology of diabetic heart disease is diverse and a source of on-going research, patients eventually develop evidence of increased myocardial fibrosis.[102] These structural changes result in increased LV stiffness and impairment of diastolic and systolic performance. Although it is not a prerequisite for patients to have preexisting diabetic heart disease in order to develop heart failure, the presence of diabetic heart

disease increases the risk for subsequent development of heart failure. Thus, early detection of diabetic heart disease may permit early treatment and prevention of heart failure progression.

Currently, diagnosis of diabetic heart disease requires the demonstration of myocardial dysfunction that is independent of other causes such as significant coronary stenosis or hypertension. Thus, in diabetic patients with overt heart failure symptoms, the presence of echocardiographic features of LV dysfunction without other explanatory causes is often confirmatory for the diagnosis of diabetic cardiomyopathy. However, non-invasive imaging is usually required for the diagnosis of diabetic heart disease in patients without clinical signs and symptoms of heart failure. Often, echocardiography is utilized to demonstrate LV diastolic and systolic dysfunction in diabetic heart disease.

1. Diastolic function

Traditionally, LV diastolic function is categorized into normal, impaired relaxation, pseudonormal and restrictive filling patterns based on transmitral flow on echocardiography. These filling patterns occur sequentially with progressively worsening LV diastolic function. However, the interpretation of transmitral inflow pattern is severely hampered by its load- and age-dependency, and is also influenced by other factors such as atrial and ventricular compliance, mitral valve competency and left atrial pressures.[103]

With the advent of tissue Doppler imaging, quantification of longitudinal myocardial velocities has significantly simplified the interpretation of LV diastolic function (Figure 16). Previous studies have demonstrated that the peak early diastolic e' velocity correlated significantly with the time constant of LV isovolumic relaxation (Tau), the gold standard of LV diastolic function.[104, 105] Transmitral inflow goes through a pseudonormalized pattern which can potentially be misinterpreted as normal, early diastolic e' velocity progressively declines with worsening LV diastolic function. However, tissue Doppler myocardial velocity imaging may be influenced by the passive translational motion and tethering effects from surrounding myocardial tissues. In contrast, myocardial strain and strain rate imaging permits site-specific quantification of active myocardial deformation that is independent of the translational motion and tethering artifacts.[106] Using strain rate imaging, LV diastolic function could be quantified by strain rate e' (Figures 17 and 18).[107] More recently, newer sophisticated echocardiographic techniques such as 2-dimensional speckle tracking have also been used to evaluate LV diastolic function (Figure 19).[108-110] Unlike tissue Doppler imaging, 2-dimensional speckle tracking is angle independent and may be more accurate than tissue Doppler imaging in evaluating LV diastolic function.[108, 110]

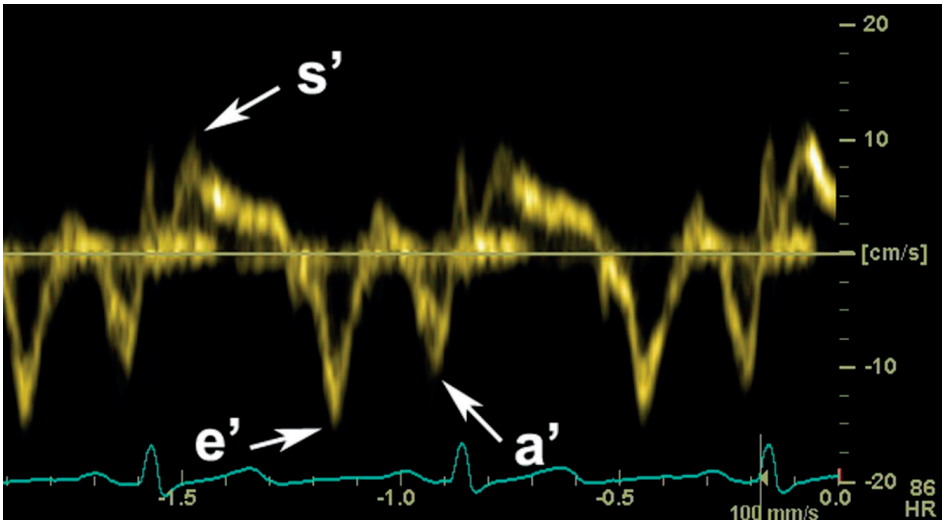


Figure 16. *Example of pulsed wave tissue Doppler trace at the lateral mitral annulus. The cardiac cycle is presented by s' during systole, followed by early diastolic relaxation (e') and late diastolic atrial contraction (a') during diastole. LV systolic and diastolic function can be quantified by the peak s' (9.8 cm/s) and peak e' (15.2 cm/s) velocities respectively.*

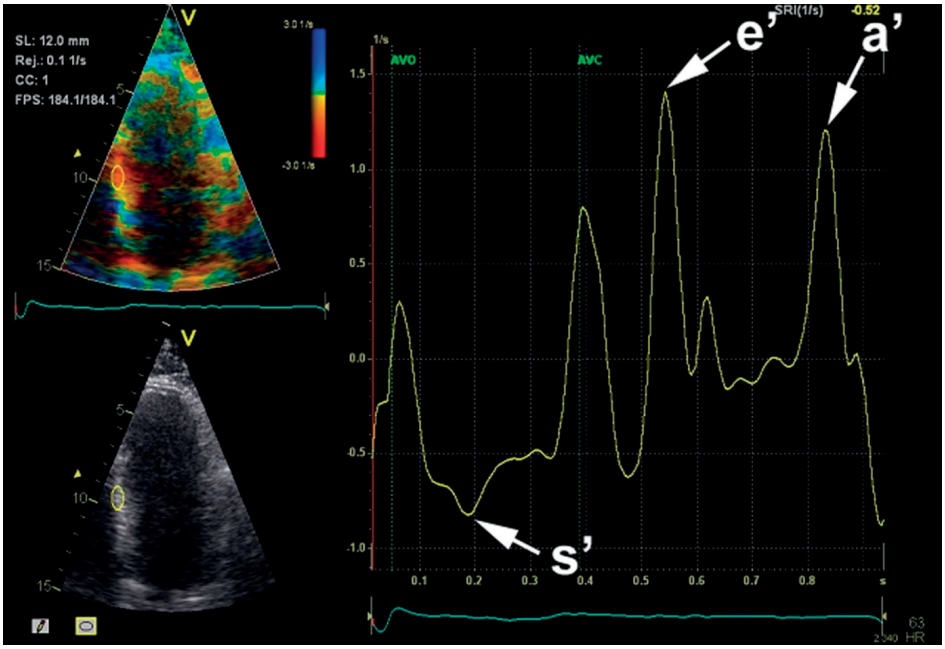


Figure 17. *Example of strain rate tracing derived from color-coded tissue Doppler imaging of the mid septum. Similar to myocardial velocity imaging, myocardial strain rate can be divided into systolic (s'), early diastolic (e'), and late diastolic atrial (a') contractions. Myocardial systolic and diastolic function can be quantified by the peak s' (-0.84 s^{-1}) and e' (1.40 s^{-1}) strain rates respectively. AVO: aortic valve opening; AVC: aortic valve closure.*

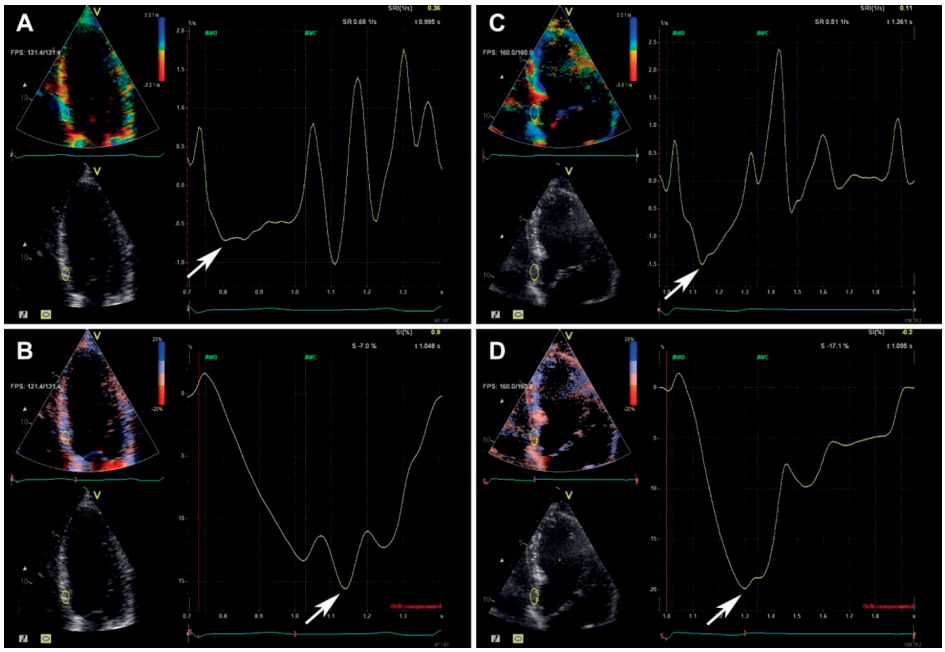


Figure 18. *Examples of tissue Doppler derived strain rate and strain in a type 2 diabetic patient (Panels A and B respectively) and a normal healthy control (Panels C and D). Both the diabetic patient and normal control had comparable left ventricular ejection fraction (63% versus 66% respectively). However, the diabetic patient had significantly lower basal septal peak systolic strain rate and strain (-0.72 s^{-1} and -15.8% respectively, arrows) by tissue Doppler imaging compared to the normal healthy control (-1.50 s^{-1} and -19.9% respectively, arrows). AVO: aortic valve opening; AVC: aortic valve closure.*

The most frequent finding in an asymptomatic patient with diabetic heart disease is diastolic dysfunction with normal LVEF. Even in well-controlled, normotensive and asymptomatic type 2 diabetic patients, the prevalence of diastolic dysfunction is reported to be up to 47% of patients, of which 30% had impaired relaxation and 17% had pseudo-normalized filling pattern.[111] However, newer and more sophisticated echocardiographic techniques such as tissue Doppler or 2-dimensional speckle tracking imaging are more sensitive in identifying subtle myocardial dysfunctions.[109, 112-114] For example, using tissue Doppler imaging, Fang and co-workers determined that subclinical LV diastolic dysfunction was present in 21% of type 2 diabetic patients.[114] This was in contrast to standard echocardiographic parameters such as transmitral inflow pattern, deceleration time and isovolumic relaxation time, which failed to identify subclinical diabetic heart disease. However, as the definition of significant subclinical LV dysfunction in that study was based on greater than 1 standard deviation less than the mean normal value derived from healthy controls, the true incidence of diabetic heart disease diagnosed with tissue Doppler imaging is likely to be significantly higher.[114] Accordingly, Boyer and co-workers demonstrated that using a mitral annular velocity of < 8cm/s identified up to 63% of diabetic patients as having evidence of diastolic dysfunction.[112]

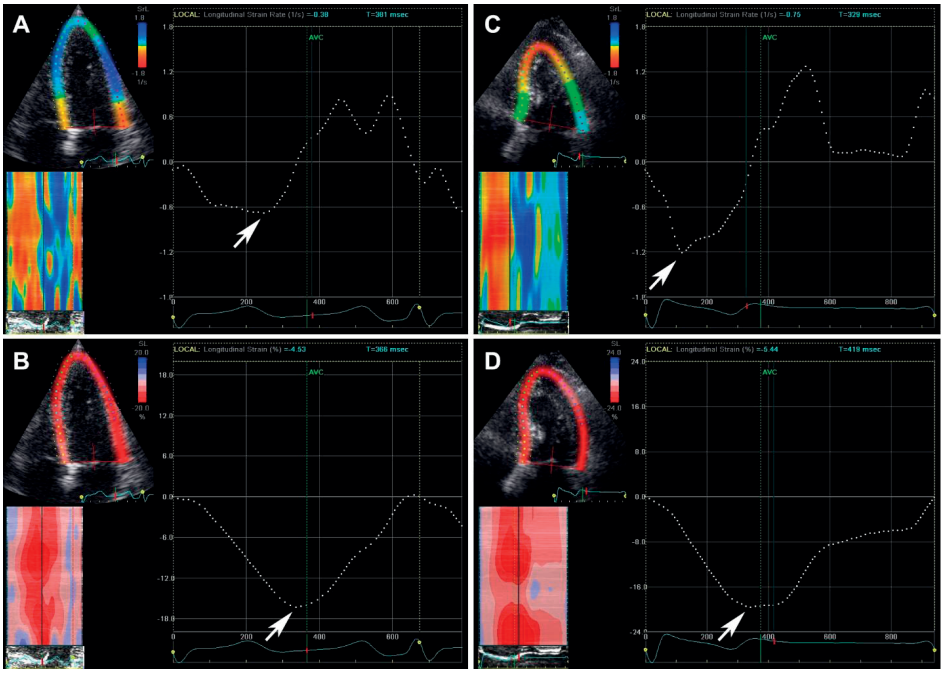


Figure 19. *Examples of 2-dimensional speckle tracking strain and strain rate in the same diabetic patient and normal control. The diabetic patient had significantly lower peak global systolic strain rate and strain (-0.69 s^{-1} and -16.3% respectively, arrows) by 2-dimensional speckle tracking compared to the normal control (-1.22 s^{-1} and -20.1% respectively, arrows). AVC: aortic valve closure.*

2. Systolic function

Traditionally, the clinical standard in the assessment of global LV systolic function is primarily based on the quantification of LV chamber volumes to derive LVEF. Although quantification of systolic function by LVEF is easily understandable and reasonably reproducible, it is highly dependent in preload and afterload. Due to the relative insensitivity of LVEF in detecting subtle myocardial dysfunction, demonstrating LV systolic dysfunction in diabetic patients has been more difficult. In contrast, myocardial velocity, strain and strain rate imaging are more sensitive systolic markers than LVEF. Similarly, quantification of systolic function by myocardial velocity (Figure 16), strain and strain rate imaging (Figures 17-19) has been shown to be significantly correlated with global LV systolic function.[106, 115-117]

Previous studies have demonstrated subclinical myocardial systolic dysfunction in diabetic patients.[97, 109, 113, 118, 119] Using color-coded tissue Doppler imaging, Fang and co-workers demonstrated reduced myocardial longitudinal systolic function in diabetic patients compared to age-matched controls.[113] In that study, diabetic patients had significantly lower peak systolic strain rate compared to controls (1.4 ± 0.3 s^{-1} vs. 1.6 ± 0.3

s^{-1}, p = 0.006), suggesting the presence of subtle myocardial contractile dysfunction despite normal LVEF. Similarly, Galderisi and co-workers examined the value of myocardial systolic velocity and strain rate during dobutamine stress echocardiography in 24 diabetic patients and 16 normal controls.[119] The group demonstrated that diabetic patients had evidence of reduced myocardial contractile reserve compared to non-diabetics. Therefore, tissue Doppler imaging is more sensitive than conventional LVEF in detecting subclinical myocardial systolic dysfunction. More recently, Ng and co-workers utilized 2-dimensional speckle tracking echocardiography to compare type 2 diabetic patients with normal healthy controls.[109] Despite all the diabetic patients having good glycemic control and asymptomatic without evidence of diabetic complications, coronary artery disease and hypertension, 2-dimensional speckle tracking was able to identify significant subclinical LV dysfunction compared to the controls.[109] Diabetic patients had significantly lower global longitudinal strain (-18.3 ± 2.2% vs. -19.9 ± 1.9%, p < 0.001) and systolic strain rate (-0.99 ± 0.17 s^{-1} vs. -1.07 ± 0.13 s^{-1}, p = 0.009) compared to healthy controls.[109]

3. Regional differences in myocardial dysfunction in diabetic heart disease

The LV myocardial architecture is a complex array of longitudinally and circumferentially orientated fibres located predominately in the epicardium/endocardium and mid-wall respectively.[120] Newer and more sophisticated echocardiographic techniques allow site-specific and multidirectional assessments of myocardial strain and strain rate, thereby permitting exploration of regional differences in myocardial functional changes in subclinical diabetic heart disease. Using color-coded tissue Doppler imaging, both Fang et al. and Vinereanu et al. demonstrated reduced longitudinal myocardial function with a compensatory increase in radial function.[113, 118] Similarly, using multidirectional speckle tracking analyses, Ng and co-workers demonstrated reduced longitudinal strain and strain rate (predominantly derived from epicardial/endocardial fibre contraction) but preserved circumferential and radial strains and strain rates (predominantly derived from mid-wall circumferential fibres contraction) in asymptomatic diabetic patients.[109] These findings suggest that myocardial dysfunction in early diabetic cardiomyopathy may start in the subendocardium, and the preservation of circumferential and radial functions account for the initial preservation of LV volumes and EF.

C) CONCLUSIONS

Over the last few decades, there is increasing recognition that diabetic heart disease is a real disease entity rather than a nebulous concept, supported by evidence from epi-

demiological and experimental studies that demonstrated an independent association between diabetes and heart failure. Numerous studies have explored the underlying pathophysiological mechanisms triggering the disease onset and progression to overt clinical heart failure. However, the etiology of diabetic heart disease remains unclear and is likely to be multifactorial, such as altered myocardial metabolism, endothelial dysfunction, autonomic neuropathy, coronary atherosclerosis and increased myocardial fibrosis. Multimodality imaging including echocardiography, nuclear imaging, CT and MRI all provide valuable insights into the disease process. In addition, cardiac imaging is essential for diagnosing diabetic heart disease by demonstrating LV myocardial dysfunction that is independent of significant coronary artery disease and hypertension. Finally, multimodality cardiac imaging may be useful for monitoring disease progression and evaluate the effectiveness of medical interventions.

REFERENCE LIST

(1) World Health Organization. Definition and diagnosis of diabetes mellitus and intermediate hyperglycemia. 2006.

(2) Wild S, Roglic G, Green A, Sicree R, King H. Global Prevalence of Diabetes. *Diabetes Care* 2004;27:1047-1053.

(3) Kannel WB, McGee DL. Diabetes and cardiovascular disease. The Framingham study. *JAMA* 1979;241:2035-2038.

(4) From AM, Scott CG, Chen HH. The Development of Heart Failure in Patients With Diabetes Mellitus and Pre-Clinical Diastolic Dysfunction: A Population-Based Study. *J Am Coll Cardiol* 2010;55:300-305.

(5) Coughlin SS, Pearle DL, Baughman KL, Wasserman A, Tefft MC. Diabetes mellitus and risk of idiopathic dilated cardiomyopathy. The Washington, DC Dilated Cardiomyopathy Study. *Ann Epidemiol* 1994;4:67-74.

(6) Redfield MM, Jacobsen SJ, Burnett JC, Jr., Mahoney DW, Bailey KR, Rodeheffer RJ. Burden of systolic and diastolic ventricular dysfunction in the community: appreciating the scope of the heart failure epidemic. *JAMA* 2003;289:194-202.

(7) Nichols GA, Gullion CM, Koro CE, Ephross SA, Brown JB. The incidence of congestive heart failure in type 2 diabetes: an update. *Diabetes Care* 2004;27:1879-1884.

(8) Rubler S, Dlugash J, Yuceoglu YZ, Kumral T, Branwood AW, Grishman A. New type of cardiomyopathy associated with diabetic glomerulosclerosis. *Am J Cardiol* 1972;30:595-602.

(9) Boudina S, Abel ED. Diabetic Cardiomyopathy Revisited. *Circulation* 2007;115:3213-3223.

(10) Marwick T. The diabetic myocardium. *Curr Diab Rep* 2006;6:36-41.

(11) Lindsey JB, Marso SP. Steatosis and Diastolic Dysfunction: The Skinny on Myocardial Fat. *J Am Coll Cardiol* 2008;52:1800-1802.

(12) Schaffer JE. Lipotoxicity: when tissues overeat. *Curr Opin Lipidol* 2003;14:281-287.

(13) McGavock JM, Victor RG, Unger RH, Szczepaniak LS. Adiposity of the Heart, Revisited. *Ann Intern Med* 2006;144:517-524.

(14) Lopaschuk GD, Ussher JR, Folmes CD, Jaswal JS, Stanley WC. Myocardial fatty acid metabolism in health and disease. *Physiol Rev* 2010;90:207-258.

(15) Unger RH. Lipotoxic Diseases. *Annu Rev Med* 2002;53:319.

(16) Szczepaniak LS, Dobbins RL, Metzger GJ, Sartoni-D'Ambrosia G, Arbique D, Vongpatanasin W, Unger R, Victor RG. Myocardial triglycerides and systolic function in humans: in vivo evaluation by localized proton spectroscopy and cardiac imaging. *Magn Reson Med* 2003;49:417-423.

(17) van der Meer RW, Doornbos J, Kozerke S, Schar M, Bax JJ, Hammer S, Smit JW, Romijn JA, Diamant M, Rijzewijk LJ, De Roos A, Lamb HJ. Metabolic imaging of myocardial triglyceride content: reproducibility of 1H MR spectroscopy with respiratory navigator gating in volunteers. *Radiology* 2007;245:251-257.

(18) Hammer S, Snel M, Lamb HJ, Jazet IM, van der Meer RW, Pijl H, Meinders EA, Romijn JA, De Roos A, Smit JW. Prolonged caloric restriction in obese patients with type 2 diabetes mellitus decreases myocardial triglyceride content and improves myocardial function. *J Am Coll Cardiol* 2008;52:1006-1012.

(19) Iozzo P, Lautamaki R, Borra R, Lehto HR, Bucci M, Viljanen A, Parkka J, Lepomaki V, Maggio R, Parkkola R, Knuuti J, Nuutila P. Contribution of glucose tolerance and gender to cardiac adiposity. *J Clin Endocrinol Metab* 2009;94:4472-4482.

(20) Rijzewijk LJ, van der Meer RW, Smit JWA, Diamant M, Bax JJ, Hammer S, Romijn JA, De Roos A, Lamb HJ. Myocardial Steatosis Is an Independent Predictor of Diastolic Dysfunction in Type 2 Diabetes Mellitus. *J Am Coll Cardiol* 2008;52:1793-1799.

(21) van der Meer RW, Rijzewijk LJ, Diamant M, Hammer S, Schar M, Bax JJ, Smit JW, Romijn JA, De Roos A, Lamb HJ. The ageing male heart: myocardial triglyceride content as independent predictor of diastolic function. *Eur Heart J* 2008;29:1516-1522.

(22) van der Meer RW, Rijzewijk LJ, de Jong HWAM, Lamb HJ, Lubberink M, Romijn JA, Bax JJ, De Roos A, Kamp O, Paulus WJ, Heine RJ, Lammertsma AA, Smit JWA, Diamant M. Pioglitazone Improves Cardiac Function and Alters Myocardial Substrate Metabolism Without Affecting Cardiac Triglyceride Accumulation and High-Energy Phosphate Metabolism in Patients With Well-Controlled Type 2 Diabetes Mellitus. *Circulation* 2009;119:2069-2077.

(23) McGavock JM, Lingvay I, Zib I, Tillery T, Salas N, Unger R, Levine BD, Raskin P, Victor RG, Szczepaniak LS. Cardiac Steatosis in Diabetes Mellitus: A 1H-Magnetic Resonance Spectroscopy Study. *Circulation* 2007;116:1170-1175.

(24) Sharma S, Adrogue JV, Golfman L, Uray I, Lemm J, Youker K, Noon GP, Frazier OH, Taegtmeyer H. Intramyocardial lipid accumulation in the failing human heart resembles the lipotoxic rat heart. *FASEB J* 2004;18:1692-1700.

(25) Zhou YT, Grayburn P, Karim A, Shimabukuro M, Higa M, Baetens D, Orci L, Unger RH. Lipotoxic heart disease in obese rats: Implications for human obesity. *Proc Natl Acad Science USA* 2000;97:1784-1789.

(26) Schrauwen-Hinderling VB, Hesselink MK, Meex R, van der MS, Schar M, Lamb H, Wildberger JE, Glatz J, Snoep G, Kooi ME, Schrauwen P. Improved Ejection Fraction after Exercise Training in Obesity Is Accompanied by Reduced Cardiac Lipid Content. *J Clin Endocrinol Metab* 2010;95:1932-1938.

(27) Zib I, Jacob AN, Lingvay I, Salinas K, McGavock JM, Raskin P, Szczepaniak LS. Effect of pioglitazone therapy on myocardial and hepatic steatosis in insulin-treated patients with type 2 diabetes. *J Investig Med* 2007;55:230-236.

(28) Kinlay S, Libby P, Ganz P. Endothelial function and coronary artery disease. *Curr Opin Lipidol* 2001;12:383-389.

(29) Radomski MW, Palmer RM, Moncada S. The role of nitric oxide and cGMP in platelet adhesion to vascular endothelium. *Biochem Biophys Res Commun* 1987;148:1482-1489.

(30) Kubes P, Suzuki M, Granger DN. Nitric oxide: an endogenous modulator of leukocyte adhesion. *Proc Natl Acad Sci U S A* 1991;88:4651-4655.

(31) Sarkar R, Meinberg EG, Stanley JC, Gordon D, Webb RC. Nitric oxide reversibly inhibits the migration of cultured vascular smooth muscle cells. *Circ Res* 1996;78:225-230.

(32) Creager MA, Luscher TF, Cosentino F, Beckman JA. Diabetes and vascular disease: pathophysiology, clinical consequences, and medical therapy: Part I. *Circulation* 2003;108:1527-1532.

(33) Tan KC, Chow WS, Ai VH, Metz C, Bucala R, Lam KS. Advanced glycation end products and endothelial dysfunction in type 2 diabetes. *Diabetes Care* 2002;25:1055-1059.

(34) McDaid EA, Monaghan B, Parker AI, Hayes JR, Allen JA. Peripheral autonomic impairment in patients newly diagnosed with type II diabetes. *Diabetes Care* 1994;17:1422-1427.

(35) Celermajer DS, Sorensen KE, Gooch VM, Spiegelhalter DJ, Miller OI, Sullivan ID, Lloyd JK, Deanfield JE. Non-invasive detection of endothelial dysfunction in children and adults at risk of atherosclerosis. *Lancet* 1992;340:1111-1115.

(36) Anderson TJ, Uehata A, Gerhard MD, Meredith IT, Knab S, Delagrange D, Lieberman EH, Ganz P, Creager MA, Yeung AC, . Close relation of endothelial function in the human coronary and peripheral circulations. *J Am Coll Cardiol* 1995;26:1235-1241.

(37) Deanfield JE, Halcox JP, Rabelink TJ. Endothelial function and dysfunction: testing and clinical relevance. *Circulation* 2007;115:1285-1295.

(38) Bots ML, Westerink J, Rabelink TJ, de Koning EJ. Assessment of flow-mediated vasodilatation (FMD) of the brachial artery: effects of technical aspects of the FMD measurement on the FMD response. *Eur Heart J* 2005;26:363-368.

(39) Kang X, Berman DS, Lewin H, Miranda R, Erel J, Friedman JD, Amanullah AM. Comparative ability of myocardial perfusion single-photon emission computed tomography to detect coronary artery disease in patients with and without diabetes mellitus. *Am Heart J* 1999;137:949-957.

(40) Djaberi R, Roodt J, Schuijf JD, Rabelink TJ, de Koning EJ, Pereira AM, Stokkel MP, Smit JW, Bax JJ, Jukema JW. Endothelial dysfunction in diabetic patients with abnormal myocardial perfusion in the absence of epicardial obstructive coronary artery disease. *J Nucl Med* 2009;50:1980-1986.

(41) Fang ZY, Najos-Valencia O, Leano R, Marwick TH. Patients with early diabetic heart disease demonstrate a normal myocardial response to dobutamine. *J Am Coll Cardiol* 2003;42:446-453.

(42) Moir S, Hanekom L, Fang ZY, Haluska B, Wong C, Burgess M, Marwick TH. Relationship between myocardial perfusion and dysfunction in diabetic cardiomyopathy: a study of quantitative contrast echocardiography and strain rate imaging. *Heart* 2006;92:1414-1419.

(43) Wei K, Ragosta M, Thorpe J, Coggins M, Moos S, Kaul S. Noninvasive quantification of coronary blood flow reserve in humans using myocardial contrast echocardiography. *Circulation* 2001;103:2560-2565.

(44) Hansen CL, Goldstein RA, Akinboboye OO, Berman DS, Botvinick EH, Churchwell KB, Cooke CD, Corbett JR, Cullom SJ, Dahlberg ST, Druz RS, Ficaro EP, Galt JR, Garg RK, Germano G, Heller GV, Henzlova MJ, Hyun MC, Johnson LL, Mann A, McCallister BD, Jr., Quaife RA, Ruddy TD, Sundaram SN, Taillefer R, Ward RP, Mahmarian JJ. Myocardial perfusion and function: single photon emission computed tomography. *J Nucl Cardiol* 2007;14:e39-e60.

(45) Amanullah AM, Berman DS, Hachamovitch R, Kiat H, Kang X, Friedman JD. Identification of severe or extensive coronary artery disease in women by adenosine technetium-99m sestamibi SPECT. *Am J Cardiol* 1997;80:132-137.

(46) Hasdai D, Gibbons RJ, Holmes DR, Jr., Higano ST, Lerman A. Coronary endothelial dysfunction in humans is associated with myocardial perfusion defects. *Circulation* 1997;96:3390-3395.

(47) Wackers FJ, Young LH, Inzucchi SE, Chyun DA, Davey JA, Barrett EJ, Taillefer R, Wittlin SD, Heller GV, Filipchuk N, Engel S, Ratner RE, Iskandrian AE. Detection of silent myocardial ischemia in asymptomatic diabetic subjects: the DIAD study. *Diabetes Care* 2004;27:1954-1961.

(48) Valensi P, Paries J, Brulport-Cerisier V, Torremocha F, Sachs RN, Vanzetto G, Cosson E, Lormeau B, Attali JR, Marechaud R, Estour B, Halimi S. Predictive value of silent myocardial ischemia for

cardiac events in diabetic patients: influence of age in a French multicenter study. *Diabetes Care* 2005;28:2722-2727.

(49) Zellweger MJ, Hachamovitch R, Kang X, Hayes SW, Friedman JD, Germano G, Pfisterer ME, Berman DS. Prognostic relevance of symptoms versus objective evidence of coronary artery disease in diabetic patients. *Eur Heart J* 2004;25:543-550.

(50) Kang X, Berman DS, Lewin HC, Cohen I, Friedman JD, Germano G, Hachamovitch R, Shaw LJ. Incremental prognostic value of myocardial perfusion single photon emission computed tomography in patients with diabetes mellitus. *Am Heart J* 1999;138:1025-1032.

(51) Pancholy SB, Fattah AA, Kamal AM, Ghods M, Heo J, Iskandrian AS. Independent and incremental prognostic value of exercise thallium single-photon emission computed tomographic imaging in women. *J Nucl Cardiol* 1995;2:110-116.

(52) Ross R. The pathogenesis of atherosclerosis: a perspective for the 1990s. *Nature* 1993;362:801-809.

(53) Egashira K, Hirooka Y, Kai H, Sugimachi M, Suzuki S, Inou T, Takeshita A. Reduction in serum cholesterol with pravastatin improves endothelium-dependent coronary vasomotion in patients with hypercholesterolemia. *Circulation* 1994;89:2519-2524.

(54) Wackers FJ, Chyun DA, Young LH, Heller GV, Iskandrian AE, Davey JA, Barrett EJ, Taillefer R, Wittlin SD, Filipchuk N, Ratner RE, Inzucchi SE. Resolution of asymptomatic myocardial ischemia in patients with type 2 diabetes in the Detection of Ischemia in Asymptomatic Diabetics (DIAD) study. *Diabetes Care* 2007;30:2892-2898.

(55) Bateman TM, Heller GV, McGhie AI, Friedman JD, Case JA, Bryngelson JR, Hertenstein GK, Moutray KL, Reid K, Cullom SJ. Diagnostic accuracy of rest/stress ECG-gated Rb-82 myocardial perfusion PET: comparison with ECG-gated Tc-99m sestamibi SPECT. *J Nucl Cardiol* 2006;13:24-33.

(56) Bengel FM, Higuchi T, Javadi MS, Lautamaki R. Cardiac positron emission tomography. *J Am Coll Cardiol* 2009;54:1-15.

(57) Bergmann SR, Herrero P, Markham J, Weinheimer CJ, Walsh MN. Noninvasive quantitation of myocardial blood flow in human subjects with oxygen-15-labeled water and positron emission tomography. *J Am Coll Cardiol* 1989;14:639-652.

(58) Lortie M, Beanlands RS, Yoshinaga K, Klein R, Dasilva JN, DeKemp RA. Quantification of myocardial blood flow with 82Rb dynamic PET imaging. *Eur J Nucl Med Mol Imaging* 2007;34:1765-1774.

(59) Kaufmann PA, Gnecchi-Ruscone T, Yap JT, Rimoldi O, Camici PG. Assessment of the reproducibility of baseline and hyperemic myocardial blood flow measurements with 15O-labeled water and PET. *J Nucl Med* 1999;40:1848-1856.

(60) Campisi R, Czernin J, Schoder H, Sayre JW, Marengo FD, Phelps ME, Schelbert HR. Effects of long-term smoking on myocardial blood flow, coronary vasomotion, and vasodilator capacity. *Circulation* 1998;98:119-125.

(61) Pitkanen OP, Raitakari OT, Niinikoski H, Nuutila P, Iida H, Voipio-Pulkki LM, Harkonen R, Wegelius U, Ronnemaa T, Viikari J, Knuuti J. Coronary flow reserve is impaired in young men with familial hypercholesterolemia. *J Am Coll Cardiol* 1996;28:1705-1711.

(62) Kjaer A, Meyer C, Nielsen FS, Parving HH, Hesse B. Dipyridamole, cold pressor test, and demonstration of endothelial dysfunction: a PET study of myocardial perfusion in diabetes. *J Nucl Med* 2003;44:19-23.

(63) Momose M, Abletshauser C, Neverve J, Nekolla SG, Schnell O, Standl E, Schwaiger M, Bengel FM. Dysregulation of coronary microvascular reactivity in asymptomatic patients with type 2 diabetes mellitus. *Eur J Nucl Med Mol Imaging* 2002;29:1675-1679.

(64) Prior JO, Quinones MJ, Hernandez-Pampaloni M, Facta AD, Schindler TH, Sayre JW, Hsueh WA, Schelbert HR. Coronary circulatory dysfunction in insulin resistance, impaired glucose tolerance, and type 2 diabetes mellitus. *Circulation* 2005;111:2291-2298.

(65) Taskiran M, Fritz-Hansen T, Rasmussen V, Larsson HB, Hilsted J. Decreased myocardial perfusion reserve in diabetic autonomic neuropathy. *Diabetes* 2002;51:3306-3310.

(66) Vinik AI, Freeman R, Erbas T. Diabetic autonomic neuropathy. *Semin Neurol* 2003;23:365-372.

(67) Boulton AJ, Vinik AI, Arezzo JC, Bril V, Feldman EL, Freeman R, Malik RA, Maser RE, Sosenko JM, Ziegler D. Diabetic neuropathies: a statement by the American Diabetes Association. *Diabetes Care* 2005;28:956-962.

(68) Nagamachi S, Fujita S, Nishii R, Futami S, Tamura S, Mizuta M, Nakazato M, Kurose T, Wakamatsu H. Prognostic value of cardiac I-123 metaiodobenzylguanidine imaging in patients with non-insulin-dependent diabetes mellitus. *J Nucl Cardiol* 2006;13:34-42.

(69) Vinik AI, Ziegler D. Diabetic cardiovascular autonomic neuropathy. *Circulation* 2007;115:387-397.

(70) Vinik AI, Maser RE, Mitchell BD, Freeman R. Diabetic autonomic neuropathy. *Diabetes Care* 2003;26:1553-1579.

(71) Vinik AI, Ziegler D. Diabetic cardiovascular autonomic neuropathy. *Circulation* 2007;115:387-397.

(72) Vinik AI, Ziegler D. Diabetic cardiovascular autonomic neuropathy. *Circulation* 2007;115:387-397.

(73) Vinik AI, Ziegler D. Diabetic cardiovascular autonomic neuropathy. *Circulation* 2007;115:387-397.

(74) Ziegler D, Weise F, Langen KJ, Piolot R, Boy C, Hubinger A, Muller-Gartner HW, Gries FA. Effect of glycaemic control on myocardial sympathetic innervation assessed by [123I]metaiodobenzylguanidine scintigraphy: a 4-year prospective study in IDDM patients. *Diabetologia* 1998;41:443-451.

(75) Stevens MJ, Raffel DM, Allman KC, Dayanikli F, Ficaro E, Sandford T, Wieland DM, Pfeifer MA, Schwaiger M. Cardiac sympathetic dysinnervation in diabetes: implications for enhanced cardiovascular risk. *Circulation* 1998;98:961-968.

(76) Patel AD, Iskandrian AE. MIBG imaging. *J Nucl Cardiol* 2002;9:75-94.

(77) Allman KC, Stevens MJ, Wieland DM, Hutchins GD, Wolfe ER, Jr., Greene DA, Schwaiger M. Noninvasive assessment of cardiac diabetic neuropathy by carbon-11 hydroxyephedrine and positron emission tomography. *J Am Coll Cardiol* 1993;22:1425-1432.

(78) Nagamachi S, Jinnouchi S, Kurose T, Nishii R, Kawai K, Futami S, Tamura S, Matsukura S. Serial change in 123I-MIBG myocardial scintigraphy in non-insulin-dependent diabetes mellitus. *Ann Nucl Med* 2002;16:33-38.

(79) Verberne HJ, Brewster LM, Somsen GA, Eck-Smit BL. Prognostic value of myocardial 123I-metaiodobenzylguanidine (MIBG) parameters in patients with heart failure: a systematic review. *Eur Heart J* 2008;29:1147-1159.

(80) Turpeinen AK, Vanninen E, Kuikka JT, Uusitupa MI. Demonstration of regional sympathetic denervation of the heart in diabetes. Comparison between patients with NIDDM and IDDM. *Diabetes Care* 1996;19:1083-1090.

(81) Goraya TY, Leibson CL, Palumbo PJ, Weston SA, Killian JM, Pfeifer EA, Jacobsen SJ, Frye RL, Roger VL. Coronary atherosclerosis in diabetes mellitus: a population-based autopsy study. *J Am Coll Cardiol* 2002;40:946-953.

(82) Pundziute G, Schuijf JD, Jukema JW, Boersma E, de RA, van der Wall EE, Bax JJ. Prognostic value of multislice computed tomography coronary angiography in patients with known or suspected coronary artery disease. *J Am Coll Cardiol* 2007;49:62-70.

(83) Ambrose JA, Tannenbaum MA, Alexopoulos D, Hjemdahl-Monsen CE, Leavy J, Weiss M, Borrico S, Gorlin R, Fuster V. Angiographic progression of coronary artery disease and the development of myocardial infarction. *J Am Coll Cardiol* 1988;12:56-62.

(84) Little WC, Constantinescu M, Applegate RJ, Kutcher MA, Burrows MT, Kahl FR, Santamore WP. Can coronary angiography predict the site of a subsequent myocardial infarction in patients with mild-to-moderate coronary artery disease? *Circulation* 1988;78:1157-1166.

(85) Sarwar A, Shaw LJ, Shapiro MD, Blankstein R, Hoffman U, Cury RC, Abbara S, Brady TJ, Budoff MJ, Blumenthal RS, Nasir K. Diagnostic and prognostic value of absence of coronary artery calcification. *J Am Coll Cardiol Img* 2009;2:675-688.

(86) Budoff MJ, Shaw LJ, Liu ST, Weinstein SR, Mosler TP, Tseng PH, Flores FR, Callister TQ, Raggi P, Berman DS. Long-term prognosis associated with coronary calcification: observations from a registry of 25,253 patients. *J Am Coll Cardiol* 2007;49:1860-1870.

(87) Raggi P, Shaw LJ, Berman DS, Callister TQ. Prognostic value of coronary artery calcium screening in subjects with and without diabetes. *J Am Coll Cardiol* 2004;43:1663-1669.

(88) Anand DV, Lim E, Hopkins D, Corder R, Shaw LJ, Sharp P, Lipkin D, Lahiri A. Risk stratification in uncomplicated type 2 diabetes: prospective evaluation of the combined use of coronary artery calcium imaging and selective myocardial perfusion scintigraphy. *Eur Heart J* 2006;27:713-721.

(89) Burgstahler C, Beck T, Reimann A, Kuettner A, Kopp AF, Heuschmid M, Claussen CD, Schroeder S. Diagnostic accuracy of multislice computed tomography for the detection of coronary artery disease in diabetic patients. *J Diabetes Complications* 2007;21:69-74.

(90) Schuijf JD, Bax JJ, Jukema JW, Lamb HJ, Vliegen HW, Salm LP, De Roos A, Van Der Wall E. Noninvasive angiography and assessment of left ventricular function using multislice computed tomography in patients with type 2 diabetes. *Diabetes Care* 2004;27:2905-2910.

(91) Pundziute G, Schuijf JD, Jukema JW, Boersma E, Scholte AJ, Kroft LJ, van der Wall EE, Bax JJ. Noninvasive assessment of plaque characteristics with multislice computed tomography coronary angiography in symptomatic diabetic patients. *Diabetes Care* 2007;30:1113-1119.

(92) Pundziute G, Schuijf JD, Jukema JW, van Werkhoven JM, Nucifora G, Decramer I, Sarno G, Vanhoenacker PK, Reiber JH, Wijns W, Bax JJ. Type 2 diabetes is associated with more advanced coronary atherosclerosis on multislice computed tomography and virtual histology intravascular ultrasound. *J Nucl Cardiol* 2009;16:376-383.

(93) Scholte AJ, Schuijf JD, Kharagjitsingh AV, Jukema JW, Pundziute G, van der Wall EE, Bax JJ. Prevalence of coronary artery disease and plaque morphology assessed by multi-slice computed tomography coronary angiography and calcium scoring in asymptomatic patients with type 2 diabetes. *Heart* 2008;94:290-295.

(94) van Werkhoven JM, Cademartiri F, Seitun S, Maffei E, Palumbo A, Martini C, Tarantini G, Kroft LJ, De Roos A, Weustink AC, Jukema JW, Ardissino D, Mollet NR, Schuijf JD, Bax JJ. Prognostic Value

of Computed Tomographic Coronary Angiography in Patients with Diabetes: Comparison with a Non-diabetic Population. Radiology. In press 2010.

(95) Kawaguchi M, Techigawara M, Ishihata T, Asakura T, Saito F, Maehara K, Maruyama Y. A comparison of ultrastructural changes on endomyocardial biopsy specimens obtained from patients with diabetes mellitus with and without hypertension. *Heart Vessels* 1997;12:267-274.

(96) Adeghate E. Molecular and cellular basis of the aetiology and management of diabetic cardiomyopathy: a short review. *Mol Cell Biochem* 2004;261:187-191.

(97) Loganathan R, Bilgen M, Al Hafez B, Smirnova IV. Characterization of alterations in diabetic myocardial tissue using high resolution MRI. *Int J Cardiovasc Imaging* 2006;22:81-90.

(98) Picano E, Pelosi G, Marzilli M, Lattanzi F, Benassi A, Landini L, L'Abbate A. In vivo quantitative ultrasonic evaluation of myocardial fibrosis in humans. *Circulation* 1990;81:58-64.

(99) Di B, V, Talarico L, Picano E, Di MC, Landini L, Paterni M, Matteucci E, Giusti C, Giampietro O. Increased echodensity of myocardial wall in the diabetic heart: an ultrasound tissue characterization study. *J Am Coll Cardiol* 1995;25:1408-1415.

(100) Fang ZY, Yuda S, Anderson V, Short L, Case C, Marwick TH. Echocardiographic detection of early diabetic myocardial disease. *J Am Coll Cardiol* 2003;41:611-617.

(101) Regan TJ, Wu CF, Yeh CK, Oldewurtel HA, Haider B. Myocardial composition and function in diabetes. The effects of chronic insulin use. *Circ Res* 1981;49:1268-1277.

(102) Bhimji S, Godin DV, McNeill JH. Biochemical and functional changes in hearts from rabbits with diabetes. *Diabetologia* 1985;28:452-457.

(103) Kim RJ, Fieno DS, Parrish TB, Harris K, Chen EL, Simonetti O, Bundy J, Finn JP, Klocke FJ, Judd RM. Relationship of MRI delayed contrast enhancement to irreversible injury, infarct age, and contractile function. *Circulation* 1999;100:1992-2002.

(104) Kwong RY, Sattar H, Wu H, Vorobiof G, Gandla V, Steel K, Siu S, Brown KA. Incidence and prognostic implication of unrecognized myocardial scar characterized by cardiac magnetic resonance in diabetic patients without clinical evidence of myocardial infarction. *Circulation* 2008;118:1011-1020.

(105) Aneja A, Tang WH, Bansilal S, Garcia MJ, Farkouh ME. Diabetic cardiomyopathy: insights into pathogenesis, diagnostic challenges, and therapeutic options. *Am J Med* 2008;121:748-757.

(106) Nagueh SF, Appleton CP, Gillebert TC, Marino PN, Oh JK, Smiseth OA, Waggoner AD, Flachskampf FA, Pellikka PA, Evangelista A. Recommendations for the evaluation of left ventricular diastolic function by echocardiography. *J Am Soc Echocardiogr* 2009;22:107-133.

(107) Nagueh SF., Middleton KJ., Kopelen HA., Zoghbi WA., Quinones MA. Doppler Tissue Imaging: A Noninvasive Technique for Evaluation of Left Ventricular Relaxation and Estimation of Filling Pressures. *J Am Coll Cardiol* 1997;30:1527-1533.

(108) Nagueh SF, Sun H, Kopelen HA, Middleton KJ, Khoury DS. Hemodynamic determinants of the mitral annulus diastolic velocities by tissue Doppler. *J Am Coll Cardiol* 2001;37:278-285.

(109) Leung DY, Ng AC. Emerging clinical role of strain imaging in echocardiography. *Heart Lung Circ* 2010;19:161-174.

(110) Marwick TH. Measurement of Strain and Strain Rate by Echocardiography: Ready for Prime Time? *J Am Coll Cardiol* 2006;47:1313-1327.

(111) Ng ACT, Tran DT, Newman M, Allman C, Vidaic J, Kadappu KK, Boyd A, Thomas L, Leung DY. Comparison of Myocardial Tissue Velocities Measured by Two-Dimensional Speckle Tracking and Tissue Doppler Imaging. *Am J Cardiol* 2008;102:784-789.

(112) Ng ACT, Delgado V, Bertini M, van der Meer RW, Rijzewijk LJ, Shanks M, Nucifora G, Smit JWA, Diamant M, Romijn JA, De Roos A, Leung DY, Lamb HJ, Bax JJ. Findings from left ventricular strain and strain rate imaging in asymptomatic patients with type 2 diabetes mellitus. *Am J Cardiol* 2009;104:1398-1401.

(113) van Dalen BM, Bosch JG, Kauer F, Soliman OI, Vletter WB, ten Cate FJ, Geleijnse ML. Assessment of mitral annular velocities by speckle tracking echocardiography versus tissue Doppler imaging: validation, feasibility, and reproducibility. *J Am Soc Echocardiogr* 2009;22:1302-1308.

(114) Zabalgoitia M, Ismaeil MF, Anderson L, Maklady FA. Prevalence of diastolic dysfunction in normotensive, asymptomatic patients with well-controlled type 2 diabetes mellitus. *Am J Cardiol* 2001;87:320-323.

(115) Boyer JK, Thanigaraj S, Schechtman KB, Përez JE. Prevalence of ventricular diastolic dysfunction in asymptomatic, normotensive patients with diabetes mellitus. *Am J Cardiol* 2004;93:870-875.

(116) Fang ZY, Leano R, Marwick TH. Relationship between longitudinal and radial contractility in subclinical diabetic heart disease. *Clin Sci* 2004;106:53-60.

(117) Fang ZY, Schull-Meade R, Downey M, Prins J, Marwick TH. Determinants of subclinical diabetic heart disease. *Diabetologia* 2005;48:394-402.

(118) Gulati V, Katz W, Follansbee W, Gorcsan III J. Mitral annular descent velocity by tissue Doppler echocardiography as an index of global left ventricular function. *Am J Cardiol* 1996;77:979-984.

(119) Delgado V, Mollema SA, Ypenburg C, Tops LF, van der Wall EE, Schalij MJ, Bax JJ. Relation Between Global Left Ventricular Longitudinal Strain Assessed with Novel Automated Function Imaging and Biplane Left Ventricular Ejection Fraction in Patients with Coronary Artery Disease. *J Am Soc Echocardiogr* 2008;21:1244-1250.

(120) Greenberg NL, Firstenberg MS, Castro PL, Main M, Travaglini A, Odabashian JA, Drinko JK, Rodriguez LL, Thomas JD, Garcia MJ. Doppler-Derived Myocardial Systolic Strain Rate Is a Strong Index of Left Ventricular Contractility. *Circulation* 2002;105:99-105.

(121) Vinereanu D, Nicolaides E, Tweddel AC, Mädler CF, Holst B, Boden LE, Cinteza M, Rees AE, Fraser AG. Subclinical left ventricular dysfunction in asymptomatic patients with Type II diabetes mellitus, related to serum lipids and glycated haemoglobin. *Clin Sci* 2003;105:591-599.

(122) Galderisi M, de Simone G, Innelli P, Turco A, Turco S, Capaldo B, Riccardi G, de Divitiis O. Impaired Inotropic Response in Type 2 Diabetes Mellitus: A Strain Rate Imaging Study. *Am J Hypertens* 2007;20:548-555.

(123) Greenbaum RA, Ho SY, Gibson DG, Becker AE, Anderson RH. Left ventricular fibre architecture in man. *Br Heart J* 1981;45:248-263.

2

Findings from Left Ventricular Strain and Strain Rate Imaging in Asymptomatic Patients with Type 2 Diabetes Mellitus

Arnold C.T. Ng, Victoria Delgado, Matteo Bertini, Rutger W. van der Meer, Luuk J. Rijzewijk, Miriam Shanks, Gaetano Nucifora, Johannes W.A. Smit, Michaela Diamant, Johannes A. Romijn, Albert de Roos, Dominic Y Leung, Hildo J. Lamb, Jeroen J. Bax

Am J Cardiol. 2009;104(10):1398-401

ABSTRACT

Background: Regional left ventricular (LV) myocardial functional changes in early diabetic cardiomyopathy are not well documented.

Methods: LV multidirectional strain and strain rate (SR) analyses by 2D speckle tracking were utilized to detect subtle myocardial dysfunction in 47 asymptomatic, male patients (57 ± 6years) with type 2 diabetes mellitus. Results were compared to 53 male controls matched by age, body mass index and body surface area.

Results: There were no differences in LV end-diastolic volume index (40.7 ± 8.9 vs. 44.1 ± 7.8mL/m^2, p = ns), end-systolic volume index (16.0 ± 4.8 vs. 17.8 ± 4.3mL/m^2, p = ns), ejection fraction (61.0 ± 5.5 vs. 59.8 ± 5.3%, p = ns). Transmitral E/A (0.95 ± 0.21 vs. 1.12 ± 0.32, p = 0.007) and pulmonary S/D ratios (1.45 ± 0.28 vs. 1.25 ± 0.27, p = 0.001) were more impaired in diabetic patients. Importantly, diabetic patients had impaired longitudinal but preserved circumferential and radial systolic and diastolic function. Diabetes mellitus was an independent predictor for longitudinal strain, systolic SR and early diastolic SR on multiple linear regression analysis (all p < 0.001).

Conclusion: LV longitudinal systolic and diastolic functions were impaired but circumferential and radial functions were preserved in uncomplicated type 2 diabetic patients.

INTRODUCTION

Diabetic cardiomyopathy is defined as left ventricular (LV) dysfunction that occurs independently of coronary artery disease and hypertension.[1] The pathogenesis of diabetic cardiomyopathy is likely to be multifactorial, including microvascular disease, altered myocardial metabolism, and altered myocardial structure with fibrosis. Patients with early diabetic cardiomyopathy often have evidence of global diastolic dysfunction but preserved systolic function as reflected by a normal LV ejection fraction (EF).[2] Compared to LVEF, myocardial velocity, strain and strain rate (SR) analyses are more sensitive indices of LV function and have been demonstrated to be abnormal in diabetic patients.[3-8] However, these studies often included patients with diabetic complications or associated co-morbidities which may introduce important biases on LV functional evaluation.[3-8] Currently, there is no extensive information on the effects of diabetes mellitus on LV mechanics. Thus, we evaluated multidirectional LV myocardial systolic and diastolic functions in a group of truly uncomplicated, normotensive, diabetic patients using 2-dimensional (2D) speckle tracking echocardiography.

METHODS

Forty-seven patients with type 2 diabetes mellitus were recruited in this study. The inclusion and exclusion criteria for all the diabetic patients have previously been reported.[2] Briefly, women were not recruited to avoid possible confounding influences of gender and plasma estrogen levels on lipid metabolism and myocardial triglyceride accumulation. Inclusion criteria for all diabetic patients included: 1) Type 2 diabetes mellitus diagnosed according to World Health Organization criteria[9] and treated with sulfonylurea derivatives in stable doses, 2) HbA1c below 8.5%, and 3) resting blood pressure < 150/85 mmHg, with or without antihypertensive medication. In addition, as an inclusion criterion, the presence of myocardial ischemia was excluded in all patients by a negative high-dose dobutamine stress echocardiogram.[2] Exclusion criteria included known cardiovascular disease or diabetes related complications including proliferative retinopathy, autonomic neuropathy as excluded by Ewing's tests[10], and microalbuminuria as excluded by measurements of albumin/creatinine ratio in a urine sample.

Fifty-three male control subjects recruited were frequency matched for age, body mass index and body surface area (BSA). All control subjects had normal physical examinations and normal echocardiograms. Exclusion criteria for the control subjects included history of diabetes mellitus, smoking, hypertension and cardiomyopathy. The institutional ethics review board of the hospital approved the study and all subjects gave informed consent.

Transthoracic echocardiography was performed with the subjects at rest using commercially available ultrasound transducer and equipment (M3S probe, Vivid 7, GE-Vingmed, Horten, Norway). All images were digitally stored on hard disks for offline analysis (EchoPAC version 07.00, GE-Vingmed, Horten, Norway). A complete 2D, color, pulsed and continuous-wave Doppler echocardiogram was performed according to standard techniques.[11, 12] Left ventricular mass index was calculated from 2D echocardiographic measurements using the area-length formula at end-diastole [13], and corrected for BSA.[14] LV end-diastolic volume index (EDVI) and end-systolic volume index (ESVI) were calculated using Simpson's biplane method of discs and corrected for BSA. LVEF was calculated and expressed as a percentage.

Mitral inflow and pulmonary venous velocities were recorded using conventional pulsed-wave Doppler echocardiography in the apical 4 chamber view using a 2 mm sample volume. Transmitral early (E wave) and late (A wave) diastolic velocities as well as deceleration time were recorded at the mitral leaflet tips. LV isovolumic relaxation time was also recorded. The pulmonary venous peak systolic (S) and diastolic (D) velocities were recorded with the sample volume positioned 1 cm below the orifice of the right superior pulmonary vein in the left atrium. Septal E/E' ratio was determined using color-coded tissue Doppler imaging (frame rates > 100 frames/sec) with the sample volume placed in the basal septum.

2D speckle tracking analyses were performed on grey scale images of the LV obtained in the apical 2-, 3- and 4-chamber views and short-axis mid-ventricular views. Left ventricular radial and circumferential functions were determined in the mid-ventricular short-axis view, and longitudinal function was determined in the 3 apical views. During analysis, the endocardial border was manually traced at end-systole and the region of interest width adjusted to include the entire myocardium. The software then automatically tracks and accepts segments of good tracking quality and rejects poorly tracked segments, while allowing the observer to manually override its decisions based on visual assessments of tracking quality. Peak systolic strain, peak systolic SR (SR Sm) and peak early diastolic SR (SR Em) for the 3 orthogonal myocardial functions were determined. Mean global longitudinal strain/SR were calculated from the 3 individual apical global longitudinal strain/SR curves respectively whereas mean global circumferential strain/SR and mean radial strain/SR were obtained from the mid-ventricular short-axis view. All strain and SR measurements were exported to a spreadsheet (Microsoft ® Excel 2002, Microsoft Corporation, Redmond, WA).

To define intra- and inter-observer variability, strain and SR measurements were repeated for 10 randomly selected patients at least 4 weeks apart by the same observer on the same echocardiographic images, and by a second independent observer.

Statistical analysis

Continuous variables were presented as mean ± 1 SD unless otherwise stated. Unpaired Student's t test and Mann-Whitney U test were used to compare 2 groups of unpaired data of Gaussian and non-Gaussian distribution respectively. Multivariate linear regression analysis (enter method) was used to identify independent clinical determinants of LV strain/SR. To avoid multicolinearity between the univariate predictors, a tolerance of > 0.5 was set. Intra- and inter-observer variability of strain and SR measurements by 2D speckle tracking were expressed as mean absolute differences and assessed by Bland-Altman analysis.[15] A 2-tailed p value of < 0.05 was considered significant. All statistical analyses were performed using SPSS for Windows (SPSS Inc, Chicago), version 16.

RESULTS

The mean age, body mass index and body surface area were 57.1 ± 6.2 years, 27.0 ± 3.1 kg/m^2, and 2.07 ± 0.18 m^2 respectively, and there were no significant differences between diabetic patients and controls (Table 1). The median diabetes mellitus diagnosis duration was 4 years (range 1 to 11 years), and the mean HbA1c level was 6.4 ± 0.7%. Although there was no evidence of autonomic neuropathy in the patients as documented by Ewing's test, the mean heart rate and systolic blood pressure of the diabetic patients was increased relative to the controls.

Table 1. *Clinical Parameters in Patients with Diabetes and Healthy Subjects*

Variable	Patients with diabetes (n = 47)	Healthy subjects (n = 53)	p value
Demographics			
Age (years)	58.0 ± 5.5	56.2 ± 6.6	NS
Body mass index (kg/m^2)	27.6 ± 3.2	26.4 ± 3.0	NS
Body surface area (m^2)	2.10 ± 0.18	2.05 ± 0.18	NS
Mean heart rate (beats/min)	72.5 ± 10.5	65.8 ± 8.2	0.001
Systolic blood pressure (mmHg)	137 ± 11	128 ± 13	< 0.001
Medications			
Beta blockers (%)	2.1	-	-
Calcium channel antagonist (%)	6.4	-	-
Angiotensin converting enzyme inhibitors (%)	27.7	-	-
Angiotensin receptor blocker (%)	12.8	-	-

Table 2 outlines the echocardiographic parameters. There were no significant differences in the indexed LV volumes and EF between the diabetic patients and healthy controls. Transmitral E/A and pulmonary S/D ratios were significantly impaired in diabetic patients as compared to controls. There was also no significant difference in septal E/E' ratio between diabetic patients and healthy controls.

Table 2. *Echocardiographic Parameters in Patients with Diabetes and Healthy Subjects*

Variable	Patients with diabetes (n = 47)	Healthy subjects (n = 53)	p value
Left ventricular mass index (g/m^2)	87.4 ± 13.8	83.9 ± 15.6	NS
Left ventricular end-diastolic volume index (mL/m^2)	40.7 ± 8.9	44.1 ± 7.8	NS
Left ventricular end-systolic volume index (mL/m^2)	16.0 ± 4.8	17.8 ± 4.3	NS
Left ventricular ejection fraction (%)	61.0 ± 5.5	59.8 ± 5.3	NS
Doppler			
Transmitral E/A ratio	0.95 ± 0.21	1.12 ± 0.32	0.007
Deceleration time (ms)	192.2 ± 37.5	196.1 ± 39.3	NS
Isovolumic relaxation time (ms)	83.3 ± 13.9	84.6 ± 19.9	NS
Pulmonary S/D ratio	1.45 ± 0.28	1.25 ± 0.27	0.001
Septal E/E' ratio	9.21 ± 1.80	8.50 ± 1.96	NS
Longitudinal function			
Mean global strain (%)	-18.3 ± 2.2	-19.9 ± 1.9	< 0.001
Mean global systolic strain rate (s^{-1})	-0.99 ± 0.17	-1.07 ± 0.13	0.009
Mean global early diastolic strain rate (s^{-1})	1.04 ± 0.25	1.26 ± 0.26	< 0.001
Circumferential function			
Global strain (%)	-22.7 ± 2.9	-23.0 ± 3.2	NS
Global systolic strain rate (s^{-1})	-1.40 ± 0.28	-1.37 ± 0.23	NS
Global early diastolic strain rate (s^{-1})	1.79 ± 0.46	1.99 ± 0.61	NS
Radial function			
Mean strain (%)	40.6 ± 11.1	42.7 ± 12.1	NS
Mean systolic strain rate (s^{-1})	1.71 ± 0.45	1.80 ± 0.48	NS
Mean early diastolic strain rate (s^{-1})	-1.98 ± 0.57	-2.14 ± 0.70	NS

The mean frame rates for the apical and short-axis views were 82.3 ± 18.2 and 90.0 ± 19.5 frames/s respectively. Compared to healthy controls, diabetic patients had significantly impaired longitudinal systolic and diastolic strain and SR, but preserved circumferential and radial strains and SR (Table 2).

To investigate the independent clinical determinants of LV longitudinal strain, SR Sm and SR Em, multivariate linear regression analyses were performed with age, body mass index, mean heart rate, systolic blood pressure and presence of diabetes mellitus

entered as covariates (Table 3). The presence of diabetes mellitus was an independent correlate of longitudinal strain (multiple R = 0.496, p = 0.001), SR Sm (multiple R = 0.612, p < 0.001) and SR Em (multiple R = 0.552, p < 0.001) on all the linear regression models. Intra- and inter-observer variabilities for the myocardial strain and SR measurement were evaluated (Table 4). Assessments of LV longitudinal strain/SR had the lowest intra- and inter-observer measurement variability compared to assessments of circumferential and radial strains/SR. Bland and Altman analysis showed small biases with no significant trend for all the intra- and inter-observer strain and strain rate measurements.

Table 3. *Independent Correlates of Global Longitudinal Strain, Global Longitudinal Systolic Strain Rate, and Global Longitudinal Diastolic Strain Rate*

Variable	Global Longitudinal Strain		Global Longitudinal Systolic Strain Rate		Global Longitudinal Diastolic Strain Rate	
	β	p value	β	p value	β	p value
Age (years)	-0.216	0.052	-0.095	0.341	-0.129	0.223
Body mass index (kg/m^2)	0.118	0.272	0.129	0.189	-0.153	0.140
Mean heart rate (beats/min)	-0.232	0.038	-0.551	< 0.001	0.167	0.118
Systolic blood pressure (mmHg)	-0.055	0.638	-0.084	0.429	-0.053	0.637
Presence of diabetes	0.508	< 0.001	0.513	< 0.001	-0.477	< 0.001

Table 4. *Intra-observer and Inter-observer Variability of Left Ventricular Strain and Strain Rate Measurements*

Variable	Intra-observer Absolute Difference	Inter-observer Absolute Difference
Longitudinal function		
Mean global strain (%)	1.2 ± 0.5	0.9 ± 1.0
Mean global systolic strain rate (s^{-1})	0.10 ± 0.06	0.09 ± 0.08
Mean global early diastolic strain rate (s^{-1})	0.08 ± 0.05	0.13 ± 0.09
Circumferential function		
Global strain (%)	1.2 ± 1.0	2.3 ± 2.4
Global systolic strain rate (s^{-1})	0.08 ± 0.08	0.16 ± 0.09
Global early diastolic strain rate (s^{-1})	0.31 ± 0.27	0.39 ± 0.45
Radial function		
Mean strain (%)	4.3 ± 2.3	6.5 ± 5.4
Mean systolic strain rate (s^{-1})	0.27 ± 0.18	0.34 ± 0.24
Mean early diastolic strain rate (s^{-1})	0.37 ± 0.34	0.39 ± 0.23

DISCUSSION

The present study demonstrated the presence of subclinical myocardial systolic and diastolic dysfunctions in type 2 diabetic patients with no diabetic related complications and good glycemic control. Despite normal LV mass, volumes and EF, the diabetic population showed impairments of LV longitudinal strain and SR but preserved circumferential and radial strain and SR. The presence of diabetes mellitus was an independent predictor of LV longitudinal strain, systolic SR and diastolic SR on multiple linear regression analysis.

The pathogenesis of diabetic cardiomyopathy is likely to be multifactorial, ranging from microvascular disease, altered myocardial metabolism, and structural changes in the myocardium with increased fibrosis. Increasingly, evidence is emerging on the role of myocardial lipotoxic injury from lipid oversupply. Visceral adipose tissue insulin resistance leads to increased myocardial fatty acid delivery and uptake with associated myocardial triglyceride accumulation.[16, 17] It is assumed that the subsequent accumulation of fatty acid intermediates is associated with mitochondrial dysfunction, leading to cell damage, apoptosis, replacement with fibrosis and myocardial contractile dysfunction.[17] Recent studies have evaluated the relationship between increased myocardial steatosis and LV dysfunction in patients with type 2 diabetes mellitus.[2, 18] Rijzewijk et al demonstrated diastolic dysfunction in a group of uncomplicated diabetic patients with documented myocardial steatosis on magnetic resonance spectroscopy.[2] In contrast, McGavock et al showed no association between myocardial triglyceride accumulation and LV function in a heterogeneous group of diabetic patients.[18] Of note, their results could be influenced by the use of insulin (a lipogenic agent) and the presence of undiagnosed coronary artery disease in their patient population, whereas Rijzewijk et al excluded patients with potential confounding comorbid conditions such as hypertension and coronary artery disease (excluded by dobutamine stress echocardiography).[2, 18] Both studies demonstrated normal global systolic function as reflected by a normal LVEF. Similarly, the present study demonstrated the presence of diastolic dysfunction (indicated by significantly greater impairments of transmitral E/A and pulmonary S/D ratios) but preserved global LVEF in diabetic patients compared to normal controls.

Previous epidemiological studies have demonstrated increased prevalence of diabetes mellitus in heart failure populations, and this increased prevalence is seen particularly in heart failure patients with normal LVEF.[19] However, LVEF is a relatively insensitive measure of LV systolic function compared to strain and strain rate imaging, especially in the context of subclinical LV systolic dysfunction.[3-8] As the LV myocardial architecture is a complex array of longitudinally and circumferentially orientated fibres located predominately in the epicardium/endocardium and mid-wall respectively[20], multidirec-

tional analyses of longitudinal, circumferential and radial function allow understanding of regional LV myocardial functional changes in subclinical diabetic heart disease.

Both Fang et al and Vinereanu et al demonstrated decreased LV longitudinal function but compensatory increase in radial function in diabetic patients.[3, 4] However, due to the angle limitations associated with tissue Doppler imaging, both studies could only assess the impact of diabetes mellitus on LV longitudinal and radial functions in a few limited myocardial segments, and circumferential myocardial function was not evaluated. Using 2D speckle tracking to assess all myocardial segments, the present study demonstrated reduced longitudinal strain and SR (predominantly derived from epicardial/endocardial fibre contraction) but preserved circumferential and radial strains and SR (predominantly derived from mid-wall circumferential fibres contraction) in diabetic patients. This finding suggests that myocardial dysfunction in early diabetic cardiomyopathy may start in the subendocardium. On multivariate analysis, the presence of diabetes mellitus was an independent predictor of impaired longitudinal strain and SR in this unique group of truly uncomplicated type 2 diabetic patients.

CONCLUSION

The novel aspect of the current study is the multidirectional strain and SR analysis by 2D speckle tracking in patients with uncomplicated type 2 diabetes mellitus. The associated myocardial systolic and diastolic dysfunction detected on echocardiography was independent of age, body mass index and blood pressure. However, current 2D speckle tracking analysis cannot take into account “through plane” cardiac motion and that may influence the absolute strain/SR values. Furthermore, the exclusion of women in the study limits its generalizability. However, the widespread availability of echocardiography and ease of use with 2D speckle tracking may allow serial assessments of patients with diabetic heart disease and monitor disease progression.

REFERENCE LIST

(1) Boudina S, Abel ED. Diabetic cardiomyopathy revisited. *Circulation* 2007;115:3213-3223.

(2) Rijzewijk LJ, van der Meer RW, Smit JWA, Diamant M, Bax JJ, Hammer S, Romijn JA, De Roos A, Lamb HJ. Myocardial steatosis is an independent predictor of diastolic dysfunction in type 2 diabetes mellitus. *J Am Coll Cardiol* 2008;52:1793-1799.

(3) Fang ZY, Leano R, Marwick TH. Relationship between longitudinal and radial contractility in subclinical diabetic heart disease. *Clin Sci* 2004;106:53-60.

(4) Vinereanu D, Nicolaides E, Tweddel AC, Mädler CF, Holst B, Boden LE, Cinteza M, Rees AE, Fraser AG. Subclinical left ventricular dysfunction in asymptomatic patients with Type II diabetes mellitus, related to serum lipids and glycated haemoglobin. *Clin Sci* 2003;105:591-599.

(5) Moir S, Hanekom L, Fang ZY, Haluska B, Wong C, Burgess M, Marwick TH. Relationship between myocardial perfusion and dysfunction in diabetic cardiomyopathy: a study of quantitative contrast echocardiography and strain rate imaging. *Heart* 2006;92:1414-1419.

(6) Fang ZY, Schull-Meade R, Downey M, Prins J, Marwick TH. Determinants of subclinical diabetic heart disease. *Diabetologia* 2005;48:394-402.

(7) Fang ZY, Yuda S, Anderson V, Short L, Case C, Marwick TH. Echocardiographic detection of early diabetic myocardial disease. *J Am Coll Cardiol* 2003;41:611-617.

(8) Galderisi M, de Simone G, Innelli P, Turco A, Turco S, Capaldo B, Riccardi G, de Divitiis O. Impaired inotropic response in type 2 diabetes mellitus: a strain rate imaging study. *Am J Hypertens* 2007;20:548-555.

(9) Alberti KG, Zimmet PZ. Definition, diagnosis and classification of diabetes mellitus and its complications. Part 1: diagnosis and classification of diabetes mellitus provisional report of a WHO consultation. *Diabet Med* 1998;15:539-553.

(10) Ewing DJ, Martyn CN, Young RJ, Clarke BF. The value of cardiovascular autonomic function tests: 10 years experience in diabetes. *Diabetes Care* 1985;8:491-498.

(11) Nishimura R, Miller FJ, Callahan M, Benassi R, Seward J, Tajik A. Doppler echocardiography: theory, instrumentation technique and application. *Mayo Clin Proc* 1985;60:321-343.

(12) Tajik A, Seward J, Hagler D, Mair D, Lie J. Two dimensional real-time ultrasonic imaging of the heart and great vessels: technique, image orientation, structure identification and validation. *Mayo Clin Proc* 1978;53:271-303.

(13) Reichek N, Helak J, Plappert T, Sutton MS, Weber KT. Anatomic validation of left ventricular mass estimates from clinical two-dimensional echocardiography: initial results. *Circulation* 1983;67:348-352.

(14) Mosteller RD. Simplified calculation of body-surface area. *N Engl J Med* 1987;317:1098.

(15) Bland JM, Altman DG. Statistical methods for assessing agreement between two methods of clinical measurement. *Lancet* 1986;1:307-310.

(16) Unger RH. Lipotoxic Diseases. *Annu Rev Med* 2002;53:319.

(17) Watts GF, Marwick TH. Ventricular dysfunction in early diabetic heart disease: detection, mechanisms and significance. *Clin Sci* 2003;105:537-540.

(18) McGavock JM, Lingvay I, Zib I, Tillery T, Salas N, Unger R, Levine BD, Raskin P, Victor RG, Szczepaniak LS. Cardiac steatosis in diabetes mellitus: A 1H-magnetic resonance spectroscopy study. *Circulation* 2007;116:1170-1175.

(19) Redfield MM, Jacobsen SJ, Burnett JC, Jr., Mahoney DW, Bailey KR, Rodeheffer RJ. Burden of systolic and diastolic ventricular dysfunction in the community: appreciating the scope of the heart failure epidemic. *JAMA* 2003;289:194-202.

(20) Greenbaum RA, Ho SY, Gibson DG, Becker AE, Anderson RH. Left ventricular fibre architecture in man. *Br Heart J* 1981;45:248-263.

3

Impact of Diabetes and Increasing Body Mass Index Category on Left Ventricular Systolic and Diastolic Function

Arnold C.T. Ng, Francesca Prevedello, Giulia Dolci, Cornelis J. Roos, Roxana Djaberi, Matteo Bertini, See Hooi Ewe, Christine Allman, Dominic Y. Leung, Nina Ajmone Marsan, Victoria Delgado, Jeroen J. Bax

J Am Soc Echocardiogr. 2018;31(8):916-925

ABSTRACT

Background: Diabetes and obesity are both a world-wide growing epidemic, and both are independently associated with an increased risk for heart failure and death. We aimed at examining the additive detrimental effect of both diabetes and increasing body mass index (BMI) category on left ventricular (LV) myocardial systolic and diastolic functions.

Methods: The present retrospective multicenter study included 653 patients (337 type 2 diabetic and 316 non-diabetic) of increasing BMI category. All patients had normal LV ejection fraction. LV myocardial systolic (peak systolic global longitudinal strain, peak systolic global longitudinal strain rate) and diastolic (average mitral annular e' velocity and early diastolic global longitudinal strain rate) functions were quantified by echocardiography.

Results: Increasing BMI category was associated with progressively more impaired LV myocardial function in diabetic patients ($p < 0.001$). Diabetic patients had significantly more impaired LV myocardial function at all BMI categories compared to non-diabetic patients ($p < 0.001$). On multivariate analysis, both diabetes and obesity were independently associated with an additive detrimental effect on LV myocardial systolic and diastolic functions. However, obesity was associated with greater LV myocardial dysfunction than diabetes.

Conclusion: Both diabetes and increasing BMI category had an additive detrimental effect on LV myocardial systolic and diastolic functions. Furthermore, increasing BMI category was associated with greater LV myocardial dysfunction than diabetes. As they frequently coexist together, future studies on diabetic patients should also focus on obesity.

INTRODUCTION

There is currently a worldwide epidemic of obesity and type 2 diabetes. The latest projection by the World Health Organization estimated that globally in 2005, approximately 1.6 billion adults over the age of 15 years were overweight, and at least 400 million adults were obese (www.WHO.int). Due to the obesity epidemic, there is a concomitant increase in the prevalence of type 2 diabetes. In the year 2000, the World Health Organization estimated more than 170 million people worldwide had diabetes and the prevalence was projected to double in the next 20 years.[1] Both obesity and diabetes are independently associated with an increased risk of heart failure.[2] Although the pathophysiological mechanisms underlying obesity and diabetic cardiomyopathy are not identical, the combination of insulin resistance, hyperinsulinemia and hyperglycemia leads to inflammation, neurohormonal activation of the renin-angiotensin-aldosterone system, and eventual myocardial structural and functional changes.[3-8] Despite previous studies showing obesity to be an independent risk factor for subsequent development of diabetes and heart failure,[2, 9, 10] few have examined the simultaneous impact of increasing body mass index (BMI) category and concomitant diabetes on changes in left ventricular (LV) myocardial function. We hypothesized that both increasing BMI category and diabetes are independently associated with progressive impairment of LV myocardial systolic and diastolic functions, and that the association is additive and not synergistic. Thus, we conducted a multicenter retrospective study (Leiden University Medical Center, The Netherlands, and Liverpool Hospital, Australia) whereby both diabetic and non-diabetic patients without coronary artery disease were evaluated with the aim to:

1. examine the impact of increasing BMI category on LV myocardial systolic (peak systolic global longitudinal strain, peak systolic global longitudinal strain rate) and diastolic functions average mitral annular e' velocity and early diastolic global longitudinal strain rate) as quantified by echocardiography in type 2 diabetic patients;
2. compare LV myocardial systolic and diastolic functions with increasing BMI category between diabetic and non-diabetic patients; and
3. determine the independent and additive detrimental effect of increasing BMI category and diabetes on LV myocardial systolic and diastolic functions.

METHODS

Patient population

The overall patient population consisted of a mix of 653 patients recruited from 2 institutions (104 from Liverpool Hospital [Australia] and 549 from Leiden University Medical Center [The Netherlands]). All patients were identified over a 10 year period

from each Australian and Dutch departmental combined echocardiographic and clinical databases. Of these, 337 had type 2 diabetes, which was diagnosed according to World Health Organization criteria.[11] Although BMI does not take into account the wide variation in body fat distribution, it is the most useful population-level measure of obesity and is recommended by the World Health Organization to define overweight and obesity within a population and the risks associated with it.[12] Furthermore, several multicenter and epidemiology studies have demonstrated the independent prognostic value of BMI as a measure of general obesity for predicting all-cause mortality.[13-15] As there were only 2 diabetic patients with BMI < 20 kg/m^2 measured at the time of echocardiography, all 337 diabetic patients were divided into 3 categorical groups: 80 lean diabetics (BMI < 25 kg/m^2); 139 overweight diabetics (BMI 25 – 29.9 kg/m^2); and 118 obese diabetics (BMI ≥ 30kg/m^2).

Type 2 diabetic patients were compared against 316 non-diabetic patients of similar age, gender and BMI. All non-diabetic patients were clinically referred for assessment of LV and/or valvular function, and had structurally normal heart on echocardiography. Similarly, as there were only 5 non-diabetic patients with BMI < 20kg/m^2, all 316 non-diabetic patients were divided into 3 categorical groups: 89 lean non-diabetics (BMI < 25 kg/m^2); 134 overweight non-diabetics (BMI 25 – 29.9 kg/m^2); and 93 obese non-diabetics (BMI ≥ 30kg/m^2).

The exclusion criteria for all diabetic and non-diabetic patients included age < 18 years, rhythm other than sinus rhythm, LV ejection fraction (EF) < 50%, moderate or severe valvular stenosis or regurgitation, and congenital heart disease. To avoid coronary artery disease as a potential confounding factor for any changes observed in myocardial function, all patients with known significant underlying coronary artery disease, previous myocardial infarction, previous coronary artery bypass surgery or percutaneous coronary intervention, presence of segmental wall motion abnormalities on echocardiography, or positive stress testing were excluded.

All patients underwent a history, physical, biochemical, and transthoracic echocardiographic examination. Baseline biochemical analyses included hemoglobin level, glomerular filtration rate (GFR) calculated by the Modification of Diet in Renal Disease formula as recommended by the National Kidney Foundation, Kidney Disease Outcomes Quality Initiative Guidelines[16], and glycated hemoglobin (HbA1c) level. The definition of hypertension was different between diabetic and non-diabetic patients. In diabetic patients, the cut-off was > 130/80 mmHg on 2 separate occasions after > 5min of rest. In non-diabetic patients, the cut-off was > 140/90 mmHg on 2 separate occasions after

> 5min of rest. All clinical and biochemical variables were collected by an independent observer blinded to the echocardiographic results.

The impact of increasing BMI categories on LV structure (LV volumes, mass) and function were initially assessed in the type 2 diabetic patients. LV myocardial function within each BMI category (lean, overweight, obese) in the diabetic population were then compared against non-diabetic patients. Finally, to determine the independent and additive detrimental effect of increasing obesity and diabetes on LV myocardial function, multivariate analysis was performed with BMI categories and the presence/absence of diabetes entered as covariates, adjusted for baseline age, gender, systolic blood pressure, heart rate, LV mass and LV volume. Echocardiographic analyses for all diabetic and non-diabetic patients, including 2D speckle tracking, were performed offline. Therefore, the present evaluation does not tabulate the results summarized in clinical reports.

The institutional review boards approved the study. The institutional review board of the Leiden University Medical Center waived the need for patient written informed consent for retrospective analysis of clinically acquired data anonymously handled.

Echocardiography

Transthoracic echocardiography was performed in all subjects at rest using commercially available ultrasound systems (Vivid 7 and E9, GE-Vingmed, Horten, Norway). All images were digitally stored on hard disks for offline analysis (EchoPAC version 108.1.5, GE-Vingmed, Horten, Norway). A complete 2D, color, pulsed and continuous-wave Doppler echocardiogram was performed according to standard techniques.[17, 18] LV end-diastolic volume (EDV) and end-systolic volume (ESV) were calculated using the Simpson's biplane method of discs. LVEF was calculated and expressed as a percentage. LV mass was calculated from the formula as recommended by the American Society of Echocardiography.[19]

Transmitral inflow velocities were recorded using conventional pulsed-wave Doppler echocardiography in the apical 4-chamber view using a 2 mm sample volume. Transmitral early (E wave) and late (A wave) diastolic velocities as well as deceleration time were recorded at the mitral leaflet tips. Average mitral annular e' velocity and average E/e' ratio were obtained from the septal and lateral annulus as recommended by current guidelines.[20] Maximal left atrial volume was calculated using the Simpson's biplane method of discs in the 4- and 2-chamber views.

Myocardial functional assessment by 2D speckle tracking

Quantification of longitudinal myocardial function was performed using 2D speckle tracking echocardiography in the 3 apical (2-, 3- and 4 chamber) views. During image analysis, the LV endocardial border was manually traced at end-systole and the region of interest width adjusted to include the entire myocardium. The 2D speckle tracking software then automatically tracks the motion of LV myocardial segments throughout the entire cardiac cycle. LV myocardial segments of good tracking quality were automatically accepted for further analyses whereas poorly tracked segments were rejected, while simultaneously allowing the user to manually override the software's decisions based on visual assessments of tracking quality. From the 3 individual apical views, peak systolic global longitudinal strain, peak systolic global longitudinal strain rate and early diastolic global longitudinal strain rate were calculated.

Variability analysis

Intraobserver and interobserver measurement variabilities were performed in 20 randomly selected patients and expressed as mean absolute difference ± 1 standard deviation (SD). The respective intraobserver and interobserver measurement variabilities for peak systolic global longitudinal strain were 1.2 ± 0.6% and 1.2 ± 1.0%, peak systolic global longitudinal strain rate were 0.10 ± 0.06s^{-1} and 0.11 ± 0.08s^{-1}, and early diastolic global longitudinal strain rate were 0.09 ± 0.05s^{-1} and 0.16 ± 0.09s^{-1}.

Statistical analysis

All continuous variables were tested for Gaussian distribution as determined by Kolmogorov-Smirnov test. Continuous variables were presented as mean ± 1 SD and categorical variables were presented as frequencies and percentages. Unpaired Student's t-test was used to compare 2 independent groups of continuous variables and the Chi-square test with Yates' correction was used to compare categorical variables. To assess the univariable linear relationship between 2 variables: Pearson correlation was performed between 2 continuous variables, Spearman correlation was performed between 1 continuous variable and 1 ordinal variable (e.g. BMI categories), and point-biserial correlation was performed between 1 continuous and 1 dichotomous variable (e.g. gender and presence of diabetes categories).

One-way analysis of variance (ANOVA) was initially used to examine the influence of increasing BMI subgroup categories on LV myocardial function (peak systolic global longitudinal strain, peak systolic global longitudinal strain rate, average mitral annular e' velocities, average E/e' ratio and early diastolic global longitudinal strain rate) in type 2 diabetic patients. Next, factorial ANOVA was used to compare peak systolic global longitudinal strain, peak systolic global longitudinal strain rate, average mitral annular

e' velocities, average E/e' ratio and early diastolic global longitudinal strain rate changes with increasing BMI category between diabetic and non-diabetic patients. Finally, multiple linear regression analyses were used to determine the independent and additive detrimental effect of increasing BMI category and diabetes on peak systolic global longitudinal strain, peak systolic global longitudinal strain rate, average mitral annular e' velocities and early diastolic global longitudinal strain rate, with correction for baseline age, gender, systolic blood pressure, heart rate, LV mass and LVESV. Standardized coefficients were presented to demonstrate the relative contribution of each variable to the multivariable linear regression model. To avoid multicolinearity, a tolerance of > 0.5 was set. All post-hoc multiple pairwise comparisons were performed with Bonferroni corrections. A 2-tailed p value of < 0.05 was considered significant. All statistical analyses were performed using SPSS for Windows (SPSS Inc, Chicago), version 17.

RESULTS

Increasing BMI category in diabetic patients

Table 1 outlines the clinical, biochemical and echocardiographic characteristics of the entire cohort of type 2 diabetic patients, and the 3 diabetic groups categorized according to BMI category. The mean age was 57 ± 12 years, 63.2% men. With increasing BMI category, there were progressive increases in systolic (p by one-way ANOVA = 0.002) and diastolic (p by one-way ANOVA < 0.001) blood pressures, and higher HbA1c level (p by one-way ANOVA = 0.046).

On echocardiography, increasing BMI category was associated with LV structural changes with progressive increases in LVEDV, LVESV and LV mass. Assessment of LV systolic function showed that LVEF did not differ significantly across the diabetic BMI subgroups. However, increasing BMI category was significantly associated with progressively more impaired peak systolic global longitudinal strain (p by one-way ANOVA < 0.001). Multiple pairwise comparisons with Bonferroni corrections showed that peak systolic global longitudinal strain became increasingly more impaired with each increase in BMI category (both p < 0.001). Similarly, increasing BMI category was also significantly associated with progressively more impaired peak systolic global longitudinal strain rate (p by one-way ANOVA < 0.001), and multiple pairwise comparisons with Bonferroni corrections showed that peak systolic global longitudinal strain rate was significantly more impaired in overweight versus lean diabetic patients (p = 0.008), and in obese versus overweight diabetic patients (p = 0.003).

Assessment of LV diastolic function showed that increasing BMI category in the diabetic patients was significantly associated with progressive prolongation of transmitral deceleration time, and a non-significant trend towards worsening of transmitral E/A ratio. Increasing BMI category was also significantly associated with progressively more impaired average mitral annular e' velocity (p by one-way ANOVA < 0.001) and average E/e' ratio (p by one-way ANOVA = 0.004). Similarly, increasing BMI was significantly associated with progressively more impaired early diastolic global longitudinal strain rate (p by one-way ANOVA < 0.001). On multiple pairwise comparisons with Bonferroni corrections, early diastolic global longitudinal strain rate was significantly more impaired in overweight versus lean diabetic patients (p = 0.001), and in obese versus overweight diabetic patients (p = 0.004).

Table 1. *Clinical, biochemical and echocardiographic characteristics of diabetic patient population*

Variable	Total diabetic population (n = 337)	Lean diabetic BMI < 25 kg/m^2 (n = 80)	Overweight diabetic BMI 25–29.9 kg/m^2 (n = 139)	Obese diabetic BMI≥30 kg/m^2 (n = 118)	p value*
Clinical					
Age (years)	57 ± 12	56 ± 12	57 ± 12	56 ± 11	0.63
Male gender (%)	63.2	67.5	74.1	47.5	< 0.001
Height (cm)	173 ± 10	173 ± 10	172 ± 11	173 ± 10	0.83
Weight (kg)	84 ± 17	69 ± 10	81 ± 11	101 ± 15	< 0.001
BMI (kg/m^2)	28.9 ± 5.6	22.8 ± 1.5	27.2 ± 1.4	35.0 ± 4.4	< 0.001
Hypertension (%)	56.4	42.5	56.1	66.1	0.005
Hyperlipidemia (%)	51.0	40.0	54.0	55.1	0.076
Family history of ischemic heart disease (%)	15.7	20.0	16.5	11.9	0.29
Current smoker (%)	29.4	28.8	25.9	33.9	0.37
Systolic blood pressure (mmHg)	139 ± 20	134 ± 20	139 ± 19	144 ± 20	0.002
Diastolic blood pressure (mmHg)	81 ± 11	78 ± 11	81 ± 10	85 ± 11	< 0.001
Biochemical					
Hemoglobin (g/dL)	13.9 ± 1.6	13.6 ± 1.8	14.1 ± 1.5	13.9 ± 1.6	0.076
Glomerular filtration rate (mL/min/1.73m^2)	87.7 ± 26.9	85.2 ± 22.8	87.1 ± 27.7	90.2 ± 28.6	0.42
HbA1c (%)	7.3 ± 1.5	7.1 ± 1.4	7.2 ± 1.5	7.6 ± 1.4	0.046
Echocardiography					
Heart rate (beats/min)	74 ± 13	72 ± 13	74 ± 12	75 ± 14	0.20
Left ventricular end-diastolic volume (mL)	93 ± 24	88 ± 23	93 ± 25	98 ± 24	0.020
Left ventricular end-systolic volume (mL)	38 ± 12	36 ± 12	37 ± 12	40 ± 12	0.048
Left ventricular ejection fraction (%)	59 ± 5	59 ± 5	60 ± 5	59 ± 5	0.53
Left ventricular mass (g)	183 ± 49	161 ± 42	182 ± 47	200 ± 48	< 0.001

Table 1. *Clinical, biochemical and echocardiographic characteristics of diabetic patient population (continued)*

Variable	Total diabetic population (n = 337)	Lean diabetic BMI < 25 kg/m² (n = 80)	Overweight diabetic BMI 25–29.9 kg/m² (n = 139)	Obese diabetic BMI≥30 kg/m² (n = 118)	p value*
Transmitral E/A ratio	0.97 ± 0.32	1.04 ± 0.40	0.96 ± 0.28	0.94 ± 0.30	0.084
Deceleration time (msec)	198 ± 54	190 ± 58	192 ± 45	209 ± 58	0.016
Average mitral annular e' velocity (cm/s)	6.7 ± 2.0	7.5 ± 2.2	6.5 ± 1.9	6.3 ± 1.8	< 0.001
Average E/e' ratio	10.9 ± 5.3	9.5 ± 4.6	10.7 ± 4.1	12.1 ± 6.6	0.004
Maximal left atrial volume (mL)	58.5 ± 17.9	54.6 ± 14.7	57.3 ± 16.7	62.5 ± 20.3	0.006
Peak systolic global longitudinal strain (%)	-17.6 ± 2.3	-18.9 ± 2.2	-17.7 ± 1.9	-16.6 ± 2.3	< 0.001
Peak systolic global longitudinal strain rate (s^{-1})	-0.93 ± 0.16	-1.01 ± 0.17	-0.94 ± 0.14	-0.88 ± 0.16	< 0.001
Early diastolic global longitudinal strain rate (s^{-1})	0.99 ± 0.27	1.13 ± 0.28	1.00 ± 0.25	0.89 ± 0.25	< 0.001

* p value by one-way analysis of variance. BMI: body mass index; HbA1c: glycated hemoglobin.

Comparisons between diabetic and non-diabetic patients

Table 2 compares the clinical and echocardiographic characteristics of the diabetic patients versus non-diabetic patients. There were no significant differences in age, gender and BMI. Diabetic patients were more likely to have a positive history of hypertension and hyperlipidemia. However, there were no significant differences in systolic and diastolic blood pressure at the time of echocardiographic examination.

On echocardiography, there were no significant differences in LVEDV, LVESV and LV mass. Assessment of LV systolic function demonstrated that there was no significant difference in LVEF between diabetic and non-diabetic patients (59 ± 5 vs. 60 ± 5%, p = 0.40). However, diabetic patients had significantly more impaired peak systolic global longitudinal strain compared to non-diabetic patients (-17.6 ± 2.3 vs. -18.9 ± 2.4%, p < 0.001). Furthermore, diabetic patients had more impaired peak systolic global longitudinal strain than non-diabetic patients across all BMI subgroups (p by factorial ANOVA < 0.001), and there was no significant interaction between the presence of diabetes and BMI categories (p by factorial ANOVA = 0.31, Figure 1). Thus, lean diabetic patients had similar peak systolic global longitudinal strain as overweight non-diabetic patients (-18.9 ± 2.2 vs. -19.0 ± 2.2%, p > 0.99 with Bonferroni correction); overweight diabetic patients had similar peak systolic global longitudinal strain as obese non-diabetic patients (-17.7 ± 1.9 vs. -17.4 ± 2.3%, p = 0.70 with Bonferroni correction); and obese diabetic patients had the most impaired peak systolic global longitudinal strain (-16.6 ± 2.3%).

Table 2. *Comparison of clinical and echocardiographic characteristics between non-diabetic and diabetic patients*

Variable	Non-diabetic (n = 316)	Diabetic (n = 337)	p value
Clinical			
Age (years)	57 ± 14	57 ± 12	0.83
Male gender (%)	62.7	63.2	0.89
BMI (kg/m^2)	28.0 ± 4.9	28.9 ± 5.6	0.074
Lean (%) (BMI < 25kg/m^2)	28.2	23.8	0.24
Overweight (%) (BMI 25–29.9 kg/m^2)	42.4	41.2	-
Obese (%) (BMI≥30 kg/m^2)	29.4	35.0	-
Hypertension (%)	27.5	56.4	< 0.001
Hyperlipidemia (%)	14.2	51.0	< 0.001
Current smoker (%)	11.4	15.7	0.11
Systolic BP (mmHg)	136 ± 24	139 ± 20	0.08
Diastolic BP (mmHg)	82 ± 12	81 ± 11	0.29
Echocardiography			
Heart rate (beats/min)	71 ± 13	74 ± 13	0.010
Left ventricular end-diastolic volume (mL)	95 ± 25	93 ± 24	0.30
Left ventricular end-systolic volume (mL)	39 ± 12	38 ± 12	0.57
Left ventricular ejection fraction (%)	60 ± 5	59 ± 5	0.40
Left ventricular mass (g)	183 ± 51	183 ± 49	0.94
Transmitral E/A ratio	1.10 ± 0.47	0.97 ± 0.32	< 0.001
Deceleration time (msec)	212 ± 60	198 ± 54	0.001
Average mitral annular e' velocity (cm/s)	7.5 ± 2.5	6.7 ± 2.0	< 0.001
Average E/e' ratio	10.2 ± 4.1	10.9 ± 5.3	0.06
Maximal left atrial volume (mL)	59.4 ± 21.3	58.5 ± 17.9	0.56
Peak systolic global longitudinal strain (%)	-18.9 ± 2.4	-17.6 ± 2.3	< 0.001
Peak systolic global longitudinal strain rate (s^{-1})	-0.99 ± 0.16	-0.93 ± 0.16	< 0.001
Early diastolic global longitudinal strain rate (s^{-1})	1.15 ± 0.32	0.99 ± 0.27	< 0.001

BMI: body mass index

Similarly, diabetic patients had more impaired peak systolic global longitudinal strain rate than non-diabetic patients across all BMI subgroups (p by factorial ANOVA < 0.001), and there was no significant interaction between the presence of diabetes and BMI categories (p by factorial ANOVA = 0.67, Figure 2). Thus, lean diabetic patients had similar peak systolic global longitudinal strain rate as overweight non-diabetic patients (-1.01 ± 0.17 vs. -0.98 ± 0.16s^{-1}, p = 0.68 with Bonferroni correction); overweight diabetic patients had similar peak systolic global longitudinal strain rate as obese non-diabetic patients (-0.94 ± 0.14 vs. -0.92 ± 0.15s^{-1}, p = 0.80 with Bonferroni correction); and obese diabetic patients had the most impaired peak systolic global longitudinal strain rate (-0.88 ± 0.16s^{-1}).

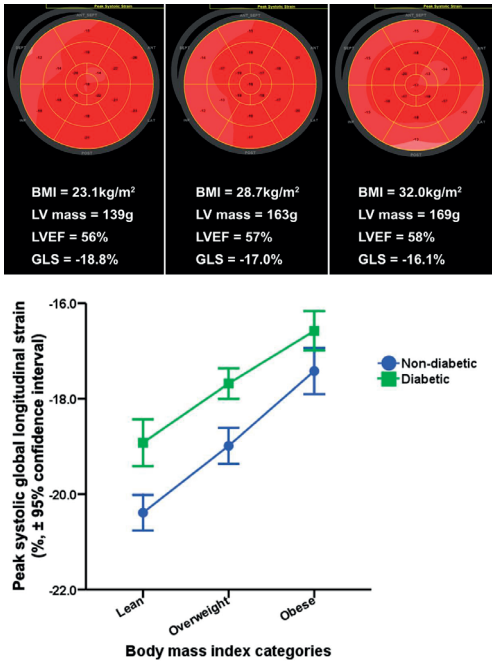


Figure 1. *Comparisons of peak systolic global longitudinal strain in diabetic versus non-diabetic patients across body mass index (BMI) categories. Increasing BMI was associated with progressive impairment of peak systolic global longitudinal strain. Furthermore, diabetic patients had more impaired peak systolic global longitudinal strain across all BMI categories.*

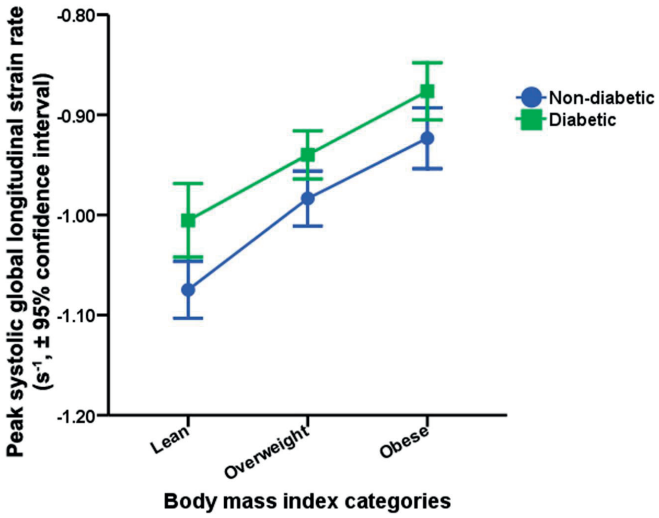


Figure 2. *Comparisons of peak systolic global longitudinal strain rate in diabetic versus non-diabetic patients across body mass index (BMI) categories. Increasing BMI was associated with progressive impairment of peak systolic global longitudinal strain rate. Diabetic patients had more impaired peak systolic global longitudinal strain across all BMI categories.*

On assessment of LV diastolic function, diabetic patients had more impaired LV diastolic function as measured by average mitral annular e' velocity (6.7 ± 2.0 vs. 7.5 ± 2.5cm/s, p < 0.001), and across all BMI categories (p by factorial ANOVA < 0.001, Figure 3). There was no significant interaction between the presence of diabetes and BMI categories in average mitral annular e' velocity (p by factorial ANOVA = 0.63). As shown in Figure 3, lean diabetic patients had similar average mitral annular e' velocity as overweight non-diabetic patients (7.5 ± 2.2 vs. 7.3 ± 2.8cm/s, p > 0.99 with Bonferroni correction); overweight diabetic patients had similar peak systolic global longitudinal strain rate as obese non-diabetic patients (6.5 ± 1.9 vs. 6.8 ± 2.0cm/s, p = 0.56 with Bonferroni correction); and obese diabetic patients had the most impaired peak systolic global longitudinal strain rate (6.3 ± 1.8cm/s).

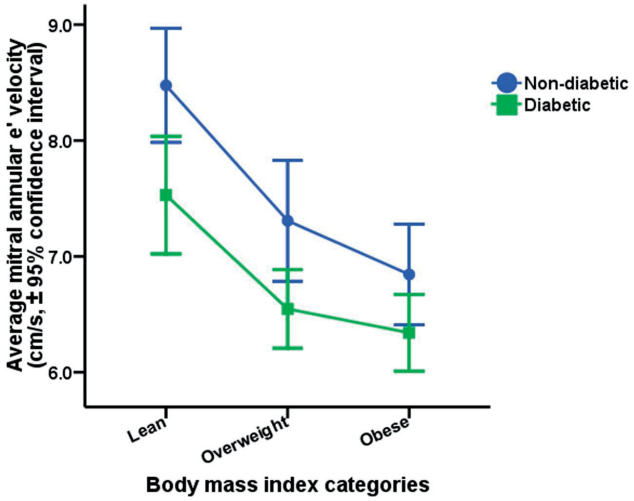


Figure 3. *Comparisons of average mitral annular e' velocity in diabetic versus non-diabetic patients across body mass index (BMI) categories. Increasing BMI was associated with progressive impairment of average mitral annular e' velocity. Diabetic patients had more impaired average mitral annular e' velocity across all BMI categories.*

In contrast, there was no significant difference in the assessment of LV filling pressure between diabetic and non-diabetic patients as quantified by average E/e' ratio in diabetic patients (10.9 ± 5.3 vs. 10.2 ± 4.1, p = 0.06).

Finally, diabetic patients also had more impaired early diastolic global longitudinal strain rate than non-diabetic patients across all BMI categories (p by factorial ANOVA < 0.001). Interestingly, there was a significant interaction between presence of diabetes and increasing BMI categories (p by factorial ANOVA = 0.005). Evaluation of Figure 4 demonstrated that non-diabetic patients had a greater initial decline in early diastolic

global longitudinal strain rate from normal weight to overweight compared to diabetic patients. Similarly, lean diabetic patients had similar early diastolic global longitudinal strain rate as overweight non-diabetic patients (1.13 ± 0.28 vs. 1.11 ± 0.29s^{-1}, p > 0.99 with Bonferroni correction); overweight diabetic patients had similar early diastolic global longitudinal strain rate as obese non-diabetic patients (1.00 ± 0.25 vs. 0.99 ± 0.26s^{-1}, p > 0.99 with Bonferroni correction); and obese diabetic patients had the most impaired early diastolic global longitudinal strain rate (0.89 ± 0.25s^{-1}).

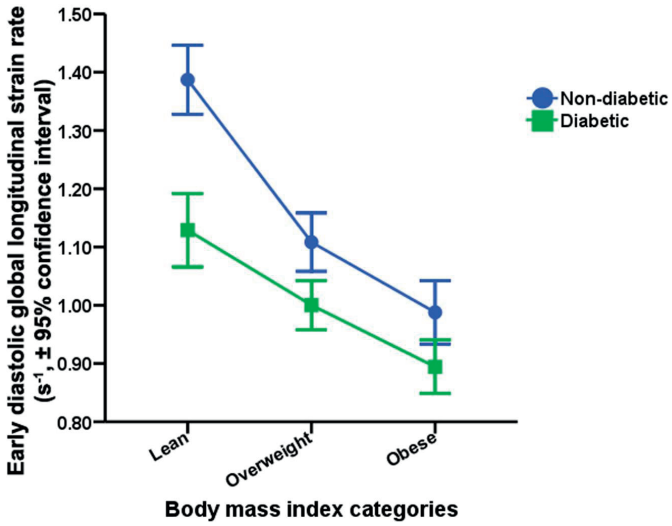


Figure 4. *Comparisons of early diastolic global longitudinal strain rate in diabetic versus non-diabetic patients across body mass index (BMI) categories. Increasing BMI was associated with progressive impairment of early diastolic global longitudinal strain rate. Diabetic patients had more impaired early diastolic global longitudinal strain across all BMI categories. However, non-diabetic patients with a normal BMI had a greater decline in early diastolic global longitudinal strain rate with increasing BMI.*

Diabetes, obesity and myocardial dysfunction

To examine the independent and additive detrimental effect of both increasing obesity and diabetes on peak systolic global longitudinal strain, peak systolic global longitudinal strain rate, average mitral annular e' velocity and early diastolic global longitudinal strain rate, multiple linear regression analyses were performed with the presence of diabetes and BMI categories entered as covariates, corrected for baseline age, gender, systolic blood pressure, heart rate, LV mass and LVESV.

Table 3 shows that both increasing BMI category and the presence of diabetes were independently associated with peak systolic global longitudinal strain (model R = 0.56, p < 0.001). Furthermore, increasing BMI (standardized beta = 0.379, p < 0.001) was associated with greater LV myocardial dysfunction than diabetes (standardized beta = 0.231, p

< 0.001). There was no significant interaction between the presence of diabetes and increasing obesity, suggesting an additive (not synergistic) detrimental effect of diabetes and obesity on LV myocardial function. Similar results were also obtained when BMI was modeled as a continuous variable (standardized beta = 0.355, p < 0.001), when systolic blood pressure was substituted by diastolic blood pressure or history of hypertension, or when all hypertensive patients were excluded from the multivariate analysis.

Table 3. *Independent determinants of left ventricular peak systolic global longitudinal strain*

Variable	Peak systolic global longitudinal strain			
	*Univariable r	p value	Standardized β	p value
Age	-0.027	0.49	0.027	0.49
Male gender	0.063	0.11	0.063	0.087
Systolic blood pressure	0.124	0.002	-0.022	0.55
Heart rate	0.196	< 0.001	0.190	< 0.001
Left ventricular mass	0.200	< 0.001	-0.035	0.41
Left ventricular end-systolic volume	0.265	< 0.001	0.246	< 0.001
Presence of diabetes	0.274	< 0.001	0.231	< 0.001
BMI categories	0.434	< 0.001	0.379	< 0.001

BMI: body mass index. *Pearson correlation performed for 2 continuous variables, Spearman correlation performed for 1 continuous variable and 1 ordinal variable (i.e. BMI categories), and point-biserial correlation performed for 1 continuous variable and 1 dichotomous variable (i.e. gender, presence of diabetes).

Table 4 shows the multivariable regression analysis for peak systolic global longitudinal strain rate (model R = 0.53, p < 0.001). Similarly, increasing BMI category (standardized beta = 0.285, p < 0.001) was associated with greater LV myocardial dysfunction by peak systolic global longitudinal strain rate compared to the presence of diabetes (standard-

Table 4. *Independent determinants of left ventricular peak systolic global longitudinal strain rate*

Variable	Peak systolic global longitudinal strain rate			
	*Univariable r	p value	Standardized β	p value
Age	-0.019	0.63	0.060	0.13
Male gender	-0.118	0.003	-0.177	< 0.001
Systolic blood pressure	0.088	0.027	0.014	0.72
Heart rate	-0.199	< 0.001	-0.202	< 0.001
Left ventricular mass	0.145	< 0.001	-0.069	0.12
Left ventricular end-systolic volume	0.324	< 0.001	0.332	< 0.001
Presence of diabetes	0.179	< 0.001	0.180	< 0.001
BMI categories	0.352	< 0.001	0.285	< 0.001

BMI: body mass index. *Pearson correlation performed for 2 continuous variables, Spearman correlation performed for 1 continuous variable and 1 ordinal variable (i.e. BMI categories), and point-biserial correlation performed for 1 continuous variable and 1 dichotomous variable (i.e. gender, presence of diabetes).

ized beta = 0.180, p < 0.001). Similar results were also obtained when BMI was modeled as a continuous variable (standardized beta = 0.247, p < 0.001).

Table 5 shows the multivariable regression analysis for average mitral annular e' velocity (model R = 0.68, p < 0.001). Increasing BMI (standardized beta = -0.157, p < 0.001) was associated with greater LV diastolic dysfunction by average mitral annular e' velocity compared to the presence of diabetes (standardized beta = -0.146, p < 0.001).

Table 5. *Independent determinants of average mitral annular e' velocity*

Variable	Average mitral annular e' velocity			
	*Univariable r	p value	Standardized β	p value
Age	-0.591	< 0.001	-0.520	< 0.001
Male gender	0.069	0.09	0.043	0.21
Systolic blood pressure	-0.367	< 0.001	-0.078	0.027
Heart rate	-0.165	< 0.001	-0.105	0.001
Left ventricular mass	-0.240	< 0.001	-0.103	0.010
Left ventricular end-systolic volume	0.167	< 0.001	0.080	0.034
Presence of diabetes	-0.175	< 0.001	-0.146	< 0.001
BMI categories	-0.238	< 0.001	-0.157	< 0.001

BMI: body mass index. *Pearson correlation performed for 2 continuous variables, Spearman correlation performed for 1 continuous variable and 1 ordinal variable (i.e. BMI categories), and point-biserial correlation performed for 1 continuous variable and 1 dichotomous variable (i.e. gender, presence of diabetes).

Finally, Table 6 shows the multivariable regression analysis for early diastolic global longitudinal strain rate (model R = 0.64, p < 0.001). Increasing BMI category (standardized beta = -0.337, p < 0.001) was associated with greater LV myocardial dysfunction by early diastolic global longitudinal strain rate compared to the presence of diabetes (standard-

Table 6. *Independent determinants of left ventricular early diastolic global longitudinal strain rate*

Variable	Early diastolic global longitudinal strain rate			
	*Univariable r	p value	Standardized β	p value
Age	-0.400	< 0.001	-0.399	< 0.001
Male gender	-0.068	0.08	-0.071	0.039
Systolic blood pressure	-0.298	< 0.001	-0.020	0.56
Heart rate	-0.128	0.001	-0.098	0.002
Left ventricular mass	-0.313	< 0.001	-0.043	0.28
Left ventricular end-systolic volume	-0.095	0.015	-0.119	0.002
Presence of diabetes	-0.257	< 0.001	-0.230	< 0.001
BMI categories	-0.392	< 0.001	-0.337	< 0.001

BMI: body mass index. *Pearson correlation performed for 2 continuous variables, Spearman correlation performed for 1 continuous variable and 1 ordinal variable (i.e. BMI categories), and point-biserial correlation performed for 1 continuous variable and 1 dichotomous variable (i.e. gender, presence of diabetes).

ized beta = -0.230, $p < 0.001$). Finally, similar results were also obtained when BMI was modeled as a continuous variable (standardized beta = -0.297, $p < 0.001$).

DISCUSSION

The present multicenter observational study demonstrated that increasing BMI category was associated with progressive and detrimental changes in LV structure, systolic and diastolic functions in diabetic patients. Compared to non-diabetic patients of similar age, gender and BMI, diabetic patients had more impaired LV function at all categories of BMI. Multivariate analysis showed that both increasing BMI category and diabetes were independent predictors of impaired LV myocardial systolic and diastolic functions despite preserved LVEF. Furthermore, both diabetes and increasing BMI category had an additive detrimental effect on LV myocardial function, and increasing BMI was a stronger determinant of impaired LV myocardial function than diabetes.

Pathogenesis of diabetic and obesity cardiomyopathy

Various mechanisms underlie the etiology of diabetic cardiomyopathy, including processes such as altered myocardial metabolism with subsequent steatosis and lipotoxicity, endothelial dysfunction with microvascular disease, autonomic neuropathy, altered myocardial structure with fibrosis and atherosclerosis.[21-26] Often, these processes act together and result in myocardial hypertrophy, increased interstitial fibrosis with increased LV stiffness, and manifesting as diastolic dysfunction in early diabetic heart disease.[5] Over time, there is progressive loss of myocardial contractile function resulting in global LV systolic dysfunction.

Recent large epidemiological studies had unequivocally demonstrated increased all-cause mortality in patients with higher levels of BMI.[15, 27] Furthermore, increasingly obese patients had progressively higher cardiovascular mortality.[15] Compared to diabetic cardiomyopathy, obesity cardiomyopathy is a clinically less well-recognized phenomenon. Obesity cardiomyopathy is characterized by a variety of cardiac structural and hemodynamic changes.[6] Previous studies have shown that obese patients have larger LV chamber sizes and increased hypertrophy compared to their lean counterparts.[28-31] These cardiac structural changes are associated with changes in cardiovascular hemodynamics, including an increased total blood volume, cardiac output and reduced systemic vascular resistance.[6, 32] Although it has been suggested that the association between obesity and incident heart failure may be secondary to these hemodynamic and cardiac structural changes[6], recent evidence suggests that the relationship may be mediated by obesity-related metabolic, inflammatory and neurohormonal changes.[2, 7, 8]

The presence of obesity-related insulin resistance, systemic vascular and adipose tissue inflammation, increased free fatty acid delivery, and activation of the renin-angiotensin-aldosterone system all contribute to atherosclerosis, myocardial hypertrophy, increased interstitial fibrosis and subsequent myocardial dysfunction.[2, 7, 8, 29]

Although the underlying pathogenesis of diabetic and obesity cardiomyopathy may not be identical, the final common pathway appears to be an increased interstitial fibrosis followed by initial myocardial diastolic dysfunction and eventually systolic dysfunction. However, few studies to date have evaluated the combined detrimental effects of both diabetes and obesity on LV function. In the present study, both diabetes and increasing BMI category were associated with LV myocardial systolic and diastolic dysfunction. Figure 4 demonstrated that non-diabetic patients had a greater initial decline in early diastolic global longitudinal strain rate from normal weight to overweight compared to diabetic patients. This suggests that early diastolic global longitudinal strain rate is most sensitive to the detrimental LV myocardial functional changes secondary to diabetes or increasing BMI, and is in agreement with the pathophysiological process of diastolic dysfunction occurring before systolic dysfunction.

Diabetes, obesity and myocardial dysfunction

Numerous echocardiographic studies examining diabetes have demonstrated the presence of both LV diastolic and systolic dysfunction compared to normal controls.[33-35] Similarly, studies on non-diabetic obese subjects have also demonstrated LV diastolic and systolic dysfunction compared to lean controls.[29, 30, 36] Although diabetes and obesity frequently co-exist together,[37] few studies to date have evaluated the combined impact of both diabetes and obesity on LV function.[38, 39] Kuperstein and co-workers recruited a large number of predominately obese subjects and demonstrated a synergistic effect of obesity and diabetes on LV mass.[38] However, the study was confounded by the small number of diabetic patients (6% of the total study population) and that all of the obese diabetic patients were women.[38] Furthermore, the combined impact of diabetes and obesity on LV function in their study was unknown. Di Stante and co-workers demonstrated LV diastolic dysfunction in 40 obese diabetic patients compared to 93 obese non-diabetic patients.[39] However, the impact of increasing obesity on LV dysfunction was not evaluated, and multivariate analysis identifying independent determinants of LV dysfunction was not performed.

In contrast, the present study is the largest to date evaluating the combined impact of diabetes and increasing BMI category on LV myocardial function. Both diabetes and increasing BMI were independent determinants of LV myocardial dysfunction. Furthermore, both increasing BMI and obesity had an additive detrimental effect on LV

myocardial function, and increasing BMI was associated with a greater impairment of LV myocardial function than diabetes. This was demonstrated in the standardized beta coefficients that demonstrated increasing BMI had a greater relative contribution to the multiple linear regression models than the presence of diabetes, despite similar p values. Importantly, the present study excluded all patients with known or suspected significant underlying coronary artery disease. Therefore, it was unlikely that the presence of undiagnosed significant coronary artery disease could have significantly influenced the results. Similarly, although increasing BMI and diabetes were associated with a higher incidence of hypertension, the independent associations between diabetes, obesity and myocardial dysfunction were still significant despite adjusting for differences in systolic blood pressure on multivariate analysis. Similar results were also obtained when systolic blood pressure was substituted by diastolic blood pressure or history of hypertension, or when all hypertensive patients were excluded from analysis.

Study Limitations

As the present study was a cross-sectional analysis on the effects of diabetes and BMI on myocardial function, there were no longitudinal follow-up clinical outcome data. Similarly, there was no information on the influences of weight loss and intensity of diabetic control on myocardial function. Finally, there was a potential enrolment/selection bias as clinical patients were referred for a clinical echocardiogram, thereby possibly increasing the incidence of subclinical myocardial dysfunction despite a normal LVEF.

Clinical implications

Both obesity and diabetes are world-wide growing epidemics. Previous epidemiological studies demonstrated that both diabetes and obesity were independent risk factors for the development of heart failure.[9, 13, 40, 41] These studies have shown that diabetes and obesity were each associated with an approximately 2-fold increased risk of heart failure.[9, 13, 41] However, these studies generally examined the prognostic impact of diabetes and obesity separately. The present study demonstrated that diabetes and obesity was independently associated with an additive detrimental effect on LV myocardial function, and increasing obesity was associated with greater LV myocardial dysfunction than diabetes. Thus, future clinical studies on diabetic patients should also focus on the frequently associated obesity problem in this patient population.

CONCLUSION

Both diabetes and obesity were independently associated with an additive detrimental effect on LV myocardial function. Furthermore, increasing BMI category was associated with greater LV myocardial dysfunction than diabetes. Therapies aiming at reducing cardiac morbidity and mortality in diabetic patients should also focus on weight reduction.

REFERENCE LIST

(1) Boudina S, Abel ED. Diabetic Cardiomyopathy Revisited. *Circulation* 2007;115:3213-3223.

(2) Rijzewijk LJ, van der Meer RW, Smit JWA, Diamant M, Bax JJ, Hammer S, Romijn JA, De Roos A, Lamb HJ. Myocardial Steatosis Is an Independent Predictor of Diastolic Dysfunction in Type 2 Diabetes Mellitus. *J Am Coll Cardiol* 2008;52:1793-1799.

(3) Fang ZY, Leano R, Marwick TH. Relationship between longitudinal and radial contractility in subclinical diabetic heart disease. *Clin Sci* 2004;106:53-60.

(4) Vinereanu D, Nicolaides E, Tweddel AC, Mädler CF, Holst B, Boden LE, Cinteza M, Rees AE, Fraser AG. Subclinical left ventricular dysfunction in asymptomatic patients with Type II diabetes mellitus, related to serum lipids and glycated haemoglobin. *Clin Sci* 2003;105:591-599.

(5) Moir S, Hanekom L, Fang ZY, Haluska B, Wong C, Burgess M, Marwick TH. Relationship between myocardial perfusion and dysfunction in diabetic cardiomyopathy: a study of quantitative contrast echocardiography and strain rate imaging. *Heart* 2006;92:1414-1419.

(6) Fang ZY, Schull-Meade R, Downey M, Prins J, Marwick TH. Determinants of subclinical diabetic heart disease. *Diabetologia* 2005;48:394-402.

(7) Fang ZY, Yuda S, Anderson V, Short L, Case C, Marwick TH. Echocardiographic detection of early diabetic myocardial disease. *J Am Coll Cardiol* 2003;41:611-617.

(8) Galderisi M, de Simone G, Innelli P, Turco A, Turco S, Capaldo B, Riccardi G, de Divitiis O. Impaired Inotropic Response in Type 2 Diabetes Mellitus: A Strain Rate Imaging Study. *Am J Hypertens* 2007;20:548-555.

(9) Alberti KG, Zimmet PZ. Definition, diagnosis and classification of diabetes mellitus and its complications. Part 1: diagnosis and classification of diabetes mellitus provisional report of a WHO consultation. *Diabet Med* 1998;15:539-553.

(10) Ewing DJ, Martyn CN, Young RJ, Clarke BF. The value of cardiovascular autonomic function tests: 10 years experience in diabetes. *Diabetes Care* 1985;8:491-498.

(11) Nishimura R, Miller FJ, Callahan M, Benassi R, Seward J, Tajik A. Doppler echocardiography: theory, instrumentation technique and application. *Mayo Clin Proc* 1985;60:321-343.

(12) Tajik A, Seward J, Hagler D, Mair D, Lie J. Two dimensional real-time ultrasonic imaging of the heart and great vessels: technique, image orientation, structure identification and validation. *Mayo Clin Proc* 1978;53:271-303.

(13) Reichek N, Helak J, Plappert T, Sutton MS, Weber KT. Anatomic validation of left ventricular mass estimates from clinical two-dimensional echocardiography: initial results. *Circulation* 1983;67:348-352.

(14) Mosteller RD. Simplified calculation of body-surface area. *N Engl J Med* 1987;317:1098.

(15) Bland JM, Altman DG. Statistical methods for assessing agreement between two methods of clinical measurement. *Lancet* 1986;1:307-310.

(16) Unger RH. Lipotoxic Diseases. *Annu Rev Med* 2002;53:319.

(17) Watts GF, Marwick TH. Ventricular dysfunction in early diabetic heart disease: detection, mechanisms and significance. *Clin Sci* 2003;105:537-540.

(18) McGavock JM, Lingvay I, Zib I, Tillery T, Salas N, Unger R, Levine BD, Raskin P, Victor RG, Szczepaniak LS. Cardiac Steatosis in Diabetes Mellitus: A 1H-Magnetic Resonance Spectroscopy Study. *Circulation* 2007;116:1170-1175.

(19) Redfield MM, Jacobsen SJ, Burnett JC, Jr., Mahoney DW, Bailey KR, Rodeheffer RJ. Burden of Systolic and Diastolic Ventricular Dysfunction in the Community: Appreciating the Scope of the Heart Failure Epidemic. *JAMA* 2003;289:194-202.

(20) Greenbaum RA, Ho SY, Gibson DG, Becker AE, Anderson RH. Left ventricular fibre architecture in man. *Br Heart J* 1981;45:248-263.

4

Myocardial Steatosis and Biventricular Strain and Strain Rate Imaging in Patients with Type 2 Diabetes Mellitus

Arnold C.T. Ng, Victoria Delgado, Matteo Bertini, Rutger W. van der Meer, Luuk J. Rijzewijk, See Hooi Ewe, Hans-Marc Siebelink, Johannes W.A. Smit, Michaela Diamant, Johannes A. Romijn, Albert de Roos, Dominic Y Leung, Hildo J. Lamb, Jeroen J. Bax

Circulation. 2010;122(24):2538-44

ABSTRACT

Background: Magnetic resonance (MR) spectroscopy can quantify myocardial triglyceride content in type 2 diabetic patients. Its relation to alterations in left and right ventricular (LV/RV) myocardial functions is unknown.

Methods: A total of 42 men with type 2 diabetes were recruited. Exclusion criteria included HbA1c > 8.5%, known cardiovascular disease or diabetes-related complications, blood pressure > 150/85 mmHg. Myocardial ischemia was excluded by a negative dobutamine stress test. LV and RV volumes and ejection fraction (EF) were quantified by magnetic resonance imaging. LV global longitudinal and RV free wall longitudinal strain, systolic strain rate (SR) and diastolic SR were quantified by echocardiographic speckle tracking analyses. Myocardial triglyceride content was quantified by MR spectroscopy and dichotomized based on the median value of 0.76%.

Results: The median age was 59 years (25th and 75th percentiles [54, 62 years]). Median diabetes diagnosis duration was 4 years, and median glycated hemoglobin level was 6.2% (5.9, 6.8%). There were no differences in LV and RV end-diastolic and end-systolic volume indices and EF between patients with high (≥ 0.76%) versus low (< 0.76%) myocardial triglyceride content. However, patients with high myocardial triglyceride content had greater impairment of LV and RV myocardial strain and strain rate. The myocardial triglyceride content was an independent correlate of LV and RV longitudinal strain, systolic SR and diastolic SR.

Conclusions: High myocardial triglyceride content is associated with more pronounced impairment of LV and RV functions in men with uncomplicated type 2 diabetes.

INTRODUCTION

The etiological mechanisms underlying diabetic heart disease are likely to be multifactorial, ranging from altered myocardial metabolism, endothelial dysfunction, microvascular disease, autonomic neuropathy, and altered myocardial structure with fibrosis.[1] Increasingly, evidence is emerging on the role of altered myocardial metabolism with subsequent lipotoxic injury from lipid oversupply. Recent studies have evaluated the role of myocardial triglyceride accumulation (steatosis) and diastolic dysfunction in patients with type 2 diabetes.[2,3] Although differences in transmitral flow patterns indicative of diastolic dysfunction were seen in diabetics compared to normal controls, there was no significant difference in global systolic function as determined by ejection fraction (EF).[2,3] In contrast, strain and strain rate (SR) imaging are more sensitive indices of myocardial function and have been shown to be impaired in diabetic patients.[4-10] However, no studies to date have evaluated the relationship between myocardial triglyceride content and both left (LV) and right ventricular (RV) myocardial functions. Therefore, the aim of the present study was to relate myocardial triglyceride content as determined by magnetic resonance (MR) spectroscopy, with biventricular myocardial strain and SR as determined by echocardiographic 2-dimensional (2D) speckle tracking analysis.

METHODS

Patient sample

The original PIRAMID (Pioglitazone Influence on tRiglyceride Accumulation in the Myocardium In Diabetes) trial included a total of 78 diabetic patients recruited from 2 centers (Leiden University Medical Center, Leiden, and VU University Medical Center, Amsterdam, The Netherlands).[11] The present study only included 42 diabetic patients who underwent a comprehensive MR (including spectroscopy) and echocardiographic examination at baseline from a single center (Leiden University Medical Center, Leiden, The Netherlands).

The inclusion and exclusion criteria have previously been reported.[11] Briefly, only male diabetics were recruited to avoid possible confounding influences of female gender and plasma estrogen levels on lipid metabolism and myocardial triglyceride accumulation. Inclusion criteria included: 1) Type 2 diabetes mellitus diagnosed according to World Health Organization criteria[12] and treated with sulfonylurea derivatives in stable doses, 2) glycated hemoglobin level between 6.5% to 8.5%, and 3) resting blood pressure < 150/85 mmHg, with or without antihypertensive medication. In addition, as an inclusion criterion, the presence of myocardial ischemia was excluded in all patients by a nega-

tive high-dose dobutamine stress echocardiogram.[3] Exclusion criteria included known cardiovascular disease or diabetes related complications including proliferative retinopathy, autonomic neuropathy as excluded by Ewing's tests,[13] and microalbuminuria as excluded by measurements of albumin/creatinine ratio in a urine sample.

Study protocol

All patients underwent magnetic resonance imaging (MRI) examinations with MR spectroscopy and transthoracic echocardiography at baseline. Both LV and RV volumes and EF were quantified by MRI, whereas LV and RV myocardial strain and SR were quantified by echocardiographic 2D speckle tracking analyses. The myocardial triglyceride content was measured by MR spectroscopy and the study sample was then dichotomized into 2 groups based on the median value. Biventricular volumes, EF and myocardial strain/SR were then compared between the 2 groups, and independent correlates of LV and RV myocardial functions were identified.

Cardiac magnetic resonance imaging protocol

All patients underwent MRI examinations for assessment of biventricular volumes and functions, and myocardial triglyceride content after an overnight fast with a 1.5-T whole-body MR scanner (Gyroscan ACS/NT15; Philips, Best, the Netherlands). During the examinations, the entire heart was imaged in the short-axis orientation with ECG-gated breath-hold balanced steady state free-precession imaging. Imaging parameters included the following: echo time = 1.7 ms, repetition time = 3.4 ms, flip-angle = 35°, slice thickness = 10 mm with a gap of 0 mm, field of view = 400 x 400 mm, reconstructed matrix size = 256 x 256.

LV and RV end-diastolic volume index (EDVI) and end-systolic volume index (ESVI) were measured and corrected for body surface area (BSA).[14] LVEF and RVEF were then calculated and expressed as percentages. LV mass (excluding papillary muscles) was also measured and indexed to BSA. LV mass-cavity ratio (which is conceptually similar to relative wall thickness) was calculated as previously described, with a higher mass-cavity ratio indicating increasing relative wall thickness.[15] All images were digitally stored on hard disks and analyzed offline using dedicated quantitative software (MASS, Medis, Leiden, the Netherlands).

Cardiac Proton MR Spectroscopy

Cardiac proton MR spectroscopy ([1H]-MRS) was performed as previously described.[16] Briefly, myocardial [1H]-MRS spectra were obtained from the interventricular septum to avoid contamination from epicardial fat. Spectroscopic data acquisitions were double-triggered with ECG triggering and respiratory navigator echoes to minimize motion

artifacts. Water-suppressed spectra were acquired to measure myocardial triglyceride content, and spectra without water suppression were acquired and used as an internal standard.[16] [1H]-MRS data were fitted by use of Java-based MR user interface software (jMRUI version 2.2, Leuven, Belgium) as previously described.[16] Myocardial triglyceride content relative to water was calculated and expressed as a percentage based on: (signal amplitude of triglyceride)/ (signal amplitude of water) x 100.[16]

Echocardiography

Transthoracic echocardiography was performed with the subjects at rest using commercially available ultrasound transducer and equipment (M3S probe, Vivid 7, GE-Vingmed, Horten, Norway). All images were digitally stored on hard disks for offline analysis (EchoPAC version 108.1.5, GE-Vingmed, Horten, Norway). A complete 2D, color, pulsed and continuous-wave Doppler echocardiogram was performed according to standard techniques.[17, 18]

Evaluation of the traditional parameters of LV diastolic function was performed by assessing transmitral inflow and pulmonary venous velocities using conventional pulsed-wave Doppler echocardiography in the apical 4 chamber view using a 2 mm sample volume. Transmitral early (E wave) and late (A wave) diastolic velocities as well as deceleration time were recorded at the mitral leaflet tips. LV isovolumic relaxation time was also recorded. The pulmonary venous peak systolic (S) and diastolic (D) velocities were recorded with the sample volume positioned 1 cm below the orifice of the right superior pulmonary vein in the left atrium.

Two-dimensional speckle tracking

2D speckle tracking analyses were performed on standard echocardiographic grey scale images. LV longitudinal function was determined from the 3 apical (2-, 3- and 4-chamber) views whereas the RV free wall longitudinal function was determined from the apical 4-chamber view only (Figure 1). During analysis, the endocardial border was manually traced at end-systole and the region of interest width adjusted to include the entire myocardium. The software then automatically tracks and accepts segments of good tracking quality and rejects poorly tracked segments, while allowing the observer to manually override its decisions based on visual assessments of tracking quality. Peak longitudinal strain, peak systolic SR and peak early diastolic SR for both the LV and RV myocardium were determined. Mean LV global longitudinal strain/SR were calculated from the 3 individual apical global longitudinal strain/SR curves respectively, whereas RV free wall longitudinal strain/SR were obtained from the apical 4-chamber view. All strain and SR measurements were exported to a spreadsheet (Microsoft ® Excel 2002, Microsoft Corporation, Redmond, WA).

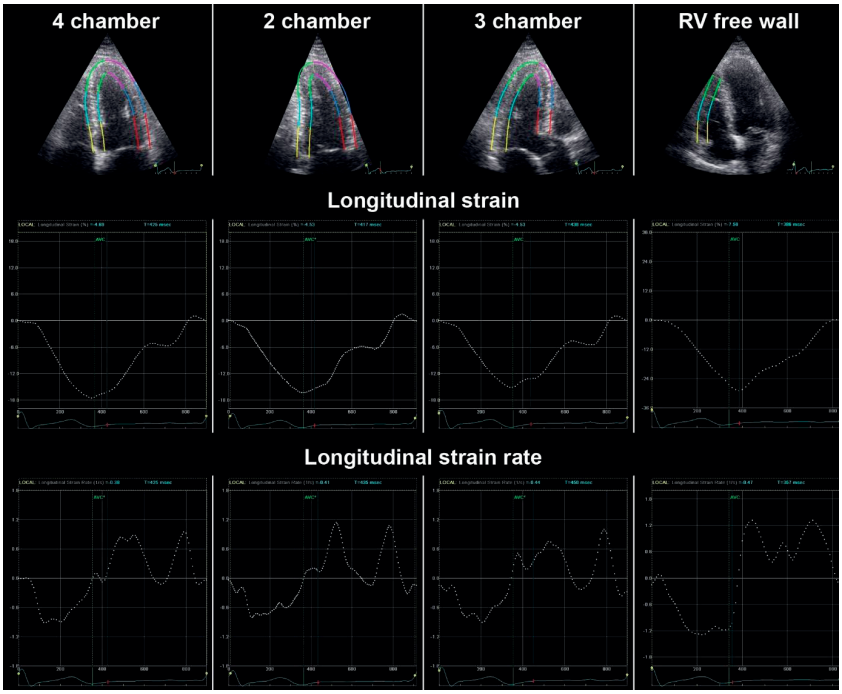


Figure 1. *Graphical example of the speckle tracking analyses to derive left and right ventricular myocardial strain and SR measurements. Mean LV global longitudinal strain/SR was calculated from the 3 individual (4-, 2- and 3-chamber) strain/SR curves, whereas the RV free wall strain/SR was derived from the 4 chamber view only. The mean global LV longitudinal strain, systolic SR and diastolic SR were -16.6%, -0.85 s-1, and 1.01 s-1 respectively. The mean RV free wall longitudinal strain, systolic SR and diastolic SR were -29.0%, -1.30 s-1, and 1.31 s-1 respectively. LV = left ventricular; RV = right ventricular; SR = strain rate.*

Previous work has reported the intra- and inter-observer variabilities in our laboratory as expressed by mean absolute difference for longitudinal strain (1.2 ± 0.5% and 0.9 ± 1.0%), systolic SR (0.10 ± 0.06 s^{-1} and 0.09 ± 0.08 s^{-1}) and early diastolic SR (0.08 ± 0.05 s^{-1} and 0.13 ± 0.09 s^{-1}).[10]

The study was approved by the local institutional ethics committee and written informed consent was obtained from all patients.

Statistical analysis

Due to the relatively small number of patients, all continuous variables were presented as median and 25th and 75th percentiles. Mann-Whitney U test was used to compare 2 groups of unpaired data. Multivariable linear regression analysis was used to identify independent correlates of LV and RV strain/SR. To generate the multivariable models, univariate variables with p value ≤ 0.20 were entered as covariates. To avoid multicolinearity between the univariate correlates, a tolerance level of > 0.5 (corresponding to

a correlation coefficient of > 0.7) was set. A 2-tailed p value of < 0.05 was considered significant. All statistical analyses were performed using SPSS for Windows (SPSS Inc, Chicago), version 17.

The authors had full access to the data and take responsibility for its integrity. All authors have read and agree to the manuscript as written.

RESULTS

The median age was 59 years (54, 62 years), and the median diabetes diagnosis duration was 4 years (range 1 to 11 years). The mean myocardial triglyceride content was 0.78 ± 0.42%. When the study sample was dichotomized based on the median myocardial triglyceride level of 0.76%, there were no significant differences in blood glucose level, glycated hemoglobin levels and lipid profiles between the 2 groups (Table 1).

Table 1. *Clinical and biochemical characteristics*

Variable	Total sample (n = 42)	Low myocardial triglyceride (n = 21)	High myocardial triglyceride (n = 21)	p value
Clinical				
Age (years)	59 (54, 62)	58 (51, 62)	60 (55, 63)	0.20
Body mass index (kg/m^2)	26.9 (25.0, 30.2)	26.9 (25.0, 28.9)	26.6 (25.0, 31.1)	0.67
Body surface area (m^2)	2.08 (2.00, 2.22)	2.10 (2.01, 2.20)	2.06 (1.97, 2.25)	0.89
Waist circumference (cm)	98.5 (93.9, 106.0)	98.0 (93.0, 103.0)	102.0 (95.0, 108.0)	0.26
Diabetes duration (years)	4.0 (1.0, 7.3)	3.0 (1.5, 7.0)	4.0 (1.0, 7.5)	0.83
Heart rate (beats/min)	71 (65, 82)	72 (66, 82)	70 (64, 80)	0.68
Systolic blood pressure (mmHg)	139 (130, 144)	134 (126, 140)	141 (133, 148)	0.025
Diastolic blood pressure (mmHg)	77 (71, 82)	77 (71, 84)	76 (73, 81)	0.83
Biochemical				
Blood glucose (mmol/L)	8.2 (7.3, 9.8)	8.1 (7.4, 9.0)	8.4 (7.1, 10.9)	0.35
Glycated hemoglobin (%)	6.2 (5.9, 6.8)	6.2 (5.9, 6.9)	6.0 (5.9, 6.7)	0.61
Plasma triglyceride (mmol/L)	1.50 (0.90, 2.30)	1.10 (0.85, 2.05)	1.80 (1.40, 2.80)	0.059
Total cholesterol (mmol/L)	4.60 (3.90, 5.10)	4.30 (3.85, 4.75)	4.90 (4.00, 5.30)	0.070
High-density lipoprotein cholesterol (mmol/L)	1.16 (0.98, 1.40)	1.24 (1.01, 1.44)	1.10 (0.89, 1.24)	0.097
Low-density lipoprotein cholesterol (mmol/L)	2.55 (2.00, 3.05)	2.40 (1.95, 2.90)	2.90 (2.05, 3.55)	0.17

Left ventricular volumes and functions

Table 2 summarizes the LV volumes and EF derived from MRI, and LV myocardial strain and SR derived from echocardiographic 2D speckle tracking analyses. There were no

significant differences in LV volumes and LVEF between patients with high versus low myocardial triglyceride content. In addition, there were no differences in LV mass index (48.1 g/m^2 [46.5, 53.1 g/m^2] vs. 50.9 g/m^2 [46.5, 55.8 g/m^2], p = 0.37) and LV mass-cavity ratio (0.70 [0.61, 0.80] vs. 0.73 [0.61, 0.79], p = 0.79) between the 2 groups of patients. Similarly, there were no significant differences in traditional parameters of LV diastolic function including transmitral E/A ratio (0.89 [0.75, 1.11] vs. 0.97 [0.72, 1.12], p = 0.97), deceleration time (206 ms [157, 214 ms] vs. 192 ms [165, 203 ms], p = 0.35), isovolumic relaxation time (84 ms [77, 94 ms] vs. 78 ms [73, 92 ms], p = 0.44) and pulmonary S/D ratio (1.45 [1.23, 1.68] vs. 1.35 [1.17, 1.64], p = 0.37) between the 2 groups of patients. However, patients with higher myocardial triglyceride content had greater impairment of global LV longitudinal strain and SR (Table 2).

Table 2. *Left and right ventricular volumes, ejection fraction, strain and strain rate*

Variable	Total sample (n = 42)	Low myocardial triglyceride (n = 21)	High myocardial triglyceride (n = 21)	p value
LEFT VENTRICLE				
Magnetic Resonance Imaging				
LVEDVI (mL/m^2)	71.6 (64.5, 78.1)	73.2 (66.6, 80.8)	68.0 (63.4, 78.3)	0.31
LVESVI (mL/m^2)	32.0 (27.6, 37.0)	32.2 (30.0, 37.3)	31.1 (25.6, 36.3)	0.23
LVEF (%)	54.6 (51.3, 58.1)	54.0 (50.5, 56.8)	55.1 (52.8, 58.8)	0.22
2D Speckle Tracking				
LV global strain (%)	-17.9 (-17.0, -19.6)	-19.3 (-18.5, -20.1)	-17.1 (-16.3, -17.7)	< 0.001
LV global systolic SR (s^{-1})	-0.98 (-0.87, -1.06)	-1.02 (-0.96, -1.14)	-0.87 (-0.82, -0.98)	< 0.001
LV global diastolic SR (s^{-1})	1.05 (0.91, 1.16)	1.11 (1.05, 1.23)	0.93 (0.77, 1.11)	0.003
RIGHT VENTRICLE				
Magnetic Resonance Imaging				
RVEDVI (mL/m^2)	70.7 (63.9, 73.9)	71.1 (64.0, 76.7)	69.3 (63.6, 73.0)	0.43
RVESVI (mL/m^2)	33.2 (30.1, 35.9)	34.9 (30.2, 36.9)	31.9 (29.0, 35.8)	0.31
RVEF (%)	52.0 (49.5, 53.7)	52.0 (49.6, 53.4)	53.0 (48.8, 54.4)	0.63
2D Speckle Tracking				
RV free wall strain (%)	-26.2 (-23.5, -28.4)	-27.7 (-25.1, -30.2)	-24.5 (-19.0, -27.7)	0.016
RV free wall systolic SR (s^{-1})	-1.83 (-1.62, -2.23)	-2.11 (-1.77, -2.46)	-1.74 (-1.44, -1.85)	0.005
RV free wall diastolic SR (s^{-1})	1.79 (1.44, 2.21)	2.10 (1.75, 2.61)	1.65 (1.12, 1.86)	0.001

LV = left ventricular; RV = right ventricular; EDVI = end-diastolic volume index; ESVI = end-systolic volume index; EF = ejection fraction; 2D = 2-dimensional; SR = strain rate

To identify the independent correlates of global LV longitudinal strain and SR, univariate correlates with a p value ≤ 0.20 (age, systolic blood pressure, fasting blood glucose level, high-density lipoprotein cholesterol, low-density lipoprotein cholesterol and

myocardial triglyceride content) were all entered into multiple linear regression models. Total cholesterol was not included in the model due to high colinearity with low-density lipoprotein cholesterol. Table 3 showed that the myocardial triglyceride content measured by MR spectroscopy was an independent correlate of global LV longitudinal strain, systolic SR and diastolic SR.

Table 3. *Independent correlates of left ventricular global longitudinal strain, global longitudinal systolic strain rate and global longitudinal diastolic strain rate*

Variable	Global LV longitudinal strain		Global LV longitudinal systolic SR		Global LV longitudinal diastolic SR	
	Standardized beta	p value	Standardized beta	p value	Standardized beta	p value
Age	-0.197	0.28	-0.092	0.62	-0.179	0.27
Systolic blood pressure	0.034	0.82	0.104	0.49	0.003	0.98
Blood glucose	0.192	0.23	0.209	0.20	-0.455	0.003
High-density lipoprotein cholesterol	-0.146	0.43	-0.043	0.82	-0.003	0.99
Low-density lipoprotein cholesterol	0.161	0.27	0.197	0.19	0.054	0.67
Myocardial triglyceride content	0.373	0.036	0.373	0.039	-0.326	0.038

LV = left ventricular; SR = strain rate

Right ventricular volumes and functions

Table 2 summarizes the RV volumes, EF, free wall longitudinal strain and SR. Similarly, there were no significant differences in MRI derived RV volumes and RVEF between the 2 groups of patients. However, patients with higher myocardial triglyceride content had greater impairment of RV free wall longitudinal strain and SR.

To identify independent correlates of RV free wall longitudinal strain and SR, age, fasting blood glucose level, high-density lipoprotein cholesterol, low-density lipoprotein cholesterol and myocardial triglyceride content were all entered into the multiple linear regression models. Table 4 showed that myocardial triglyceride content was an independent correlate of RV free wall longitudinal strain, systolic SR and diastolic SR.

Table 4. *Independent correlates of right ventricular free wall longitudinal strain, free wall longitudinal systolic strain rate and free wall longitudinal diastolic strain rate*

Variable	RV free wall longitudinal strain		RV free wall longitudinal systolic SR		RV free wall longitudinal diastolic SR	
	Standardized beta	p value	Standardized beta	p value	Standardized beta	p value
Age	-0.084	0.67	-0.280	0.098	0.050	0.76
Blood glucose	0.064	0.73	0.162	0.30	-0.014	0.92
High-density lipoprotein cholesterol	0.094	0.69	-0.354	0.048	0.425	0.017
Low-density lipoprotein cholesterol	-0.096	0.57	-0.331	0.024	0.288	0.044
Myocardial triglyceride content	0.457	0.020	0.321	0.048	-0.403	0.013

RV = right ventricular; SR = strain rate

DISCUSSION

In the present study, MRI assessment revealed similar LV/RV volumes and EF in type 2 diabetic patients with high versus low myocardial triglyceride content, as measured by MR spectroscopy. However, 2D speckle tracking deformation imaging demonstrated greater impairments of biventricular strain/SR in patients with higher myocardial triglyceride content. Myocardial triglyceride content was an independent correlate of LV and RV longitudinal strain, systolic SR and diastolic SR.

Myocardial substrate metabolism and steatosis

The etiology of diabetic heart disease is complex and multifactorial, ranging from altered myocardial metabolism, up-regulation of the renin-angiotensin system, increased oxidative stress, endothelial dysfunction with microvascular disease, autonomic neuropathy, and altered myocardial structure with fibrosis.[1] However, recent evidence suggests the role of myocardial lipotoxic injury from lipid oversupply contributing to diabetic heart disease.[19]

Under normal physiological conditions, fatty acids are absorbed through the intestines and stored as triglycerides within adipocytes with minimal accumulation within non-adipose tissues such as the heart. However, the combination of diabetes with its metabolic derangements, insulin resistance, visceral adiposity and increased dietary fatty acid intake, all lead to increased myocardial fatty acid delivery and uptake. This results in the accumulation of intracellular triglyceride within the myocyte cytoplasm (also known as steatosis).[19-22] However, part of the excess fatty acid is redirected into non-oxidative pathways giving rise to toxic fatty acid intermediates such as ceramide. These toxic fatty acid intermediates disrupt normal cellular signalling, leading to mito-

chondrial dysfunction, cellular damage, apoptosis, and eventual replacement fibrosis and myocardial contractile dysfunction. Thus, although it is currently accepted that intracellular triglycerides are probably inert, its intracellular concentration is reflective of an increased concentration of toxic fatty acid intermediates. Therefore, the observed relationship between intracellular triglyceride accumulation and myocardial dysfunction likely represents an association, mediated by the accumulation of toxic intermediates from increased non-oxidative fatty acid metabolism. Although animal studies have shown an association between myocardial triglyceride accumulation, eccentric LV hypertrophy and systolic dysfunction[23], human studies showing similar association between myocardial steatosis and myocardial dysfunction have been limited.

Myocardial steatosis and myocardial dysfunction

Several studies have examined the relationship between myocardial triglyceride accumulation and LV function.[2, 3] McGavock and co-workers showed that there was no association between myocardial triglyceride accumulation and LV diastolic function.[2] However, their results could be confounded by their inclusion of a heterogeneous group of diabetic patients and the use of insulin (a lipogenic agent).[2] In contrast, Rijzewijk and co-workers were able to demonstrate diastolic dysfunction in a group of uncomplicated diabetic patients with myocardial steatosis when compared to healthy controls.[3] However, both groups could not demonstrate a correlation between myocardial triglyceride content and LVEF.[2, 3] Thus, these diabetic patients have traditionally been labeled as having diastolic dysfunction with normal systolic function. However, this is largely a misnomer due to the insensitivity of conventional systolic parameters such as LVEF in identifying subtle changes in myocardial contractility.[24] In contrast, 2D speckle tracking derived myocardial strain and SR indices are more sensitive in detecting subclinical myocardial dysfunction and have been shown to be impaired in diabetic patients compared to normal controls.[4, 8, 10]

To date, no studies have related myocardial strain and SR analyses by echocardiography to myocardial triglyceride accumulation. In the present study, MRI derived LV volumes and EF were similar between patients with high versus low myocardial triglyceride levels. However, the study was first to demonstrate that patients with high myocardial triglyceride levels had significantly greater impairment of LV myocardial longitudinal strain, systolic SR and diastolic SR. Furthermore, as the diabetic metabolic derangements with subsequent myocardial steatosis should hypothetically have a similar adverse effect on the RV, the present study also demonstrated RV free wall myocardial systolic and diastolic dysfunctions in patients with high myocardial triglyceride levels. The present study was first to demonstrate an independent association between myocardial triglyceride accumulation in diabetic patients and biventricular myocardial dysfunctions.

However, intracellular surplus triglyceride itself is likely to be relatively inert, while the lipid intermediates derived from non-oxidative pathways are probably responsible for lipotoxic injury and eventual cellular apoptosis.[20] Thus, the observed relationship between myocardial triglyceride accumulation and myocardial dysfunction is probably an association secondary to the adverse diabetic metabolic profile rather than a causal relationship.

Clinical implications

The novel aspect of the current study was the demonstration of the independent association between myocardial triglyceride content and biventricular myocardial systolic and diastolic functions. In animal studies, therapeutic interventions aiming at reducing myocardial triglyceride accumulation have demonstrated beneficial myocardial effects.[23] Thus, future human studies assessing the effectiveness of anti-steatotic therapy in type 2 diabetics may include quantifications of myocardial triglyceride content by spectroscopy, and assessments of myocardial functions by strain/SR imaging on 2D speckle tracking echocardiography.

Study limitations

This was a relatively small study and several characteristics such as LV and RV volumes were not statistically different between patients with high versus low myocardial triglyceride content. Thus, future studies should include more patients to avoid possible type 1 error.

CONCLUSIONS

Uncomplicated type 2 diabetic patients with high levels of myocardial triglyceride content and no ischemia showed greater impairments of biventricular myocardial strain and SR but similar biventricular volumes and EF compared to patients with low levels of myocardial triglyceride. Myocardial triglyceride accumulation was an independent correlate of biventricular myocardial strain and SR.

REFERENCE LIST

(1) Marwick T. The diabetic myocardium. *Curr Diab Rep* 2006;6:36-41.

(2) McGavock JM, Lingvay I, Zib I, Tillery T, Salas N, Unger R, Levine BD, Raskin P, Victor RG, Szczepaniak LS. Cardiac Steatosis in Diabetes Mellitus: A 1H-Magnetic Resonance Spectroscopy Study. *Circulation* 2007;116:1170-1175.

(3) Rijzewijk LJ, van der Meer RW, Smit JWA, Diamant M, Bax JJ, Hammer S, Romijn JA, De Roos A, Lamb HJ. Myocardial Steatosis Is an Independent Predictor of Diastolic Dysfunction in Type 2 Diabetes Mellitus. *J Am Coll Cardiol* 2008;52:1793-1799.

(4) Fang ZY, Leano R, Marwick TH. Relationship between longitudinal and radial contractility in subclinical diabetic heart disease. *Clin Sci* 2004;106:53-60.

(5) Vinereanu D, Nicolaides E, Tweddel AC, Mädler CF, Holst B, Boden LE, Cinteza M, Rees AE, Fraser AG. Subclinical left ventricular dysfunction in asymptomatic patients with Type II diabetes mellitus, related to serum lipids and glycated haemoglobin. *Clin Sci* 2003;105:591-599.

(6) Moir S, Hanekom L, Fang ZY, Haluska B, Wong C, Burgess M, Marwick TH. Relationship between myocardial perfusion and dysfunction in diabetic cardiomyopathy: a study of quantitative contrast echocardiography and strain rate imaging. *Heart* 2006;92:1414-1419.

(7) Fang ZY, Schull-Meade R, Downey M, Prins J, Marwick TH. Determinants of subclinical diabetic heart disease. *Diabetologia* 2005;48:394-402.

(8) Fang ZY, Yuda S, Anderson V, Short L, Case C, Marwick TH. Echocardiographic detection of early diabetic myocardial disease. *J Am Coll Cardiol* 2003;41:611-617.

(9) Galderisi M, de Simone G, Innelli P, Turco A, Turco S, Capaldo B, Riccardi G, de Divitiis O. Impaired Inotropic Response in Type 2 Diabetes Mellitus: A Strain Rate Imaging Study. *Am J Hypertens* 2007;20:548-555.

(10) Ng ACT, Delgado V, Bertini M, van der Meer RW, Rijzewijk LJ, Shanks M, Nucifora G, Smit JWA, Diamant M, Romijn JA, De Roos A, Leung DY, Lamb HJ, Bax JJ. Findings from left ventricular strain and strain rate imaging in asymptomatic patients with type 2 diabetes mellitus. *Am J Cardiol* 2009;104:1398-1401.

(11) van der Meer RW, Rijzewijk LJ, de Jong HWAM, Lamb HJ, Lubberink M, Romijn JA, Bax JJ, De Roos A, Kamp O, Paulus WJ, Heine RJ, Lammertsma AA, Smit JWA, Diamant M. Pioglitazone Improves Cardiac Function and Alters Myocardial Substrate Metabolism Without Affecting Cardiac Triglyceride Accumulation and High-Energy Phosphate Metabolism in Patients With Well-Controlled Type 2 Diabetes Mellitus. *Circulation* 2009;119:2069-2077.

(12) Alberti KG, Zimmet PZ. Definition, diagnosis and classification of diabetes mellitus and its complications. Part 1: diagnosis and classification of diabetes mellitus provisional report of a WHO consultation. *Diabet Med* 1998;15:539-553.

(13) Ewing DJ, Martyn CN, Young RJ, Clarke BF. The value of cardiovascular autonomic function tests: 10 years experience in diabetes. *Diabetes Care* 1985;8:491-498.

(14) Mosteller RD. Simplified calculation of body-surface area. *N Engl J Med* 1987;317:1098.

(15) Rodriguez CJ, Diez-Roux AV, Moran A, Jin Z, Kronmal RA, Lima J, Homma S, Bluemke DA, Barr RG. Left Ventricular Mass and Ventricular Remodeling Among Hispanic Subgroups Compared With

Non-Hispanic Blacks and Whites: MESA (Multi-Ethnic Study of Atherosclerosis). *J Am Coll Cardiol* 2010;55:234-242.

(16) van der Meer RW, Doornbos J, Kozerke S, Schar M, Bax JJ, Hammer S, Smit JW, Romijn JA, Diamant M, Rijzewijk LJ, De Roos A, Lamb HJ. Metabolic imaging of myocardial triglyceride content: reproducibility of 1H MR spectroscopy with respiratory navigator gating in volunteers. *Radiology* 2007;245:251-257.

(17) Nishimura R, Miller FJ, Callahan M, Benassi R, Seward J, Tajik A. Doppler echocardiography: theory, instrumentation technique and application. *Mayo Clin Proc* 1985;60:321-343.

(18) Tajik A, Seward J, Hagler D, Mair D, Lie J. Two dimensional real-time ultrasonic imaging of the heart and great vessels: technique, image orientation, structure identification and validation. *Mayo Clin Proc* 1978;53:271-303.

(19) McGavock JM, Victor RG, Unger RH, Szczepaniak LS. Adiposity of the Heart, Revisited. *Ann Intern Med* 2006;144:517-524.

(20) Unger RH. Lipotoxic Diseases. *Annu Rev Med* 2002;53:319.

(21) Watts GF, Marwick TH. Ventricular dysfunction in early diabetic heart disease: detection, mechanisms and significance. *Clin Sci* 2003;105:537-540.

(22) Lopaschuk GD, Ussher JR, Folmes CD, Jaswal JS, Stanley WC. Myocardial fatty acid metabolism in health and disease. *Physiol Rev* 2010;90:207-258.

(23) Zhou YT, Grayburn P, Karim A, Shimabukuro M, Higa M, Baetens D, Orci L, Unger RH. Lipotoxic heart disease in obese rats: Implications for human obesity. *Proc Natl Acad Science USA* 2000;97:1784-1789.

(24) Marwick TH. Diabetic heart disease. *Heart* 2006;92:296-300.

5

Association Between Diffuse Myocardial Fibrosis by Cardiac Magnetic Resonance Contrast-Enhanced T1 Mapping and Subclinical Myocardial Dysfunction in Diabetic Patients: A Pilot Study

Arnold C.T. Ng, Dominique Auger, Victoria Delgado, Saskia G.C. van Elderen, Matteo Bertini, Hans-Marc Siebelink, Rob J. van der Geest, Cosimo Bonetti, Enno T. van der Velde, Albert de Roos, Johannes W.A. Smit, Dominic Y. Leung, Jeroen J. Bax, Hildo J. Lamb

Circ Cardiovasc Imaging. 2012 Jan;5(1):51-9

ABSTRACT

Background: Diabetic patients have increased interstitial myocardial fibrosis on histological examination. Magnetic resonance imaging (MRI) T_1 mapping is a previously validated imaging technique that can quantify the burden of global and regional interstitial fibrosis. However, the association between MRI T_1 mapping and subtle left ventricular (LV) dysfunction in diabetic patients is unknown.

Methods: Fifty diabetic patients with normal LV ejection fraction (EF) and no underlying coronary artery disease or regional macroscopic scar on MRI delayed enhancement were prospectively recruited. Diabetic patients were compared with 19 healthy controls who were frequency matched in age, sex and body mass index.

Results: There were no significant differences in mean LV end-diastolic volume index, end-systolic volume index and LVEF between diabetic patients and healthy controls. Diabetic patients had significantly shorter global contrast-enhanced myocardial T_1 time (425 ± 72 ms vs. 504 ± 34 ms, $p < 0.001$). There was no correlation between global contrast-enhanced myocardial T_1 time and LVEF ($r = 0.14$, $p = 0.32$) in the diabetic patients. However, there was good correlation between global contrast-enhanced myocardial T_1 time and global longitudinal strain ($r = -0.73$, $p < 0.001$). Global contrast-enhanced myocardial T_1 time was the strongest independent determinant of global longitudinal strain on multivariate analysis (standardized $\beta = -0.626$, $p < 0.001$). Similarly, there was good correlation between global contrast-enhanced myocardial T_1 time and septal E' ($r = 0.54$, $p < 0.001$). Global contrast-enhanced myocardial T_1 time was also the strongest independent determinant of septal E' (standardized $\beta = 0.432$, $p < 0.001$).

Conclusions: A shorter global contrast-enhanced myocardial T_1 time was associated with more impaired longitudinal myocardial systolic and diastolic function in diabetic patients.

INTRODUCTION

Diabetic patients can develop changes in cardiac structure and myocardial dysfunction that are independent of hypertension and coronary artery disease.[1-3] Although the underlying pathogenesis is likely to be multifactorial[1-4], there is eventually accelerated cellular apoptosis and necrosis resulting in increased perivascular and diffuse interstitial fibrosis within the myocardium.[2] Importantly, previous studies have demonstrated histological evidence of increased diffuse microscopic fibrosis in the myocardium of diabetic patients.[5, 6] In magnetic resonance imaging (MRI), gadolinium-based contrast agents accumulates and have increased wash-out times within these myocardial fibrous tissues due to the absence of viable myocytes and increased volume of distribution.[7] Using MRI T1 mapping sequences, global contrast-enhanced T1 relaxation time can detect and quantify the extent of diffuse interstitial myocardial fibrosis. A recent independent study has histologically validated and demonstrated an inverse linear relationship between global contrast-enhanced myocardial T1 time and the burden of myocardial interstitial fibrosis.[8] Thus, shorter global contrast-enhanced myocardial T1 time represent more interstitial fibrosis.[8]

Diabetic patients can develop subtle left ventricular (LV) myocardial dysfunction despite normal LV ejection fraction (EF).[9, 10] Advanced echocardiographic techniques such as tissue Doppler imaging and 2-dimensional (2D) speckle tracking are highly sensitive for early detection of subclinical diabetic myocardial dysfunction.[10, 11] Therefore, increased interstitial fibrosis within the diabetic myocardium may result in subtle LV dysfunction which can be detected by these sophisticated echocardiographic techniques. Thus, the aims of the present study were:

1) to quantify and compare global contrast-enhanced myocardial T1 time between diabetic patients with normal LVEF and normal controls, and
2) to correlate global contrast-enhanced myocardial T1 time with LV myocardial functional assessment using global longitudinal strain by 2D speckle tracking analysis.[12]

METHODS

Patient population and study protocol

Sixty-five diabetic patients (35 type 1 and 30 type 2) were prospectively recruited in the present study. Inclusion criteria included diabetes mellitus diagnosed according to World Health Organization criteria.[13] Exclusion criteria included age < 18 years, rhythm other than sinus rhythm, significant coronary artery disease, previous myocardial infarction, presence of segmental wall motion abnormalities or presence of delayed

contrast enhancement (DCE) on MRI indicative of macroscopic fibrosis/scar from previous myocardial infarction, LVEF < 50%, and moderate or severe valvular stenosis or regurgitation. However, 15 type 2 diabetic patients were excluded from the study due to the presence of DCE on MRI that was indicative of previous silent myocardial infarction. Thus, a total of 50 diabetic patients (35 type 1 and 15 type 2) were included in the final analysis. The study was approved by the local institutional ethics committee and written informed consent was obtained.

In addition, 19 normal control subjects were also included. The normal controls were frequency matched against the diabetic patients for age, gender and body mass index. All control subjects were clinically referred for evaluation of atypical chest pain, palpitations or syncope without murmur and had normal MRI examinations. Exclusion criteria for the control subjects included history of diabetes mellitus, hypertension, previous myocardial infarction, presence of segmental wall motion abnormalities or presence of DCE on MRI, LVEF < 50%, and moderate or severe valvular stenosis or regurgitation.

All subjects underwent a comprehensive MRI examination (including administration of gadolinium-based contrast for DCE and quantification of global contrast-enhanced myocardial T1 time).

All diabetic patients underwent a complete transthoracic echocardiographic examination including assessment of myocardial systolic and diastolic function by 2D speckle tracking strain and tissue Doppler septal E' analyses respectively. Baseline clinical variables recorded included diabetic complications (including diabetic retinopathy, neuropathy and nephropathy), cardiac risk factors, and glomerular filtration rates (GFR) calculated by the Modification of Diet in Renal Disease formula as recommended by the National Kidney Foundation, Kidney Disease Outcomes Quality Initiative Guidelines.[14]

LV volumes, EF and mass were quantified in all the patients using MRI as gold standard. In addition, global contrast-enhanced myocardial T1 time was also quantified, with a shorter T1 time suggestive of more fibrosis.[8] Previous study has demonstrated that the assessment of global longitudinal strain by 2D speckle tracking echocardiography is the most sensitive marker of myocardial systolic function in diabetic patients compared to circumferential or radial strain.[10] Thus, to evaluate the effects of increasing interstitial fibrosis on LV systolic function, the linear correlations between global contrast-enhanced myocardial T1 time, LVEF and global longitudinal strain were explored. Similarly, the linear correlation between global contrast-enhanced myocardial T1 time and septal E' was also determined. Finally, the independent effect of global contrast-enhanced myocardial T1 time on global longitudinal strain (marker of myocardial systolic function)

and septal E' (marker of myocardial diastolic function) were determined in a multivariate analysis corrected for clinical and MRI covariates.

Cardiac magnetic resonance imaging

All patients underwent MRI examinations for assessment of LV volumes, LVEF, global contrast-enhanced myocardial T1 time and DCE with a 1.5-T whole-body MRI scanner (Gyroscan ACS/NT15; Philips, Best, the Netherlands). LV volumes and EF were assessed by imaging the entire heart in the short-axis orientation with ECG-gated breath-hold balanced steady state free-precession imaging. Cine imaging parameters included the following: echo time = 1.7 ms, repetition time = 3.4 ms, flip-angle = 35°, slice thickness = 10 mm with a gap of 0 mm, field of view = 400 x 400 mm, reconstructed matrix size = 256 x 256 pixels.

DCE images were acquired 15 minutes after bolus injection of gadolinium diethylenetriamine penta-acetic acid (Magnevist, Schering, Berlin, Germany; 0.15 mmol/kg) with an inversion recovery gradient echo sequence with parallel imaging (SENSE, acceleration factor 2). Inversion time was determined by real-time plan scan (Look-Locker sequence) to null normal myocardium signal. DCE images of the heart were acquired in 1 breath-hold using 20 – 24 short-axis slices (depending on the heart size). DCE imaging parameters were: echo time = 1.06 ms, repetition time = 3.7 ms, flip-angle = 15°, slice thickness = 5 mm, field of view = 400 x 400 mm, reconstructed matrix size = 256 x 256 pixels. All subjects included in the present study had no evidence of DCE suggestive of macroscopic myocardial scar/fibrosis.

Contrast-enhanced myocardial T1 mapping with the Look-Locker sequence was used to cycle through images over a range of inversion times.[15] The sequence consisted of an ECG-gated, inversion recovery gradient echo sequence with parallel imaging (SENSE, acceleration factor 1.8). Thirty-three images were acquired sequentially at increasing inversion times 10 minutes after bolus injection of gadolinium diethylenetriamine penta-acetic acid in 1 breath-hold. The Look-Locker sequence imaging parameters were: echo time = 1.0 ms, repetition time = 3.79 ms, flip-angle = 8°, inversion time 150 ms, slice thickness = 10 mm, field of view = 370 x 370 mm, reconstructed matrix size = 256 x 256 pixels. These images were then processed with a curve fitting technique to generate T1 maps as described below.

Evaluation of LV mass, volumes and function. All MRI images were digitally stored on hard disks and analyzed offline using dedicated quantitative software (MASS, Medis, Leiden, The Netherlands). LV endocardial and epicardial borders were outlined on the short-axis cine images. Papillary muscles were considered as part of the LV cavity, and

epicardial fat was excluded. LV end-diastolic mass index, LV end-diastolic volume index (EDVI) and LV end-systolic volume index (ESVI) were measured and corrected for body surface area.[16] LVEF was calculated and expressed as a percentage. Stroke volume was calculated as the difference between LV end-diastolic and end-systolic volumes, and cardiac output was calculated as the product of stroke volume and heart rate.

Evaluation of T1 mapping. T1 recovery is a basic fundamental parameter of magnetic resonance imaging and refers to the recovery of "longitudinal magnetization" of protons along the main magnetic field in the z-axis. The rate of this recovery can be described by the exponential equation: $M_Z(t) = M_{Z(t=\infty)}[1 - e^{-t/T1}]$, where $M_Z(t)$ is the sample magnetization observed at time = t = inversion time for an inversion recovery experiment, and $M_{Z(t=\infty)}$ denotes the equilibrium magnetization in the z-axis. To quantify contrast-enhanced myocardial T1 time, LV endocardial and epicardial borders were outlined from a single mid-ventricular short-axis Look-Locker sequence of varying inversion times using MASS research software (MASS V2010-EXP, Leiden University Medical Center, Leiden, The Netherlands) (Figure 1).

As the different inversion recovery times fall into different cardiac phases during the Look-Locker sequence, it resulted in movement of the left ventricle. Thus, the endo- and epicardial contours were manually drawn in each image (total of 33 images) to ensure the inclusion of only myocardium and the exclusion of blood pool/epicardial fat. The software then permits automatic pixel-by-pixel quantification of contrast-enhanced myocardial T1 time by fitting data acquired at the various inversion times.[17] The location of a pixel position within the myocardium can be described by its relative position across the local wall thickness (relative distance to the endocardial and epicardial contour) and its relative position along the length of the defined myocardial contours (for short-axis images, the longitudinal location is defined by the angular position relative to the posterior junction of the RV free wall with the LV). Following this definition, signal intensity curves of matching pixels were reconstructed and used for T1 fitting. Prior to fitting, the signal intensity of initial phases was inverted. The best fit for T1 value (corresponding to the smallest fitting error) was determined iteratively by inverting initial phases up to a time corresponding to the zero crossing of the longest possible T1 value and performing a fit for each case. The Levenberg-Marquardt algorithm was used to perform a nonlinear fit of the model to the measured data. Only pixels where the $\chi 2$ test for goodness of fit was significant with level of significance $\alpha = 0.05$ were included in the final average T1 value.

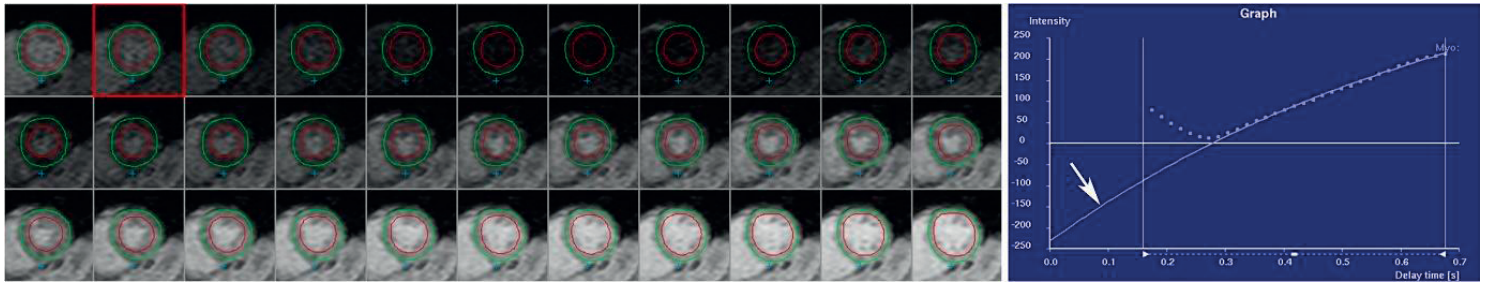


Figure 1. *Example of myocardial T1 mapping using the Look-Locker sequence with increasing inversion times. Left ventricular endocardial and epicardial borders were outlined for all 33 images (left panel). The software then automatically determines the myocardial signal intensity for every individual pixel from each image. The individual pixel intensities within the myocardium (y-axis) were subsequently plotted against the inversion time (x-axis) (right panel). Finally, the global contrast-enhanced myocardial T1 time was automatically calculated by the software which performed curve-fitting of the data points to an exponential recovery curve (arrow) representing the recovery of myocardial longitudinal magnetization. Therefore, a short global contrast-enhanced myocardial T1 time indicate a higher burden of interstitial fibrosis due to a greater concentration of gadolinium within the fibrous tissues, and vice versa.*

A global contrast-enhanced myocardial T1 time was subsequently automatically calculated as the average of all the individual contrast-enhanced myocardial T1 time from each pixel. As the function of gadolinium-based contrast agents normally shortens T1 time, and its wash-out time increases within myocardial fibrous tissues due to increased volume of distribution[7], a shorter global contrast-enhanced myocardial T1 time consequently is suggestive of more interstitial fibrosis.[8] The derived global contrast-enhanced myocardial T1 time is generally expected to be shorter than the true T1 time of myocardium due to the multiple readout gradients from the Look-Locker sequence and the presence of gadolinium-based contrast agents.

Transthoracic echocardiography

Transthoracic echocardiography was performed with the diabetic patients at rest using commercially available ultrasound transducer and equipment (M4S probe, Vivid 7, GE-Vingmed, Horten, Norway). All images were digitally stored on hard disks for offline analysis (EchoPAC version 108.1.5, GE-Vingmed, Horten, Norway). A complete 2D, color, pulsed and continuous-wave Doppler echocardiogram was performed according to standard techniques.[18, 19]

Transmitral and pulmonary venous flow velocities were recorded using conventional pulsed-wave Doppler echocardiography in the apical 4 chamber view using a 2 mm sample volume. Transmitral early (E wave) and late (A wave) diastolic velocities as well as deceleration time were recorded at the mitral leaflet tips. The pulmonary venous peak systolic (S) and diastolic (D) velocities were recorded with the sample volume positioned 1 cm below the orifice of the right superior pulmonary vein in the left atrium.

Evaluation of myocardial systolic function. Quantification of myocardial systolic function was performed using 2D speckle tracking echocardiography.[12] Briefly, 2D speckle tracking is a commercial software (EchoPAC version 108.1.5, GE-Vingmed, Horten, Norway) that performs semi-automated frame-by-frame tracking of natural acoustic markers within the myocardium seen on standard 2D gray-scale echocardiographic images, and it permits direct quantification of global longitudinal myocardial function. Previous study has demonstrated that the assessment of global longitudinal strain and strain rate by 2D speckle tracking echocardiography is the most sensitive marker of myocardial systolic function in diabetic patients and is superior to LVEF, circumferential and radial strain/strain rate.[10]

To obtain global longitudinal strain/strain rate, 2D speckle tracking analyses were performed on grey scale images of the LV obtained in the 3 apical (3-, 4- and 2-chamber) views (Figure 2). During analysis, the endocardial border was manually traced at end-

systole and the region of interest width adjusted to include the entire myocardium. The software then automatically tracks and accepts segments of good tracking quality and rejects poorly tracked segments, while allowing the observer to manually override its decisions based on visual assessments of tracking quality. From the 3 individual apical views, myocardial systolic function was calculated as the average of the 3 peak global longitudinal strain.[10] All strain measurements were exported to a spreadsheet (Microsoft ® Excel 2002, Microsoft Corporation, Redmond, WA).

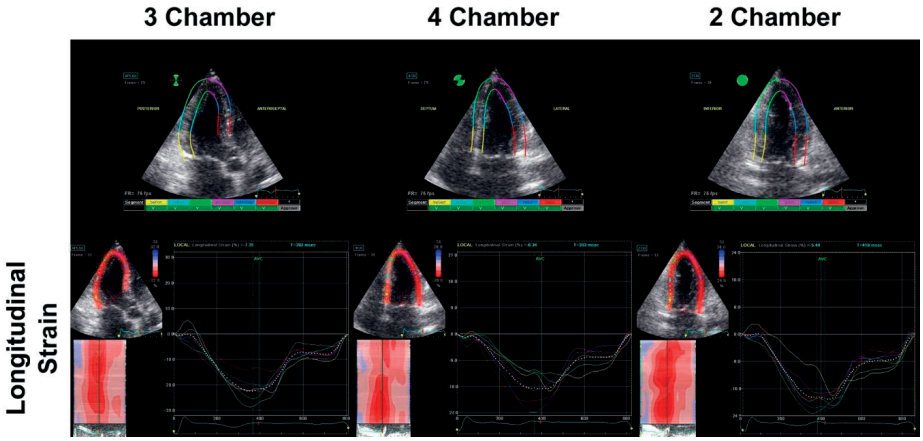


Figure 2. *Quantification of longitudinal myocardial function by 2-dimensional speckle tracking echocardiography. Longitudinal strain was quantified from the 3 apical (3-, 4- and 2 chamber) views. The 2-dimensional speckle tracking software then automatically displays the respective segmental (colored lines) and global (single white dotted line) longitudinal strain curves. Longitudinal myocardial function was then calculated as the mean of the 3 individual peak global longitudinal strain values, and expressed as a percentage. Longitudinal strain is normally expressed as a negative percentage, indicating percentage shortening of the myocardium.*

Evaluation of myocardial diastolic function. Quantification of myocardial diastolic function was performed using septal E' and E/e' ratio by tissue Doppler imaging.[20] Color-coded tissue Doppler images of the left ventricle were obtained in apical 4-chamber view acquired at the highest possible frame rates (> 150 frames/s) during end-expiration and stored for off-line analysis. Peak early diastolic myocardial velocities (E') was measured in the basal septal mitral annulus, and the ratio of peak transmitral E wave to septal E' was calculated (septal E/e' ratio).[20]

Variability analysis

To determine intra- and inter-observer variabilities for global contrast-enhanced myocardial T1 time, measurements were repeated in 10 randomly selected patients. The intra- and inter-observer variabilities for global contrast-enhanced myocardial T1 time expressed as mean absolute differences ± 1 standard deviation were 12.6 ± 12.7 ms and 12.4 ± 10.0 ms respectively.

Previous work from our laboratory has reported the intra- and inter-observer variabilities for mean global longitudinal strain as mean absolute differences ± 1 standard deviation of 1.2 ± 0.5% and 0.9 ± 1.0% respectively.[10]

Statistical analysis

All continuous variables were presented as mean ± 1 SD unless otherwise stated. Categorical variables were presented as frequencies and percentages. Comparisons between diabetic and control patients were performed using Mann-Whitney U test and Chi square test for continuous and categorical variables respectively. Pearson correlation was employed to examine the linear association between 2 continuous variables. Multiple linear regression analyses were then performed to identify independent clinical and echocardiographic determinants of global longitudinal strain and septal E' for diabetic patients. All univariable predictors with $p < 0.20$ were simultaneously entered into the multiple linear regression models. Validity of the multiple linear regression models were established by confirming the residuals to be normally distributed. A 2-tailed p value of < 0.05 was considered significant. All statistical analyses were performed using SPSS for Windows (SPSS Inc, Chicago), version 17.

RESULTS

Table 1 summarizes the baseline clinical characteristics of the 50 diabetic patients and 19 control subjects. There were no differences in age, gender, blood pressure, hemoglobin and GFR between the diabetic patients and control subjects. A total of 28 (56%) diabetic patients were treated for hypertension. A respective 31 (62.0%), 12 (24.0%) and 7 (14.0%) diabetic patients had evidence of diabetic retinopathy, peripheral neuropathy and nephropathy respectively. However, no diabetic patients had a history of previous myocardial infarction or underlying significant coronary artery disease by virtue of the study exclusion criteria.

Magnetic resonance imaging and echocardiography

Table 2 summarizes the baseline MRI and echocardiographic characteristics of the diabetic patients and normal controls. There were no significant differences in LVEDVI (79.1 ± 14.4 vs. 79.8 ± 17.2 mL/m^2, $p = 0.60$), LVESVI (33.3 ± 7.6 vs. 34.7 ± 7.5 mL/m^2, $p = 0.23$), LV mass index (49.0 ± 7.6 vs. 50.9 ± 8.7 g/m^2, $p = 0.24$) and LVEF (58.1 ± 4.6 vs. 56.2 ± 3.8%, $p = 0.10$) between the diabetic patients and control subjects. No patients had evidence of regional DCE suggestive of focal macroscopic scar/fibrosis by virtue of the study exclusion criteria. However, diabetic patients had significantly shorter global contrast-enhanced myocardial T1 time (425 ± 72 vs. 504 ± 34 ms, $p < 0.001$). Furthermore, there was a wide

Table 1. *Clinical and biochemical characteristics of diabetic patients and normal controls*

Variable	Diabetic patients (n = 50)	Controls (n = 19)	p value*
Demographics			
Age (years)	51 ± 10	45 ± 15	0.15
Male gender (%)	54.0	63.2	0.49
Body mass index (kg/m^2)	26.3 ± 3.7	26.1 ± 4.4	0.84
Medical history			
Retinopathy (%)	62.0	-	-
Neuropathy (%)	24.0	-	-
Nephropathy (%)	14.0	-	-
Systolic blood pressure (mmHg)	129 ± 10	123 ± 14	0.08
Diastolic blood pressure (mmHg)	76 ± 7	73 ± 8	0.14
Laboratory			
Hemoglobin (g/dL)	14.2 ± 1.3	14.1 ± 1.1	0.76
GFR (mL/min/1.73m^2)	92.8 ± 18.9	97.9 ± 18.8	0.26
HbA1c (%)	8.0 ± 1.4	-	-

*p value by Mann-Whitney U test and Chi square test for continuous and categorical variables respectively. GFR = glomerular filtration rate; HbA1c = glycated hemoglobin level.

Table 2. *Magnetic resonance imaging and echocardiographic characteristics of diabetic patients*

Variable	Diabetic patients (n = 50)	Controls (n = 19)	p value*
Magnetic resonance imaging			
LV mass index (g/m^2)	49.0 ± 7.6	50.9 ± 8.7	0.24
LVEDVI (mL/m^2)	79.1 ± 14.4	79.8 ± 17.1	0.60
LVESVI (mL/m^2)	33.3 ± 7.6	34.7 ± 7.5	0.23
LVEF (%)	58.1 ± 4.6	56.2 ± 3.8	0.10
Cardiac output (L/min)	6.5 ± 1.3	6.2 ± 2.2	0.44
Global contrast-enhanced myocardial T1 time (ms)	425 ± 72	504 ± 34	< 0.001
Echocardiography			
Heart rate (beats/min)	74 ± 12	67 ± 12	0.10
Transmitral E/A ratio	1.13 ± 0.34	1.19 ± 0.52	0.97
Deceleration time (ms)	194 ± 44	266 ± 68	< 0.001
Pulmonary S/D ratio	1.31 ± 0.28	1.22 ± 0.22	0.20
Global longitudinal strain (%)	-16.1 ± 1.4	-20.2 ± 1.0	< 0.001
Septal E' (cm/s)	7.3 ± 1.1	8.7 ± 1.8	0.005
Septal E/e' ratio	10.0 ± 3.3	8.4 ± 2.0	0.03

*p value by Mann-Whitney U test. EDVI = end-diastolic volume index; ESVI = end-systolic volume index; EF = ejection fraction; LV = left ventricular.

range of global contrast-enhanced myocardial T1 time in diabetic patients ranging from 271 ms to 604 ms. There was no difference in the global contrast-enhanced myocardial T1 time in diabetic patients with and without a history of hypertension (422 ± 83 vs. 429 ± 52 ms, p = 0.74).

Global contrast-enhanced myocardial T1 time and LV function

Table 3 outlines the univariate Pearson correlations between global contrast-enhanced myocardial T1 time and different parameters of LV function for the entire study population. There was no significant correlation between global contrast-enhanced myocardial T1 time and LVEF (r = 0.04, p = 0.76; Figure 3). Similarly, there was no significant correlation between global contrast-enhanced myocardial T1 time and transmitral E/A ratio (r = -0.10, p = 0.44). However, there was a good correlation with global longitudinal strain (r = -0.71, p < 0.001; Figure 4) and septal E' (r = 0.47, p < 0.001; Figure 5), suggesting that a shorter global contrast-enhanced myocardial T1 time was associated with more impaired myocardial systolic and diastolic function respectively.

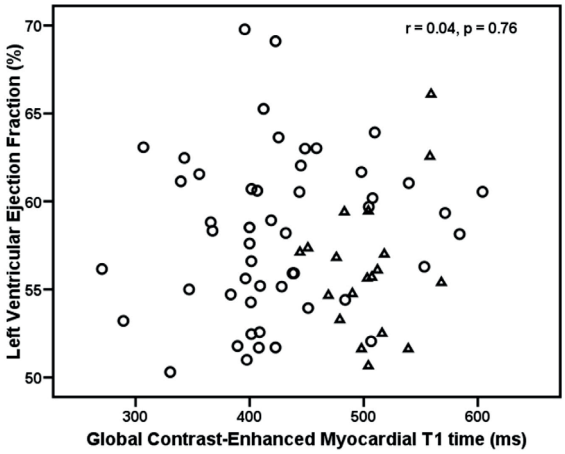


Figure 3. *Scatterplot showing no correlation between global contrast-enhanced myocardial T1 time and LVEF in diabetic patients (circles) and control subjects (triangles). Thus, LVEF may not accurately reflect the burden of diffuse interstitial fibrosis as represented by the global contrast-enhanced myocardial T1 time.*

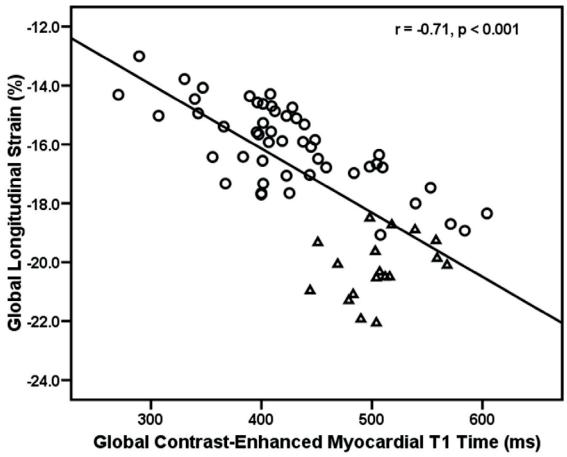


Figure 4. *Scatterplot showing correlation between global contrast-enhanced myocardial T1 time and global longitudinal strain for diabetic patients (circles) and control subjects (triangles). Thus, a higher burden of interstitial myocardial fibrosis (represented by shorter global contrast-enhanced myocardial T1 time) was associated with more impaired myocardial systolic function (represented by global longitudinal strain).*

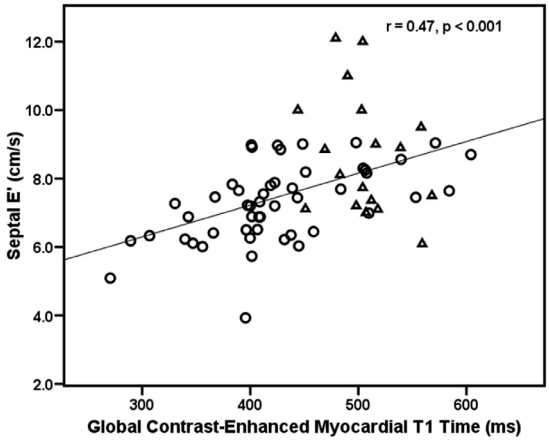


Figure 5. *Scatterplot showing correlation between global contrast-enhanced myocardial T1 time and septal E' for diabetic patients (circles) and control subjects (triangles). Thus, a higher burden of interstitial myocardial fibrosis (represented by shorter global contrast-enhanced myocardial T1 time) was associated with more impaired myocardial diastolic function (represented by septal E').*

Table 3. *Univariate Pearson correlation coefficients between global contrast-enhanced myocardial T1 time and left ventricular volume and functional parameters in diabetic patients and normal controls*

Variable	Correlation coefficient	p value
Heart rate	0.02	0.87
LV mass index	0.07	0.55
LVEDVI	0.15	0.22
LVESVI	0.09	0.47
LVEF	0.04	0.76
Cardiac output	0.32	0.01
Transmitral E/A ratio	-0.10	0.44
Deceleration time	0.36	0.003
Pulmonary S/D ratio	-0.03	0.83
Global longitudinal strain	-0.71	< 0.001
Septal E’	0.47	< 0.001
Septal E/e’ ratio	-0.33	0.007

EDVI = end-diastolic volume index; ESVI = end-systolic volume index; EF = ejection fraction; LV = left ventricular

Determinants of myocardial systolic function in diabetic patients

The mean global longitudinal strain for the diabetic patients was -16.1 ± 1.4%. Type 1 diabetic patients had significantly more preserved global longitudinal strain than type 2 diabetic patients (-16.4 ± 1.4 vs. -15.3 ± 1.2%, p = 0.009). Women had significantly more preserved global longitudinal strain than men (-16.6 ± 1.5 vs. -15.6 ± 1.2%, p = 0.017). Table 4 outlines the univariate Pearson correlations for global longitudinal strain.

Table 4. *Univariate Pearson correlation coefficients for global longitudinal strain and septal E’ in diabetic patients*

	Global longitudinal strain		Septal E’	
Variable	Correlation coefficient	p value	Correlation coefficient	p value
Age	0.14	0.32	-0.55	< 0.001
Body mass index	0.06	0.69	0.04	0.80
Systolic blood pressure	0.24	0.10	-0.17	0.23
Diastolic blood pressure	0.08	0.60	0.01	0.95
Heart rate	-0.15	0.30	0.03	0.82
LV mass index	0.20	0.17	0.18	0.20
LVEDVI	-0.21	0.15	0.45	0.001
LVESVI	0.03	0.86	0.37	0.009
Transmitral E/A ratio	-0.03	0.84	0.25	0.08
Deceleration time	-0.21	0.15	-0.08	0.58
Pulmonary S/D ratio	-0.02	0.89	-0.32	0.03
Global contrast-enhanced myocardial T1 time	-0.73	< 0.001	0.54	< 0.001

EDVI = end-diastolic volume index; ESVI = end-systolic volume index; EF = ejection fraction; LV = left ventricular

To identify independent determinants of global longitudinal strain for the diabetic patients, univariable predictors with $p < 0.20$ (including gender, type of diabetes, systolic blood pressure, deceleration time, LV mass index, LVEDVI and global contrast-enhanced myocardial T1 time) were all entered into a multiple linear regression model as covariates (Table 5). On multivariable analysis, the contrast-enhanced myocardial T1 time was an independent determinant of global longitudinal strain (model $R = 0.82$, $p < 0.001$). Furthermore, global contrast-enhanced myocardial T1 time was the strongest determinant of myocardial systolic function (standardized $\beta = -0.626$, $p < 0.001$). There were no significant interactions between global contrast-enhanced myocardial T1 time and the other significant covariates in the model. Figure 6 shows examples of 2 diabetic patients with high and low global contrast-enhanced myocardial T1 time with a corresponding normal and impaired global longitudinal strain respectively.

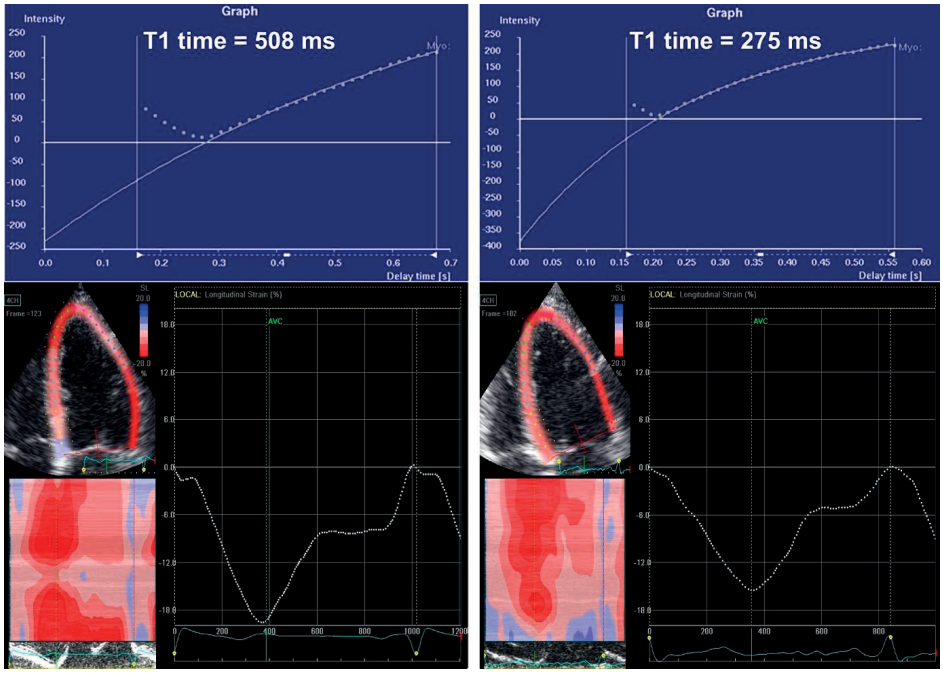


Figure 6. *Example of a diabetic patient with high global contrast-enhanced myocardial T1 time (508 ms) suggesting less interstitial fibrosis, and a corresponding global longitudinal strain of -19.0% (left panel). In contrast, another diabetic patient with a low global contrast-enhanced myocardial T1 time (275 ms) suggesting more interstitial fibrosis, and a reduced global longitudinal strain of -14.3% (right panel). Their respective LVEF on MRI were 59% and 57%.*

Determinants of myocardial diastolic function in diabetic patients

The mean septal E' for the diabetic patients was 7.3 ± 1.1 cm/s. Similarly, type 1 diabetic patients had more preserved septal E' compared to type 2 diabetic patients (7.6 ± 1.0

vs. 6.5 ± 0.9 cm/s, p < 0.001). There was no difference in the septal E' between men and women (7.3 ± 0.9 vs. 7.2 ± 1.4 cm/s, p = 0.64). Table 5 outlines the univariate Pearson correlations for septal E'.

To identify independent determinants of septal E' for the diabetic patients, univariable predictors with p < 0.20 (including age, type of diabetes, LVEDVI, transmitral E/A ratio, pulmonary S/D ratio and global contrast-enhanced myocardial T1 time) were all entered into a multiple linear regression model as covariates (Table 5). On multivariable analysis, the contrast-enhanced myocardial T1 time was an independent determinant of septal E' (model R = 0.78, p < 0.001). Similarly, global contrast-enhanced myocardial T1 time was the strongest determinant of myocardial function (standardized β = 0.432, p < 0.001). There were no significant interactions between global contrast-enhanced myocardial T1 time and the other significant covariates in the model.

Table 5. *Independent determinants of left ventricular global longitudinal strain and septal E' in diabetic patients*

Variable	Unstandardized β	Standardized β	p value
Global longitudinal strain			
Type of diabetes	0.834	0.266	0.02
Global myocardial T1 time	-0.012	-0.626	< 0.001
Septal E'			
Age	-0.036	-0.288	0.02
Type of diabetes	-0.587	-0.231	0.06
Global myocardial T1 time	0.007	0.432	< 0.001

EDVI = end-diastolic volume index; LV = left ventricular

DISCUSSION

Using MRI, the present study demonstrated that diabetic patients had a significantly shorter global contrast-enhanced myocardial T1 time compared to normal controls. Despite normal LVEF and no evidence of previous myocardial infarction, diabetic patients had a wide range of global contrast-enhanced myocardial T1 time. Furthermore, global contrast-enhanced myocardial T1 time was independently associated with and was the strongest determinant of both myocardial systolic and diastolic function.

Quantification of interstitial myocardial fibrosis by T1 mapping

A recent study by Iles and co-workers has histologically validated and demonstrated the ability of MRI T1 mapping to quantify diffuse interstitial myocardial fibrosis in chronic heart failure patients.[8] The authors showed that the global contrast-enhanced myocar-

dial T1 time by MRI T1 mapping was inversely correlated to the myocardial collagen content on endomyocardial biopsies.[8] When compared to normal control subjects, chronic heart failure patients had significantly shorter global contrast-enhanced myocardial T1 time due to an increased burden of interstitial fibrosis. Importantly, there was also a significant relationship between interstitial fibrosis and LV diastolic function, whereby patients with progressively worse LV diastolic function had increasingly shorter global contrast-enhanced myocardial T1 time.[8]

Interstitial myocardial fibrosis in diabetic patients

Although the pathogenesis of diabetic heart disease is likely to be multifactorial, the final common pathway is the activation of the renin-angiotensin-aldosterone system resulting in myocyte necrosis and deposition of collagen in the interstitial, perivascular and subendocardial regions.[2] The deposited collagen interacts with glucose to eventually form advanced glycation end-products, which is thought to contribute to myocardial stiffness, endothelial dysfunction and atherosclerosis.[2] In diabetic patients, the milieu of hyperglycemia, increased free fatty acid availability with altered metabolism, activation of renin-angiotensin-aldosterone system, and increased oxidative stress with endothelial dysfunction, all contribute to the subsequent development of replacement fibrosis, myocardial dysfunction and diabetic heart disease.[1, 2, 21, 22] In the present study, global contrast-enhanced myocardial T1 time using MRI T1 mapping was utilized as a surrogate marker of the burden of interstitial myocardial fibrosis. Consistent with previous studies, diabetic patients demonstrated evidence of interstitial myocardial fibrosis.[5, 6] Furthermore, there was a significant association between global contrast-enhanced myocardial T1 time and longitudinal myocardial systolic and diastolic function.

Global contrast-enhanced myocardial T1 time and myocardial dysfunction

Although quantification of LV systolic function by LVEF is easy to perform, it is relatively insensitive in detecting subtle myocardial dysfunction.[10, 23] This was reflected in the present study where there was a lack of relationship between LVEF and global contrast-enhanced myocardial T1 time. In contrast, advanced echocardiographic techniques such as global longitudinal strain analysis by 2D speckle tracking are more sensitive markers of myocardial systolic function.[10] Recently, in asymptomatic diabetic patients with normal LVEF, it has been demonstrated impaired global longitudinal systolic and diastolic function indicative of early subtle myocardial dysfunction.[10] By quantifying both global contrast-enhanced myocardial T1 time, global longitudinal strain and septal E', the present study demonstrated the independent association between global contrast-enhanced myocardial T1 time and associated myocardial systolic and dia-

stolic dysfunction in diabetic patients, thereby contributing to the understanding of the pathogenesis of diabetic heart disease.

Clinical implications

Contrast-enhanced myocardial T1 mapping may non-invasively quantify diffuse interstitial myocardial fibrosis in diabetic patients. The present study demonstrated a linear and independent relationship between global contrast-enhanced myocardial T1 time and myocardial systolic and diastolic dysfunction. Early diagnosis of diabetic heart disease by contrast-enhanced myocardial T1 mapping and 2D speckle tracking analyses may permit identification of patients at risk of subsequent development of clinical heart failure. Furthermore, a number of therapies have been postulated to inhibit the progression of heart failure, principally through the inhibition of the renin-angiotensin-aldosterone system and subsequent reduction of myocardial fibrosis.[10, 24-26] Similarly, recent studies have demonstrated the role of diffuse interstitial myocardial fibrosis in hypertensive heart disease.[27, 28] Thus, contrast-enhanced myocardial T1 mapping may permit non-invasive monitoring of the effectiveness of these anti-fibrotic therapies targeted at patients with diabetic or hypertensive heart disease.

Study limitations

The present study initially recruited approximately equal proportions of type 1 and 2 diabetic patients. However, 15 patients were excluded due to the unexpected presence of DCE indicative of previous myocardial infarction, resulting in disproportionally less type 2 diabetic patients. This could have influenced the multivariable analysis demonstrating a small but significantly different relationship between type of diabetes, global contrast-enhanced myocardial T1 time and global longitudinal strain. Therefore, the presence of underlying significant but undiagnosed coronary artery disease could have affected the results. Future larger studies will be needed to compare interstitial myocardial fibrosis in type 1 versus type 2 diabetes. Furthermore, although previous studies have validated global contrast-enhanced myocardial T1 time with interstitial fibrosis on histopathology[8, 29], the presence of myocardial inflammation may also have potentially confounded the present results.

There are currently several different MRI inversion pulse sequences that are available for generating contrast-enhanced myocardial T1 maps.[8, 30, 31] Furthermore, T1 recovery time naturally increases with higher MRI field strength, and is influenced by the dosage and type of contrast agent used, the timing of T1 map acquisition from time of injection, and cardiac output (which influences gadolinium wash-out rate from the myocardium). Thus, the derived global myocardial T1 time from one study is not directly comparable

across different studies that use different protocols. Furthermore, pre-contrast T1 maps were not acquired during the present study.

CONCLUSIONS

A shorter global contrast-enhanced myocardial T1 time (suggestive of a higher burden of interstitial myocardial fibrosis) in diabetic patients is independently associated with more impaired longitudinal myocardial systolic and diastolic function. Future larger studies are needed to confirm the present findings.

REFERENCE LIST

(1) Marwick T. The diabetic myocardium. *Curr Diab Rep* 2006;6:36-41.

(2) Aneja A, Tang WH, Bansilal S, Garcia MJ, Farkouh ME. Diabetic cardiomyopathy: insights into pathogenesis, diagnostic challenges, and therapeutic options. *Am J Med* 2008;121:748-757.

(3) Maya L, Villarreal FJ. Diagnostic approaches for diabetic cardiomyopathy and myocardial fibrosis. *J Mol Cell Cardiol* 2010;48:524-529.

(4) Shivu GN, Phan TT, Abozguia K, Ahmed I, Wagenmakers A, Henning A, Narendran P, Stevens M, Frenneaux M. Relationship Between Coronary Microvascular Dysfunction and Cardiac Energetics Impairment in Type 1 Diabetes Mellitus. *Circulation* 2010;121:1209-1215.

(5) Konduracka E, Gackowski A, Rostoff P, Galicka-Latala D, Frasik W, Piwowarska W. Diabetes-specific cardiomyopathy in type 1 diabetes mellitus: no evidence for its occurrence in the era of intensive insulin therapy. *Eur Heart J* 2007;28:2465-2471.

(6) Frustaci A, Kajstura J, Chimenti C, Jakoniuk I, Leri A, Maseri A, Nadal-Ginard B, Anversa P. Myocardial cell death in human diabetes. *Circ Res* 2000;87:1123-1132.

(7) Kim HW, Farzaneh-Far A, Kim RJ. Cardiovascular Magnetic Resonance in Patients With Myocardial Infarction: Current and Emerging Applications. *J Am Coll Cardiol* 2010;55:1-16.

(8) Iles L, Pfluger H, Phrommintikul A, Cherayath J, Aksit P, Gupta SN, Kaye DM, Taylor AJ. Evaluation of Diffuse Myocardial Fibrosis in Heart Failure With Cardiac Magnetic Resonance Contrast-Enhanced T1 Mapping. *J Am Coll Cardiol* 2008;52:1574-1580.

(9) Berg TJ, Snorgaard O, Faber J, Torjesen PA, Hildebrandt P, Mehlsen J, Hanssen KF. Serum levels of advanced glycation end products are associated with left ventricular diastolic function in patients with type 1 diabetes. *Diabetes Care* 1999;22:1186-1190.

(10) Ng ACT, Delgado V, Bertini M, van der Meer RW, Rijzewijk LJ, Shanks M, Nucifora G, Smit JWA, Diamant M, Romijn JA, De Roos A, Leung DY, Lamb HJ, Bax JJ. Findings from left ventricular strain and strain rate imaging in asymptomatic patients with type 2 diabetes mellitus. *Am J Cardiol* 2009;104:1398-1401.

(11) Fang ZY, Schull-Meade R, Downey M, Prins J, Marwick TH. Determinants of subclinical diabetic heart disease. *Diabetologia* 2005;48:394-402.

(12) Leung DY, Ng AC. Emerging clinical role of strain imaging in echocardiography. *Heart Lung Circ* 2010;19:161-174.

(13) Alberti KG, Zimmet PZ. Definition, diagnosis and classification of diabetes mellitus and its complications. Part 1: diagnosis and classification of diabetes mellitus provisional report of a WHO consultation. *Diabet Med* 1998;15:539-553.

(14) K/DOQI clinical practice guidelines for chronic kidney disease: evaluation, classification and stratification. *Am J Kidney Dis* 2002;39:S1-S266.

(15) Karlsson M, Nordell B. Phantom and in vivo study of the Look-Locher T1 mapping method. *Magn Reson Imaging* 1999;17:1481-1488.

(16) Mosteller RD. Simplified calculation of body-surface area. *N Engl J Med* 1987;317:1098.

(17) Gai N, Turkbey EB, Nazarian S, van der Geest RJ, Liu CY, Lima JA, Bluemke DA. T1 mapping of the gadolinium-enhanced myocardium: adjustment for factors affecting interpatient comparison. *Magn Reson Med* 2011;65:1407-1415.

(18) Nishimura R, Miller FJ, Callahan M, Benassi R, Seward J, Tajik A. Doppler echocardiography: theory, instrumentation technique and application. *Mayo Clin Proc* 1985;60:321-343.

(19) Tajik A, Seward J, Hagler D, Mair D, Lie J. Two dimensional real-time ultrasonic imaging of the heart and great vessels: technique, image orientation, structure identification and validation. *Mayo Clin Proc* 1978;53:271-303.

(20) Shanks M, Ng AC, van de Veire NR, Antoni ML, Bertini M, Delgado V, Nucifora G, Holman E, Choy JB, Leung DY, Schalij MJ, Bax JJ. Incremental prognostic value of novel left ventricular diastolic indexes for prediction of clinical outcome in patients with ST-elevation myocardial infarction. *Am J Cardiol* 2010;105:592-597.

(21) Boudina S, Abel ED. Diabetic Cardiomyopathy Revisited. *Circulation* 2007;115:3213-3223.

(22) Hammer S, Snel M, Lamb HJ, Jazet IM, van der Meer RW, Pijl H, Meinders EA, Romijn JA, De Roos A, Smit JW. Prolonged caloric restriction in obese patients with type 2 diabetes mellitus decreases myocardial triglyceride content and improves myocardial function. *J Am Coll Cardiol* 2008;52:1006-1012.

(23) Marwick TH. Diabetic heart disease. *Heart* 2006;92:296-300.

(24) Diez J, Querejeta R, Lopez B, Gonzalez A, Larman M, Martinez Ubago JL. Losartan-dependent regression of myocardial fibrosis is associated with reduction of left ventricular chamber stiffness in hypertensive patients. *Circulation* 2002;105:2512-2517.

(25) Maron BA, Leopold JA. Aldosterone Receptor Antagonists: Effective but Often Forgotten. *Circulation* 2010;121:934-939.

(26) Pitt B, Zannad F, Remme WJ, Cody R, Castaigne A, Perez A, Palensky J, Wittes J, The Randomized Aldactone Evaluation Study Investigators. The Effect of Spironolactone on Morbidity and Mortality in Patients with Severe Heart Failure. *N Engl J Med* 1999;341:709-717.

(27) Diez J, Frohlich ED. A translational approach to hypertensive heart disease. *Hypertension* 2010;55:1-8.

(28) Berk BC, Fujiwara K, Lehoux S. ECM remodeling in hypertensive heart disease. *J Clin Invest* 2007;117:568-575.

(29) Maceira AM, Joshi J, Prasad SK, Moon JC, Perugini E, Harding I, Sheppard MN, Poole-Wilson PA, Hawkins PN, Pennell DJ. Cardiovascular Magnetic Resonance in Cardiac Amyloidosis. *Circulation* 2005;111:186-193.

(30) Messroghli DR, Walters K, Plein S, Sparrow P, Friedrich MG, Ridgway JP, Sivananthan MU. Myocardial T1 mapping: application to patients with acute and chronic myocardial infarction. *Magn Reson Med* 2007;58:34-40.

(31) Flett AS, Hayward MP, Ashworth MT, Hansen MS, Taylor AM, Elliott PM, McGregor C, Moon JC. Equilibrium Contrast Cardiovascular Magnetic Resonance for the Measurement of Diffuse Myocardial Fibrosis. Preliminary Validation in Humans. *Circulation* 2010;122:138-144.

6

Impact of Epicardial Adipose Tissue, Left Ventricular Myocardial Fat Content and Interstitial Fibrosis on Myocardial Contractile Function

Arnold C.T. Ng, Mark Strudwick, Rob J. van der Geest, Austin C.C. Ng, Lisa Gillinder, Shi Yi Goo, Gary Cowin, Victoria Delgado, William Y.S. Wang, Jeroen J. Bax

Circ Cardiovasc Imaging. 2018;11(8):e007372

ABSTRACT

Background: Current understanding of metabolic heart disease consists of myriad of different pathophysiological mechanisms. Epicardial adipose tissue (EAT) is increasingly recognized as metabolically active and associated with adverse cardiovascular outcomes. The present study aimed to investigate the effect of increased EAT volume index on left ventricular (LV) myocardial fat content (LV-myoFat) and burden of interstitial myocardial fibrosis, and their subsequent effects on LV myocardial contractile function.

Methods: 40 volunteers (mean age 35 ± 10 years, 26 males) of varying body mass index (BMI: 25.0 ± 4.1 kg/m^2, range 19.3–36.3 kg/m^2) and without diabetes or hypertension were prospectively recruited. EAT volume index, LV-myoFat and extracellular volume (ECV) were quantified by magnetic resonance imaging (MRI). LV myocardial contractile function was quantified by speckle tracking echocardiography global longitudinal strain (GLS) on the same day as MRI examination.

Results: Mean total EAT volume index, LV-myoFat and ECV were 30.0 ± 19.6 cm^3/m^2, 5.06 ± 1.18% and 27.5 ± 0.5% respectively. On multivariable analyses, increased EAT volume index and insulin resistance were independently associated with both increased LV-myoFat content and higher burden of interstitial myocardial fibrosis. Furthermore, increased EAT volume index was independently associated with LV GLS.

Conclusions: Increased EAT volume index and insulin resistance were independently associated with increased myocardial fat accumulation and interstitial myocardial fibrosis. Increased EAT volume index was associated with detrimental effects on myocardial contractile function as evidenced by a reduction in LV GLS.

INTRODUCTION

There is a growing body of evidence that the altered metabolic milieu seen in obese and diabetic patients causes myocardial structural changes and contractile dysfunction.[1] Commonly referred to as metabolic heart disease, we have previously shown that impaired left ventricular (LV) myocardial systolic function as quantified by 2-dimensional (2D) global longitudinal strain (GLS) echocardiography was associated with increased myocardial fat accumulation, coronary artery disease, increased interstitial fibrosis, and increased epicardial adipose tissue (EAT) volume.[2-5] EAT is depot of visceral fat directly overlying the myocardium, and is of similar embryological origin as abdominal mesenteric and omental visceral fat.[6] Increasingly, EAT is recognized as a metabolically active endocrine organ that secretes adipokines associated with detrimental myocardial and coronary vascular dysfunction.[7] Several studies have demonstrated a direct correlation between EAT and myocardial fat (i.e. triglyceride [TG]) accumulation,[8, 9] and animal research suggested that EAT may directly channel fatty acids to the myocardium as a local energy source.[10, 11] However, when the amount of free fatty acid uptake by the heart exceeds its oxidative capacity, it is converted and stored as intracellular TG.[12] It is currently accepted that the intracellular myocardial TG is probable inert, but increased shunting of free fatty acid into the non-oxidative pathway leads to accumulation of toxic fatty acid intermediates such as ceramide that disrupt normal cellular signaling and eventually leads to cellular apoptosis and replacement fibrosis.[13]

Magnetic resonance imaging (MRI) techniques such as proton magnetic resonance spectroscopy ([1H]-MRS) and multi-echo Dixon water and fat separated imaging with variable projection (VARPRO) can quantify LV myocardial fat (LV-myoFat) content.[14, 15] Similarly, the modified Look-Locker inversion recovery (MOLLI) sequence can quantify the burden of interstitial fibrosis by extracellular volume (ECV) expansion.[16, 17] In the present study, volunteers of normal weight, as well as overweight and obese individuals without the confounding influences of diabetes or hypertension were evaluated to determine the effect of increased EAT volume index on LV-myoFat content and burden of LV interstitial fibrosis. We hypothesize that: 1) increased EAT volume index is independently associated with increased myocardial fat accumulation and interstitial fibrosis; and 2) EAT volume index is independently associated with myocardial contractile function.

METHODS

Study population and study protocol

A total of 40 volunteers with a wide range of body mass index (BMI) were prospectively recruited from the community. Exclusion criteria included age < 18 years, pregnancy, rhythm other than sinus rhythm, hypertension, diabetes mellitus, previously known underlying coronary artery disease, LV systolic dysfunction or previous myocardial infarction, moderate or severe valvular stenosis or regurgitation, pre-existing hepatic or renal disorders, active smoker, current use of any regular medications, inability to provide informed consent, and inability to undergo a cardiac MRI. All participants' blood tests, transthoracic echocardiogram and cardiac MRI examinations were performed on the same day after an overnight fast.

Figure 1 outlines the study protocol. In brief, a subset of 15 randomly selected volunteers underwent "clinical reference standard" [1H]-MRS to validate LV-myoFat content by VARPRO. All 40 volunteers underwent cardiac MRI to quantify LV volumes, LV mass, EAT volume, LV-myoFat content by the VARPRO, and burden of LV interstitial fibrosis by ECV using the MOLLI sequence. [4, 16, 17] All 40 volunteers also underwent echocardiograms to quantify myocardial contractile function by 2D LV GLS.

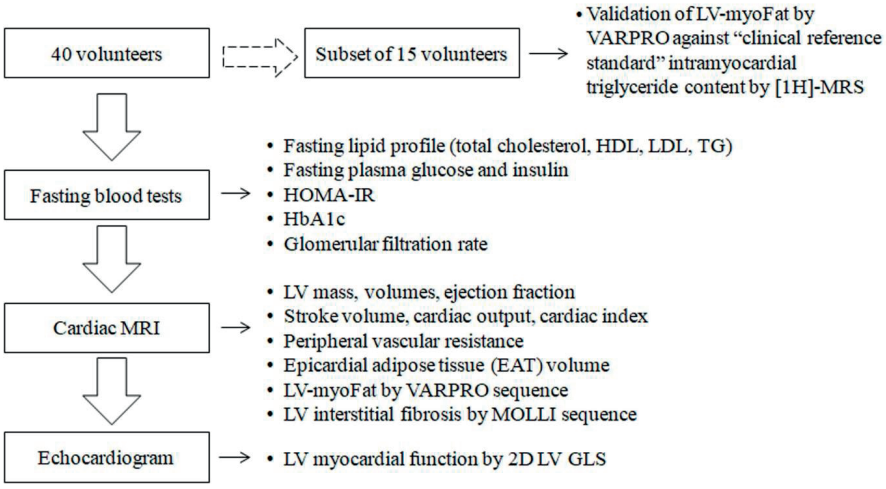


Figure 1. *Outline of study protocol. Subset of 15 volunteers underwent quantification of myocardial TG by [1H]-MRS to validate LV-myoFat by the VARPRO sequence. All 40 volunteers underwent fasting blood tests, cardiac MRI and echocardiography on the same day after an overnight fast. LV-myoFat = left ventricular myocardial fat; [1H]-MRS = proton magnetic resonance imaging; HDL = high density lipoprotein; LDL = low density lipoprotein; TG = triglyceride; HOMA-IR = homeostatic model assessment index of insulin resistance; HbA1c = glycated hemoglobin; VARPRO = variable projection; MOLLI = modified Look-Locker inversion recovery; LV = left ventricle/ventricular; 2D = 2-dimensional; GLS = global longitudinal strain.*

The study was approved by the institutional ethics committee and all subjects provided written informed consent. The data, analytic methods, and study materials will not be made available to other researchers for purposes of reproducing the results or replicating the procedure for competitive reasons.

Demographic, anthropomorphic and metabolic data

All subjects underwent an overnight fast of at least 8 hours. Clinical data collected included age, gender, height, weight, waist/hip ratio, and resting blood pressures. Waist circumference was measured midway between the lower rib margin and iliac crest. Hip circumference was measured at the level of widest circumference over greater trochanters.[18] Blood tests included fasting lipid profile, fasting plasma glucose, glycated hemoglobin (HbA1c), insulin, and glomerular filtration rates (GFR) calculated by the Modification of Diet in Renal Disease formula.[19]

High-density lipoprotein (HDL) cholesterol was measured as a homogeneous assay in liquid phase (Boehringer Mannheim, Mannheim, Germany) on a Hitachi 747 autoanalyzer. Low-density lipoprotein (LDL) cholesterol was calculated according to the Friedewald equation: LDL-cholesterol (mmol/L) = Total cholesterol – HDL-cholesterol – TG / 2.2.

Fasting plasma glucose was measured by enzymatic assay (Dade Behring, Newark, DE, USA). Serum insulin was evaluated using a chemiluminescent enzyme immunoassay (Immulite 2000; Diagnostic Products, Los Angeles, CA, USA). The homeostatic model assessment (HOMA) index of insulin resistance (HOMA-IR) was computed using the HOMA calculator that utilizes the HOMA2 model as previously reported.[20] HbA1c measurements were performed using high performance liquid chromatography cation-exchange analyzers by Bio-Rad D-10™ Hemoglobin Testing System (Bio-Rad Laboratories, Inc., Hercules, CA). This assay is National Glycohemoglobin Standardization Program (NGSP) and International Federation of Clinical Chemistry and Laboratory Medicine (IFCC) certified, and standardized to the Diabetes Control and Complications Trial (DCCT) assay.

Cardiac magnetic resonance imaging

All participants underwent a cardiac MRI examination using a 1.5T Siemens Magnetom Avanto (Erlangen, Germany) system on the same day as their transthoracic echocardiogram and blood tests. During the examination, the entire heart was imaged in the short-axis orientation with retrospective ECG-gating and breath-hold. Typical imaging parameters were: balanced steady state free-precession imaging, echo time (TE) = 1.0 ms, repetition time (TR) = 3.1 ms, flip angle = 54°, slice thickness = 8 mm with a gap of 2 mm, field of view = 340x340 mm, reconstructed matrix size = 156x192.

LV end-diastolic mass index, LV end-diastolic volume index (EDVI) and LV end-systolic volume index (ESVI) were measured and corrected for body surface area.[21] LV ejection fraction (LVEF) was calculated and expressed as a percentage. Differences in LV end-diastolic and end-systolic volumes were used to calculate stroke volume, multiplied by heart rate to calculate cardiac output, and corrected for body surface area to calculate cardiac index. Peripheral vascular resistance was calculated as the ratio of mean blood pressure to cardiac output. Images were digitally stored on hard disks and analyzed offline using dedicated quantitative software (MASS V2010-EXP, Leiden University Medical Center, Leiden, The Netherlands).

MRI quantification of myocardial triglyceride/fat content

Quantification of myocardial TG content by [1H]-MRS is considered the "clinical reference standard", but is time consuming to perform (mean scan duration 13.2 ± 4.5min).[13, 22] In contrast, newer MRI techniques such as VARPRO can rapidly obtain fat and water separated images to quantify LV-myoFat content in a single breath-hold. Furthermore, it can avoid contamination from EAT. Therefore, a subset of 15 volunteers underwent concomitant [1H]-MRS to validate LV-myoFat by VARPRO.

Quantification of myocardial triglyceride content by [1H]-MRS

Cardiac [1H]-MRS was performed as previously described (Figure 2, top panels).[2,22] Briefly, [1H]-MRS spectra were obtained by point resolved spectroscopy sequence (PRESS) with an 6mL voxel (1x2x3 cm) placed in the interventricular septum using the 4-chamber and short-axis views at end-diastole. Spectroscopic data acquisitions were double-triggered with ECG triggering and respiratory navigator echoes to minimize motion artifacts. End-diastolic spectra were acquired with the following parameters: TE = 25 ms, TR = 2000 ms, 1024 data points, bandwidth 1000Hz. Automatic shimming was performed before the spectroscopy data acquisition using the gradient-recalled echo shim technique whereby a field map was generated from a single-slab double-echo 3D gradient-recalled echo acquisition with two in-phase TEs with respect to fat and water, which were then used to calculate the shim currents to improve B0 homogeneity. Water-suppressed spectra were acquired with 128 signal averages to quantify myocardial TG. Non-water suppressed spectra were acquired with 16 signal averages and used as an internal standard.

[1H]-MRS data were then fitted by use of Java-based MR user interface software (jMRUI version 2.2, Leuven, Belgium) AMARES algorithm as previously described.[2] Resonance frequency estimates for myocardial TG were described by assuming Gaussian line shapes and summing the amplitudes of lipid resonances at 0.9 and 1.3 ppm. Resonance frequency estimate for water used for internal standardization was described by assuming a Lorentzian line shape that peaks at 4.7ppm. Myocardial TG content relative

to water was calculated and expressed as a percentage based on: (signal amplitude of myocardial TG)/(signal amplitude of water)x100%.[2]

Quantification of LV-myoFat content by VARPRO sequence

The VARPRO multi-point Dixon algorithm is a multi-echo gradient sequence with fat and water separation.[14, 23, 24] This multi-echo Dixon fat-water separation jointly estimates the fieldmap, fat, and water images (Figure 2, middle panel). The sequence was ECG triggered, with 2 R-R intervals between inversions, and used an echo-train readout with 4 echoes. Typical imaging parameters were: gradient echo, TE = 1.27, 3.18, 5.09, 7.00 ms, TR = 11.2 ms, flip angle = 24°, slice thickness 6 mm, field of view = 360 x 292 mm, reconstructed matrix size = 256x218, bandwidth = 1502 Hz/pixel. The LV basal and mid-ventricular short-axis slices by the VARPRO sequence were obtained at exactly the same LV level as quantification of interstitial fibrosis by MOLLI sequence (see below).

During analysis, the LV contours at the basal and mid-ventricular short axis slices were deliberately drawn in the mid-myocardium to exclude and avoid contamination by EAT and the LV blood pool using MASS research software. Although the LV apical segments were also acquired during the VARPRO image acquisitions, it was not included in the analyses due to partial volume effects from EAT and LV blood pool secondary to the curvature of the LV apex that will compromise accurate quantifications of LV-myoFat content. LV-myoFat fat content was calculated and expressed as a percentage based on: (mean pixel signal intensity of LV fat-only image)/(mean pixel signal intensity of LV water-only image)x100%.

MRI quantification of LV interstitial fibrosis by MOLLI sequence

The MOLLI T1 mapping sequence was used to quantify the burden of interstitial fibrosis by ECV.[16, 17] All participants received 0.1mmol/kg of gadolinium diethylenetriamine penta-acetic acid. The MOLLI sequence imaging parameters were: single-shot steady-state free precession read out with trigger delay to coincide with end-diastole, TE = 1.0 ms, TR = 2.7 ms, flip angle = 35°, slice thickness = 8mm, field of view = 340x340 mm, reconstructed matrix size = 106x192 pixels, trigger delay = 300ms. The LV basal and mid-ventricular short-axis slices by the MOLLI sequence were obtained at exactly the same LV level as quantification of LV-myoFat content by VARPRO. These images were then processed with a curve fitting technique to generate T1 maps as described below.

To quantify the ECV, LV endocardial and epicardial borders were outlined using MASS research software.[4, 25] Contours were deliberately drawn to ensure the inclusion of only myocardium and the exclusion of EAT and LV blood pool. The software then performs automatic pixel-by-pixel quantification of myocardial T1 time by fitting data acquired

at the various inversion times.[4, 25] A mean global native and post-contrast myocardial T1 time were subsequently automatically calculated as the average of all the individual myocardial T1 time from each pixel. ECV was calculated as per previous publication and expressed as a percentage [16]:

$$Myocardial\ ECV = (1 - haematocrit) \times \frac{\left(\frac{1}{post\ contrast\ myocardial\ T1} - \frac{1}{native\ myocardial\ T1}\right)}{\left(\frac{1}{post\ contrast\ blood\ T1} - \frac{1}{native\ blood\ T1}\right)}$$

A higher ECV is indicative of increased collagen deposition and thus a greater degree of myocardial interstitial fibrosis.

MRI quantification of epicardial adipose tissue volume

Total EAT volume was quantified using a T1 weighted double inversion recovery Half-Fourier-Acquired Single-shot Turbo spin Echo (HASTE) black blood imaging (Figure 2, bottom panels). Manual contours were drawn whereby mediastinal fat and pericardial fat (outside the visceral pericardium and on the external surface of the parietal pericardium) were excluded. The volumes of EAT in all the slices were calculated by converting the number of pixels to square centimetres multiplied by the slice thickness. Total EAT volume was subsequently calculated by summing the volumes of all slices from the level of pulmonary artery bifurcation to the diaphragm and indexed to body surface area. Typical imaging parameters were: turbo spin echo, TE = 26.0 ms, TR = 1000 ms depending on RR interval, flip angle = 160°, slice thickness 6 mm with a gap of 6 mm, field of view = 440x440 mm, reconstructed matrix size = 256x176.

MRI quantification of visceral adiposity

Abdominal visceral fat depots were quantified by using the VARPRO sequence with similar imaging parameters as outlined previously. Six consecutive transverse images were obtained with the middle image at the middle of the fourth lumbar vertebra. Similarly, manual contours were drawn to include only the abdominal visceral fat, and the volumes of the visceral fat depots in each slice was calculated by converting the number of pixels to square centimeters multiplied by the slice thickness. The total L4 visceral fat volume was calculated by summing the volumes of all 6 slices.

Echocardiography

Transthoracic echocardiography was performed with the subjects at rest using a commercially available ultrasound system (Vivid E9, 4V probe, GE-Vingmed, Horten, Norway) on the same day as their cardiac MRI and blood tests. A complete 2D, color, pulsed

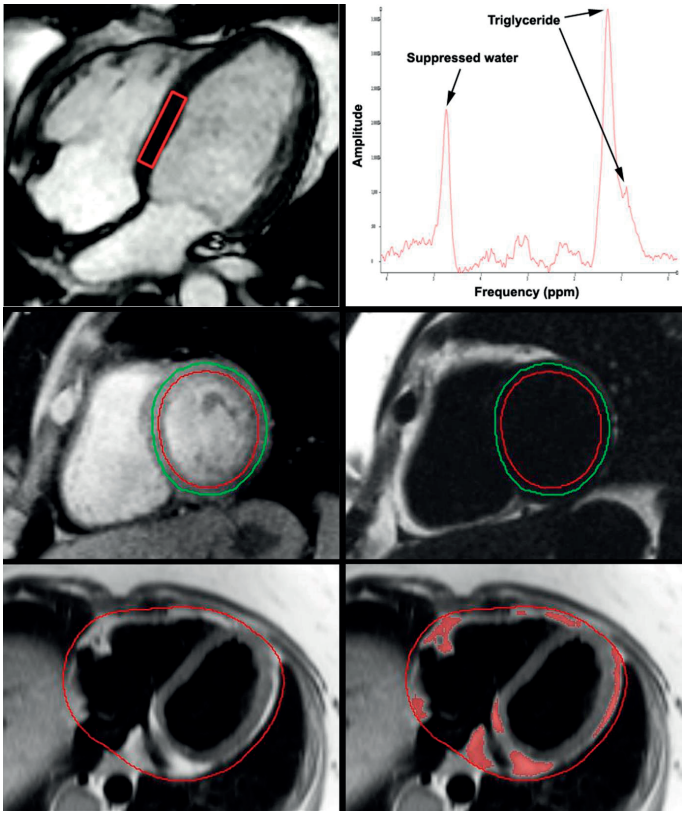


Figure 2. *Quantification of myocardial TG by "clinical reference standard" [1H]-MRS with the voxel of interest placed in the interventricular septum (top left panel). Myocardial TG was calculated from the summation of the lipid resonance amplitudes at 0.9 and 1.3ppm (top right panel). Quantification of LV-myoFat by VARPRO where epicardial and endocardial borders were deliberately drawn in the mid-myocardium to avoid contamination from EAT and LV blood pool (middle panels). The "water only" (middle left panel) and "fat only" (middle right panel) were obtained simultaneously from VARPRO, and both the endocardial and epicardial contours were identical on both images. Example of quantification of EAT volume (bottom panels).*

and continuous-wave Doppler echocardiogram was performed according to standard techniques.[26] All images were digitally stored on hard disks for offline analysis (EchoPAC version 113, GE-Vingmed, Horten, Norway).

Doppler assessment

Mitral inflow velocities were recorded using conventional pulsed-wave Doppler echocardiography in the apical 4-chamber view using a 2 mm sample volume. Transmitral early (E wave) and late (A wave) diastolic velocities as well as deceleration time were recorded at the mitral leaflet tips. Pulsed-wave tissue Doppler velocities were recorded at the septal mitral annulus in the apical 4-chamber view at end-expiration as recommended to obtain the mitral annular early diastolic (e') velocity.[27] LV filling pressure (septal E/e') was calculated as the ratio of transmitral E wave to septal mitral annular e' velocity.

Two-dimensional speckle tracking

2D speckle tracking analyses were performed on standard grey scale images in the apical 2-, 3- and 4-chamber views. During analysis, the endocardial border was manually traced at end-systole and the region of interest width adjusted to include the entire myocardium. LV GLS was calculated from the 3 individual apical global longitudinal strain curves.

Statistical analysis

All continuous variables were tested for Gaussian distribution. Continuous variables were presented as mean ±1 SD unless otherwise stated, and categorical variables were presented as frequencies and percentages. Unpaired Student's t-test and Mann-Whitney U test were used to compare 2 groups of continuous variables of Gaussian and non-Gaussian distribution respectively. Pearson correlation was used to determine the association between 2 continuous variables. Intraclass correlation and Bland-Altman plot were used to validate VARPRO to quantify LV-myoFat content against "clinical reference standard" myocardial TG content by [1H]-MRS. Multiple linear regression analyses were performed to identify independent variables associated with LV-myoFat content by VARPRO sequence, ECV as a measure of LV interstitial fibrosis, and 2D LV GLS by speckle tracking echocardiography. In each multiple linear regression model, significant univariables with $p < 0.05$ were entered as covariates and independent variables were identified using the backward elimination method. To avoid potential multicollinearity, a tolerance of > 0.4 (equating to a Variance Inflation Factor of > 2.5) was set. To determine if EAT volume index was independently associated with LV-myoFat, ECV, and 2D LV GLS (rather than just a measure of overall visceral adiposity), all multivariable analyses were repeated with L4 visceral fat volume forced into the models. A 2-tailed p value of < 0.05 was considered significant. All statistical analyses were performed using IBM SPSS Statistics for Windows, version 21.0 (Armonk, NY).

RESULTS

A total of 40 volunteers (26 males) with a mean age of 35 ± 10 years were recruited. The mean heart rate, LVEDVI, LVESVI, LVEF and LV mass index were 61 ± 9 beats/min, 90 ± 15 mL/m^2, 40 ± 8 mL/m^2, 55 ± 4% and 43 ± 8 g/m^2 respectively.

The mean BMI was 25.0 ± 4.1 kg/m^2 (range 19.3 to 36.3 kg/m^2), and the mean waist/hip ratio was 0.88 ± 0.11 (range 0.74 to 1.33). Twenty-two volunteers (55.0%) were identified as overweight/obese based on waist/hip ratio as classified by the World Health Organization cut-off values. The mean total EAT volume index was 30.0 ± 19.6 cm^3/m^2, and there was no gender difference in EAT volume index ($p = 0.28$).

Table 1. *Clinical, MRI and echocardiographic characteristics of study population.*

Variable	All Volunteers (n = 40)	Volunteers without [1H]-MRS (n = 25)	Volunteers with [1H]-MRS (n = 15)	p value*
Clinical				
Age (years)	35 ± 10	35 ± 11	36 ± 9	0.79
Male gender	26 (65%)	16 (64%)	10 (67%)	0.86
Waist/hip ratio	0.88 ± 0.11	0.88 ± 0.10	0.89 ± 0.14	0.92
Heart rate (beats/min)	61 ± 9	61 ± 10	60 ± 8	0.83
Systolic BP (mmHg)	128 ± 11	129 ± 11	126 ± 12	0.51
Diastolic BP (mmHg)	79 ± 9	79 ± 9	79 ± 10	0.97
Biochemical				
Total cholesterol (mmol/L)	4.82 ± 0.72	4.85 ± 0.72	4.78 ± 0.74	0.77
LDL cholesterol (mmol/L)	2.92 ± 0.56	2.93 ± 0.51	2.91 ± 0.66	0.89
HDL cholesterol (mmol/L)	1.44 ± 0.39	1.47 ± 0.47	1.40 ± 0.23	0.60
Plasma triglyceride (mmol/L)	1.03 ± 0.52	1.02 ± 0.48	1.04 ± 0.59	0.93
Fasting plasma glucose (mmol/L)	5.0 ± 0.5	5.0 ± 0.6	5.0 ± 0.3	0.67
HbA1c (%)	5.2 ± 0.2	5.2 ± 0.2	5.2 ± 0.3	0.93
Fasting Insulin (mU/L)	5.8 ± 5.1	6.2 ± 5.7	5.2 ± 4.1	0.99
HOMA-IR	1.30 ± 1.11	1.39 ± 1.24	1.16 ± 0.88	0.92
GFR (mL/min/1.73m^2)	99 ± 16	97 ± 17	101 ± 13	0.52
MRI				
LV mass index (g/m^2)	43 ± 8	43 ± 6	43 ± 10	0.89
LVEDVI (mL/m^2)	90 ± 15	91 ± 11	89 ± 21	0.74
LVESVI (mL/m^2)	40 ± 8	41 ± 6	39 ± 10	0.48
LVEF (%)	55 ± 4	55 ± 3	55 ± 4	0.58
Stroke volume (mL)	95 ± 19	95 ± 15	96 ± 25	0.81
Cardiac output (L/min)	5.7 ± 1.1	5.7 ± 1.1	5.7 ± 1.2	0.96
Cardiac index (L/min/m^2)	3.0 ± 0.6	3.0 ± 0.6	2.9 ± 0.6	0.80
Peripheral vascular resistance (dyn.s/cm^5)	1385 ± 288	1393 ± 318	1371 ± 240	0.82
L4 visceral fat volume (cm^3)	324 ± 239	227 ± 200	264 ± 219	0.60
EAT volume index (cm^3/m^2)	30.0 ± 19.6	27.3 ± 16.0	34.6 ± 24.3	0.26
LV-myoFat content (%)	5.1 ± 1.2	5.0 ± 1.1	5.2 ± 1.3	0.51
ECV (%)	27.5 ± 0.5	27.3 ± 0.5	27.8 ± 0.4	0.037
Echocardiography				
Transmitral E velocity (m/s)	0.77 ± 0.17	0.77 ± 0.18	0.78 ± 0.16	0.98
Transmitral E/A ratio	1.8 ± 0.8	1.8 ± 0.9	1.9 ± 0.6	0.77
Deceleration time (ms)	166 ± 28	169 ± 31	159 ± 20	0.26
Septal E' velocity (cm/s)	12.3 ± 3.0	11.9 ± 3.1	12.9 ± 2.6	0.30
Septal E/e' ratio	6.6 ± 1.8	6.8 ± 1.8	6.2 ± 1.8	0.33
2D LV GLS	-19.0 ± 2.4	-19.0 ± 2.7	-19.2 ± 2.0	0.77

*p value by unpaired Student's t-test or Mann-Whitney U test for continuous variables of Gaussian and non-Gaussian distribution respectively, and Chi square test for categorical variables. 2D: 2-dimensional; BP: blood pressure; EAT: epicardial adipose tissue; ECV: extracellular volume; EDVI: end-diastolic volume index; ESVI: end-systolic volume index; EF: ejection fraction; GFR: glomerular filtration rate; GLS: global longitudinal strain; HbA1c: glycated hemoglobin; HDL: high density lipoprotein; LDL: low density lipoprotein; HOMA-IR: homeostatic model assessment index of insulin resistance; LV: left ventricular; LV-myoFat: left ventricular myocardial fat content by VARPRO sequence.

Validation of VARPRO sequence against [1H]-MRS

A subset of 15 randomly volunteers underwent "clinical reference standard" [1H]-MRS to quantify myocardial TG content. Table 1 outlines the baseline clinical, MRI and echocardiographic characteristics between the 15 randomly selected volunteers against the rest of the cohort. Other than a slight difference in ECV between these 2 groups (27.3 ± 0.5 vs. 27.8 ± 0.4%, p = 0.037), there were no significant differences in other variables. Figures 3 and 4 show LV-myoFat content by VARPRO overestimated myocardial TG content compared to [1H]-MRS:

$$\textit{LV-myoFat content by VARPRO} = 1.31 \times (\textit{Intramyocardial TG by } [1H]\text{-}MRS) + 3.84$$

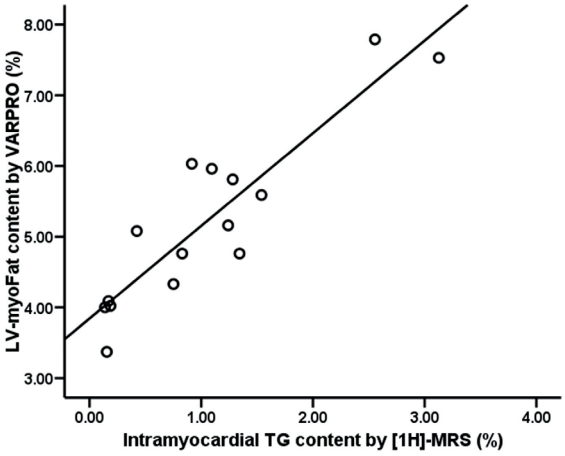


Figure 3. *Scatterplot showing excellent reliability of VARPRO quantification of LV-myoFat against "clinical reference standard" quantification of myocardial TG content by [1H]-MRS.*

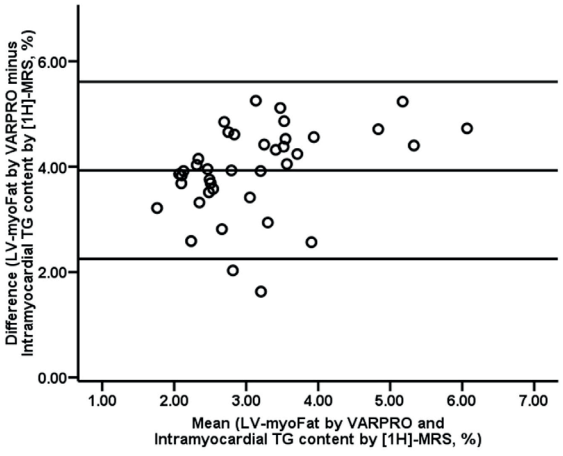


Figure 4. *Bland-Altman plot showing overestimation of VARPRO quantification of LV-myoFat against "clinical reference standard" quantification of myocardial TG content by [1H]-MRS.*

However, LV-myoFat content quantification by VARPRO had excellent reliability compared to the "clinical reference standard" myocardial TG quantification by [1H]-MRS with an intraclass correlation for consistency of r = 0.92 (95% confidence interval 0.75-0.97).

Determinants of LV-myoFat content

The mean LV-myoFat content by VARPRO for all 40 volunteers was 5.06 ± 1.18%. There was no gender difference in LV-myoFat content (p = 0.36). LV-myoFat content increased with older age (r = 0.51, p = 0.001), higher insulin resistance (HOMA-IR, r = 0.51, p = 0.001) and increasing measures of obesity by EAT volume index (r = 0.61, p < 0.001), waist/hip ratio (r = 0.59, p < 0.001) and L4 visceral fat volume (r = 0.60, p < 0.001). There was also a correlation between LV-myoFat content and plasma TG (r = 0.48, p = 0.002), LDL-cholesterol (r = 0.33, p = 0.038) and HDL-cholesterol (r = -0.37, p = 0.018), but not total cholesterol (p = 0.23).

To identify the independent variables associated with LV-myoFat content, significant univariables (age, HOMA-IR, EAT volume index, waist/hip ratio, plasma TG, LDL-cholesterol and HDL-cholesterol) were entered as covariates into a multiple linear regression model. On multivariable analysis, only HOMA-IR (standardized β = 0.32, p = 0.024) and EAT volume index (standardized β = 0.47, p = 0.002) were independently associated with LV-myoFat content.

To determine if increased EAT volume index was truly independently associated with LV-myoFat content rather than just a measure of overall visceral adiposity, waist/hip ratio was replaced with L4 visceral fat volume in the multiple linear regression model. Although L4 visceral fat volume was highly correlated with EAT volume index (r = 0.69, p < 0.001), it was forced into the multivariable model. Despite that, similar results were obtained with only HOMA-IR (standardized β = 0.32, p = 0.024) and EAT volume index (standardized β = 0.47, p = 0.002) remaining as significantly associated with LV-myoFat content.

Determinants of burden of LV interstitial fibrosis

The mean ECV was 27.5 ± 0.5%, and there was no gender difference (p = 0.88). On univariable analysis, ECV was significantly correlated with higher LV-myoFat content (r = 0.71, p < 0.001), older age (r = 0.64, p = 0.002), higher HOMA-IR (r = 0.51, p = 0.021) and increasing EAT volume index (r = 0.69, p = 0.001).

To identify the independent variables associated with ECV, significant univariables (age, LV-myoFat, HOMA-IR and EAT volume index) were entered as covariates into a multiple linear regression model. EAT volume index (standardized β = 0.46, p = 0.025)

and LV-myoFat content (standardized β = 0.41, p = 0.045) were independently associated with ECV. The results did not change when L4 visceral fat volume was forced into the multivariable model.

Determinants of LV myocardial function

The mean 2D LV GLS was -19.0 ± 2.4%, and women had significantly higher GLS than men (-20.3 ± 2.2 vs. -18.4 ± 2.3%, p = 0.013). 2D LV GLS was significantly correlated with age (r = 0.44, p = 0.005), HOMA-IR (r = 0.60, p < 0.001), EAT volume index (r = 0.66, p < 0.001), LV-myoFat (r = 0.50, p < 0.001) and ECV (r = 0.70, p < 0.001).

On multivariable analysis whereby age, gender, HOMA-IR, EAT volume index, LV-myoFat and ECV were entered into the model, only EAT volume index was independently associated with 2D LV GLS (standardized β = 0.44, p = 0.041). Similarly, when L4 visceral fat volume was forced into the model, only EAT volume index remained independently associated with 2D LV GLS.

Variability analysis

We have previously reported the intra- and inter-observer measurement variabilities for LV GLS expressed as mean absolute difference ± 1 SD were 1.2 ± 0.5% and 0.9 ± 1.0% respectively.[28] Table 2 outlines the intra- and inter-observer measurement variabilities for ECV, LV-myoFat content and EAT volume index expressed as mean absolute differences ± 1 SD and intraclass correlation for agreement in 10 randomly selected subjects.

Table 2. *Intra-observer and inter-observer measurement variability*

Variable	Intra-observer		Inter-observer	
	Absolute difference	ICC (95% CI)	Absolute difference	ICC (95% CI)
ECV	0.21 ± 0.08	0.97 (0.80 – 0.99)	0.28 ± 0.13	0.93 (0.73 – 0.98)
LV-myoFat	0.26 ± 0.19	0.98 (0.91 – 0.99)	0.42 ± 0.50	0.91 (0.67 – 0.98)
EAT volume index	3.0 ± 1.5	0.99 (0.96 – 0.99)	3.6 ± 2.2	0.99 (0.95 – 0.99)

CI: Confidence interval; EAT: Epicardial adipose tissue; ECV: Extracellular volume; ICC: Intraclass correlation; LV-myoFat: left ventricular myocardial fat content by VARPRO sequence.

DISCUSSION

The present study evaluated the complex interplay between insulin resistance, increased EAT volume, myocardial fat accumulation and LV interstitial fibrosis, leading to LV myocardial systolic dysfunction in volunteers with normal weight, as well as over-

weight and obese individuals. This study showed that insulin resistance and EAT volume index were independently associated with increased myocardial fat accumulation and LV interstitial fibrosis. On multivariable analyses, EAT volume index was independently associated with impaired LV myocardial systolic contractile function.

Quantification of LV-myoFat by VARPRO versus [1H]-MRS

In the present study, VARPRO significantly overestimated LV-myoFat content compared to [1H]-MRS. This is likely secondary to its inherent T1 bias, especially with its high flip angle. As previously shown by Kühn et al and Liu et al, increasing flip angle (≥5-10°) will overestimate fat fraction by chemical shift imaging compared to [1H]-MRS.[29, 30] However, a lower flip angle will significantly reduce the signal-to-noise ratio, and the noise can lead to incorrect estimation of the true fat fraction.[30] Although VARPRO significantly overestimated LV-myoFat content, it still had excellent correlation and reliability when compared to [1H]-MRS (Figure 3).

However, VARPRO has significant advantages over [1H]-MRS. Firstly, it permits regional and global LV quantification of LV-myoFat, whereas [1H]-MRS is limited to the interventricular septum due to the risk of contamination from EAT. Secondly, VARPRO is performed with a single breath-hold, whereas [1H]-MRS will require double respiratory and cardiac gating that will significantly increase scan duration.[22] Finally, slice positioning for various imaging sequences (e.g. VARPRO for LV-myoFat and MOLLI for interstitial fibrosis) can be consistently and completely matched as demonstrated in the present study.

Epicardial adipose tissue, insulin resistance and myocardial steatosis

The myocardium has a very high energy demand in order to perform cardiac contraction and relaxation. Under normal physiological conditions, it predominately metabolizes free fatty acids through β-oxidation which accounts for approximately 50-70% of its energy production.[7] Although the source of this free fatty acid is generally derived from circulating plasma triglyceride and free fatty acid, it is now recognized that EAT is a readily available local store of TG that directly release free fatty acid to the myocardium at times of increased cardiac fatty acid metabolism.[10, 11, 31] As such, the present study demonstrated that both increased EAT volume index and insulin resistance were independently associated with increased myocardial fat accumulation. This is consistent with previous studies that showed increased EAT volume in obese patients was associated with increased myocardial fat accumulation.[8, 9] In addition, type 2 diabetes, the archetypal disease where pathophysiology is characterized by insulin resistance, is also associated with increased myocardial fat accumulation.[2]

Epicardial adipose tissue and myocardial interstitial fibrosis

However, EAT is also now increasingly recognized as an endocrine organ that secretes adipokines.[7] Both EAT and the underlying myocardium share the same coronary microcirculation with no anatomical fascial boundary separating the 2 structures. As such, adipokines and cytokines secreted by EAT have a direct vasocrine and paracrine effect on coronary and myocardial function.[32] Secretions of pro-inflammatory adipokines such as IL-6, MCP-1, leptin and visfatin are increased with larger EAT volumes, while the secretions of anti-inflammatory adipokines such as adiponectin and adrenomedullin are decreased, all leading to increased coronary vasoconstriction, inflammation and atherosclerosis.[7] Furthermore, increased secretion of TNF-α from EAT has also been shown to induce cardiomyocyte apoptosis leading to replacement fibrosis.[33] Mazurek and colleagues previously demonstrated higher levels of pro-inflammatory cytokines such as IL-6 and TNF-α in EAT harvested from patients undergoing coronary artery bypass grafting compared to subcutaneous adipose tissue.[33] TNF-α worsens insulin resistance and causes vasoconstriction, which is also associated with increased production of angiotensin II and endothelin-1.[34, 35]

Previous studies have shown increased TNF-α is associated with cardiac dilatation, increased interstitial inflammatory infiltrates, abnormal calcium homeostasis, increased apoptosis, extracellular matrix remodeling, ventricular arrhythmias and death.[36, 37] To the best of the authors' knowledge, the present in-vivo study is the first to demonstrate larger EAT volumes is associated with increased myocardial interstitial fibrosis in humans.

Epicardial adipose tissue and myocardial contractility

In-vitro studies of EAT derived from guinea pigs fed a high fat diet [38] and diabetic patients undergoing coronary bypass surgery [39] showed that unlike subcutaneous adipose tissue, EAT have altered secretory profiles that directly contribute to cardiomyocyte contractile dysfunction. Mediated through adipokines including activin A and angiopoietin-2, they adversely affect cytosolic Ca^{2+} metabolism and reduce sarcomere shortening in a dose dependent manner.[38, 39] We have previously shown increased EAT volume was associated with myocardial systolic contractile dysfunction.[5] The present study extends these findings by showing that the observed myocardial contractile dysfunction often seen in obese and diabetic patients is likely secondary to functional (i.e. direct cardio-depressant effects of adipokines) and structural changes (i.e. increased myocardial interstitial fibrosis from inflammation secondary to adipokines) in the myocardium mediated by an increased EAT volume.

Clinical implications

The present findings suggest that EAT is a marker of visceral adiposity with direct adverse effects on myocardial structure and function. Therefore, it may be a target for pharmacological therapy and serve as a prognostic indicator. Previous small studies using hydroxymethyl glutaryl-CoAreductase inhibitors (i.e. statins) [40], dipeptidyl peptidase 4 inhibitors (e.g. sitagliptin) [41] and glucagon-like peptide-1 (e.g. liraglutide) [42] have been shown to reduce EAT volume. The effects of EAT volume reduction on myocardial structural and functional changes need to be assessed in future studies.

Study limitations

While the present study provides new and novel findings on myocardial structural and functional changes associated with EAT, the study only recruited volunteers of varying BMI but without diabetes or hypertension. This was to avoid potential confounding influences of diabetes and hypertension on myocardial interstitial fibrosis and altered myocardial contractile function. Therefore, the present results serve as a pilot for future studies in diabetic patients. Secondly, although the present study demonstrated significant independent associations between increased EAT volume index, increased LV-myoFat, increased interstitial fibrosis and LV myocardial contractile dysfunction, it does not equate to causality in humans despite various published in-vitro basic science as well as animal studies.

CONCLUSIONS

The current findings demonstrate that increased EAT was associated with LV myocardial fat accumulation and increased interstitial fibrosis. Both increased EAT and increased interstitial fibrosis were independently associated with myocardial contractile function. Therefore, therapeutic interventions targeting EAT may serve to modulate the detrimental effects of metabolic heart disease.

REFERENCE LIST

(1) Horwich TB, Fonarow GC. Glucose, Obesity, Metabolic Syndrome, and Diabetes: Relevance to Incidence of Heart Failure. *J Am Coll Cardiol* 2010;55(4):283-293.

(2) Ng AC, Delgado V, Bertini M, van der Meer RW, Rijzewijk LJ, Hooi ES, Siebelink HM, Smit JW, Diamant M, Romijn JA, de RA, Leung DY, Lamb HJ, Bax JJ. Myocardial steatosis and biventricular strain and strain rate imaging in patients with type 2 diabetes mellitus. *Circulation* 2010;122(24):2538-2544.

(3) Nucifora G, Schuijf JD, Delgado V, Bertini M, Scholte AJ, Ng AC, van Werkhoven JM, Jukema JW, Holman E, Van Der Wall E, Bax JJ. Incremental value of subclinical left ventricular systolic dysfunction for the identification of patients with obstructive coronary artery disease. *Am Heart J* 2010;159(1):148-157.

(4) Ng AC, Auger D, Delgado V, van Elderen SG, Bertini M, Siebelink HM, van der Geest RJ, Bonetti C, van der Velde ET, De Roos A, Smit JW, Leung DY, Bax JJ, Lamb HJ. Association between diffuse myocardial fibrosis by cardiac magnetic resonance contrast-enhanced T1 mapping and subclinical myocardial dysfunction in diabetic patients: a pilot study. *Circ Cardiovasc Imaging* 2012;5(1):51-59.

(5) Ng AC, Goo SY, Roche N, van der Geest RJ, Wang WY. Epicardial Adipose Tissue Volume and Left Ventricular Myocardial Function Using 3-Dimensional Speckle Tracking Echocardiography. *Can J Cardiol* 2016;32(12):1485-1492.

(6) Sacks HS, Fain JN. Human epicardial adipose tissue: a review. *Am Heart J* 2007;153(6):907-917.

(7) Patel VB, Shah S, Verma S, Oudit GY. Epicardial adipose tissue as a metabolic transducer: role in heart failure and coronary artery disease. *Heart Fail Rev* 2017;22(3):889-902.

(8) Kankaanpaa M, Lehto HR, Parkka JP, Komu M, Viljanen A, Ferrannini E, Knuuti J, Nuutila P, Parkkola R, Iozzo P. Myocardial triglyceride content and epicardial fat mass in human obesity: relationship to left ventricular function and serum free fatty acid levels. *J Clin Endocrinol Metab* 2006;91(11):4689-4695.

(9) Malavazos AE, Di LG, Secchi F, Lupo EN, Dogliotti G, Coman C, Morricone L, Corsi MM, Sardanelli F, Iacobellis G. Relation of echocardiographic epicardial fat thickness and myocardial fat. *Am J Cardiol* 2010;105(12):1831-1835.

(10) Marchington JM, Pond CM. Site-specific properties of pericardial and epicardial adipose tissue: the effects of insulin and high-fat feeding on lipogenesis and the incorporation of fatty acids in vitro. *Int J Obes* 1990;14(12):1013-1022.

(11) Nelson RH, Prasad A, Lerman A, Miles JM. Myocardial uptake of circulating triglycerides in nondiabetic patients with heart disease. *Diabetes* 2007;56(2):527-530.

(12) McGavock JM, Victor RG, Unger RH, Szczepaniak LS. Adiposity of the Heart, Revisited. *Ann Intern Med* 2006;144(7):517-524.

(13) Ng AC, Delgado V, Djaberi R, Schuijf JD, Boogers MJ, Auger D, Bertini M, De Roos A, van der Meer RW, Lamb HJ, Bax JJ. Multimodality imaging in diabetic heart disease. *Curr Probl Cardiol* 2011;36(1):9-47.

(14) Kellman P, Hernando D, Shah S, Zuehlsdorff S, Jerecic R, Mancini C, Liang ZP, Arai AE. Multiecho dixon fat and water separation method for detecting fibrofatty infiltration in the myocardium. *Magn Reson Med* 2009;61(1):215-221.

(15) Hernando D, Kellman P, Haldar JP, Liang ZP. Robust water/fat separation in the presence of large field inhomogeneities using a graph cut algorithm. *Magn Reson Med* 2010;63(1):79-90.

(16) Schelbert EB, Testa SM, Meier CG, Ceyrolles WJ, Levenson JE, Blair AJ, Kellman P, Jones BL, Ludwig DR, Schwartzman D, Shroff SG, Wong TC. Myocardial extravascular extracellular volume fraction measurement by gadolinium cardiovascular magnetic resonance in humans: slow infusion versus bolus. *J Cardiovasc Magn Reson* 2011;13:16.

(17) Messroghli DR, Greiser A, Frohlich M, Dietz R, Schulz-Menger J. Optimization and validation of a fully-integrated pulse sequence for modified look-locker inversion-recovery (MOLLI) T1 mapping of the heart. *J Magn Reson Imaging* 2007;26(4):1081-1086.

(18) World Health Organization. Waist circumference and waist-hip ratio: report of a WHO expert consultation. Geneva, 8-11 December 2008. Geneva, Switzerland: WHO. 2011.

(19) K/DOQI clinical practice guidelines for chronic kidney disease: evaluation, classification and stratification. *Am J Kidney Dis* 2002;39:S1-S266.

(20) Wallace TM, Levy JC, Matthews DR. Use and abuse of HOMA modeling. *Diabetes Care* 2004;27(6):1487-1495.

(21) Mosteller RD. Simplified calculation of body-surface area. *N Engl J Med* 1987;317(17):1098.

(22) Gillinder L, Goo SY, Cowin G, Strudwick M, van der Geest RJ, Wang WY, Ng AC. Quantification of Intramyocardial Metabolites by Proton Magnetic Resonance Spectroscopy. *Front Cardiovasc Med* 2015;2:24.

(23) Hernando D, Haldar JP, Sutton BP, Ma J, Kellman P, Liang ZP. Joint estimation of water/fat images and field inhomogeneity map. *Magn Reson Med* 2008;59(3):571-580.

(24) Kellman P, Hernando D, Arai AE. Myocardial Fat Imaging. *Curr Cardiovasc Imaging Rep* 2010;3(2):83-91.

(25) Gai N, Turkbey EB, Nazarian S, van der Geest RJ, Liu CY, Lima JA, Bluemke DA. T1 mapping of the gadolinium-enhanced myocardium: adjustment for factors affecting interpatient comparison. *Magn Reson Med* 2011;65(5):1407-1415.

(26) Lang RM, Badano LP, Mor-Avi V, Afilalo J, Armstrong A, Ernande L, Flachskampf FA, Foster E, Goldstein SA, Kuznetsova T, Lancellotti P, Muraru D, Picard MH, Rietzschel ER, Rudski L, Spencer KT, Tsang W, Voigt JU. Recommendations for cardiac chamber quantification by echocardiography in adults: an update from the American Society of Echocardiography and the European Association of Cardiovascular Imaging. *Eur Heart J Cardiovasc Imaging* 2015;16(3):233-270.

(27) Nagueh SF, Smiseth OA, Appleton CP, Byrd BF, III, Dokainish H, Edvardsen T, Flachskampf FA, Gillebert TC, Klein AL, Lancellotti P, Marino P, Oh JK, Popescu BA, Waggoner AD. Recommendations for the Evaluation of Left Ventricular Diastolic Function by Echocardiography: An Update from the American Society of Echocardiography and the European Association of Cardiovascular Imaging. *J Am Soc Echocardiogr* 2016;29(4):277-314.

(28) Ng ACT, Delgado V, Bertini M, van der Meer RW, Rijzewijk LJ, Shanks M, Nucifora G, Smit JWA, Diamant M, Romijn JA, De Roos A, Leung DY, Lamb HJ, Bax JJ. Findings from left ventricular strain and strain rate imaging in asymptomatic patients with type 2 diabetes mellitus. *Am J Cardiol* 2009;104(10):1398-1401.

(29) Kuhn JP, Jahn C, Hernando D, Siegmund W, Hadlich S, Mayerle J, Pfannmoller J, Langner S, Reeder S. T1 bias in chemical shift-encoded liver fat-fraction: role of the flip angle. *J Magn Reson Imaging* 2014;40(4):875-883.

(30) Liu CY, McKenzie CA, Yu H, Brittain JH, Reeder SB. Fat quantification with IDEAL gradient echo imaging: correction of bias from T(1) and noise. *Magn Reson Med* 2007;58(2):354-364.

(31) Stanley WC, Recchia FA, Lopaschuk GD. Myocardial substrate metabolism in the normal and failing heart. *Physiol Rev* 2005;85(3):1093-1129.

(32) Cherian S, Lopaschuk GD, Carvalho E. Cellular cross-talk between epicardial adipose tissue and myocardium in relation to the pathogenesis of cardiovascular disease. *Am J Physiol Endocrinol Metab* 2012;303(8):E937-E949.

(33) Mazurek T, Zhang L, Zalewski A, Mannion JD, Diehl JT, Arafat H, Sarov-Blat L, O'Brien S, Keiper EA, Johnson AG, Martin J, Goldstein BJ, Shi Y. Human epicardial adipose tissue is a source of inflammatory mediators. *Circulation* 2003;108(20):2460-2466.

(34) Zhang H, Park Y, Wu J, Chen X, Lee S, Yang J, Dellsperger KC, Zhang C. Role of TNF-alpha in vascular dysfunction. *Clin Sci (Lond)* 2009;116(3):219-230.

(35) Salazar J, Luzardo E, Mejias JC, Rojas J, Ferreira A, Rivas-Rios JR, Bermudez V. Epicardial Fat: Physiological, Pathological, and Therapeutic Implications. *Cardiol Res Pract* 2016;2016:1291537.

(36) Higuchi Y, McTiernan CF, Frye CB, McGowan BS, Chan TO, Feldman AM. Tumor necrosis factor receptors 1 and 2 differentially regulate survival, cardiac dysfunction, and remodeling in transgenic mice with tumor necrosis factor-alpha-induced cardiomyopathy. *Circulation* 2004;109(15):1892-1897.

(37) Sinagra E, Perricone G, Romano C, Cottone M. Heart failure and anti tumor necrosis factor-alpha in systemic chronic inflammatory diseases. *Eur J Intern Med* 2013;24(5):385-392.

(38) Greulich S, de Wiza DH, Preilowski S, Ding Z, Mueller H, Langin D, Jaquet K, Ouwens DM, Eckel J. Secretory products of guinea pig epicardial fat induce insulin resistance and impair primary adult rat cardiomyocyte function. *J Cell Mol Med* 2011;15(11):2399-2410.

(39) Greulich S, Maxhera B, Vandenplas G, de Wiza DH, Smiris K, Mueller H, Heinrichs J, Blumensatt M, Cuvelier C, Akhyari P, Ruige JB, Ouwens DM, Eckel J. Secretory products from epicardial adipose tissue of patients with type 2 diabetes mellitus induce cardiomyocyte dysfunction. *Circulation* 2012;126(19):2324-2334.

(40) Park JH, Park YS, Kim YJ, Lee IS, Kim JH, Lee JH, Choi SW, Jeong JO, Seong IW. Effects of statins on the epicardial fat thickness in patients with coronary artery stenosis underwent percutaneous coronary intervention: comparison of atorvastatin with simvastatin/ezetimibe. *J Cardiovasc Ultrasound* 2010;18(4):121-126.

(41) Lima-Martinez MM, Paoli M, Rodney M, Balladares N, Contreras M, D'Marco L, Iacobellis G. Effect of sitagliptin on epicardial fat thickness in subjects with type 2 diabetes and obesity: a pilot study. *Endocrine* 2016;51(3):448-455.

(42) Iacobellis G, Mohseni M, Bianco SD, Banga PK. Liraglutide causes large and rapid epicardial fat reduction. *Obesity (Silver Spring)* 2017;25(2):311-316.

7

Defining Subclinical Myocardial Dysfunction and Implications for Patients with Diabetes Mellitus and Preserved Ejection Fraction

Arnold C.T. Ng, Matteo Bertini, See Hooi Ewe, Enno T van der Velde, Dominic Y. Leung, Victoria Delgado, Jeroen J. Bax

Am J Cardiol. 2019;124(6):892-898

ABSTRACT

Background: Left ventricular (LV) global longitudinal strain (GLS) can detect subclinical myocardial systolic dysfunction in individuals with diabetes. The present study investigates the clinical usefulness and incremental net benefit of identifying subclinical myocardial systolic dysfunction in individuals with diabetes.

Methods: A cohort of 397 type 2 diabetic individuals were followed up for the occurrence of all-cause mortality. Both clinical and echocardiographic data of diabetic patients were assessed retrospectively. LV GLS was evaluated on transthoracic echocardiography using speckle tracking imaging.

Results: Subclinical LV systolic dysfunction was defined as LV GLS > -17.0% from 104 healthy volunteers recruited from the community. A total of 178 (44.8%) diabetic individuals had evidence of subclinical LV systolic dysfunction and 46 (11.6%) died during follow up. The presence of subclinical LV systolic dysfunction was independently associated with all-cause mortality on follow-up (HR 2.83, 95% CI 1.40 – 5.71, p = 0.004). Diabetic individuals without subclinical LV systolic dysfunction had similar survival as the general population (standardized mortality ratio 0.94, 95% CI 0.52 – 1.58). Decision curve analysis showed identification of subclinical LV systolic dysfunction and quantification of LV GLS provided an incremental net clinical benefit at risk stratifying patients for risk of death at 5 years.

Conclusions: Subclinical LV systolic dysfunction is independently associated with all-cause mortality in diabetic patients. Decision curve analyses suggest use of LV GLS and identification of subclinical LV systolic dysfunction is clinically useful, and provided incremental net clinical benefit for diabetic individuals.

INTRODUCTION

Diabetes mellitus is the most common endocrinological disease in the world and its presence portends an increased risk for the subsequent development of cardiovascular disease, heart failure and death. [1,2] Echocardiographic techniques such as 2-dimensional (2D) speckle tracking global longitudinal strain analysis permits early identification of subclinical left ventricular (LV) systolic dysfunction despite preserved LV ejection fraction (EF) in asymptomatic type 2 diabetic individuals.[3] However, limited data exist on the prevalence and prognostic implications of subclinical LV systolic dysfunction with preserved LVEF in diabetic population. Thus, we conducted a multicenter study aimed to:

4. evaluate the prevalence of subclinical LV systolic dysfunction with preserved LVEF in type 2 diabetic individuals by using 2D speckle tracking global longitudinal strain cut-off value derived from normal healthy volunteers; and
5. determine the prognostic implications of subclinical LV systolic dysfunction in type 2 diabetic patients and compare it with the general population; and
6. determine the clinical usefulness and incremental net benefit of identifying subclinical LV systolic dysfunction on echocardiography.

METHODS

A total of 104 healthy volunteers were prospectively recruited from the community (Liverpool Hospital, Australia; and Princess Alexandra Hospital, Australia) to derive a cut-off value for normal global longitudinal strain and define subclinical LV systolic dysfunction. All the healthy volunteers had normal physical examinations, in normal sinus rhythm and had normal echocardiograms. Exclusion criteria for the healthy volunteers included history of diabetes, hypertension, smoking, use of cardiac medications, known underlying significant coronary artery disease, previous myocardial infarction and cardiomyopathy. As the LV global longitudinal strain from this normal population demonstrated a unimodal Gaussian distribution, the lower limit of normal was defined as 2 standard deviations from the mean. Thus, subclinical LV systolic dysfunction was defined as an LV global longitudinal strain > 2 standard deviations from the mean.

The definition of subclinical LV systolic dysfunction was subsequently applied to 397 type 2 diabetic patients (Leiden University Medical Center, The Netherlands) who were followed-up to evaluate the adverse risk of subclinical LV systolic dysfunction. These patients were identified from the departmental echocardiographic database, and all

clinical data were originally prospectively entered in the departmental Cardiology Information System (EPD-Vision®, Leiden University Medical Center).

Type 2 diabetes was diagnosed according to World Health Organization criteria.[4] All diabetic patients were in normal sinus rhythm and had normal LVEF defined as ≥ 50%. Exclusion criteria for all the diabetic patients included history of heart failure, known pre-existing underlying significant coronary artery disease, previous myocardial infarction, presence of segmental wall motion abnormalities on echocardiogram, or ≥ moderate valvular stenosis or regurgitation.

Baseline clinical variables that were recorded included cardiac risk factors, hemoglobin level, glycated hemoglobin (HbA1c) and glomerular filtration rates (GFR) calculated by the Modification of Diet in Renal Disease formula as recommended by the National Kidney Foundation, Kidney Disease Outcomes Quality Initiative Guidelines.[5] Heart rate and blood pressures were recorded at the time of echocardiographic examination. Baseline echocardiographic variables recorded included LV volumes, LVEF, and LV global longitudinal strain.

All diabetic individuals were followed-up after the baseline echocardiographic examination for the occurrence of death. The prognostic significance of subclinical LV systolic dysfunction was determined. Furthermore, to validate the cut-off value for the definition of subclinical LV dysfunction in the diabetic population, their survival was compared to the general Dutch population matched by age, gender, and time period using life-tables provided by the Dutch Central Bureau of Statistics. The clinical usefulness of identifying subclinical LV systolic dysfunction was also analyzed using decision curve analysis.

All the institutional review boards approved the study. All healthy volunteers prospectively recruited from the community provided written informed consent (Liverpool Hospital and Princess Alexandra Hospital, Australia). For the diabetic population, the Leiden University Medical Center institutional review board waived the need for patient written informed consent as all clinically acquired data were retrospectively analyzed and anonymously handled.

Transthoracic echocardiography was performed in all subjects at rest using commercially available ultrasound systems (Vivid 7 and E9, GE-Vingmed, Horten, Norway). All images were digitally stored on hard disks. All offline analyses were performed using a single software system (EchoPAC version 108.1.5, GE-Vingmed, Horten, Norway) at the Leiden University Medical Center echocardiography core laboratory by 2 operators (ACTN and MB). A complete 2D, color, pulsed and continuous-wave Doppler echocardiogram was

performed. LV end-diastolic volume index (EDVI) and end-systolic volume index (ESVI) were calculated using Simpson's biplane method of discs and corrected for body surface area. LVEF was calculated and expressed as a percentage. LV mass index was calculated from the formula as recommended by the American Society of Echocardiography and the European Association of Cardiovascular Imaging.[6]

Quantification of LV global longitudinal strain was performed using 2D speckle tracking echocardiography in the 3 apical (2-, 3- and 4 chamber) views. During image analysis, the LV endocardial border was manually traced at end-systole and the region of interest width adjusted to include the entire myocardium. The 2D speckle tracking software then automatically tracks the motion of LV myocardial segments throughout the entire cardiac cycle. From the 3 individual apical views, peak LV global longitudinal strain was calculated. Previous work has reported that the intra- and inter-observer variabilities (expressed as mean absolute difference ± 1 standard deviation and intraclass correlation coefficient) for LV global longitudinal strain were 1.2 ± 0.5% and 0.939 and 0.9 ± 1.0% and 0.942, respectively.[3]

Statistical analysis

All continuous variables were tested for Gaussian distribution using the Kolmogorov-Smirnov test for normality. Continuous variables are presented as mean ± 1 standard deviation and categorical variables are presented as frequencies and percentages. The unpaired Student's t-test was used to compare 2 independent groups of continuous variables and the Chi-square test was used to compare categorical variables. Cumulative event rates were calculated using the Kaplan-Meier method and between group comparisons were made using the log-rank tests with respect to the primary outcome of all-cause mortality.[7]

Comparison of the diabetic cohort against the mortality of the total Dutch population matched by age, gender and time period was performed using standardized mortality ratios (SMR). The SMR is the ratio of the observed number of deaths in the study cohort relative to the expected number of deaths in the general population. Multivariate Cox proportional-hazards models were then constructed to determine the independent prognostic value of subclinical LV systolic dysfunction and LV global longitudinal strain, adjusted for baseline clinical, biochemical and echocardiographic characteristics (age, hemoglobin, GFR, and LV mass index).[8] These variables were selected as they were significant determinants of all-cause mortality on univariable analysis. The first model included LV global longitudinal strain as a categorical variable defined as the presence or absence of subclinical LV systolic dysfunction. The second model included LV global longitudinal strain as a continuous variable in increments of per unit (1%) worsening.

The Cox proportional-hazards models were used to estimate hazard ratios (HR) and 95% confidence intervals (CI) for all independent predictors of all-cause mortality. A Pearson's correlation coefficient of > 0.7 was used to identify high colinearity between the univariable predictors and avoid concurrent inclusion in the multivariable Cox regression model. Validity of the Cox regression assumption of proportionality was confirmed for all continuous covariates by scaled Schoenfeld residuals. For categorical variables, the assumption of proportionality was confirmed by log minus log plots.

To determine the incremental prognostic value of identifying subclinical LV systolic dysfunction using LV global longitudinal strain, the integrated discrimination improvement (IDI) and the continuous net reclassification improvement (NRI) were initially used.[9, 10] Next, a formal cost-benefit analysis using decision curve analysis was undertaken to determine the clinical usefulness of identifying subclinical LV systolic dysfunction using LV global longitudinal strain to predict all-cause mortality at 5 years.[11] It compares the clinical usefulness and net benefits of the model 1 (i.e. "traditional" risk factors that included age, GFR, hemoglobin and LV mass index) versus model 2 (model 1 + subclinical LV dysfunction/LV global longitudinal strain), against 2 default clinical strategies: 1) assume all diabetic patients have subclinical LV systolic dysfunction and therefore perform an echocardiographic quantification of LV global longitudinal strain in everyone, or 2) assume all diabetic individuals are well and do not have subclinical LV dysfunction and therefore quantify LV global longitudinal strain in no one.[11]

A 2-tailed p value of < 0.05 was considered significant. All statistical analyses were performed using SPSS for Windows (SPSS Inc, Chicago) version 16, STATA version 10 (StatCorp, Texas) and R version 3.3.2 (R Foundation for Statistical Computing, Vienna, Austria).

RESULTS

The mean age of the 104 normal healthy volunteers was 50 ± 9 years, and 56.7% were male. The mean heart rate, systolic and diastolic blood pressures were 68 ± 11 beats/min, 123 ± 12 mmHg and 82 ± 9 mmHg respectively. All normal healthy volunteers had normal echocardiograms by virtue of the inclusion criteria. The mean LV mass index, LVEDVI, LVESVI and LVEF were 69.2 ± 12.4 g/m^2, 52.9 ± 8.1 mL/m^2, 12.5 ± 3.8 mL/m^2 and 57.8 ± 4.6% respectively. The mean LV global longitudinal strain for the healthy volunteers was -20.5 ± 1.8%. Although there was no correlation between LV global longitudinal strain and age, there was a significant gender difference (men -19.8 ± 1.6%, women -21.4 ± 1.7%, $p < 0.001$). To define subclinical myocardial dysfunction, the lower limit of normal

is calculated as 2 standard deviations from the mean. Therefore, in order to simplify and increase clinical utility, the lower cut-off value of -17% for LV global longitudinal strain was used (Figure 1). Thus, all diabetic individuals with normal LVEF but LV global longitudinal strain worse than -17% (less negative) were considered to have subclinical LV systolic dysfunction.

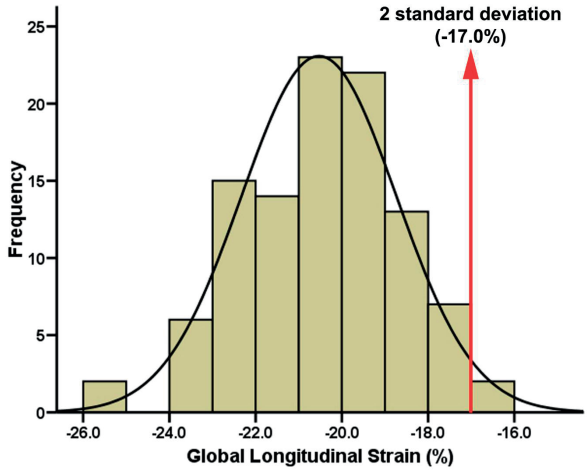


Figure 1. *Distribution of LV global longitudinal strain values in the normal controls. The mean LV global longitudinal strain was -20.5 ± 1.8%. Therefore, the normal global longitudinal strain cut-off value was -17.0% (based on 2 standard deviations below the mean).*

Table 1 outlines the clinical, biochemical and echocardiographic characteristics of the 397 diabetic individuals. Using the LV global longitudinal strain cut-off value of -17.0%, 178 (44.8%) diabetic individuals had evidence of subclinical LV systolic dysfunction.

After a mean follow-up period of 3.6 ± 1.6 years (median 3.5 years, 25th and 75th percentile 2.8 and 4.5 years respectively), 46 diabetic individuals died. Patients who died were significantly older (68.3 ± 11.7 vs. 57.1 ± 11.8 years, $p < 0.001$), and had lower hemoglobin (13.2 ± 1.6 vs. 13.9 ± 1.6 g/dL, $p = 0.009$) and lower GFR (63.5 ± 34.0 vs. 86.3 ± 26.3 mL/min/1.73m^2, $p < 0.001$). On echocardiography, patients who died had significantly higher LV mass index (108.9 ± 23.9 vs. 91.8 ± 22.9 g/m^2, $p < 0.001$) and worse LV global longitudinal strain (-15.4 ± 2.3 vs. -17.5 ± 2.2%, $p < 0.001$) compared to patients who were alive. There were no significant differences in LV volumes or LVEF. The Kaplan Meier survival curves in Figure 2 show the patients with subclinical LV systolic dysfunction had significantly lower survival compared to patients with preserved LV systolic function (log rank $p < 0.001$), and significantly lower survival compared to the general population (SMR 2.61, 95% CI 1.78 – 3.68, one-sided log rank $p < 0.001$). A SMR above unity indicates

Table 1. *Clinical, biochemical and echocardiographic characteristics of diabetic patients*

Variable	Diabetic population (n = 397)	Preserved LV systolic function (n = 219)	Subclinical LV systolic dysfunction (n = 178)	p value
Age (years)	58 ± 12	58 ± 12	59 ± 12	0.34
Men	63.7%	62.6%	65.2%	0.59
Body mass index (kg/m^2)	28.8 ± 5.5	27.3 ± 5.0	30.5 ± 5.7	< 0.001
Systolic blood pressure (mmHg)	141 ± 22	139 ± 20	143 ± 23	0.032
Diastolic blood pressure (mmHg)	81 ± 11	80 ± 11	83 ± 12	0.023
Hyperlipidemia	50.0%	48.6%	51.7%	0.54
Hypertension	57.8%	55.7%	60.5%	0.34
Smoker	16.9%	15.6%	18.5%	0.44
Hemoglobin (g/dL)	13.8 ± 1.6	13.9 ± 1.6	13.8 ± 1.7	0.56
HbA1c (%)	7.3 ± 1.5	7.1 ± 1.5	7.6 ± 1.4	0.013
GFR (mL/min/1.73m^2)	83.8 ± 28.1	86.3 ± 27.4	80.7 ± 28.7	0.052
Heart rate (beats/min)	74 ± 13	72 ± 13	75 ± 12	0.05
Transmitral E velocity (m/s)	0.66 ± 0.17	0.70 ± 0.18	0.65 ± 0.18	0.014
Transmitral E/A ratio	0.98 ± 0.33	1.00 ± 0.34	0.91 ± 0.28	0.005
Deceleration time (ms)	197 ± 54	198 ± 54	201 ± 54	0.60
LV mass index (g/m^2)	93.8 ± 23.7	91.2 ± 23.2	96.7 ± 23.9	0.016
LVEDVI (mL/m^2)	46.0 ± 11.2	45.9 ± 10.7	46.2 ± 11.8	0.75
LVESVI (mL/m^2)	18.7 ± 5.6	18.1 ± 5.1	19.6 ± 6.0	0.007
LVEF (%)	59.5 ± 5.4	60.8 ± 5.3	57.9 ± 5.0	< 0.001
Global longitudinal strain (%)	-17.3 ± 2.3	-18.9 ± 1.5	-15.3 ± 1.4	< 0.001

* p value by unpaired Student's t-test and Chi-square test for continuous and categorical variables respectively. EDVI: end-diastolic volume index; ESVI: end-systolic volume index; EF: ejection fraction; GFR: glomerular filtration rate; HbA1c: glycated hemoglobin; LV: left ventricular.

that the mortality of the study cohort is higher than the general population, adjusted for age distribution, gender, and calendar time. Thus, diabetic individuals with subclinical myocardial dysfunction were 161% more likely to die on follow-up compared to the general population. In contrast, there was no difference in survival between diabetic individuals with preserved LV systolic function and the general population (SMR 0.94, 95% CI 0.52 – 1.58, one-sided log rank p = not significant).

Table 2 outlines the all significant univariable determinants of all-cause mortality on follow up (including presence of subclinical LV systolic dysfunction, age, hemoglobin, GFR and LV mass index). On multivariate Cox proportional-hazards models, the presence of subclinical LV systolic dysfunction (HR 2.83, 95% CI 1.40 – 5.71, p = 0.004) in diabetic individuals was independently associated with increased all-cause mortality on follow-up after adjusting for baseline clinical and echocardiographic characteristics.

Similarly, when LV global longitudinal strain was modeled as a continuous variable, it was still independently associated with increased all-cause mortality on follow-up (HR 1.29, 95% CI 1.14 – 1.46, p < 0.001) (Table 3).

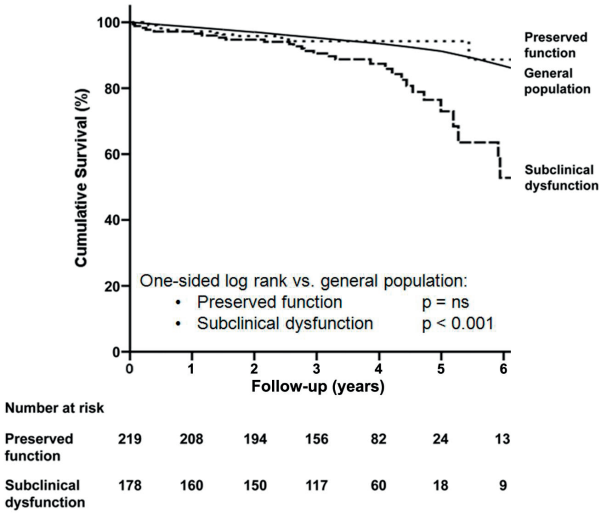


Figure 2. *Kaplan Meier survival curves for diabetic individuals with subclinical LV systolic dysfunction and preserved LV systolic function compared to the general population. There was no significant difference in long-term survival for diabetic individuals with preserved LV systolic function and the general population (p = ns). In contrast, diabetic individuals with normal LVEF but with subclinical LV systolic dysfunction had significantly lower long term survival compared to the general population (p < 0.001).*

Table 2. *Univariable and multivariable Cox proportional hazard models for all-cause mortality in diabetic patients*

Variable	Univariable		Multivariable	
	Hazard ratio (95% CI)	p value	Hazard ratio (95% CI)	p value
Presence of subclinical LV systolic dysfunction	2.78 (1.48 – 5.23)	0.002	2.83 (1.40 – 5.71)	0.004
Age (per 10 year increase)	1.89 (1.43 – 2.50)	< 0.001	1.44 (1.08 – 1.91)	0.013
LV mass index (per 10 g/m^2 increase)	1.14 (1.03 – 1.26)	0.012		
GFR (per 10 mL/min/1.73m^2 decrease)	1.29 (1.14 – 1.45)	< 0.001	1.18 (1.03 – 1.35)	0.015
Hemoglobin (per 1g/dL decrease)	1.25 (1.06 – 1.47)	0.008		

CI: confidence interval; GFR: glomerular filtration rate; LV: left ventricular.

Table 3. *Univariable and multivariable Cox proportional hazard models for all-cause mortality in diabetic patients*

Variable	Univariable		Multivariable	
	Hazard ratio (95% CI)	**p value**	**Hazard ratio (95% CI)**	**p value**
LV global longitudinal strain (per unit [1%] worsening)	1.37 (1.22 – 1.54)	< 0.001	1.29 (1.14 – 1.46)	< 0.001
Age (per 10 year increase)	1.89 (1.43 – 2.50)	< 0.001	1.37 (1.03 – 1.82)	0.029
LV mass index (per 10 g/m^2 increase)	1.14 (1.03 – 1.26)	0.012		
GFR (per 10 mL/min/1.73m^2 decrease)	1.29 (1.14 – 1.45)	< 0.001	1.16 (1.02 – 1.32)	0.021
Hemoglobin (per 1g/dL decrease)	1.25 (1.06 – 1.47)	0.008		

CI: confidence interval; GFR: glomerular filtration rate; LV: left ventricular.

Figure 3 graphically illustrates the IDI and continuous NRI between the baseline Cox model 1 (age, GFR, hemoglobin and LV mass index [thick line]) and Cox model 2 (model 1 + subclinical myocardial dysfunction [thin line]). The identification of subclinical LV systolic dysfunction significantly improved the predictive value of the Cox model based on the IDI (point estimate 0.054, 95% confidence interval 0.002 – 0.163, p = 0.040) and continuous NRI (point estimate 0.362, 95% confidence interval 0.062 – 0.587, p = 0.013).

Figures 4 and 5 are the decision curve analyses illustrating the net clinical benefit of identifying subclinical LV systolic dysfunction and LV global longitudinal strain respectively. In these figures, the net benefit in risk stratifying diabetic individuals using echocardiography to identify subclinical LV systolic dysfunction is represented by the y-axis, and plotted over varying thresholds of risk for death at 5 years on the x-axis. This is compared against the 2 “extreme theoretical” clinical strategies: perform echocardiograms in all diabetic individual (gray solid line) vs. not performing any echocardiograms in all diabetic individual (black solid line). Both figures demonstrate that using LV global longitudinal strain either as a categorical variable (i.e. presence of subclinical LV systolic dysfunction, Figure 4) or continuous variable (Figure 5) to inform clinical decisions will lead to superior predictive outcomes when the threshold probability of death at 5 years is above 8% (arrow, Figure 4) to 10% (arrow, Figure 5). Importantly, once the patient’s 5 year probability of death is > 50-70%, there is no net benefit in identifying subclinical LV systolic dysfunction or quantifying LV global longitudinal strain respectively on echocardiogram.

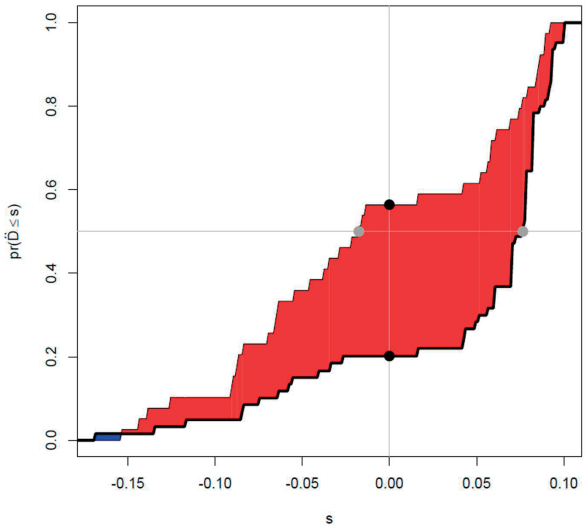


Figure 3. *Graphical representation of the incremental prognostic value of subclinical LV systolic dysfunction in predicting all-cause mortality in the overall multivariable Cox regression model in diabetic individuals at 5 years. Model 1 (age, GFR, hemoglobin and LV mass index) and model 2 (model 1 + subclinical myocardial dysfunction as categorical variable) are represented by the thick and thin lines respectively. The difference between the 2 curves (area under the curve) represents the IDI, and the distances between the 2 black dots vertically and the 2 gray dots horizontally represents the continuous NRI and difference in medians for the 2 curves respectively. The larger the separation between the 2 curves, the larger the improvement in model performance when including subclinical LV systolic dysfunction as a prognostic marker.*

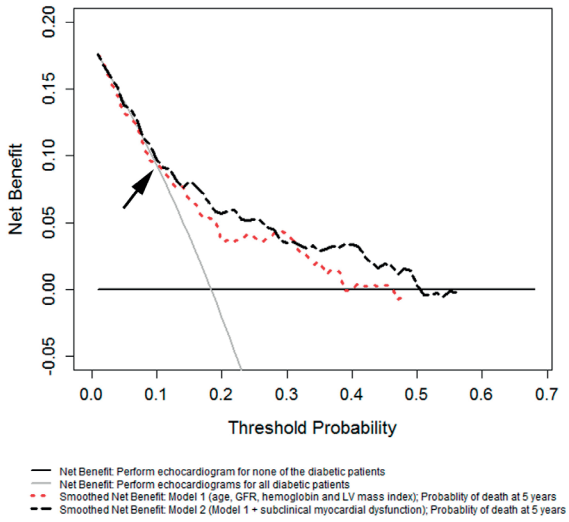


Figure 4. *Decision curve analysis for model 1 (age, GFR, hemoglobin and LV mass index) and model 2 (model 1 + subclinical LV systolic dysfunction as categorical variable). Once the threshold probability of death approaches 10% (arrow), performing echocardiograms to identify subclinical LV systolic dysfunction (model 2) provide a superior net clinical benefit across a large range of death risk at 5 years follow up. GFR: glomerular filtration rate, LV: left ventricular.*

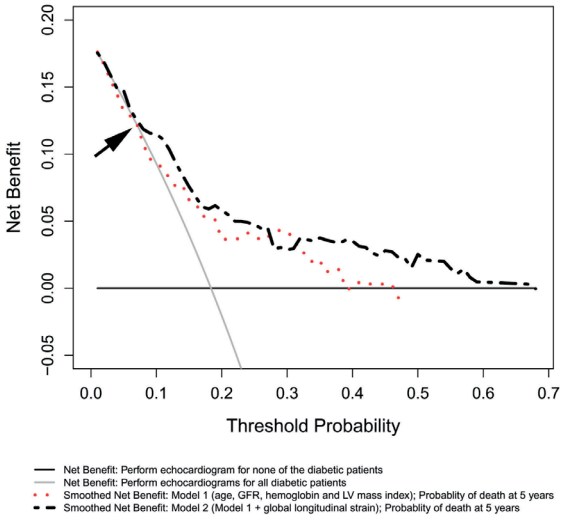


Figure 5. *Decision curve analysis for model 1 (age, GFR, hemoglobin and LV mass index) and model 2 (model 1 + LV global longitudinal strain as continuous variable). Once the threshold probability of death approaches 8% (arrow), quantifying LV global longitudinal strain (model 2) provide a superior net clinical benefit across a large range of death risk at 5 years follow up. GFR: glomerular filtration rate, LV: left ventricular.*

DISCUSSION

It is well recognized that LVEF is a poor marker for identifying myocardial dysfunction as it remains well preserved until significant impairment of longitudinal, circumferential and radial deformations.[3] Depending on the echocardiographic modality used, the prevalence of myocardial dysfunction in diabetics ranged from 21% to 63%.[12, 13] In the present study, up to 45% of diabetic individuals had evidence of subclinical LV systolic dysfunction as defined by 2D speckle tracking LV global longitudinal strain. This was identical to a previous publication by Holland et al.[14]

Myocardial dysfunction in diabetics has a multifactorial pathophysiology. Proposed mechanisms include metabolic derangements, autonomic dysfunction, abnormal calcium homeostasis, endothelial dysfunction, altered structural proteins and interstitial fibrosis.[15, 16] As such, the diabetic myocardium has accentuated cellular damage, reduced structural and function reserve, and is more prone to future decompensation and eventual failure when exposed to adverse cardiac events. This was highlighted in the seminal work by From et al that showed increased incidence of new-onset heart failure in diabetic patients with pre-clinical diastolic dysfunction.[17] Although it is traditionally held that diastolic dysfunction precedes systolic dysfunction, recent work suggested that subclinical LV systolic dysfunction detected by LV global longitudinal strain may be

the first sign of diabetic heart disease instead.[18] Even though it is clear that prognosis is very poor once clinical heart failure is established,[19] there is a paucity of research data on prognosis of the earlier subclinical dysfunction stage.

To our knowledge, only 2 previous publications have demonstrated adverse long-term prognosis associated with subclinical LV systolic dysfunction using LV global longitudinal strain.[14, 20] Holland et al included 230 diabetic patients and showed increased all-cause mortality and hospitalization in patients with subclinical LV systolic dysfunction compared to those with preserved LV global longitudinal strain.[14] However, the primary outcome was primarily driven by hospitalization, and the causes of hospitalizations were unknown. Liu et al included 247 diabetic patients and showed that an impaired LV global longitudinal strain was associated with an increased incidence of cardiovascular events defined as a composite of acute coronary syndrome, cerebrovascular stroke, cardiovascular death and hospitalization for heart failure.[20] In contrast, the present study is the largest to date to include 397 diabetic patients with a primary end-point of all-cause mortality. Not only did our results corroborate the previous 2 publications demonstrating similar adverse prognosis associated with subclinical LV systolic dysfunction, it is also first to show diabetic individuals with preserved LV systolic function had similar long term survival rates as the general population.

In both studies by Holland et al [14] and Liu et al [20], the "incremental" prognostic value of LV global longitudinal strain were based on the Chi square change in the multivariable Cox model, which is a statistical measure of the overall model performance related to the concept of "goodness-of-fit" (i.e. a better model results in smaller distances between predicted and observed outcomes).[21] However, it fails to inform both the doctor and patient if the test is clinically useful. In contrast, the use of a decision curve analysis in the present study illustrated the net clinical benefit of identifying subclinical LV systolic dysfunction (binary data, Figure 4) and LV global longitudinal strain (continuous data, Figure 5) in diabetic individuals over the baseline prediction model (age, GFR, hemoglobin and LV mass index) by incorporating the clinical consequences across a large range of all-cause mortality risk. As the relative weights of benefits and harms in identifying subclinical LV systolic dysfunction in asymptomatic diabetic population will differ individually, the decision curve analysis allows the setting of individual patient's thresholds for predicting the probability of death at 5 years. It showed that the identification of subclinical LV systolic dysfunction is only of incremental net clinical benefit if the risk of death at 5 years is between 10% and 50%. As for quantification of LV global longitudinal strain as a continuous variable, the incremental net clinical benefit is present if the risk of death at 5 years is between 8% and 70%. Therefore, the identification of

subclinical LV systolic dysfunction provided superior net clinical benefit across a wide range of probabilities of death at 5 years.

Although the present study included healthy volunteers and diabetic individuals across 3 different institutions, all diabetic individuals were recruited from a single center. Sub-group analyses based on cardiovascular and non-cardiovascular mortality were not available. Finally, by virtue of the study design, we did not evaluate the progression of subclinical LV systolic dysfunction over time. However, that research was previously reported by our group.[22]

CONCLUSIONS

Diabetic patients with subclinical LV systolic dysfunction have increased risk of all-cause mortality compared to diabetic patients without subclinical LV systolic dysfunction. Furthermore, diabetic patients without subclinical LV systolic dysfunction had similar survival as the general population. Decision curve analyses suggest that identifying subclinical LV systolic dysfunction is clinically useful.

REFERENCE LIST

(1) Wild S, Roglic G, Green A, Sicree R, King H. Global Prevalence of Diabetes. *Diabetes Care* 2004;27:1047-1053.

(2) Kannel WB, McGee DL. Diabetes and cardiovascular disease. The Framingham study. *JAMA* 1979;241:2035-2038.

(3) Ng ACT, Delgado V, Bertini M, van der Meer RW, Rijzewijk LJ, Shanks M, Nucifora G, Smit JWA, Diamant M, Romijn JA, De Roos A, Leung DY, Lamb HJ, Bax JJ. Findings from left ventricular strain and strain rate imaging in asymptomatic patients with type 2 diabetes mellitus. *Am J Cardiol* 2009;104:1398-1401.

(4) Alberti KG, Zimmet PZ. Definition, diagnosis and classification of diabetes mellitus and its complications. Part 1: diagnosis and classification of diabetes mellitus provisional report of a WHO consultation. *Diabet Med* 1998;15:539-553.

(5) K/DOQI clinical practice guidelines for chronic kidney disease: evaluation, classification and stratification. *Am J Kidney Dis* 2002;39:S1-S266.

(6) Lang RM, Badano LP, Mor-Avi V, Afilalo J, Armstrong A, Ernande L, Flachskampf FA, Foster E, Goldstein SA, Kuznetsova T, Lancellotti P, Muraru D, Picard MH, Rietzschel ER, Rudski L, Spencer KT, Tsang W, Voigt JU. Recommendations for cardiac chamber quantification by echocardiography in adults: an update from the American Society of Echocardiography and the European Association of Cardiovascular Imaging. *Eur Heart J Cardiovasc Imaging* 2015;16:233-270.

(7) Kaplan E, Meier P. Nonparametric estimation from incomplete observations. *J Am Stat Assoc* 1958;53:457-481.

(8) Cox D. Regression models and life-tables. *J R Stat Soc* 1972;34:187-220.

(9) Pencina MJ, D'Agostino RB, Pencina KM, Janssens AC, Greenland P. Interpreting incremental value of markers added to risk prediction models. *Am J Epidemiol* 2012;176:473-481.

(10) Uno H, Tian L, Cai T, Kohane IS, Wei LJ. A unified inference procedure for a class of measures to assess improvement in risk prediction systems with survival data. *Stat Med* 2013;32:2430-2442.

(11) Vickers AJ, Elkin EB. Decision curve analysis: a novel method for evaluating prediction models. *Med Decis Making* 2006;26:565-574.

(12) Boyer JK, Thanigaraj S, Schechtman KB, Përez JE. Prevalence of ventricular diastolic dysfunction in asymptomatic, normotensive patients with diabetes mellitus. *Am J Cardiol* 2004;93:870-875.

(13) Fang ZY, Schull-Meade R, Downey M, Prins J, Marwick TH. Determinants of subclinical diabetic heart disease. *Diabetologia* 2005;48:394-402.

(14) Holland DJ, Marwick TH, Haluska BA, Leano R, Hordern MD, Hare JL, Fang ZY, Prins JB, Stanton T. Subclinical LV dysfunction and 10-year outcomes in type 2 diabetes mellitus. *Heart* 2015;101:1061-1066.

(15) Ng AC, Delgado V, Djaberi R, Schuijf JD, Boogers MJ, Auger D, Bertini M, De Roos A, van der Meer RW, Lamb HJ, Bax JJ. Multimodality imaging in diabetic heart disease. *Curr Probl Cardiol* 2011;36:9-47.

(16) Falcao-Pires I, Leite-Moreira AF. Diabetic cardiomyopathy: understanding the molecular and cellular basis to progress in diagnosis and treatment. *Heart Fail Rev* 2012;17:325-344.

(17) From AM, Scott CG, Chen HH. The development of heart failure in patients with diabetes mellitus and pre-clinical diastolic dysfunction a population-based study. *J Am Coll Cardiol* 2010;55:300-305.

(18) Ernande L, Bergerot C, Rietzschel ER, De Buyzere ML, Thibault H, Pignonblanc PG, Croisille P, Ovize M, Groisne L, Moulin P, Gillebert TC, Derumeaux G. Diastolic dysfunction in patients with type 2 diabetes mellitus: is it really the first marker of diabetic cardiomyopathy? *J Am Soc Echocardiogr* 2011;24:1268-1275.

(19) Dandamudi S, Slusser J, Mahoney DW, Redfield MM, Rodeheffer RJ, Chen HH. The prevalence of diabetic cardiomyopathy: a population-based study in Olmsted County, Minnesota. *J Card Fail* 2014;20:304-309.

(20) Liu JH, Chen Y, Yuen M, Zhen Z, Chan CW, Lam KS, Tse HF, Yiu KH. Incremental prognostic value of global longitudinal strain in patients with type 2 diabetes mellitus. *Cardiovasc Diabetol* 2016;15:22.

(21) Steyerberg EW, Vickers AJ, Cook NR, Gerds T, Gonen M, Obuchowski N, Pencina MJ, Kattan MW. Assessing the performance of prediction models: a framework for traditional and novel measures. *Epidemiology* 2010;21:128-138.

(22) Roos CJ, Scholte AJ, Kharagjitsingh AV, Bax JJ, Delgado V. Changes in multidirectional LV strain in asymptomatic patients with type 2 diabetes mellitus: a 2-year follow-up study. *Eur Heart J Cardiovasc Imaging* 2014;15:41-47.



Summary and conclusions

Both obese and diabetic patients can develop changes in myocardial structure and function independent of coronary artery disease. Collectively known as metabolic heart disease, this thesis attempted to illuminate its pathogenesis and prognostic implications.

The thesis began by summarizing the various imaging modalities used to quantifying changes in myocardial structure and contractile function. Specifically, magnetic resonance imaging techniques such as spectroscopy and T1 mapping can be used to quantify myocardial energy substrate utilization and extent of interstitial fibrosis respectively. In addition, myocardial deformation imaging using 2-dimensional speckle tracking echocardiography provides an accurate quantification of myocardial contractility. This technique has previously been validation against the “gold standard” myocardial strain imaging using magnetic resonance imaging myocardial tagging sequence.

In Chapter 2, asymptomatic type 2 male diabetic patients without any associated diabetic complications were prospectively recruited to undergo 2-dimensional speckle tracking echocardiography. These diabetic patients were compared to male controls matched to age and body mass index. This study was first to demonstrate impaired myocardial contractility in asymptomatic diabetic patients, with an impaired longitudinal but preserved circumferential and radial functions. This study established global longitudinal strain as the most sensitive marker for identifying subclinical myocardial dysfunction in diabetic patients.

Chapter 3 explored the combined detrimental effects of increasing body mass index and diabetes on myocardial contractile. In this multicenter study, we demonstrated that both diabetes and increasing body mass index were independent determinants of global longitudinal strain. Secondly, the adverse impact of increasing body mass index and diabetes were additive. Finally, increasing body mass index was a stronger determinant of impaired global longitudinal strain compared to diabetes.

In Chapters 4 to 6, we attempted to evaluate the pathogenesis of subclinical myocardial dysfunction associated with diabetes and increasing body mass index. In a process analogous to fatty liver disease, diabetic patients can accumulate triglyceride within the cytoplasm of myocytes. Under normal physiological conditions, the heart uses both free fatty acids and glucose as its energy source. However, diabetes is characterized by insulin resistance and the heart preferentially uses free fatty acid for metabolism despite the prevailing hyperglycemia. The intracellular triglyceride is a source of free fatty acid and eventually, the excessive triglyceride/free fatty acid concentration exceeds the myocardial β-oxidative capacity. Consequently, there is accumulation of toxic intermediates such as ceramide and diacylglycerol that results in cellular dysfunction. Using proton

magnetic resonance spectroscopy double gated to ECG and respiratory motion, we can quantify the concentration of intramyocardial triglyceride. Furthermore, recent advances in magnetic resonance imaging using post-contrast T1 mapping techniques, we can also quantify the extent of interstitial myocardial fibrosis (i.e. myocardial structural change).

In Chapter 4, intramyocardial triglyceride concentration was quantified using proton magnetic resonance spectroscopy in asymptomatic male diabetic patients, and patients were dichotomized into 2 groups based on the median intramyocardial triglyceride concentration. In this study, patients with higher intramyocardial triglyceride concentration was independently associated with impaired left and right ventricular global longitudinal strain.

In Chapter 5, the burden of interstitial fibrosis was quantified using post-contrast T1 maps in 50 diabetic patients without underlying coronary artery disease or macroscopic scar. Compared to healthy controls, diabetic patients had more interstitial fibrosis was reflected by a shorter post-contrast T1 time. Furthermore, post-contrast T1 time was the strongest determinant of global longitudinal strain on multivariable analysis (standardized $\beta = -0.626$, $p < 0.001$).

In Chapter 6, we evaluated the combined effects of myocardial steatosis and interstitial fibrosis on myocardial contractile function in patients with increasing body mass index. Importantly, patients with underlying diabetes and hypertension were excluded to avoid any potential confounding influences. In this study, epicardial fat volume (a measure of visceral adiposity) was an independent determinant of both intramyocardial triglyceride accumulation and the burden of interstitial fibrosis. On univariable analysis, epicardial fat volume, intramyocardial triglyceride concentration and interstitial fibrosis were associated with left ventricular global longitudinal strain. However, only epicardial fat volume was independently associated with global longitudinal strain on multivariable analysis.

Finally, in Chapter 7, we aimed to determine the prognostic implications of subclinical myocardial dysfunction as identified by global longitudinal strain. In this multicenter study, “normal” global longitudinal strain cut-off value of > -17.0% was defined from 104 healthy volunteers recruited from the community. Applying this normal global longitudinal strain cut-off value to 397 type 2 diabetic patients with normal left ventricular ejection fraction, up to 45% of patients had evidence of subclinical myocardial dysfunction. At follow-up, the presence of subclinical myocardial dysfunction in diabetic patients was independently associated with increased all-cause mortality on follow-up (hazard ratio

2.83, 95% confidence interval 1.40 – 5.71, p = 0.004). Vice versa, diabetic patients without subclinical myocardial dysfunction had similar survival as the general population (standardized mortality ratio 0.94, 95% confidence interval 0.52 – 1.58). Using decision curve analysis, quantifying global longitudinal strain and identifying subclinical myocardial dysfunction was clinically useful and provided incremental net clinical benefit for diabetic patients.

Conclusions and future directions

Echocardiographic 2-dimensional speckle tracking analysis is now a well-established tool that is widely used in routine clinical practice. It is now well accepted that global longitudinal strain is superior to "traditional" left ventricular ejection fraction in detecting early subtle changes and prognosticating adverse outcomes on follow-up. In this thesis, we determined that up to 45% of diabetic patients had evidence of subclinical myocardial dysfunction despite normal left ventricular ejection fraction or known underlying significant coronary artery disease. Using state-of-the-art cardiac magnetic resonance imaging, we have attempted to elucidate the pathophysiology of metabolic heart disease. We have identified increased epicardial adipose tissue, myocardial steatosis and interstitial fibrosis were associated with myocardial contractile dysfunction. Future research should aim at corroborating these findings, risk stratify patients, and identifying effective therapeutic interventions (e.g. medically or surgically induced weight loss, diabetic medications such as sodium-glucose transport protein 2 (SGLT2) inhibitors, etc.) that can potentially reverse subclinical myocardial dysfunction and improve patient outcome.

SAMENVATTING EN CONCLUSIES

Zowel obese als diabetische patiënten kunnen onafhankelijk van coronairlijden veranderingen in myocardstructuur en -functie ontwikkelen. In deze thesis is geprobeerd de pathogenese en de prognostische implicaties van deze veranderingen, algemeen bekend als metabole hartziekten, te belichten.

De thesis begon met het samenvatten van de verschillende beeldvormingstechnieken die worden gebruikt om de veranderingen in myocardstructuur en contractiele functie te kwantificeren. Met name beeldvorming met magnetische resonantie (MRI) zoals spectroscopie en T1 gewogen opnames kunnen worden gebruikt om respectievelijk het myocardiale energie substraat en de mate van interstitiële fibrose te kwantificeren. Daarnaast kan beeldvorming van myocardiale deformatie door middel van 2-dimensionale *speckle tracking* echocardiografie de myocardiale contractiliteit accuraat kwantificeren. Deze techniek is eerder gevalideerd tegen de "gouden standaard" van myocardiale *strain* beeldvorming door MRI met *myocardial tagging*.

In hoofdstuk 2 werden asymptomatische mannen met diabetes type 2 zonder diabetische complicaties prospectief onderzocht met 2-dimensionale *speckle tracking* echocardiografie. Deze patiënten werden vergeleken met mannelijke controles die waren gematcht voor leeftijd en *body mass index* (BMI). Deze studie was de eerste die verminderde myocardiale contractiliteit, met een verminderde longitudinale *strain* maar een behouden circumferente en radiale *strain*, in asymptomatische diabetici aantoonde. De studie stelde vast dat globale longitudinale *strain* de meest sensitieve marker is voor het identificeren van subklinische myocardiale dysfunctie in patiënten met diabetes.

In hoofdstuk 3 werd het gecombineerde schadelijke effect van toename van BMI en diabetes op myocardiale contractiliteit onderzocht. In deze multicenter studie werd gedemonstreerd dat zowel diabetes als toename van BMI onafhankelijke determinanten van globale longitudinale *strain* waren. Daarnaast waren de negatieve impact van toename van BMI en diabetes additief. Tenslotte was toename van BMI een sterkere determinant van verminderde globale longitudinale *strain* vergeleken met diabetes.

In hoofdstukken 4 tot 6 hebben we gepoogd de pathogenese van subklinische myocardiale dysfunctie geassocieerd met diabetes en toename van BMI te evalueren. In een proces dat analoog is aan leververvetting kunnen diabetici triglyceriden accumuleren in het cytoplasma van myocyten. Onder normale fysiologische omstandigheden gebruikt het hart vrije vetzuren en glucose als energiebron. Echter wordt diabetes gekarakteriseerd door insuline resistentie en waardoor het hart vrije vetzuren gebruikt voor het

metabolisme ondanks de continue hyperglycemie. De intracellulaire triglyceriden zijn een bron van vrije vetzuren en uiteindelijk zal de verhoogde concentratie triglyceriden/ vrije vetzuren de capaciteit van de myocardiale β-oxidatieve capaciteit overschrijden. Daardoor ontstaat een accumulatie van toxische tussenproducten zoals ceramide en diacylglycerol wat resulteert in cellulaire dysfunctie. Door middel van proton magnetische resonantie spectroscopie gekoppeld aan het elektrocardiogram en ademhalingsbewegingen, kunnen we de concentratie van de intramyocardiale triglyceriden kwantificeren. Daarnaast kunnen we door recente vooruitgang in MRI technieken met post-contrast T1 gewogen opnames de omvang van interstitiële myocardiale fibrose kwantificeren (bijvoorbeeld myocardiale structurele veranderingen).

In hoofdstuk 4 is de concentratie intramyocardiale tryglyceriden gekwantificeerd behulp van proton magnetische resonantie spectroscopie in mannelijke, asymptomatische patiënten met diabetes. Patienten werden onderverdeeld in 2 groepen gebaseerd op de mediane intramyocardiale triglyceride concentratie. In deze studie was een hogere intramyocardiale triglyceride concentratie onafhankelijk geassocieerd met verminderde linker en rechter ventriculaire globale longitudinale *strain*.

In hoofdstuk 5 werd de hoeveelheid interstitiële fibrose gekwantificeerd door middel van post-contrast T1 gewogen opnames in 50 patiënten met diabetes zonder onderliggend coronairlijden of macroscopisch littekenweefsel. Vergeleken met gezonde controles hadden de patiënten met diabetes meer interstitiële fibrose, wat gereflecteerd werd door een kortere post-contrast T1 tijd. Daarnaast was post-contrast T1 tijd de sterkste determinant van globale longitudinale *strain* in multivariate analyse (gestandaardiseerde $\beta = -0.626$, $p < 0.001$).

In hoofdstuk 6 is het gecombineerde effect van myocardiale steatose en interstitiele fibrose op myocardiale contractiele functie in patiënten met toename van BMI geëvalueerd. Hierbij werden patiënten met onderliggende diabetes en hypertensie als potentiele confounders geëxcludeerd. In deze studie was epicardiaal vetvolume (een maat van viscerale adipositas) een onafhankelijke determinant voor accumulatie van intramyocardiale tryglyceriden en voor de hoeveelheid interstitiële fibrose. In univariate analyse waren epicardiaal vetvolume, intramyocardiale tryglyceride concentratie en interstitiële fibrose geassocieerd met linker ventriculaire globale longitudinale *strain*. Echter was alleen epicardiaal vetvolume in de multivariate analyse onafhankelijk geassocieerd met globale longitudinale *strain*.

Tenslotte werd in hoofdstuk 7 de prognostische implicatie van subklinische myocardiale dysfunctie, vastgesteld met globale longitudinale *strain*, onderzocht. In deze multicen-

ter studie werd een "normale" globale longitudinale *strain* gedefinieerd als > -17.0% op basis van 104 gezonde vrijwilligers uit de algemene populatie. Bij het toepassen van deze afkapwaarde voor normale globale longitudinale *strain* op 397 patiënten met diabetes type 2 en een normale linker ventriculaire ejectiefractie, bleek 45% van de patiënten subklinische myocardiale dysfunctie te hebben. Bij *follow-up* was de aanwezigheid van subklinische myocardiale dysfunctie in diabetici onafhankelijk geassocieerd met verhoogde kans op sterfte (hazard ratio 2.83, 95% betrouwbaarheidsinterval 1.40 – 5.71, p = 0.004). Patiënten met diabetes zonder subklinische myocardiale dysfunctie hadden daarentegen een vergelijkbare overleving met de algemene populatie (gestandaardiseerde sterfte ratio 0.94, 95% betrouwbaarheidsinterval 0.52 – 1.58). Volgens de *decision curve* analyse was het kwantificeren van globale longitudinale *strain* en het identificeren van subklinische myocardiale dysfunctie bruikbaar in de kliniek, en verschafte het incrementeel klinisch voordeel voor patiënten met diabetes.

Conclusies en toekomstperspectieven

Echocardiografische 2-dimensionale *speckle tracking* analyse is een hulpmiddel dat momenteel veel gebruikt wordt in routine onderzoeken in de klinische praktijk. Het is tegenwoordig algemeen geaccepteerd dat globale longitudinale *strain* superieur is aan de "traditionele" linker ventriculaire ejectie fractie in het detecteren van vroege subtiele veranderingen en het voorspellen van ongunstige uitkomsten tijdens *follow-up*. In deze thesis hebben we vastgesteld dat tot 45% van de patiënten met diabetes aanwijzingen hadden voor subklinische myocardiale dysfunctie, ondanks normale linker ventriculaire ejectie fractie en de afwezigheid van bekend onderliggend coronairlijden. Door middel van *state-of-the-art* cardiale MRI hebben we geprobeerd de pathofysiologie van metabole hartziekten te verhelderen. Toekomstig onderzoek zou als doel moeten hebben om deze uitkomsten te bevestigen, risicostratificatie voor patiënten te ontwikkelen en effectieve therapeutische interventies te identificeren (bijvoorbeeld medicamenteus of chirurgisch geïnduceerd gewichtsverlies, diabetes medicatie zoals natrium-glucose-cotransporter 2 (SGLT2) remmers, etc) waardoor potentieel subklinische myocardiale dysfunctie omgekeerd en patiënten uitkomsten verbeterd kunnen worden.

LIST OF PUBLICATIONS

1. **Arnold CT Ng**, David Taylor, Craig Juergens. Infected left ventricular pseudoaneurysm. *Heart* 2006; 92(9): 1237

2. **Arnold CT Ng**, Da T Tran, Mark Newman, Christine Allman, Jane Vidaic, Sidney T Lo, Andrew P Hopkins, Dominic Y Leung. Left Ventricular Longitudinal and Radial Synchrony and Their Determinants in Normal Subjects. *J Am Soc Echocardiogr* 2008;21(9):1042-1048.

3. **Arnold CT Ng**, Da T Tran, Mark Newman, Christine Allman, Jane Vidaic, Kishor K Kadappu, Anita Boyd, Liza Thomas, Dominic Y Leung. Comparison Of Myocardial Tissue Velocities Measured By Two-Dimensional Speckle Tracking And Tissue Doppler Imaging. *Am J Cardiol* 2008;102(6):784-789.

4. **Arnold CT Ng**, Da T Tran, Mark Newman, Christine Allman, Jane Vidaic, Dominic Y Leung. Comparison of Left Ventricular Dyssynchrony by Two-Dimensional Speckle Tracking Versus Tissue-Doppler Imaging in Patients With Non-ST Elevation Myocardial Infarction and Preserved Left Ventricular Systolic Function. *Am J Cardiol* 2008;102(9):1146-1150.

5. Dominic Y Leung, Anita Boyd, **Arnold CT Ng**, Cecilia Chi, Liza Thomas. Echocardiographic Evaluation of Left Atrial Size and Function: Current Understanding, Pathophysiologic Correlates, and Prognostic Implications. *Am Heart J* 2008;156(6):1056-1064.

6. **Arnold CT Ng**, Frank van der Kley, Victoria Delgado, Miriam Shanks, Rutger J van Bommel, Eduard R Holman, Joanne D Schuijf, Nico R van de Veire, Martin J Schalij, Jeroen J Bax. Percutaneous Valve-in-Valve Procedure For Severe Paravalvular Regurgitation In Aortic Bioprosthesis. *J Am Coll Cardiol: Imaging* 2009;2(4):522-523.

7. **Arnold CT Ng**, Christine Allman, Jane Vidaic, H Tie, AP Hopkins, DY Leung. Long Term Impact of Right Ventricular Septal Versus Apical Pacing On Left Ventricular Synchrony And Function in Patients with Second or Third Degree Heart Block. *Am J Cardiol* 2009;103(8):1096-1101.

8. Matteo Bertini, Sjoerd A Mollema, Victoria Delgado, Louisa Antoni, **Arnold CT Ng**, Eduard Holman, Giuseppe Boriani, Martin J Schalij, Jeroen J Bax. Impact of Time

to Reperfusion after Acute Myocardial Infarction on Myocardial Damage Assessed by Left Ventricular Longitudinal Strain. *Am J Cardiol* 2009;104(4):480-485.

9. **Arnold CT Ng**, Victoria Delgado, Matteo Bertini, Gaetano Nucifora, Miriam Shanks, Nina Ajmone Marsan, Eduard Holman, Nico R.L. van de Veire, Dominic Y. Leung, Jeroen J. Bax. Advanced Applications of 3-Dimensional Echocardiography. *Minerva Cardioangiologica* 2009;57(4):415-441.

10. **Arnold CT Ng**, Victoria Delgado, Matteo Bertini, Rutger W. van der Meer, Luuk J Rijzewijk, Miriam Shanks, Gaetano Nucifora, Johannes W.A. Smit, Michaela Diamant, Johannes A. Romijn, Albert de Roos, Dominic Y Leung, Hildo J. Lamb, Jeroen J. Bax. Findings from Left Ventricular Strain and Strain Rate Imaging in Asymptomatic Patients with Type 2 Diabetes Mellitus. *Am J Cardiol* 2009;104(10):1398-1401.

11. **Arnold CT Ng**, Marta Sitges, Phuong N Pham, Da T Tran, Victoria Delgado, Matteo Bertini, Gaetano Nucifora, Jane Vidaic, Christine Allman, Eduard Holman, Jeroen J Bax, Dominic Y Leung. Incremental Value Of Two-Dimensional Speckle Tracking Strain Imaging To Wall Motion Analysis For Detection Of Coronary Artery Disease In Patients Undergoing Dobutamine Stress Echocardiography. *Am Heart J* 2009;158(5):836-844.

12. **Arnold CT Ng**, Victoria Delgado, Frank van der Kley, Rutger J. van Bommel, Miriam Shanks, Arend de Weger, Giuseppe Tavilla, Nico R.L. van de Veire, Matteo Bertini, Gaetano Nucifora, Dominic Y Leung, Joanne Schuijf, Martin J Schalij, Jeroen J. Bax. Comparison of Aortic Root Dimensions and Geometries Pre- and Post-Transcatheter Aortic Valve Implantation by 2- and 3-Dimensional Transesophageal Echocardiography and Multislice Computed Tomography. *Circ Cardiovasc Imaging* 2010;3(1):94-102.

13. Matteo Bertini, Victoria Delgado, Dennis den Ujil, Gaetano Nucifora, **Arnold CT Ng**, Rutger J van Bommel, C Jan Willem Borleffs, Giuseppe Boriani, Martin J Schalij, Jeroen J Bax. Prediction of cardiac resynchronization therapy response: value of calibrated integrated backscatter imaging. *Circ Cardiovasc Imaging* 2010;3(1):86-93.

14. Arend de Weger, Giuseppe Tavilla, **Arnold CT Ng**, Victoria Delgado, Frank van der Kley, Joanne D Schuijf, Jeroen J Bax, Robert JM Klautz. Successful Transapical

Transcatheter Valve Implantation within a Dysfunctional Mitral Bioprosthesis. *J Am Coll Cardiol: Imaging* 2010;3(2):222-223.

15. Gaetano Nucifora, Matteo Bertini, Nina Ajmone Marsan, Victoria Delgado, Arthur J. Scholte, **Arnold CT Ng**, Jacob M. van Werkhoven, Hans-Marc J. Siebelink, Eduard R. Holman, Martin J. Schalij, Ernst E. van der Wall, Jeroen J. Bax. Impact of Left Ventricular Dyssynchrony Early on Left Ventricular Function After First Acute Myocardial Infarction. *Am J Cardiol* 2010;105(3):306-311.

16. Matteo Bertini, Partho Sengupta, Gaetano Nucifora, Victoria Delgado, **Arnold CT Ng**, Nina Ajmone Marsan, Miriam Shanks, Rutger RJ van Bommel, Martin J Schalij, Jagat Narula, Jeroen J Bax. Role of Left Ventricular Twist Mechanics in the Assessment of Cardiac Dyssynchrony in Heart Failure. *J Am Coll Cardiol: Imaging* 2010;2(12):1425-1435.

17. **Arnold CT Ng**, Da T Tran, Christine Allman, Jane Vidaic, Dominic Y Leung. Prognostic Implications of Left Ventricular Dyssynchrony Early After Non-ST Elevation Myocardial Infarction Without Congestive Heart Failure. *Eur Heart J* 2010;31(3):298-308.

18. Gaetano Nucifora, Joanne D Schuijf, Victoria Delgado, Matteo Bertini, Arthur AJ Scholte, **Arnold CT Ng**, Jacob M van Werkhoven, J. Wouter Jukema, Eduard R Holman, Ernst E. van der Wall, Jeroen J Bax. Incremental Value of Subclinical Left Ventricular Systolic Dysfunction For The Identification Of Patients With Obstructive Coronary Artery Disease. *Am Heart J* 2010;159(1):148-157.

19. Miriam Shanks*, **Arnold CT Ng***, Louisa M. Antoni, Sjoerd A. Mollema, Martin J. Schalij, Jeroen J. Bax. Incremental Prognostic Value of the Novel Diastolic Indices for Prediction of Clinical Outcome in Patients with ST Elevation Myocardial Infarction. *Am J Cardiol* 2010;105(5):592-597.

20. Dominic Y Leung, **Arnold CT Ng**. Emerging clinical role of strain imaging in echocardiography. *Heart Lung Circ* 2010;19(3):161-174.

21. Dominic Y Leung, Cecelia Chi, Christine Allman, Anita Boyd, **Arnold CT Ng**, Kishor Kadappu, Liza Thomas. Prognostic Implications of Left Atrial Volume Index In A Large Consecutive Series Of Patients In Sinus Rhythm: A Long Term Follow Up Study. *Am J Cardiol* 2010;105(11):1635-1639.

22. Victoria Delgado, **Arnold CT Ng**, Miriam Shanks, Frank van der Kley, Joanne D Schuijf, Nico R van de Veire, Lucia J Kroft, Albert de Roos, Martin J Schalij, Jeroen J Bax. Transcatheter Aortic Valve Implantation: Role of Multimodality Cardiac Imaging. *Expert Rev Cardiovasc Ther* 2010;8(1):113-123.

23. Victoria Delgado, **Arnold CT Ng**, Nico R van de Veire, Frank van der Kley, Joanne D Schuijf, Laurens F Tops, Arend de Weger, Giuseppe Tavilla, Albert de Roos, Lucia J Kroft, Martin J Schalij, Jeroen J Bax. Transcatheter Aortic Valve Implantation: Role of Multi-slice Computed Tomography to Evaluate Prosthesis Positioning and Deployment in Relation to Valve Function. *Eur Heart J* 2010;31(9):1114-1123.

24. **Arnold CT Ng**, Liza Thomas, Dominic Leung. Tissue Doppler Echocardiography. *Minerva Cardioangiologica* 2010;58(3):357-378

25. Matteo Bertini, Victoria Delgado, Gaetano Nucifora, Nina Ajmone Marsan, **Arnold CT Ng**, Miriam Shanks, Rutger J van Bommel, C Jan Willem Borleffs, See Hooi Ewe, Giuseppe Boriani, Mauro Biffi, Martin J Schalij, Jeroen J Bax. Effect of Cardiac Resynchronization Therapy on Subendo- and Subepicardial Left Ventricular Twist Mechanics and Relation to Favorable Outcome. *Am J Cardiol* 2010;106(5):682-687.

26. Miriam Shanks, Matteo Bertini, Victoria Delgado, **Arnold CT Ng**, Gaetano Nucifora, Rutger J van Bommel, C Jan Willem Borleffs, Eduard R Holman, Nico RL van de Veire, Martin J Schalij, Jeroen J Bax. Effect of Biventricular Pacing on Diastolic Dyssynchrony. *J Am Coll Cardiol* 2010;56(19):1567-1575.

27. **Arnold CT Ng***, Victoria Delgado*, Roxana Djaberi, Joanne D Schuijf, Mark J Boogers, Dominique Auger, Matteo Bertini, Albert de Roos, Rutger W van der Meer, Hildo J Lamb, Jeroen J Bax. Multimodality Imaging in Diabetic Heart Disease. *Curr Probl Cardiol* 2011;36(1):9-47.

28. Victoria Delgado, Eline AQ Mooyaart, **Arnold CT Ng**, Dominique Auger, Matteo Bertini, Rutger J van Bommel, Kai-Hung Yiu, See Hooi Ewe, Tomasz G Witkowski, Nina Ajmone Marsan, Joanne D Schuijf, Ernst E van der Wall, Martin J Schalij, Jeroen J Bax. Echocardiography and Non-Invasive Imaging in Cardiac Resynchronization Therapy. *Minerva Cardioangiologica* 2010;58(3):313-332.

29. Matteo Bertini, C Jan Willem Borleffs, Victoria Delgado, **Arnold CT Ng**, Sebastiaan R Piers, Miriam Shanks, M Louisa Antoni, Mauro Biffi, Giuseppe Boriani, Martin J

Schalij, Jeroen J Bax, Nico R van der Veire. Prediction of Atrial Fibrillation in Patients with Implantable Cardioverter-Defibrillator and Heart Failure. *Eur J Heart Fail* 2010;12(10):1101-1110.

30. Matteo Bertini*, **Arnold CT Ng***, C Jan Willem Borleffs, Victoria Delgado, Adrianus P Wijnmaalen, Gaetano Nucifora, See Hooi Ewe, Miriam Shanks, Joep Thijssen, Katja Zeppenfeld, Mauro Biffi, Dominic Y Leung, Martin J Schalij, Jeroen J Bax. Longitudinal Mechanics of the Peri-Infarct Zone and Ventricular Tachycardia Inducibility in Patients with Chronic Ischemic Cardiomyopathy. *Am Heart J* 2010;160(4):729-736.

31. Miriam Shanks, Victoria Delgado, **Arnold CT Ng**, Frank van der Kley, Joanne D. Schuijf, Eric Boersma, Nico R.L. van de Veire, Gaetano Nucifora, Matteo Bertini, Albert de Roos, Lucia Kroft, Martin J. Schalij, Jeroen J. Bax. Mitral Valve Morphology Assessment: Three-dimensional Transesophageal Echocardiography versus Computed Tomography. *Ann Thorac* Surg 2010;90(6):1922-1929.

32. **Arnold CT Ng***, Matteo Bertini*, C Jan Willem Borleffs, Victoria Delgado, Sebastiaan RD Piers, Joep Thijssen, Gaetano Nucifora, Miriam Shanks, See Hooi Ewe, Mauro Biffi, Nico RL van de Veire, Dominic Y Leung, Martin J Schalij, Jeroen J Bax. Predictors of Death and Occurrence of Appropriate Implantable Defibrillator Therapies in Patients with Chronic Ischemic Cardiomyopathy. *Am J Cardiol* 2010;106(11):1566-1573.

33. Randa M Abdulrahman, Victoria Delgado, **Arnold CT Ng**, See Hooi Ewe, Matteo Bertini, Eduard Holman, Guido C Hovens, AM Pereira, Johannes A Romijn, Jeroen J Bax, Johannes WA Smit. Abnormal Cardiac Contractility in Long Term Exogenous Subclinical Hyperthyriod Patients as Demonstrated by Two-Dimensional Echocardiography Speckle Tracking Imaging. *Eur J Endocrinol* 2010;163(3):435-441.

34. Victoria Delgado, See Hooi Ewe, **Arnold CT Ng**, Frank van der Kley, Nina Ajmone Marsan, Joanne D Schuijf, Martin J Schalij, Jeroen J Bax. Multimodality Imaging in Transcatheter Aortic Valve Implantation: Key Steps to Assess Procedural Feasibility. *EuroIntervention* 2010;6(5):643-652.

35. Dominique Auger, Rutger J van Bommel, Matteo Bertini, Victoria Delgado, **Arnold CT Ng**, See Hooi Ewe, Miriam Shanks, Nina Ajmone Marsan, Eline AQ Mooyaart, Tomasz Witkowski, Don Poldermans, Martin J Schalij, Jeroen J Bax. Prevalence

and Characteristics of Patients with Clinical Improvements But Not Significant Left Ventricular Reverse Remodeling After Cardiac Resynchronization Therapy. *Am Heart J* 2010;160(4):737-743.

36. Miriam Shanks, Hans-Marc Siebelink, Victoria Delgado, Nico R van de Veire, **Arnold CT Ng**, Allard Sieders, Joanne D Schuijf, Hildo J Lamb, Nina Ajmone Marsan, Jos J Westenberg, Lucia Kroft, Albert de Roos, Jeroen J Bax. Quantitative Assessment of Mitral Regurgitation: Comparison Between Three-dimensional Transesophageal Echocardiography and Magnetic Resonance Imaging. *Circ Cardiovasc Imaging* 2010;3(6):694-700.

37. Anita C Boyd, **Arnold CT Ng**, Da T Tran, Ee May Chia, John K French, Dominic Y Leung, Liza Thomas. Left Atrial Enlargement and Phasic Function in Patients Following Non-ST Elevation Myocardial Infarction. *J Am Soc Echocardiogr* 2010;23(12):1251-1258.

38. Matteo Bertini, Victoria Delgado, Gaetano Nucifora, Nina Ajmone Marsan, **Arnold CT Ng**, Miriam Shanks, M Louisa Antoni, Nico RL van de Veire, Rutger J van Bommel, Claudio Rapezzi, Martin J Schalij, Jeroen J Bax. Left ventricular rotational mechanics in patients with coronary artery disease: differences in subendocardial and subepicardial layers. *Heart* 2010;96(21):1737-1743.

39. Gaetano Nucifora, Victoria Delgado, Matteo Bertini, Nina Ajmone Marsan, Nico R van de Veire, **Arnold CT Ng**, Hans-Marc Siebelink, Martin J Schalij, Eduard R Holman, Partho P Sengupta, Jeroen J Bax. Left ventricular muscle and fluid mechanics in acute myocardial infarction. *Am J Cardiol* 2010;106(10):1404-1409.

40. **Arnold CT Ng**, Victoria Delgado, Matteo Bertini, Rutger W van der Meer, Luuk J Rijzewijk, See Hooi Ewe, Hans-Marc Siebelink, Johannes WA Smit, Michaela Diamant, Johannes A Romijn, Albert de Roos, Dominic Y Leung, Hildo Lamb, Jeroen J Bax. Myocardial Steatosis and Biventricular Strain and Strain Rate Imaging in Patients with Type 2 Diabetes Mellitus. *Circulation* 2010;122(24):2545-2550.

41. Dennis W den Uijl, Victoria Delgado, Laurens F Tops, **Arnold CT Ng**, Eric Boersma, Serge A Trines, Katja Zeppenfeld, Martin J Schalij, Arnoud van der Laarse, Jeroen J Bax. Natriuretic Peptide Levels Predict Recurrent of Atrial Fibrillation After Radiofrequency Catheter Ablation. *Am Heart J* 2011;161(1):197-203.

42. Victoria Delgado*, **Arnold CT Ng*,** Joanne D Schuijf, Frank van der Kley, Laurens F Tops, Nico R van de Veire, Albert de Roos, Lucia J Kroft, Martin J Schalij, Jeroen J Bax. Automated Assessment of the Aortic Root Dimensions with Multidetector Row Computed Tomography. *Ann Thorac Surg* 2010;91(3):716-723.

43. See Hooi Ewe, Nina Ajmone Marsan, Mauro Pepi, Victoria Delgado, Gloria Tamborini, Manuela Muratori, **Arnold CT Ng**, Frank van der Kley, Arend de Weger, Melissa Fusari, Paolo Biglioli, Jeroen J Bax. Impact of Left Ventricular Systolic Function on Clinical and Echocardiographic Outcomes Following Transcatheter Aortic Valve Implantation for Severe Aortic Stenosis. *Am Heart J* 2010;160(6):1113-1120.

44. Tomasz Witkowski, Ellen A ten Brinke, Victoria Delgado, **Arnold CT Ng**, Matteo Bertini, Nina Ajmone Marsan, See Hooi Ewe, Dominique Auger, Kelvin H Yiu, J Braun; Patrick Klein, Paul Steendijk, MI Versteegh; Robert J Klautz, Jeroen J Bax. Surgical Ventricular Restoration for Patients with Ischemic Heart Failure Patients: Determinants of Two-Year Survival. *Ann Thorac Surg* 2011;91(2):491-498.

45. **Arnold CT Ng***, Victoria Delgado*, Matteo Bertini, M Louisa Antoni, Rutger van Bommel, Frank van der Kley, See Hooi Ewe, Gaetano Nucifora, Joanne Schuijf, Don Poldermans, Dominic Y Leung, Martin Schalij, Jeroen J Bax. Alterations in Multidirectional Myocardial Functions in Patients with Aortic Stenosis and Preserved Ejection Fraction: A Two-Dimensional Speckle Tracking Analysis. *Eur Heart J* 2011;32(12):1542-1550.

46. Victoria Delgado, Rutger J van Bommel, Matteo Bertini, C Jan Willem Borleffs, Nina Ajmone Marsan, Gaetano Nucifora, Nico RL van de Veire, Eric Boersma, Claudia Ypenburg, **Arnold CT Ng**, Eduard R Holman, Martin J Schalij, Jeroen J Bax. Relative Merits of Left Ventricular Dyssynchrony, Left Ventricular Lead Position, and Myocardial Scar to Predict Long-Term Survival of Ischemic Heart Failure Patients Undergoing Cardiac Resynchronization Therapy. *Circulation* 2011;123(1):70-78.

47. Miriam Shanks, Victoria Delgado, **Arnold CT Ng**, Dominique Auger, Eline A Mooyaart, Matteo Bertini, Nina Ajmone Marsan, Rutger J van Bommel, Eduard R Holman, Don Poldermans, Martin J Schalij, Jeroen J Bax. Clinical and echocardiographic predictors of nonresponse to cardiac resynchronization therapy. *Am Heart J* 2011;161(3):552-557.

48. See Hooi Ewe, Victoria Delgado, **Arnold CT Ng**, M Louisa Antoni, Frank van der Kley, Nina Ajmone Marsan, Aren de Weger, Giuseppe Tavilla, Eduard R Hol-

man, Martin J Schalij, Jeroen J Bax. Outcomes After Transcatheter Aortic Valve Implantation: Transfemoral Versus Transapical Approach. *Ann Thorac Surg* 2011;92(4):1244-1251.

49. Randa M Abdulrahman, Victoria Delgado, Hendrieke C Hoftijzer, **Arnold CT Ng**, See Hooi Ewe, Nina Ajmone Marsan, Eduard R Holman, Guido C Hovens, Eleonora P Corssmit, Johannes A Romijn, Jeroen J Bax, Johannes WA Smit. Both Exogenous Subclinical Hyperthyroidism and Short-Term Overt Hypothyroidism Affect Myocardial Strain in Patients with Differentiated Thyroid Carcinoma. *Thyroid* 2011;21(5):471-476.

50. Dominique Auger, Matteo Bertini, Nina Ajmone Marsan, Ulas Hoke, See Hooi Ewe, Joep Thijssen, Tomasz Witkowski, Kai Hang Yiu, **Arnold CT Ng**, Ernst E van der Wall, Martin J Schalij, Jeroen J Bax, Victoria Delgado. Prediction of Response to Cardiac Resynchronizaion Therapy Combining Two Different Three-Dimensional Analyses of Left Ventricular Dyssynchrony. *Am J Cardiol* 2011;108(5):711-717.

51. **Arnold CT Ng***, Kai-Hang Yiu*, Victoria Delgado, Frank van der Kley, M Louisa Antoni, See Hooi Ewe, Matteo Bertini, Arend de Weger, Albert de Roos, Lucia J Kroft, Dominic Y Leung, Joanne D Schuijf, Martin J Schalij, Jeroen J Bax. Influence of left ventricular geometry and function on aortic annular dimensions as assessed with multi-detector row computed tomography: implications for transcatheter aortic valve implantation. *Eur Heart J* 2011;32(22):2806-2813.

52. See Hooi Ewe; **Arnold CT Ng**, Joanne D Schuijf, Frank van der Kley, Andrea Colli, Meindert Palmen, Arend de Weger, Nina Ajmone Marsan, Eduard R Holman, Albert de Roos, Martin J Schalij, Jeroen J Bax, Victoria Delgado. Location and Severity of Aortic Valve Calcium and Implications for Aortic Regurgitation After Transcatheter Aortic Valve Implantation. *Am J Cardiol* 2011;108(10):1470-1477.

53. Miriam Shanks, M Louisa Antoni, Ulas Hoke, Matteo Bertini, **Arnold CT Ng**, Dominique Auger, Nina Ajmone Marsan, Lieselot van Erven, Eduard R Holman, Martin J Schalij, Jeroen J Bax, Victoria Delgado. The effect of cardiac resynchronization therapy on left ventricular diastolic function assessed with speckle-tracking echocardiography. *Eur J Heart Fail* 2011;13(10):1133-1139.

54. **Arnold CT Ng***, Dominique Auger*, Victoria Delgado, Saskia GC van Elderen, Hans-Marc Siebelink, Rob J van der Geest, Cosimo Bonetti, Enno T van der Velde, Albert de Roos, Don Poldermans, Johannes WA Smit, Dominic Y Leung, Hildo J

Lamb, Jeroen J Bax. Diffuse Myocardial Fibrosis by Cardiac Magnetic Resonance Contrast-Enhanced T1 Mapping and Subclinical Myocardial Dysfunction in Diabetic Heart Disease. *Circ Cardiovasc Imaging* 2012;5(1):51-59

55. Matteo Bertini*, **Arnold CT Ng***, M. Louisa Antoni, Gaetano Nucifora, See H. Ewe, Dominique Auger, Nina Ajmone Marsan, Martin J Schalij, Jeroen J. Bax, Victoria Delgado. Global Longitudinal Strain Predicts Long-Term Survival in Patients with Chronic Ischemic Cardiomyopathy. *Circ Cardiovasc Imaging* 2012;5(3):383-391

56. Tomasz G Witkowski, James D Thomas, Victoria Delgado, Eva van Rijnsoever, **Arnold CT Ng**,Ulas Hoke, See H Ewe, Dominique Auger, Kai H Yiu, Eduard R Holman, Robert JM Klautz, Martin J Schalij, Jeroen J Bax, Nina Ajmone Marsan. Changes in Left Ventricular Function After Mitral Valve Repair for Severe Organic Mitral Regurgitation. *Ann Thorac Surg* 2012;93(3):754-760.

57. Dominique Auger, Gabe B Bleeker, Matteo Bertini, See H Ewe, Rutger J van Bommel, Tomasz G Witkowski, **Arnold CT Ng**, Lieselot van Erven, Martin J Schalij, Jeroen J Bax, Victoria Delgado. Effect of Cardiac Resynchronization Therapy in Patient Without Left Intraventricular Dyssynchrony. *Eur Heart J* 2012;33(7):913-920.

58. Kai Hang Yiu, Douwe E Atsma, Victoria Delgado, **Arnold CT Ng**, Tomasz G Witkowski, See Hooi Ewe, Dominique Auger, Eduard R Holman, Anneke M van Mil, Martijn H Breuning, Hung Fat Tse, Jeroen J Bax, Martin J Schalij, Nina Ajmone Marsan. Myocardial structural alteration and systolic dysfunction in preclinical hypertrophic cardiomyopathy mutation carriers. *PLoS One* 2012;7(5):e36115.

59. Paola Gripari, See Hooi Ewe, Laura Fusini, Manuela Muratori, **Arnold CT Ng**, Claudia Cefalu, Victoria Delgado, Martin J Schalij, Jeroen J Bax, Nina Ajmone Marsan, Gloria Tamborini, Mauro Pepi. Intraoperative 2D and 3D transoesophageal echocardiographic predictors of aortic regurgitation after transcatheter aortic valve implantation. *Heart* 2012;98(16):1229-1236.

60. Victoria Delgado, **Arnold CT Ng**. Assessment of Left Ventricular Systolic Function in Aortic Stenosis and Prognostic Implications. *Eur Heart J Cardiovasc Imaging* 2012;13(10):805-807.

61. Linda D van Schinkel, Dominique Auger. Saskia GC van Elderen, Nina Ajmone Marsan, Victoria Delgado, Hildo J Lamb, **Arnold C T Ng**, Johannes WA Smit,

Jeroen J Bax, Jos JM Westenberg, Albert de Roos. Aortic stiffness is related to left ventricular diastolic function in patients with diabetes mellitus type 1: assessment with MRI and speckle tracking strain analysis. *Int J Cardiovasc Imaging* 2013; 29 (3):633-641.

62. Jacqueline S Mourer, See Hooi Ewe, Marko JK Mallat, **Arnold CT Ng**, Ton J Rabelink, Jeroen J. Bax, Victoria Delgado, and Johan W de Fijter. Late Calcineurin Inhibitor Withdrawal Prevents Progressive Left Ventricular Diastolic Dysfunction in Renal Transplant Recipients. *Transplantation* 2012;94(7):721-728.

63. Matteo Bertini, Ulas Höke, Rutger J van Bommel, **Arnold CT Ng**, Miriam Shanks, Gaetano Nucifora, Dominique Auger, Jan C Willem Borleffs, Eva P van Rijnsoever, Lieselot van Erven, Martin J Schalij, Nina A Marsan, Jeroen J Bax, Victoria Delgado. Impact of clinical and echocardiographic response to cardiac resynchronization therapy on long-term survival. *Eur Heart J Cardiovasc Imaging* 2013;14(8):774-781.

64. Stuart J Butterly, Mathivathana Indrajith, Paul Garrahy, **Arnold CT Ng**, Paul A Gould, William YS Wang. Stress-induced takotsubo cardiomyopathy in survivors of the 2011 Queensland floods. *Med J Aust* 2013, 198(2):109-110.

65. Terri Hall, Tony Stanton, William YS Wang, **Arnold CT Ng**. Stroke Prevention in Atrial Fibrillation: An Update on Current Management. *Panminerva Medica* 2013, 55(1):43-58.

66. Doughty, R.N. , Gardin, J.M., Hobbs, F.D.R., McMurray, J.J.V., Nagueh, S.F., Poppe, K.K., Senior, R., Thomas, L., Whalley, G.A., Aune, E., Brown, A., Badano, L.P., Cameron, V., Chadha, D.S., Chahal, N., Chien, K.L., Daimon, M., Dalen, H., Detrano, R., Akif Duzenli, M., Ezekowitz, J., De Simone, G., Di Pasquale, P., Fukuda, S., Gill, P.S., Grossman, E., Hobbs, F.D.R., Kim, H.-K., Kuznetsova, T., Leung, N.K.W., Linhart, A., McDonagh, T.A., McGrady, M., McMurray, J.J.V., Mill, J.G., Mogelvang, R., Muiesan, M.L., **Ng, A.C.T.**, Ojji, D., Otterstad, J.E., Petrovic, D.J., Poppe, K.K., Prendergast, B., Rietzschel, E., Schirmer, H., Schvartzman, P., Senior, R., Simova, I., Sliwa, K., Stewart, S., Squire, I.B., Takeuchi, M., Thomas, L., Whalley, G.A., Altman, D., Perera, R., Poppe, K.K., Triggs, C.M., Au Yeung, H., Beans Picón, G.A., Poppe, K.K., Whalley, G.A. A meta-Analysis of echocardiographic measurements of the left heart for the development of normative reference ranges in a large international cohort: The EchoNoRMAL study. *Eur Heart J Cardiovasc Imaging* 2014,15(3):341.

67. Danielle Harrop, William YS Wang, **Arnold CT Ng**. Imaging Diabetic Heart Disease. *EMJ Diabet* 2014;2:88-98.

68. Matthew Salamonsen, Ada Lo, **Arnold Ng**, William Wang, Bashirzadeh Bashirzadeh, David Fielding. Novel Use of Pleural Ultrasound Techniques Can Identify Malignant Trapped Lung Prior to Effusion Drainage. *Chest* 2014,146(5):1286-1293.

69. Vasileios Kamperidis, Philippe J van Rosendael, **Arnold C.T. Ng**, Spyridon Katsanos, Frank van der Kley, Philippe Debonnaire, Emer Joyce, Georgios Sianos, Nina Ajmone Marsan, Jeroen J Bax, Victoria Delgado. Impact of Flow and Left Ventricular Strain on Outcome of Patients With Preserved Left Ventricular Ejection Fraction and Low Gradient Severe Aortic Stenosis Undergoing Aortic Valve Replacement. *Am J Cardiol* 2014;114(12):1875-1881.

70. Josh PJ Tsai, Jenny Tian, William YS Wang, **Arnold CT Ng**. Glycated Hemoglobin vs.Fasting Plasma Glucose as a Predictor of Left Ventricular Dysfunction After ST-Elevation Myocardial Infarction. *Can J Cardiol.* 2015;31(1):44-49.

71. EchoNoRMAL collaborators. Ethnic-specific normative reference values for echocardiographic LA and LV size, LV mass, and systolic function: The EchoNoRMAL study. *J Am Coll Cardiol: Imaging* 2015; 8(6):656-665.

72. Lisa Gillinder, Shi Yi Goo, Gary Cowin, Mark Strudwick, Rob J van der Geest, William YS Wang, **Arnold CT Ng**. Quantification of Intramyocardial Metabolites by Proton Magnetic Resonance Spectroscopy**.** *Front Cardiovasc Med* 2015;2:24.

73. Yash Singbal, William Vollbon, Luan T Huynh, William YS Wang, **Arnold CT Ng**, Sudhir Wahi. Exploring the Role of Non-invasive Tricuspid dP/dt as A Marker of Right Ventricular Function. *Echocardiography*, 2015;32(9):1347-1351.

74. Ewe SH, Haeck ML, **Ng AC**, Witkowski TG, Auger D, Leong DP, Abate E, Ajmone Marsan N, Holman ER, Schalij MJ, Bax JJ, Delgado V. Detection of subtle left ventricular systolic dysfunction in patients with significant aortic regurgitation and preserved left ventricular ejection fraction: speckle tracking echocardiographic analysis. *Eur Heart J Cardiovasc Imaging*, 2015;16(9):992-999.

75. **Arnold CT Ng**, William KF Kong, Vasileios Kamperidis, Matteo Bertini, M. Louisa Antoni, Dominic Y Leung, Nina Ajmone Marsan, Victoria Delgado, Jeroen J. Bax.

Anemia in Patients with Aortic Stenosis: Influence on Long-Term Prognosis. *Eur J Heart Fail*, 2015;17(10):1042-1049

76. Christopher C.Y. Wong; Austin C.C. Ng; Jerrett K. Lau; Vincent Chow; Vivien Chen; **Arnold C.T. Ng**; Andy S.C. Yong; Andrew P. Sindone; Thomas H. Marwick; Leonard Kritharides. High mortality in patients presenting with acute pulmonary embolism and elevated INR not on anticoagulant therapy. *Thromb Haemost*, 2016;115(6):1191-1199.

77. W. Phillip Law, William Y.S. Wang, Peter T. Moore, Peter N. Mollee, **Arnold C.T. Ng**. Cardiac amyloid imaging with 18F-florbetaben positron emission tomography: a pilot study. *J Nucl Med*, 2016;57(11):1733-1739.

78. Peter T Moore, **Arnold CT Ng**, Paul A Gould, William YS Wang. An unusual cause of out-of-hospital cardiac arrest recorded on a heartrate monitor. *Heart Lung Circ,* 2016;25(10):e130-2.

79. **Arnold CT Ng,** Shi Yi Goo, Nicole Roche, Lisa Gillinder, Rob J van der Geest, William YS Wang. Epicardial Adipose Tissue Volume and Left Ventricular Myocardial Function Using 3-Dimensional Speckle Tracking Echocardiography. *Can J Cardiol,* 2016;32(12):1485-1492

80. Matthew Burrage, Arun Dahiya, **Arnold CT Ng**, Dariusz Korczyk. Multimodality imaging of a rare case of cardiac lipomatosis. *Eur Heart J Cardiovasc Imaging*, 2017;18(1):115

81. William KF Kong, Victoria Delgado, Kian Keong Poh, Madelien V. Regeer, **Arnold CT Ng**, Louise McCormack, Tiong Cheng Yeo, Miriam Shanks, Sarah Parent, Roxana Enache, Bogdan A. Popescu, Michael Liang, James W. Yip, Lawrence CW Ma, Vasileios Kamperidis, Philippe J van Rosendael, Enno T van der Velde, Nina Ajmone Marsan, Jeroen J Bax. Prognostic implications of raphe in bicuspid aortic valve anatomy. *JAMA Cardiol,* 2017;2(3):285-292.

82. William KF Kong, Madelien V. Regeer, **Arnold CT Ng**, Louise McCormack, Kian Keong Poh, Tiong Cheng Yeo, Miriam Shanks, Sarah Parent, Roxana Enache, Bogdan A. Popescu, James W Yip, Lawrence Ma, Vasilis Kamperidis, Enno T van der Velde, Bart Mertens, Nina Ajmone Marsan, Victoria Delgado, Jeroen J Bax. Sex Differences in Phenotypes of Bicuspid Aortic Valve and Aortopathy: Insights From a Large Multicenter, International Registry. *Circ Cardiovasc Imaging,* 2017;10(3):e005155.

83. **Arnold CT Ng**, William YS Wang, Victoria Delgado, Jeroen J Bax. Bicuspid Aortic Valve Disease: New Insights. *Structural Heart,* 2017;1(1):9-17.

84. Edgard A Prihadi, Melissa Leung, E Mara Vollema, **Arnold CT Ng**, Nina Ajmone Marsan, Jeroen J Bax, Victoria Delgado. Prevalence and Prognostic Relevance of Ventricular Conduction Disturbances in Patients with Aortic Stenosis. *Am J Cardiol*, 2017;120(12):2226-2232.

85. **Arnold CT Ng**, Edgard Prihadi, M. Louisa Antoni, Matteo Bertini, See Hooi Ewe, Nina Ajmone Marsan, Dominic Y Leung, Victoria Delgado, Jeroen J Bax. Left Ventricular Myocardial Deformation is Predictive of All-Cause Mortality Independent of Aortic Stenosis Severity and Ejection Fraction. *Eur Heart J Cardiovasc Imaging*, 2018;19(8):859-867

86. **Arnold CT Ng**, Prevedello F, Dolci G, Roos CJ, Djaberi R, Bertini M, Ewe SH, Allman C, Leung DY, Marsan NA, Delgado V, Bax JJ. Impact of Diabetes and Increasing Body Mass Index Category on Left Ventricular Systolic and Diastolic Function. *J Am Soc Echocardiol*, 2018;31(8):916-925.

87. **Arnold CT Ng**, Mark Strudwick, Rob J van der Geest, Austin CC Ng, Lisa Gillinder, Shi Yi Goo, Gary Cowin, Victoria Delgado, William YS Wang, Jeroen J Bax. Impact of Epicardial Adipose Tissue, Left Ventricular Myocardial Fat Content and Interstitial Fibrosis on Myocardial Contractile Function. *Circ Cardiovasc Imaging*, 2018; 11(8): e007372.

88. Edgard A Prihadi, Melissa Leung, E Mara Vollema, **Arnold CT Ng**, Nina Ajmone Marsan, Victoria Delgado, Jeroen J Bax. Electrocardiographic Pattern of Left Ventricular Hypertrophy with Strain and Survival In Calcific Aortic Valve Disease. *Structural Heart,* 2018; 2(3): 240-246.

89. Lei Zhao, Danielle L Harrop, **Arnold CT Ng**, William YS Wang. Epicardial adipose tissue is associated with left atrial dysfunction in people without obstructive coronary artery disease or atrial fibrillation. *Can J Cardiol,* 2018; 34(8):1019-1025

90. **Arnold CT Ng**, Victoria Delgado, William KF Kong, Jeroen J Bax. Lessons from an International Bicuspid Aortic Valve disease registry: the Raphe and Beyond. *Heart Lung Circ,* 2018; 27(7):782-784

91. **Arnold CT Ng**, Victoria Delgado, Jeroen J Bax. Application of Left Ventricular Strain in patients with Aortic and Mitral Valve Disease. *Curr Opin Cardiol,* 2018;33(5):470-478.

92. Gerald Kaye, Jun Yen Ng, Shameer Ahmed, Diana Valencia, Danielle Harrop, **Arnold CT Ng**. The prevalence of pacing-induced cardiomyopathy (PICM) in patients with long term right ventricular pacing - is it a matter of definition? *Heart Lung Circ,* 2018; 28(7): 1027-1033.

93. **Arnold CT Ng**, Jeroen J Bax. Pre-Operative Hyperglycemia and Risk of Myocardial Injury in Non-Cardiac Surgery. *Lancet Diabetes Endocrinol*, 2018; 6(10): 757-759.

94. E. Mara Vollema, Tadafumi Sugimoto, Mylène Shen, Lionel Tastet, **Arnold CT Ng**, Rachid Abou, Nina Ajmone Marsan, Raluca Dulgheru, Patrizio Lancellotti, Marie-Annick Clavel, Philippe Pibarot, Philippe Genereux, Martin B. Leon, Victoria Delgado, Jeroen J Bax. Association of Left Ventricular Global Longitudinal Strain With Asymptomatic Severe Aortic Stenosis: Natural Course and Prognostic Value. *JAMA Cardiol*, 2018; 3(9): 839-847.

95. Edgard A Prihadi, E Mara Vollema, **Arnold CT Ng**, Nina Ajmone Marsan, Jeroen J Bax, Victoria Delgado. Determinants and prognostic implications of left ventricular mechanical dispersion in aortic stenosis. *Eur Heart J Cardiovasc Imaging*, 2019; 20(7): 740-748.

96. Kristyan B Guppy-Coles, Sandhir B Prasad, Kym C Smith, Ada Lo, Patrick Beard, **Arnold CT Ng**, John J Atherton. Accuracy of Cardiac Nurse Acquired and Measured Three-dimensional Echocardiographic Left Ventricular Ejection Fraction: Comparison to Echosonographer. *Heart Lung Circ*, 2019; S1443-9506(19)30347-6

97. Vollema EM, Singh GK, Prihadi EA, Regeer MV, Ewe SH, Ng ACT, Mertens BJA, Klautz RJM, Ajmone Marsan N, Bax JJ, Delgado V. Time course of left ventricular remodelling and mechanics after aortic valve surgery: aortic stenosis vs. aortic regurgitation. *Eur Heart J Cardiovasc Imaging*, 2019; 20(10): 1105-1111.

98. **Arnold CT Ng**, Matteo Bertini, See Hooi Ewe, Enno T van der Velde, Dominic Y Leung, Victoria Delgado. Jeroen J. Bax. Defining Subclinical Myocardial Dysfunction and Implications for Patients with Diabetes Mellitus and Preserved Ejection Fraction. *Am J Cardiol*, 2019; 124(6): 892-898.

99. E. Mara Vollema, Mohammed R. Amanullah, **Arnold C.T. Ng**, Pieter van der Bijl, Francesca Prevedello, Yoong Kong Sin, Edgard A. Prihadi, Nina Ajmone Marsan, Zee Pin Ding, Philippe Généreux, Philippe Pibarot, Martin B. Leon, Jagat Narula, See Hooi Ewe, Victoria Delgado, Jeroen J. Bax, Staging Cardiac Damage in Patients With Symptomatic Aortic Valve Stenosis. *J Am Coll Cardiol*, 2019; 74(4): 538-549.

100. Ha T, Korczyk D, **Ng ACT**, Wang WYS. When can heart failure treatment be stopped safely? *Lancet*, 2019; 394(10194): 217.

101. **Arnold CT Ng**, Jeroen J Bax. Hyperdynamic Left Ventricular Function and the Prognostic Implications for Heart Failure with Preserved Ejection Fraction. *Eur Heart J*, 2019 In Press

102. **Arnold CT Ng**, Jeroen J Bax. Diagnostic Value of Hybrid Imaging with Computed Tomography Coronary Angiogram and Stress Positron Emission Tomography in Patient with Coronary Artery Bypass Grafting. *Eur Heart J Cardiovasc Imaging*, 2019; 20(11): 1296-1297.

103. Zhao L, Gould PA, **Ng ACT**, Wang WYS. Cardiac autonomic nerve system and epicardial fat in atrial fibrillation. *Int J Cardiol*, 2019; 34(8): 1019-1025.

104. Huang LYI, Fogarty SJ, **Ng ACT**, Wang WYS. Rates and predictors of general practitioner (GP) follow-up postdischarge from a tertiary hospital cardiology unit: a retrospective cohort study. *BMJ Open*, 2019; 9(10): e031627.

105. Kong WKF, Vollema EM, Prevedello F, Perry R, **Ng ACT**, Poh KK, Almeida AG, González A, Shen M, Yeo TC, Shanks M, Popescu BA, Galian Gay L, Fijałkowski M, Liang M, Chen RW, Ajmone Marsan N, Selvanayagam J, Pinto F, Zamorano JL, Pibarot P, Evangelista A, Delgado V, Bax JJ. Prognostic implications of left ventricular global longitudinal strain in patients with bicuspid aortic valve disease and preserved left ventricular ejection fraction. *Eur Heart J Cardiovasc Imaging*, 2019 In Press

106. Vollema EM, Prihadi EA, **Ng ACT**, Gegenava T, Ajmone Marsan N, Bax JJ, Delgado V. Prognostic Implications of Renal Dysfunction in Patients With Aortic Stenosis. *Am J Cardiol*, 2020 In Press

107. **Arnold CT Ng**, Victoria Delgado, Jeroen J Bax. Individualized Patient Risk Stratification Using Machine Learning and Topological Data Analysis. *JACC Cardiovasc Imaging*, 2020 In Press

108. **Ng ACT**, Delgado V, Bax JJ. Autonomic dysfunction in Huntington's disease: A 123 I-MIBG study. J Nucl Cardiol, 2020 In Press

109. **Ng ACT**, Delgado V, Bax JJ. An international, multicentre survey of echocardiographic abnormalities in COVID-19 patients. Eur Heart J Cardiovasc Imaging. 2020 Sep 1;21(9):959-960.

110. **Ng ACT**, Bax JJ. Hyperdynamic left ventricular function and the prognostic implications for heart failure with preserved ejection fraction. Eur Heart J. 2020 Mar 21;41(12):1258-1259.

111. **Ng ACT**, Holmes DR, Mack MJ, Delgado V, Makkar R, Blanke P, Leipsic JA, Leon MB, Bax JJ. Leaflet immobility and thrombosis in transcatheter aortic valve replacement. Eur Heart J, 2020; 41(33):3184-3197.

112. E Mara Vollema, Mohammed R Amanullah, Edgard A Prihadi, **Arnold CT Ng**, Pieter van der Bijl, Yoong Kong Sin, Nina Ajmone Marsan, Zee Pin Ding, Philippe Généreux, Martin B Leon, See Hooi Ewe, Victoria Delgado, Jeroen J Bax. Incremental value of left ventricular global longitudinal strain in a newly proposed staging classification based on cardiac damage in patients with severe aortic stenosis. Eur Heart J Cardiovasc Imaging, 2020 In Press

113. Borlaug BA, **Ng ACT**. Cardiac Magnetic Resonance to Enhance Phenotypic Characterization of HFpEF. JACC Cardiovasc Imaging, 2020 In Press

114. **Arnold CT Ng**, Barry A Borlaug, Victoria Delgado, Jeroen J Bax. Diabesity: the combined burden of obesity and diabetes on heart disease and the role of imaging. Nature Reviews Cardiology, 2020 In Press

CURRICULUM VITAE

Dr. Arnold Ng was born on December 22nd, 1976, in Malaysia and emigrated to Australia in 1991. He obtained his high school diploma in 1993 from Hale School in Perth, Western Australia. In 1999, he graduated from the Medical School at The University of New South Wales, Australia and in 2006 he completed his Cardiology training at Liverpool Hospital, New South Wales, Australia. After working as a consultant cardiologist for 8 months at Liverpool Hospital in 2008, he underwent a 2-year multimodality cardiac imaging research fellowship at Leiden University Medical Center, Leiden, The Netherlands under the mentorship of Prof. Dr. Jeroen J. Bax. Since 2010, he has been working as a consultant cardiologist at The Princess Alexandra Hospital, Queensland, Australia. He obtained his first PhD at The University of New South Wales, Australia, in 2011 on left ventricular myocardial mechanics and synchrony in patients with coronary artery disease. His primary clinical and research areas of interest include multimodality cardiac imaging (echocardiography, cardiac computed tomography, cardiac magnetic resonance and cardiac positron emission tomography), particularly in the assessment of coronary artery disease and metabolic heart disease.

ACKNOWLEDGEMENTS

I would like first thank Professor Jeroen J Bax who supervised me during the 2 years of fellowship, and continues to support me in the last 10 years. Your dedication and commitment to your fellows is an inspiration to me and something that I will always strive to emulate.

I would also like to thank Professor Dominic Leung who recommended me to come to Leiden to work with Professor Bax.

This thesis was also made possible by my friends and colleagues at LUMC. In particular, I would like to thank Victoria who always looked out for me and yet never asked anything in return. I would also like to thank Marlieke Dietz who helped with the Dutch translations.

Finally, I would like to thank my wife, Carolina, for her love and support. Thank you for putting up with me and being there all the time.